CERN-PH-TH-2010-298 KA-TP-40-2010
Cavendish-HEP-10/21 DCPT/10/202
MAN/HEP/2010/23 IPPP/10/101
SLAC-PUB-14333 LU TP 10-28
HD-THEP-10-24 MCnet-11-01

General-purpose event generators for LHC physics

Andy Buckley[a], Jonathan Butterworth[b], Stefan Gieseke[c], David Grellscheid[d], Stefan Höche[e], Hendrik Hoeth[d], Frank Krauss[d], Leif Lönnblad[f,g], Emily Nurse[b], Peter Richardson[d], Steffen Schumann[h], Michael H. Seymour[i], Torbjörn Sjöstrand[f], Peter Skands[g], Bryan Webber[j]

[a] *PPE Group, School of Physics & Astronomy, University of Edinburgh, EH25 9PN, UK*
[b] *Department of Physics & Astronomy, University College London, WC1E 6BT, UK*
[c] *Institute for Theoretical Physics, Karlsruhe Institute of Technology, D-76128 Karlsruhe*
[d] *Institute for Particle Physics Phenomenology, Durham University, DH1 3LE, UK*
[e] *SLAC National Accelerator Laboratory, Menlo Park, CA 94025, USA*
[f] *Department of Astronomy and Theoretical Physics, Lund University, Sweden*
[g] *PH Department, TH Unit, CERN, CH-1211 Geneva 23, Switzerland*
[h] *Institute for Theoretical Physics, University of Heidelberg, 69120 Heidelberg, Germany*
[i] *School of Physics and Astronomy, University of Manchester, M13 9PL, UK*
[j] *Cavendish Laboratory, J.J. Thomson Avenue, Cambridge CB3 0HE, UK*

Abstract

We review the physics basis, main features and use of general-purpose Monte Carlo event generators for the simulation of proton-proton collisions at the Large Hadron Collider. Topics included are: the generation of hard-scattering matrix elements for processes of interest, at both leading and next-to-leading QCD perturbative order; their matching to approximate treatments of higher orders based on the showering approximation; the parton and dipole shower formulations; parton distribution functions for event generators; non-perturbative aspects such as soft QCD collisions, the underlying event and diffractive processes; the string and cluster models for hadron formation; the treatment of hadron and tau decays; the inclusion of QED radiation and beyond-Standard-Model processes. We describe the principal features of the Ariadne, Herwig++, Pythia 8 and Sherpa generators, together with the Rivet and Professor validation and tuning tools, and discuss the physics philosophy behind the proper use of these generators and tools. This review is aimed at phenomenologists wishing to understand better how parton-level predictions are translated into hadron-level events as well as experimentalists wanting a deeper insight into the tools available for signal and background simulation at the LHC.

Keywords: QCD, hadron colliders, Monte Carlo simulation

Contents

1. General introduction

Understanding the final states of high energy particle collisions such as those at the Large Hadron Collider (LHC) is an extremely challenging theoretical problem. Typically hundreds of particles are produced, and in most processes of interest their momenta range over many orders of magnitude. All the particle species of the Standard Model (SM), and maybe some beyond, are involved. The relevant matrix elements are too laborious to compute beyond the first few orders of perturbation theory, and in the case of QCD processes they involve the intrinsically non-perturbative and unsolved problem of confinement. Once these matrix elements have been computed within some approximation scheme, there remains the problem of dealing with their many divergences and/or near-divergences. Finally they must be integrated over a final-state phase space of huge and variable dimension in order to obtain predictions of experimental observables.

Over the past thirty years an armoury of techniques has been developed to tackle these seemingly intractable problems. The crucial tool of factorization allows us to separate the treatment of many processes of interest into different regimes, according to the scales of momentum transfer involved. At the highest scales, the constituent partons of the incoming beams interact to produce a relatively small number of energetic outgoing partons, leptons or gauge bosons. The matrix elements of these hard subprocesses are perturbatively computable. At the very lowest scales, of the order of 1 GeV, incoming partons are confined in the beams and outgoing partons interact non-perturbatively to form the observed final-state hadrons. These soft processes cannot yet be calculated from first principles but have to be modelled. The hard and soft regimes are distinct but connected by an evolutionary process that can be calculated in principle from perturbative QCD. One consequence of this scale evolution is the production of many additional partons in the form of initial- and final-state parton showers, which eventually participate in the low-scale process of hadron formation.

All three regimes of this highly successful picture of hard collisions are eminently suited to computer simulation using Monte Carlo techniques. The large and variable dimension of the phase space, $3n - 4$ dimensions[1] plus flavour and spin labels for an n-particle final state, makes Monte Carlo the

[1]Three components of momentum per produced particle, minus four constraints of overall energy-momentum conservation.

integration method of choice: its accuracy improves inversely as the square root of the number of integration points, irrespective of the dimension. The evolution of scales that leads to parton showering is a Markov process that can be simulated efficiently with Monte Carlo techniques, and the available hadronization models are formulated as Monte Carlo processes from the outset. Furthermore the factorized nature of the problem means that the treatment of each regime can be improved systematically as more precise perturbative calculations or more sophisticated hadronization models become available.

Putting all these elements together, one has a Monte Carlo event generator capable of simulating a wide range of the most interesting processes that are expected at the LHC, which can be used for several distinct purposes in particle physics experiments. Event generators are usually required to extract a signal of new physics from the background of SM processes. Comparisons of their predictions to the data can be used to perform measurements of SM parameters. They also provide realistic input for the design of new experiments, or for new selection or reconstruction procedures within an existing experiment.

Historically, the development of event generators began shortly after the discovery of the partonic structure of hadrons and of QCD as the theory of strong interactions.[2] Some important features of hard processes, such as deep inelastic scattering and hadroproduction of jets and lepton pairs, could be understood simply in terms of parton interactions. To describe final states in more detail, at first simple models were used to fragment the primary partons directly into hadrons, but this could not account for the transverse broadening of jets and lepton pair distributions with increasing hardness of the interaction. It was soon appreciated that the primary partons, being coloured, would emit gluons in the same way that scattered charged particles emit photons, and that these gluons, unlike photons, could themselves radiate, leading to a parton cascade or shower that might account for the broadening. It was then evident that hadron formation would occur naturally as the endpoint of parton showering, when the typical scale of momentum transfers is low and the corresponding value of the QCD running coupling is large. However, this very fact renders the hadronization process non-perturbative, so hadronization models, inspired by QCD but not so far

[2]For an early review, see [1].

derivable from it, were developed with tunable parameters to describe the hadron-level properties of final states.

Although most of the signal processes of interest at the LHC fall into the category of hard interactions that can be treated by the above methods, the vast majority of collisions are soft, leading to diffractive scattering or multiparticle production with low transverse momenta. These soft processes also need to be simulated but, as in the case of hadronization, their non-perturbative nature means that we have to resort to models with tunable parameters to describe the data. A related phenomenon is the component of the final state in hard interactions that is not associated with the primary hard process – the so-called "underlying event". There is convincing evidence that this is due to secondary interactions of the other constituent partons of the colliding hadrons. The hard tails of these interactions are described by perturbative QCD, but again the soft component has to be modelled. The same multiple-parton interaction model can serve for the simulation of soft collisions, provided there is no conflict between the parameter values needed to describe the two phenomena.

The main purpose of this review is to provide a survey of how all the above components are implemented in the general-purpose event generators that are currently available for the simulation of LHC proton-proton collisions. The authors are members of MCnet,[3] a European Union funded Marie Curie Research Training Network dedicated to developing the next generation of Monte Carlo event generators and providing training of its user base; the review seeks to contribute to those objectives.

Our discussion is aimed at phenomenologists wishing to understand better the simulation of hadron-level events as well as experimentalists wanting a deeper insight into the tools available for signal and background simulation at the LHC. We have tried to start at a level that does not assume expertise beyond graduate particle physics courses. However, some sections dealing with current developments, such as the matching of matrix elements and parton showers, are necessarily more technical. In those cases the treatment is less pedagogical but we provide references to further discussion and proofs. Each section ends with a set of bullet points summarizing the main points. In many cases we illustrate points by reference to plots of event generator output, and compare with experimental data where available.

[3] http://www.montecarlonet.org/

We begin in Part I with a more detailed discussion of the physics involved in event generators, starting with an overview in Section 2 of the structure of an event and the steps by which it is generated. We then describe the hard subprocess in Section 3 before going on to the parton showers in Section 4. The precision of these perturbative components of the simulation has been improved in recent years by various schemes to include higher-order QCD corrections without double counting, which we review in Section 5.

Next we turn to the non-perturbative aspects of event generation, starting in Section 6 with the parton distribution functions of the incoming hadrons, which are used not only to compute the hard subprocess cross section but also for the generation of initial-state parton showers. We go on to discuss the modelling of soft collisions, the underlying event and diffraction in Section 7, and then in Section 8 we describe the principal hadronization models used in present-day event generators.

It is well established that a large fraction of produced particles come from the decays of unstable hadronic resonances, and therefore the accurate simulation of these decays, together with electroweak decays that occur before particles have exited a typical beampipe or detector, is an essential part of event generation, reviewed in Section 9. Next we describe the available techniques for simulating QED radiation. Part I ends with a discussion of the simulation of physics beyond the Standard Model.

Part II contains brief reviews of the individual event generators that were developed as part of the MCnet Network, referring back to Part I for the physics involved and the modelling options that are implemented. Then in Part III we discuss issues involved in the use of event generators, their validation and tuning, and the tools that have been developed for these purposes. In particular, guidelines for making experimental measurements that are optimally useful for Monte Carlo validation and tuning are given.

Part III ends with some illustrative plots of results from the MCnet event generators for a wide range of processes. It should be emphasised that these results are only "snapshots" of the current state of the generators, which have not yet been thoroughly tuned for use at the LHC. For up-to-date comparisons with LHC data one should consult the repository of plots at `mcplots.cern.ch`.

A number of Appendices deal with important technical points in more detail. Appendix A gives a brief survey of the basic Monte Carlo methods employed in event generators, while Appendix B discusses methods for evaluating hard subprocess matrix elements and phase space integration. A

BSM	Beyond Standard Model
DIS	Deep inelastic (lepton) scattering
FSR	Final-state (QCD) radiation
ISR	Initial-state (QCD) radiation
LL	Leading logarithm(ic)
LO	Leading order
MC	Monte Carlo
ME	Matrix element
MPI	Multiple parton interations
NLL	Next-to-leading logarithm(ic)
NLO	Next-to-leading order
PDF	Parton distribution function
PS	Parton shower
SM	Standard Model
UE	Underlying event

Table 1: Abbreviations used in this review.

particularly important Standard Model parameter is the top quark mass, and we devote Appendix C to the meaning of this quantity as determined by tuning the corresponding event generator parameters.

As space is limited, and the emphasis of MCnet has been on general-purpose event generation for proton colliders, some topics relevant to the LHC programme, notably heavy ion collisions, are not included. We also do not cover specialized generators for specific processes, or programs that operate only at parton level and do not generate complete hadron-level final states. In most cases the latter can be interfaced to the MCnet generators through standard file formats, as outlined in Appendix B.3, although care must be taken to avoid double counting, as discussed in Section 5.

For reference and to avoid repetition, we have collected in Tab. 1 the common abbreviations used throughout the review.

Part I
Review of physics behind MC event generators

2. Structure of an event

We start this part of the review with a brief overview of the steps by which event generators build up the structure of a hadron-hadron collision involving a hard process of interest – that is, a process in which heavy objects are created or a large momentum transfer occurs. As outlined already in Section 1, there are several basic phases of the process that need to be simulated: a primary hard subprocess, parton showers associated with the incoming and outgoing coloured participants in the subprocess, non-perturbative interactions that convert the showers into outgoing hadrons and connect them to the incoming beam hadrons, secondary interactions that give rise to the underlying event, and the decays of unstable particles that do not escape from the detector. There are corresponding steps in the event generation.

Of course, not all these steps are relevant in all processes. In particular, the majority of events that make up the total hadron-hadron cross section are of soft QCD type and rely more on phenomenological models. At the other extreme the simulation of new-physics events such as supersymmetric particle production and decay, and the SM backgrounds to them, rely on essentially all of the components.

We also briefly introduce two issues that affect all areas of the simulation: the jet structure of the final state and a widely used approximation to QCD – the large-N_c limit.

In most applications of event generators, one is interested in events of a particular type. Rather than simulating typical events and waiting for one of them to be of the required type, which can be as rare as 1 in 10^{15} in some applications, the simulation is built around the hard subprocess. The user selects hard subprocesses of given types and partonic events are generated according to their matrix elements and phase space, as described in Section 3 and in more detail in Appendix B. These are typically of LO for the given process selected (which could be relatively high order in the QCD coupling, for example for Z+4 partons) and calculated with the tree-level matrix elements. There has however been important progress in including

loop corrections into hard process generation, as described in Section 5.

Since the particles entering the hard subprocess, and some of those leaving it, are typically QCD partons, they can radiate gluons. These gluons can radiate others, and also produce quark–antiquark pairs, generating showers of outgoing partons. This process is simulated with a step-wise Markov chain, choosing probabilistically to add one more parton to the final state at a time, called a parton shower algorithm, described in Section 4. It is formulated as an evolution in some momentum-transfer-like variable downwards from a scale defined by the hard process, and as both a forwards evolution of the outgoing partons and a backwards evolution of the incoming partons progressively towards the incoming hadrons.

The incoming hadrons are complex bound states of strongly-interacting partons and it is possible that, in a given hadron-hadron collision, more than one pair of partons may interact with each other. These multiple interactions go on to produce additional partons throughout the event, which may contribute to any observable, in addition to those from the hard process and associated parton showers that we are primarily interested in. We therefore describe this part of the event structure as the underlying event. As described in Section 7, it can also be formulated as a downward evolution in a momentum-transfer-like variable.

As the event is evolved downwards in momentum scales it ultimately reaches the region, at scales of order 1 GeV, in which QCD becomes strongly interacting and perturbation theory breaks down. Therefore at this scale the perturbative evolution must be terminated and replaced by a non-perturbative hadronization model that describes the confinement of the system of coloured partons into colourless hadrons. A key feature of these models, described in Section 8, is that individual partons do not hadronize independently, but rather colour-connected systems of partons hadronize collectively. These models are not derived directly from QCD and consequently have more free parameters than the preceding components. However, to a good approximation they are universal – the hadronization of a given coloured system is independent of how that system was produced, so that once tuned on one data set the models are predictive for new collision types or energies.

Finally, many of the hadrons that are produced during hadronization are unstable resonances. Sophisticated models are used to simulate their decay to the lighter hadrons that are long-lived enough to be considered stable on the time-scales of particle physics detectors, Section 9. Since many of the particles involved with all stages of the simulation are charged, QED

radiation effects can also be inserted into the event chain at various stages, Section 10.

2.1. Jets and jet algorithms

The final states of many subprocesses of interest include hard partons. Radiation from the incoming partons is a source of additional partons in the final state. The parton shower evolution is dominated by the emission of additional partons that are either collinear with the outgoing partons or are soft. The final state of the parton shower therefore predominantly has a structure in which most of the energy is carried by localized collinear bundles of partons, called jets. The hadronization mechanism is such that this jet structure is preserved and it is experimentally observed that the final state of high-momentum-transfer hadronic events is dominated by jets of hadrons. The distributions of the total momentum of hadrons in jets are approximately described by perturbative calculations of partons with the same total momentum.

Although jets are a prominant feature of hadronic events, they are not fundamental objects that are defined by the theory. In order to classify the jet final state of a collision, define which hadrons belong to which jet and reconstruct their total momentum, we need a precise algorithmic jet definition, or jet algorithm. There has been much progress on the properties that such algorithms must satisfy in order to be convenient theoretically and experimentally. We are not able to review this work here (for a recent thorough review, see [2] for example), but we mention one important property that we require of a jet algorithm. One of the applications we will use them for is the matching of perturbative calculations at different orders and with different jet structures and in order for this to be well-defined we must use an algorithm for which jet cross sections can be calculated on the parton level to arbitrarily high order of perturbation theory. This is only true of jet algorithms that are *collinear and infrared safe*. That is, for any partonic configuration, replacing any parton with a collinear set of partons with the same total momentum, or adding any number of infinitely soft partons in any directions, should produce the identical result. One can show that, provided this property is satisfied, jet cross sections are finite at any perturbative order and have non-perturbative corrections that are suppressed by powers of the jet momenta, so that at high momentum transfers the jet structure of the hadronic final state of a collision is very well described by a parton-level calculation.

2.2. The large-N_c limit

It is of course well established that QCD is an SU(3) gauge theory. Nevertheless it is frequently useful to consider the generalization to a theory with N_c colours, SU(N_c). We will see that various aspects of event simulation simplify in the limit of large N_c. For any N_c, one can combine a fundamental colour with a fundamental anticolour to produce an adjoint colour and a colour singlet, $N_c \otimes \bar{N}_c = (N_c^2 - 1) \oplus 1$. Conversely, we can think of the colour of a gluon as being that of a quark and an antiquark, up to corrections from the fact that the gluon does not have a singlet component. One can decompose the colour structure of each of the Feynman rules, and hence of any Feynman diagram, into a set of delta-functions between external fundamental colours. We call this the colour flow of the diagram. In the limit of large N_c, only diagrams whose colour flow is planar, i.e. for which the fundamental colour connections can be drawn in a single plane, contribute. Each colour connection that needs to come out of the plane results in a suppression of $1/N_c^2$. This connection between the topology of a diagram and its colour flow is an extremely powerful organizing principle, which we will see comes into several different aspects of event modelling. One should bear in mind that whenever we use the large-N_c limit, corrections to it are expected to be suppressed by at least $1/N_c^2 \sim 10\%$ and in practice, because of the connection with the topology, are often further dynamically suppressed.

3. Hard subprocesses

Many LHC processes of interest involve large momentum transfers, for example to produce heavy particles or jets with high transverse momenta. Thus the simulation of subprocesses with large invariant momentum transfer is at the core of any simulation of collider events in contemporary experiments through Monte Carlo event generators. As QCD quanta are asymptotically free, such reactions can be described by perturbation theory, thus making it possible to compute many features of the subprocess in question by, for example, using Feynman diagrams.

3.1. Factorization formula for QCD cross sections

Cross sections for a scattering subprocess $ab \to n$ at hadron colliders can be computed in collinear factorization through [3]

$$\begin{aligned}\sigma &= \sum_{a,b} \int_0^1 \mathrm{d}x_a \mathrm{d}x_b \int f_a^{h_1}(x_a,\mu_F) f_b^{h_2}(x_b,\mu_F)\, \mathrm{d}\hat{\sigma}_{ab\to n}(\mu_F,\mu_R) \qquad (1)\\ &= \sum_{a,b} \int_0^1 \mathrm{d}x_a \mathrm{d}x_b \int \mathrm{d}\Phi_n\, f_a^{h_1}(x_a,\mu_F) f_b^{h_2}(x_b,\mu_F)\\ &\qquad \times \frac{1}{2\hat{s}} |\mathcal{M}_{ab\to n}|^2(\Phi_n;\mu_F,\mu_R)\,,\end{aligned}$$

where

- $f_a^h(x,\mu)$ are the parton distribution functions (PDFs), which depend on the light-cone momentum fraction x of parton a with respect to its parent hadron h, and on the factorization scale[4] μ_F;

- $\hat{\sigma}_{ab\to n}$ denotes the parton-level cross section for the production of the final state n through the initial partons a and b. It depends on the momenta given by the final-state phase space Φ_n, on the factorization scale and on the renormalization scale μ_R. The fully differential parton-level cross section is given by the product of the corresponding matrix element squared, averaged over initial-state spin and colour degrees of freedom, $|\mathcal{M}_{ab\to n}|^2$, and the parton flux $1/(2\hat{s}) = 1/(2x_a x_b s)$, where s is the hadronic centre-of-mass energy squared.

- The matrix element squared $|\mathcal{M}_{ab\to n}|^2(\Phi_n;\mu_F,\mu_R)$ can be evaluated in different ways. In Appendix B.1 we discuss some of the technology used for tree-level matrix elements. Here it should suffice to say that the matrix element can be written as a sum over Feynman diagrams,

$$\mathcal{M}_{ab\to n} = \sum_i \mathcal{F}^{(i)}_{ab\to n}\,. \qquad (2)$$

[4]One could imagine to have two factorization scales, one for each hadron. This may be relevant for certain processes such as the fusion of electroweak bosons into a Higgs boson, where, at leading order, the two hadrons do not interact through the exchange of colour.

However, any summation over quantum numbers can be moved outside the square, allowing one to sum over helicity and colour orderings such that

$$|\mathcal{M}_{ab\to n}|^2(\Phi_n;\mu_F,\mu_R) = \sum_{h_i;\,c_j} |\mathcal{M}^{\{ij\}}_{ab\to n}|^2(\Phi_n,\{h_i\},\{c_j\};\mu_F,\mu_R)\,. \quad (3)$$

In the computation of cross sections, this allows one to Monte Carlo sample not only over the phase space, but also over the helicities and colour configurations. Picking one of the latter in fact defines the starting conditions for the subsequent parton showering, as discussed in more detail in Section 4.

- $\mathrm{d}\Phi_n$ denotes the differential phase space element over the n final-state particles,

$$\mathrm{d}\Phi_n = \prod_{i=1}^{n} \frac{\mathrm{d}^3 p_i}{(2\pi)^3 2E_i} \cdot (2\pi)^4 \delta^{(4)}(p_a + p_b - \sum_{i=1}^{n} p_i)\,, \quad (4)$$

where p_a and p_b are the initial-state momenta. For hadronic collisions, they are given by $x_a P_a$ and $x_b P_b$, where the Bjorken variables, x_a and x_b, are also integrated over, and P_a and P_b are the fixed hadron momenta.

This equation holds to all orders in perturbation theory. However, when the subprocess cross section is computed beyond leading order there are subtleties, which will be discussed later, and therefore for the moment we consider only the use of leading-order (LO) subprocess matrix elements.

It should be noted that the integration over the phase space may contain cuts, for two reasons. First of all there are cuts reflecting the geometry and acceptance of detectors, which are relevant for the comparison with measured cross sections and other related quantities. On top of that there are other cuts, which, although their details may be dominated by similar considerations, reflect a physical necessity. These are, for instance, cuts on the transverse momentum of particles produced in t-channel processes, which exhibit the analogue of the Coulomb singularity in classical electron scattering and are related to internal particles going on their mass shell. In a similar way, especially for QCD processes, the notion of jets defined by suitable algorithms (see Section 2) shields the calculation of the cross section of a process from unphysical soft and/or collinear divergences. At

leading order, these correspond simply to a set of cuts on parton momenta, preventing them from becoming soft or collinear.

3.2. Leading-order matrix-element generators

All multi-purpose event generators provide a comprehensive list of LO matrix elements and the corresponding phase-space parameterizations for $2 \to 1$, $2 \to 2$ and some $2 \to 3$ production channels in the framework of the Standard Model and some of its new physics extensions. For higher-multiplicity final states they employ dedicated matrix-element and phase-space generators, such as AlpGen [4], AMEGIC++ [5], COMIX [6], HELAC/PHEGAS [7, 8], MadGraph/MadEvent [9, 10] and Whizard/O'Mega [11, 12], which are either interfaced (see Appendix B.3) or built-in as for the case of SHERPA. These codes specialize in the efficient generation and evaluation of tree-level matrix elements for multi-particle processes, see Appendix B.1 and Appendix B.2.

In doing so they have to overcome a number of obstacles. First of all, the number of Feynman diagrams used to construct the matrix elements increases roughly factorially with the number of final-state particles. This typically renders textbook methods based on the squaring of amplitudes through completeness relations inappropriate for final-state multiplicities of four or larger. Processes with multiplicities larger than six are even more cumbersome to compute and usually accessible through recursive relations only. Secondly, the phase space of final-state particles in such reactions necessitates the construction of dedicated integration algorithms, based on the multi-channel method. This, and other integration techniques, will be discussed in more detail in Appendix A and Appendix B.2.

3.3. Choices for renormalization and factorization scales

The cross section defined by Eq. (1) is fully specified only for a given PDF set and a certain choice for the unphysical factorization and renormalization scales. There exists no first principle defining what are the *correct* μ_F and μ_R. However, our knowledge of the logarithmic structure of QCD for different classes of hard scattering processes limits the range of reasonable values. This knowledge is used as a guide when setting the default choices in the various generators. Considering the class of $2 \to 1$ and $2 \to 2$ processes, typically one hard scale Q^2 is identified such that $\mu_F = \mu_R = Q^2$. Examples thereof are the production of an s-channel resonance of mass M, where $Q^2 = M^2$ or the production of a pair of massless particles with transverse momentum p_T, where typically $Q^2 = p_T^2$. In general-purpose event generators the hard

scale Q^2 has the further meaning of a starting scale for subsequent initial- and final-state parton showers[5]. Accordingly when choosing μ_F and μ_R for processes with final-state multiplicity larger than two, care has to be taken not to introduce any double counting between the matrix-element calculation and the parton-shower simulation, see Section 5.

3.4. Choices for PDFs

Regarding the PDF, one is in principle free to choose any parameterization that matches the formal accuracy of the cross section calculation, see Eq. (1). All generators provide access to commonly used PDF sets via the LHAPDF interface [13]. However, each generator uses a default PDF set and the predictions of certain tunes of parton shower, hadronization and underlying event model parameters might be altered when changing the default PDF set, see Section 17. For a detailed discussion on PDF issues in Monte Carlo event generators see Section 6.

3.5. Anatomy of NLO cross section calculations

Most of the current multi-purpose event generators currently employ leading-order (LO) matrix elements to drive the simulation. This means that the results are only reliable for the shape of distributions, while the absolute normalization is often badly described, due to large higher-order corrections. One therefore often introduces a so-called K-factor when comparing results from event generators with experimental data. This factor is normally just that, a single factor multiplying the LO cross section, typically obtained by the ratio of the total NLO cross section to the LO one for the relevant process. However, in this report we use the concept in a broader sense, where the K-factor can depend on the underlying kinematics of the LO process.

However, in striving for a higher accuracy and a better control of theoretical uncertainties, some processes have been made accessible at next-to-leading order accuracy and have been included in the complete simulation chain, properly matched to the subsequent parton showers. This motivates the introduction of some formalism here, which will be used in Section 5, where NLO event generation will be discussed in some detail.

[5] The precise phase-space limits of course depend on the relation between the generator's shower evolution scale and Q^2.

A cross section calculated at NLO accuracy is composed of three parts, the LO or Born-level part, and two corrections, the virtual and the real-emission one. Schematically,

$$\mathrm{d}\sigma^{\mathrm{NLO}} = \mathrm{d}\tilde{\Phi}_n \left[\mathcal{B}(\tilde{\Phi}_n) + \alpha_\mathrm{s}\mathcal{V}(\tilde{\Phi}_n)\right] + \mathrm{d}\tilde{\Phi}_{n+1}\alpha_\mathrm{s}\mathcal{R}(\tilde{\Phi}_{n+1})\,, \tag{5}$$

where the tildes over the phase space elements $\mathrm{d}\tilde{\Phi}_n$ denote integrals over the n-particle final state *and* the Bjorken variables, and include the incoming partonic flux, and where the terms $\mathcal{B}$, $\mathcal{V}$, and $\mathcal{R}$ denote the Born, virtual and real emission parts. They in turn include the PDFs, and the summation over flavours is implicit.

An obstacle in calculating these parts is the occurrence of ultraviolet and infrared divergences. The former are treated in a straightforward manner, by firstly regularizing them, usually in dimensional regularization, before the theory is renormalized. The infrared divergences, on the other hand, are a bit more cumbersome to deal with. This is due to the fact that they show up both in the virtual contributions, which lead to the same n-particle final state, and in the real corrections, leading to an $n+1$-particle final state. According to the Bloch-Nordsieck [14] and Kinoshita-Lee-Nauenberg theorems [15, 16], for sensible, i.e. infrared-safe, observables these divergences must mutually cancel. This presents some difficulty, since they are related to phase spaces of different dimensionality. In order to cure the problem several strategies have been devised, which broadly fall into two categories: phase-space slicing methods, pioneered in [17, 18], and infrared subtraction algorithms [19–26]. Current NLO calculations usually use the latter. They are based on the observation that the soft and collinear divergences in the real-emission correction $\mathcal{R}$ exhibit a universal structure. This structure can be described by the convolution of (finite) Born-level matrix elements, $\mathcal{B}$, with suitably chosen, universal splitting kernels, $\mathcal{S}$, which in turn encode the divergent structure. Therefore, the "subtracted real-emission term" $[\mathcal{R}-\mathcal{B}\otimes\mathcal{S}]$ is infrared finite and can be integrated over the full phase space Φ_{n+1} of the real-emission correction in four space-time dimensions. The subtraction terms $\mathcal{B}\otimes\mathcal{S}$ are added back in and combined with the virtual term, $\mathcal{V}$, after they have been integrated over the radiative phase space. This integration is typically achieved in D dimensions, such that the divergences emerge as poles in $4-D$. Taking everything together, the parton-level cross section at

NLO accuracy reads, schematically,

$$\sigma^{\mathrm{NLO}} = \int_n \mathrm{d}\tilde{\Phi}_n^{(4)}\, \mathcal{B} \quad + \quad \alpha_\mathrm{s} \int_{n+1} \mathrm{d}\tilde{\Phi}_{n+1}^{(4)} \left[\mathcal{R} - \mathcal{B} \otimes \mathcal{S} \right] + \quad \alpha_\mathrm{s} \int_n \mathrm{d}\tilde{\Phi}_n^{(D)} \left[\tilde{\mathcal{V}} + \mathcal{B} \otimes \int_1 \mathrm{d}\Phi_1^{(D)} \mathcal{S} \right] , \tag{6}$$

where the dimensions of the phase space elements and the number of final-state particles have been made explicit and where collinear counter-terms have been absorbed into the modified virtual contribution, $\tilde{\mathcal{V}}$.

It is worth noting that the task of evaluating the above equation can be compartmentalized in a straightforward way. A natural division is between specialized codes, so-called one-loop providers (OLPs), that provide the virtual part, $\mathcal{V}$, and generic tree-level matrix element generators which will take care of the rest, including phase space integration. For details see Appendix B.3. In the long run this will allow for an automated inclusion of NLO accuracy into the multi-purpose event generators; first steps in this direction have been made in [27–29].

In order to go to even higher accuracy, i.e. to the NNLO level, the above equation would become even more cumbersome, with more contributions to trace. This, however, will most likely remain far beyond the anticipated accuracy reach of the multi-purpose event generators for a long time to come.

3.6. Summary

- The factorization formula in Eq. (1) is employed to calculate cross sections at hadron colliders. The necessary ingredients are the parton-level matrix element, the parton distribution functions and the integration over the corresponding phase space.

- At leading order, i.e. for tree-level processes, there is a plethora of fully automated tools, constructing and evaluating the matrix elements with different methods. They typically do not rely on textbook methods but on the helicity method or recursion relations.

- Due to the complexity of the processes, the phase space integration is a complicated task, which is usually performed using Monte Carlo

sampling methods, which extend to include also treatment of the sum over polarizations and, more recently, even colours.

- The choice of the renormalization and factorization scales is not fixed by first principles, but rather by experience. Combining the matrix elements with the subsequent parton shower defines, to some extent, which choices are consistent and therefore "allowed".

- Higher-order calculations, i.e. including loop effects, are not yet fully automated. They consist of more than just one matrix element with a fixed number of final-state particles, but they include terms with extra particles in loops and/or legs. These extra emissions introduce infrared divergences, which must cancel between the various terms. This also makes the combination with the parton shower more cumbersome.

4. Parton showers

The previous section discussed the generation of a hard process according to lowest-order matrix elements. These describe the momenta of the outgoing jets well, but to give an exclusive picture of the process, including the internal structure of the jets and the distributions of accompanying particles, any fixed order is not sufficient. The effect of all higher orders can be simulated through a parton shower algorithm, which is typically formulated as an evolution in momentum transfer down from the high scales associated with the hard process to the low scales, of order 1 GeV, associated with confinement of the partons it describes into hadrons.

In this section, we describe the physics behind parton showering. Much of our language will be based on the conventional approach in which a parton shower simulates a succession of emissions from the incoming and outgoing partons. Towards the end of the section, however, we will describe a slightly different formulation based on a succession of emissions from the coloured dipoles formed by pairs of these partons. As we will discuss there, at the level of detail of our presentation, the two approaches are almost equivalent and most of this section applies equally well to dipole-based showers.

4.1. Introduction: QED bremsstrahlung in scattering processes

We are familiar with the fact that in classical electrodynamics charges radiate when scattered (see for example [30], chapter 15). Calculating a scattering process in perturbative QED, one finds that the radiation pattern

of photons at the first order agrees with this classical calculation (an important fact proved in Low's theorem [31]). One also encounters loop diagrams, which correct the non-emission process such that the sum of emission and non-emission probabilities is unity. At successively higher orders, soft photons are effectively emitted independently. The spectrum extends down to arbitrarily low frequencies, so that the total number of photons emitted is ill-defined, but the number of observable photons above a given energy is finite. The probability of no observable photons is also finite, and exponentially suppressed for small energy cutoffs (known as Sudakov suppression [32]).

One important property of this QED bremsstrahlung is the fact that emission from different particles involved in the same scattering event is coherent. One manifestation of this is that when a high energy photon produces an e^+e^- pair in the field of a nucleus and, due to the high boost factor, the pair are extremely close to each other in direction, they do not ionize subsequent atoms they pass near because, while they are closer together than the atomic size, the atoms only see their total charge, which is zero, and not their individual charges. Only once their separation has reached the atomic size do they start to ionize. In effect, the charged particles only behave independently with respect to observers in a forward cone of opening angle given by their separation and at larger angles they behave as a coherent pair. This is observed in bubble-chamber photographs as a single line of very weak ionization that becomes stronger and eventually separates into two lines and is known as the Chudakov effect [33]. We will see that there is a corresponding effect in QCD.

Having recalled these basic features of QED bremsstrahlung, we will calculate the equivalent processes in QCD and see many analogous features, as well as crucial differences arising from the non-abelian nature of QCD and the resulting strong interactions at low energy.

4.2. Collinear final state evolution

Although the utility of parton showers comes from the fact that they are universal (process-independent) building blocks, we find it instructive to motivate their main features by considering a specific process, e^+e^- annihilation to jets. The leading-order cross section is given by the electroweak process $e^+e^- \to q\bar{q}$ and is finite. We define its total cross section to be $\sigma_{q\bar{q}}$.

We are more interested in the next-order process, $e^+e^- \to q\bar{q}g$, which we hope to formulate as the production of a $q\bar{q}$ pair, accompanied by the emission of a gluon by that pair. Parameterizing the three-parton phase

space with θ, the opening angle between the quark and the gluon, and z, the energy fraction of the gluon, we obtain

$$\frac{\mathrm{d}\sigma_{q\bar{q}g}}{\mathrm{d}\cos\theta\,\mathrm{d}z} \approx \sigma_{q\bar{q}}\, C_F\, \frac{\alpha_\mathrm{s}}{2\pi}\, \frac{2}{\sin^2\theta}\, \frac{1+(1-z)^2}{z}\,, \tag{7}$$

where $C_F = \frac{N_c^2-1}{2N_c}$ is a colour factor that can be thought as the colour-charge squared of a quark. In Eq. (7) we see that the differential cross section diverges at the edges of phase space. To illustrate this, we have approximated the full expression (which can be found in [3] for example) by neglecting non-divergent terms. Recalling that the bremsstrahlung distribution was also divergent in QED, but that this did not matter for a physical description of the final state of observable photons, this divergence may not be a problem. But we will certainly want to understand its physical origin since, as we approach the divergences, the emission distribution will be large and these will be the regions that dominate the emission pattern.

In Eq. (7), we also see the structure we were hoping for: the cross section for $q\bar{q}g$ is proportional to that for $q\bar{q}$ and therefore we may interpret the rest of the expression as the probability for gluon emission, differential in the kinematics of the gluon.

The integrand of Eq. (7) can diverge in three ways: $\theta \to 0$, corresponding to the gluon being collinear to the quark; $\theta \to \pi$, corresponding to the gluon being back-to-back with the quark, i.e. collinear with the antiquark; and $z \to 0$, the gluon energy going to zero for any value of the opening angle. Each of the first two divergences can be traced to a propagator in one of the two Feynman diagrams going on-shell. However, it should be emphasized that Eq. (7) contains the sum of the two diagrams and properly includes their interference. The third divergence comes from the propagators in both diagrams going on-shell simultaneously and much more clearly involves the interference of the two diagrams. We return to discuss the soft region in Section 4.3 and for now focus on the collinear regions.

We can separate the angular distribution into two components, each of which is divergent in only one of the two collinear regions,

$$\frac{2}{\sin^2\theta} = \frac{1}{1-\cos\theta} + \frac{1}{1+\cos\theta} \approx \frac{1}{1-\cos\theta} + \frac{1}{1-\cos\bar{\theta}}, \tag{8}$$

where $\bar{\theta}$ is the angle between g and $\bar{q}$ and the approximation is as good as

the one in Eq. (7). The distribution can therefore be written as the sum of two separate distributions, describing the emission of a gluon close to the directions of the quark or the antiquark. Since the distributions are summed, they are effectively independent. We emphasize again though, that they are derived from the proper sum of amplitudes for diagrams in which the gluon is attached to either emitter; it is just convenient to separate them into pieces that can be treated independently.

We can therefore write the emission distribution as

$$\mathrm{d}\sigma_{q\bar{q}g} \approx \sigma_{q\bar{q}} \sum_{\text{partons}} C_F \, \frac{\alpha_\mathrm{s}}{2\pi} \, \frac{\mathrm{d}\theta^2}{\theta^2} \, \mathrm{d}z \frac{1+(1-z)^2}{z}, \tag{9}$$

where now θ is the opening angle between the gluon and the parton that emitted it. This is starting to look like something that can be implemented and iterated in a Monte Carlo algorithm, with an independent emission distribution for each parton. Before generalizing it, we point out one mathematically-trivial property of this equation, which will turn out to be important for the physical properties of our parton shower algorithm. In writing down Eq. (9), we have focused on the small-θ region, which gives the collinear divergence. However, we would have obtained a mathematically-identical expression if we had chosen to parameterize the phase space in terms of any other variable proportional to θ^2, for example the virtuality of the off-shell quark propagator, $q^2 = z(1-z)\,\theta^2\,E^2$, where E is its energy, or the gluon's transverse momentum with respect to the parent quark's direction, $k_\perp^2 = z^2(1-z)^2\,\theta^2\,E^2$, since

$$\frac{\mathrm{d}\theta^2}{\theta^2} = \frac{\mathrm{d}q^2}{q^2} = \frac{\mathrm{d}k_\perp^2}{k_\perp^2}. \tag{10}$$

Any of these forms would give identical results in the collinear limit, but different extrapolations away from it, i.e. different finite terms accompanying the divergence.

While it is not obvious from our derivation, the structure of Eq. (9) is completely general. For any hard process that produces partons of any flavour i, the cross section for a hard configuration that has cross section σ_0 to be accompanied by a parton j with momentum fraction z is given by

$$\mathrm{d}\sigma \approx \sigma_0 \sum_{\text{partons},i} \frac{\alpha_\mathrm{s}}{2\pi} \, \frac{\mathrm{d}\theta^2}{\theta^2} \, \mathrm{d}z \, P_{ji}(z,\phi)\mathrm{d}\phi, \tag{11}$$

with $P_{ji}(z,\phi)$ a set of universal, but flavour-dependent (and, through ϕ, the azimuth of j around the axis defined by i, spin-dependent) functions. The spin-dependence can be found in, for example, Ref. [3] – we give the spin-averaged functions:

$$\begin{aligned} P_{qq}(z) &= C_F \tfrac{1+z^2}{1-z}, & P_{gq}(z) &= C_F \tfrac{1+(1-z)^2}{z}, \\ P_{gg}(z) &= C_A \tfrac{z^4+1+(1-z)^4}{z(1-z)}, & P_{qg}(z) &= T_R(z^2+(1-z)^2), \end{aligned} \tag{12}$$

where C_F was already defined above, $C_A = N_c$ is a colour factor that can be thought as the colour-charge squared of a gluon, and T_R is a colour factor that is fixed only by convention, $T_R = \frac{1}{2}$ (a different value of T_R would be compensated by a different definition of α_s). P_{qq}, P_{gq}, P_{gg} and P_{qg} correspond to the splittings $q \to qg$, $q \to gq$, $g \to gg$ and $g \to q\bar{q}$ respectively[6]. In the collinear limit, in which these results are valid, they are independent of the precise definition of z – it could be the energy fraction, light-cone momentum fraction, or anything similar, of parton j with respect to parton i. We now have the basic building block to write an iterative algorithm: since Eq. (11) is a completely general expression for any hard process to be accompanied by a collinear splitting, we can iterate it, using it on the hard process to generate one collinear splitting and then treating the final state of that splitting as a new hard process, generating an even more collinear splitting from it, and so on.

However, we are not quite ready to do so yet, because we have not yet learnt how to deal with the divergence. We have seen where it comes from and that it is universal, but not how to tame it to produce a well-defined probability distribution. This comes when we ask what we mean by a final-state parton. The point is that any physical measurement cannot distinguish an exactly collinear pair of partons from a single parton with the same total momentum and other quantum numbers. The infinitely high probability is associated with a transition that has no physical effect. As in our discussion of QED, to produce physically-meaningful distributions, we should introduce a resolution criterion, saying that we will only generate the distributions of resolvable partons. A particular convenient choice, although by no means the only one possible, is the transverse momentum: to say that two partons are resolvable if their relative transverse momentum is above

[6] A fifth splitting function $P_{\bar{q}g}$ corresponding to $g \to \bar{q}q$ is equal to P_{qg} by symmetry.

some cutoff Q_0. This cuts off both the soft and collinear divergences, and gives a total resolvable-emission probability that is finite. To calculate the non-resolvable-emission probability, one must integrate the emission distribution below the cutoff and add it to the loop-correction to the hard process. The result is finite, but there is an easier way to obtain it: unitarity tells us that the total probability of *something* happening, either emission or non-emission, is unity, and therefore, knowing the emission probability, we can calculate the non-emission probability as one minus it. (This unitarity argument is exact in the case of soft or collinear emission, but in general hard non-collinear loops contribute a finite correction, which can be absorbed into the normalization of the total cross section, restoring unitarity.) It is sometimes said that parton shower algorithms do not include loop corrections, but if this were so the non-emission probability would be ill-defined. It is better to say that they construct the loop corrections by unitarity arguments from the tree corrections.

We are almost ready to construct the probability distribution for one emission from a hard process, the basic building block that we will iterate to produce a parton shower. To do this, we have to realize that the distribution we have been calculating so far is the inclusive emission distribution of all gluon emissions: their total energy is the total energy carried away by all gluons emitted, given by the classical result. To calculate instead the distributions of exclusive multi-gluon events, it is convenient to separate out the distributions of individual gluons, for example by introducing an ordering variable. Let us take as an illustrative example, the virtuality of the internal line, q^2. The distribution we have been calculating is the total probability for all branchings of a parton of type i between q^2 and $q^2 + \mathrm{d}q^2$,

$$\mathrm{d}\mathcal{P}_i = \frac{\alpha_\mathrm{s}}{2\pi}\,\frac{\mathrm{d}q^2}{q^2}\int_{Q_0^2/q^2}^{1-Q_0^2/q^2}\mathrm{d}z\,P_{ji}(z), \tag{13}$$

where the limits on z come from the requirement that the partons be resolvable, and their precise form depends on the definition of the resolution criterion and of z. In order to construct the probability distribution of the first branching, i.e. the one that yields the largest contribution to the virtuality of the internal line, we need to calculate the probability that there are no branchings giving virtualities greater than a given q^2 value, given that it has a maximum possible virtuality of Q^2. We define this function to be

$\Delta_i(Q^2, q^2)$. It is given by a differential equation,

$$\frac{\mathrm{d}\Delta_i(Q^2, q^2)}{\mathrm{d}q^2} = \Delta_i(Q^2, q^2)\,\frac{\mathrm{d}\mathcal{P}_i}{\mathrm{d}q^2}, \tag{14}$$

corresponding to the fact that, when changing q^2 by a small amount, the probability Δ_i can only change by the branching probability $\mathrm{d}\mathcal{P}_i$ if there are no branchings above q^2, which has probability Δ_i. It is easy to check that this equation has the solution

$$\Delta_i(Q^2, q^2) = \exp\left\{-\int_{q^2}^{Q^2} \frac{\mathrm{d}k^2}{k^2}\,\frac{\alpha_\mathrm{s}}{2\pi}\int_{Q_0^2/k^2}^{1-Q_0^2/k^2} \mathrm{d}z\, P_{ji}(z)\right\}. \tag{15}$$

This formula has a close analogy with the well-known radioactivity decay formula: if the rate of decay of nuclei is λ per unit time, then the probability that a given nucleus has not decayed by time T is given by $\exp\left\{-\int_0^T \mathrm{d}t\,\lambda\right\}$. Or, in words, the probability of non-branching over some region is given by e to the minus the total inclusive branching probability over that region.

A particular case of this non-branching probability is $\Delta_i(Q^2, Q_0^2)$, the total probability to produce *no* resolvable branchings. This is the Sudakov form factor we encountered in our discussion of QED, given by

$$\begin{aligned}\Delta_i(Q^2, Q_0^2) &= \exp\left\{-\int_{Q_0^2}^{Q^2} \frac{\mathrm{d}k^2}{k^2}\,\frac{\alpha_\mathrm{s}}{2\pi}\int_{Q_0^2/k^2}^{1-Q_0^2/k^2} \mathrm{d}z\, P_{ji}(z)\right\} &(16)\\ &\sim \exp\left\{-C_F\,\frac{\alpha_\mathrm{s}}{2\pi}\log^2\frac{Q^2}{Q_0^2}\right\}, &(17)\end{aligned}$$

for a quark, a probability that falls faster than any inverse power of Q^2.

Finally, we have the building block we need to iteratively attach additional partons to a hard process one at a time. Since Δ_i describes the probability to have no branching above q^2, its derivative, the right-hand-side of Eq. (14), is the probability distribution for the first branching. Having produced such a branching, the same procedure has to be applied to each of the child partons, with their q^2 values required to be smaller than the one we generated for this splitting, to prevent double-counting. Evolution continues until no more resolvable branchings are produced above Q_0^2. The only missing ingredient now is the starting condition: the value of Q^2 for the parton line that initiated

the shower, which we return to in Section 4.5.

The Monte Carlo implementation of Eq. (14) is remarkably straightforward in principle: a random number ρ is chosen between 0 and 1 and the equation $\Delta_i(Q^2, q^2) = \rho$ is solved for q^2. If the solution is above Q_0^2, a resolvable branching is generated at scale q^2 and otherwise there is no resolvable branching and evolution terminates. For a resolvable branching a z value is chosen according to $P_{ji}(z)$. Such a shower algorithm implements numerically the all-order summation inherent in the exponentiation of Eq. (16). Since this correctly sums the terms with the greatest number of logs of Q_0^2 at each order of α_s it is called a leading collinear logarithmic parton shower algorithm.

However, there are considerable ambiguities in constructing such an algorithm. We already mentioned that an identical form would be given by any other choice of evolution scale proportional to θ^2, we simply chose q^2 as an illustrative example. We also defined z to be the energy fraction of the emitted parton, but in fact in the exactly collinear limit in which Eq. (11) is valid, choosing the longitudinal momentum fraction, the light-cone momentum fraction, or anything else similar, would give identical results, but different extrapolations away from that limit. Finally, since the hard process matrix element deals with on-shell partons, and the parton shower process has generated a virtuality for the parton line, energy-momentum must be shuffled between partons in some way to be conserved, but the collinear approximation does not specify how this should be done. All of these are formally allowable choices, with the same leading collinear logarithmic accuracy, but they differ in the amount of subleading terms they introduce. In the case of the evolution scale, we will see in Section 4.3 that a study of the soft limit of QCD matrix elements gives us an indication of the best choice.

Before turning to the soft limit, we discuss one important source of higher-order corrections, namely running coupling effects. A certain tower of higher-order diagrams, including those with loops inserted into an emitted gluon, can be summed to all orders and absorbed by the simple replacement of α_s by $\alpha_s(k_\perp)$, the running coupling evaluated at the scale of the transverse momentum of the emitted gluon [34]. This can be easily absorbed into the algorithm above, but has a couple of important consequences. Firstly, parton multiplication becomes much faster: as q^2 decreases, α_s becomes larger and it becomes easier to emit further gluons until at small enough scales the emission probability becomes of order 1 and phase space fills with soft gluons. Secondly, since one has to avoid the region for which α_s becomes of order 1,

Q_0 has to be considerably above $\Lambda_{\rm QCD}$, and actually becomes a physical parameter affecting observable distributions at the end of the parton shower, rather than a purely technical cutoff parameter that can be taken as small as one likes, as it is without running coupling effects. These facts mean that in the parlance used in analytical resummation, the parton shower is not a purely perturbative description but induces power corrections $\sim (Q_0/Q)^p$, contributing to the non-perturbative structure of the final state. Here $p \geq 1$ is a constant that may depend on the parton shower algorithm used and the observable calculated; usually $p = 1$.

The ingredients described in this section are sufficient to construct a final-state collinear parton shower algorithm. However, recall that in $e^+e^- \to q\bar{q}g$ (Eq. (7)) we found that the matrix elements were enhanced in both the collinear and soft limits. In order to give a complete description of all dominant regions of the emission distribution, we should consider soft emission in as much detail.

4.3. Soft gluon emission

In studying the matrix elements for e^+e^- annihilation to $q\bar{q}g$, we discovered that they were divergent as the gluon energy goes to zero, in any direction of emission, as well as in the collinear limit. One may also show that this soft divergence is a general feature of QCD amplitudes and also that it can be written in a universal factorized form. However, the big difference relative to the collinear case is that the factorization is valid at the amplitude level: the amplitude is given by the product of the amplitude to produce the system of hard partons, times a universal factor describing the emission of the additional gluon. The cross section is calculated by summing all Feynman diagrams and squaring and in practice many diagrams contribute at a similar level, so that interference terms between diagrams are unavoidable. This tells us that soft gluons should be considered to be emitted by the scattering process as a whole, rather than any given parton, and appears to spoil the picture of independent evolution of each parton.

Consider, as a concrete example, the configuration shown in Fig. 1. A quark has been produced in a hard process and has gone on to emit a reasonably hard, but reasonably collinear, gluon, and we wish to calculate the probability that this event is accompanied by a soft wide-angle gluon. The soft factorization theorem tells us that the amplitude for this process should be calculated as the sum of amplitudes for the gluon to be attached to each of the external partons, as indicated by the two placements of the gluon on the

Figure 1: Illustration of QCD coherence. The emission of a soft wide-angle gluon receives contributions from Feynman diagrams in which it is attached to any of the external partons (left). The coherent sum of these diagrams is equal to the emission from a single parton with the total momentum and colour of the partons. That is, as if it were emitted before the smaller-angle harder gluon (right).

left-hand-side of the figure. The two resulting amplitudes are of exactly the same order and have a non-trivial phase structure, so that interference between them seems absolutely crucial. It appears impossible to reconcile this with the picture of independent collinear evolution discussed in the previous section.

However, the coherence that we discussed in the context of QED bremsstrahlung comes into play here and shows us that we *can* formulate soft emission within a parton shower approach. Explicitly calculating the amplitudes described above, one can show that in the region shown in the figure, in which the softer gluon is at a larger angle than the harder one, the interference is largely destructive, reducing the emission distribution from the level it would be if the two partons emitted independently to a term proportional to C_F. Specifically, the result is identical to the one that would be obtained from a configuration in which the collinear quark/gluon pair is replaced by a single *on-shell* quark with the same total longitudinal momentum. That is, we can think of the wide-angle emission as being *as if* it occurred before the more collinear one, summarized pictorially in the right-hand side of Fig. 1. However, it should be emphasized that this picture is the summary of the proper interference between quantum mechanical amplitudes and does not represent a Feynman diagram in which the gluon is emitted by the internal line. This should remind us of the Chudakov effect in QED: there, wide angle emission from the e^+e^- pair was absent, because their total charge is zero. Here, since the gluon is itself coloured, the emission pattern is more complicated, but the result is the same: the soft wide angle gluon sees the *total* colour charge of the system of partons to which it is attached.

On the other hand, calculating the case in which the angle between the soft gluon and one of the other partons is much smaller than that between

them, one finds that the two contributions have very different sizes and the cross section can be described as the sum of independent emissions from the two partons. These considerations can easily be generalized to systems of more than two emitting partons. They can be summarized in a remarkably simple result: soft gluon effects can be correctly taken into account by a collinear parton shower algorithm, provided that, out of the choice of all possible evolution scales, one uses the opening angle. This is the central result that leads to angular-ordered, or coherence-improved, parton showers, such as is implemented in HERWIG. As a result, the first emission in the shower is often not the hardest and it often happens that several soft wide-angle gluons are emitted before the hardest gluon in the shower, a fact that will lead to some complications when we try to match with matrix element calculations in Section 5.

In Section 4.7, an alternative implementation of colour coherence is discussed, based on colour dipoles between pairs of emitters. It is explained there that, at the level of detail discussed here, the $k_\perp$-ordered dipole showers and angular-ordered parton showers are effectively equivalent.

4.4. Initial state evolution

So far we have discussed the evolution of the partons produced in a hard process. According to the analogy with QED, we equally expect partons to radiate on their way in to a scattering or annihilation process, giving rise to an initial-state parton shower. In principle, the generation of initial-state showers can be set up in an extremely similar way to the final-state showers already discussed, with an incoming parton evolving through a series of $1 \to 2$ splittings to a shower of partons, one of which is ultimately involved in the hard process, with the rest being emitted as accompanying radiation. An added complication in the initial-state case is that whole showers, and branches off the sides of showers, can develop that do not ultimately participate in any hard scatter. These should be collapsed back into the proton remnant in the same way that fluctuations that develop in a freely-moving proton that does not have any interaction collapse back into it.

In practice, simulating initial-state showers in this way is extremely inefficient, because the majority of partons have low energy and virtuality and if the showers were produced with the same frequency as in nature, it would be extremely rare to produce exactly the right kinematics to produce a hard process of interest, such as Higgs production. Moreover, as we shall discuss in Section 4.5, the properties of the parton showers, both initial- and final-state,

are correlated with the hard process, and it would be difficult to build this in to such an initial-state shower. Instead, event generators actually start by selecting the hard process and then using the parton shower evolution to dress it with additional radiation. That is, our basic building block is a *backwards* step: one generates the probability distribution for a parton with given momentum fraction and value of evolution scale to have come from one at a higher momentum fraction and lower scale. This is iterated until the evolution scale reaches the infrared cutoff, whereupon a non-perturbative model of the remnant left behind by the extraction of a parton from the incoming hadron is invoked.

The evolution of the PDFs with momentum scale is given by the DGLAP equations [35–37]. They can be viewed as describing the flow of information about the PDFs to a given point in the (x, Q^2) plane from a boundary condition, usually a fixed line at some input scale $Q^2 = Q_0^2$, requiring information about all higher values of x. As pointed out in [38] and further developed in [39], one can use the solution to the DGLAP equations to guide the backward evolution just described. That is, for a parton of a given flavour at a given x and q^2 value, we can calculate the conditional distribution that it came from a parton of the same or another flavour at a higher x and lower q^2 value. Moreover, at leading order, this distribution is positive definite and we can formulate it as a probabilistic Markov chain. The final result, which we do not derive here (see the original references, [38, 39]), is that the Sudakov form factor, $\Delta_i(Q^2, q^2)$ (Eq. (15)), which gives the probability that a final-state parton does not produce any radiation at scales between q^2 and Q^2, is replaced in the initial-state case[7] by a non-emission probability $\Delta_i(Q^2, q^2; x)$,

$$\Delta_i(Q^2, q^2; x) = \exp\left\{ -\int_{q^2}^{Q^2} \frac{\mathrm{d}k^2}{k^2} \frac{\alpha_\mathrm{s}}{2\pi} \int_{Q_0^2/k^2}^{1-Q_0^2/k^2} \mathrm{d}z\, P_{ij}(z)\, \frac{x/z\, f_j(x/z, k^2)}{x\, f_i(x, k^2)} \right\}. \tag{18}$$

The inclusive emission probability, which gets exponentiated to give the non-emission probability, contains an extra factor of the ratio of parton distribution functions at the 'new', higher, value of x that the parton may evolve back to and its 'current' value. Thus, if our parton is in a region in which

[7]Note the interchange of the ij indices on P_{ij} relative to the final-state case, which comes about because this is a backward evolution.

the PDF decreases rapidly with increasing x, its non-emission probability will be close to one, i.e. its emission probability will be small, and it is more likely that the parton came straight out of the hadron at the infrared cutoff scale, rather than having been produced by evolution of a higher-x parton. In the same way, if an emission is generated, its z value is not generated according to $P_{ij}(z)$, but rather includes an extra factor of $x/z\, f_j(x/z, k^2)$. In this way, one can show that the algorithm is guaranteed to follow the same evolution as the input parton distributions, provided the limit $Q_0 \to 0$ is taken. In reality, it is modified somewhat by infrared (i.e. finite Q_0) effects. In addition, the emitted partons go on to produce final-state parton showers of their own.

The arguments concerning the coherence of radiation from different emitters and the scale of the running coupling apply equally well to initial-state showers. Indeed, one can show that along the initial-state line, the opening angle of each emission relative to the fixed direction of the incoming hadron is the correct ordering variable [39] in a parton shower algorithm and that the showers produced by the emitted partons should have opening angles limited also by this angle. Again the appropriate scale for the running coupling is the transverse momentum of emitted gluons. Ref. [40] showed that, if these conditions are met, then the shower algorithm, even with LO splitting functions, is correct to NLO accuracy in the limited phase space region $x \to 1$.

In the discussion of final-state parton showers, we emphasized that they were derived from the full amplitudes of the theory, including interference between different amplitudes, and describing a particular gluon emission as being from a particular parton is a convenient language to use, but is not truly what happens at the fundamental level. Since we properly include colour coherence effects, we do account for interference between amplitudes. The same is true for the separation into final-state and initial-state emission: the separation is arbitrary and only the sum of the two is physically meaningful and reproduces the underlying quantum mechanical amplitude. In the dipole approach to parton showering, gluons are emitted by the colour dipole that stretches between a colour–anticolour pair. This picture works also for scattered partons, where an incoming colour line behaves effectively like an outgoing anticolour line and a scattered quark in DIS, for example, radiates coherently with a radiation pattern that peaks in the incoming and outgoing directions, without the need for an explicit separation into initial- and final-state, as we shall discuss a little more in Section 4.7.

Although not the main focus of this review, we note that for scattering processes involving partons with very small momentum fractions (i.e. at given hard process kinematics, for very high energy incoming hadrons) logarithms of the momentum fraction at each splitting can be large and a different resummation is needed (BFKL [41, 42] or CCFM [43]). Such a resummation can also be formulated in a probabilistic way, either as a dipole cascade (see Section 12) or as a parton shower, as in the SmallX [44] and Cascade [45] programs. While quantifying how small a momentum fraction is needed before including these effects becomes essential has proved elusive, it seems very likely that a variety of hard processes at the LHC with momentum fractions below $10^{-4 \text{ or } 5}$ will be significantly affected by them.

4.5. Connecting parton showers to the hard process

We have discussed the evolution of partons on their way in and out of a scattering process, but not the starting conditions for the showers, i.e. the maximum values of Q^2. Here again coherence plays a crucial role. In this section we discuss the simplest case of $2 \to 2$ scattering, but the general case is intimately linked with the question of matrix element matching, which we discuss in detail in Section 5.

A first consideration involves avoidance of double counting. A QCD $2 \to 2$ scattering accompanied by an emission from one of the external legs that is much harder than the hard scale gives the hard process a strong recoil that boosts one or both of its outgoing partons to a significantly higher transverse momentum. The outcome is a configuration that is indistinguishable from one that arises from a harder hard process accompanied by a softer emission from one its external legs. The fact that one configuration can arise in two ways is a double counting and should be resolved by only allowing one of them. Since the parton shower is built on the soft and collinear approximations, the distribution of soft emission in hard scatters is more accurate than that of hard emission in soft scatters and it is the former that should be used. This can be enforced by setting the upper limit of the parton shower evolution to the scale of the hard scattering. In the case of processes for which the lowest order is purely electroweak, for example gauge boson production, there is no analogous process with which hard emission would be double-counted, but nevertheless event generators typically also in this case limit emission to be below the hard scale, where the parton shower approximations are most reliable, and instead populate the region of phase space corresponding to harder emission using matrix element corrections, as discussed in Section 5.

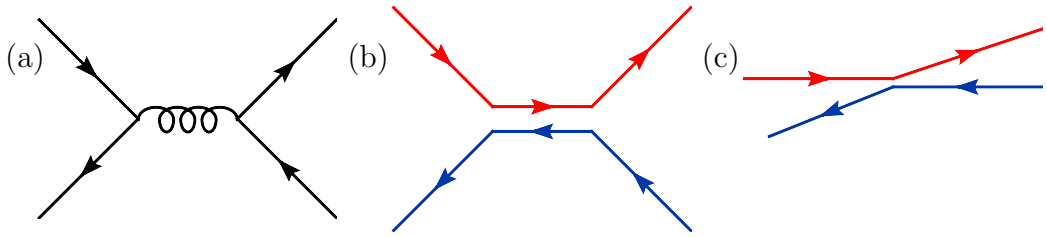

Figure 2: Illustration of colour coherence effect in hard scattering processes. In the quark–antiquark annihilation and production process (a), the quark's flavour is annihilated, but its colour flows onto the outgoing quark (b), such that in the centre-of-mass system, the colours are only scattered through small angles (c).

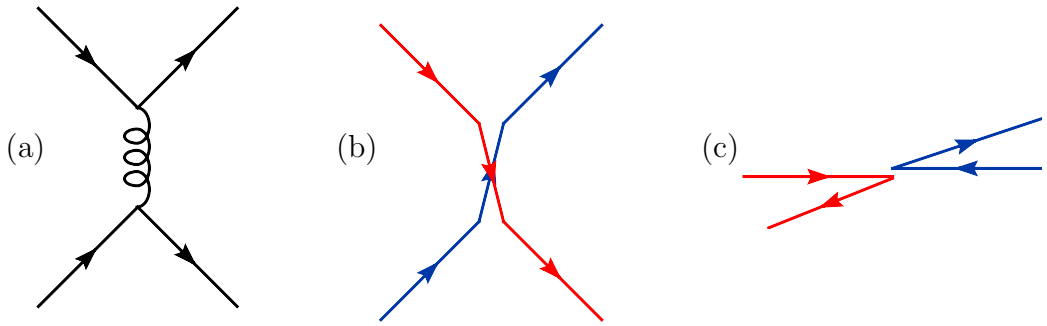

Figure 3: As Fig. 2 but for a quark scattering process.

The second consideration arises due to colour coherence. In the limit of a large number of colours, $N_c \to \infty$, the colour structure of a gluon can be considered to be a fundamental colour–anticolour pair, as discussed in Section 2.2. In a scattering process such as $q\bar{q} \to q'\bar{q}'$, illustrated in Fig. 2, although the flavour of the quark and antiquark is annihilated, their colour lines flow onto the s-channel gluon and hence onto the outgoing (anti)quarks, as illustrated in Fig. 2b. The outgoing quark–antiquark pair has a distribution over all polar angles, but the colour coherence effect is best illustrated by an event in which the outgoing quark's direction is only a small angle away from the incoming quark's (see Fig. 2c). Although the quark lines are annihilated and created, the colour lines are scattered through small angles. Detailed analysis supports the intuition that one might derive from analogy with the Chudakov effect in QED, that the radiation pattern from such an event is effectively that of two independent colour lines, each of which is scattered through only a small angle. Such a small-angle scattering does not radiate at large angles, only into a forward cone of opening angle given by

the scattering angle. This event would not, therefore, radiate significantly at central rapidities.

This radiation pattern should be contrasted with the one from a quark scattering event with identical kinematics (i.e. $qq' \to qq'$ at a small angle, Fig. 3). In this process the scattering takes place via a t-channel gluon so that the colour of the incoming q quark is carried through the gluon on to the outgoing q' quark and vice versa. Therefore, although the quarks have been scattered through a small angle, their colour charges have been scattered through a large angle, almost 180°, and they radiate throughout almost the entire event. This is actually the norm for small angle scattering, since it is dominated by t-channel gluon exchange, but in the general case it is essential that the colour connection of each parton is identified so that the coherence of the different emitters can be incorporated.

The algorithm to set the starting scale of the shower from each parton that implements this coherence can therefore be stated as follows: trace the colour line of the parton through the hard process to find the parton to which it is colour-connected, the "colour partner". Start the shower from each parton with a maximum allowed opening angle given by the angle to the colour partner.

A detailed analysis of three-jet events by the CDF collaboration [46], showed that this colour coherence effect is absolutely crucial to fit the data. They studied events with three jets, the hardest of which had transverse energy[8] $E_T > 110$ GeV and the softest had $E_T > 10$ GeV, so that the sample was dominated by configurations with a pair of roughly balancing high transverse energy jets and a relatively soft third jet. Distributions in the direction of this third jet were shown to be particularly sensitive to the colour coherence effects in the initial conditions of the shower. Despite the fact that this analysis was not corrected for detector effects, it is so important as a testing ground for event generators that it has been implemented into Rivet (see Section 17.2) with approximate detector corrections applied to the Monte Carlo events. As an example, we show in Fig. 4 the distribution of η_3, the pseudorapidity of the third hardest jet. Since colour coherence is so inherent to modern generators, to illustrate this effect we have had to return to Pythia 6 with its old virtuality-ordered parton shower (Pythia 6

[8]The transverse energy of a particle or jet is defined as $E_T = E \sin\theta$, where E is its energy and θ is the polar angle of its direction of motion with respect to the beam axis.

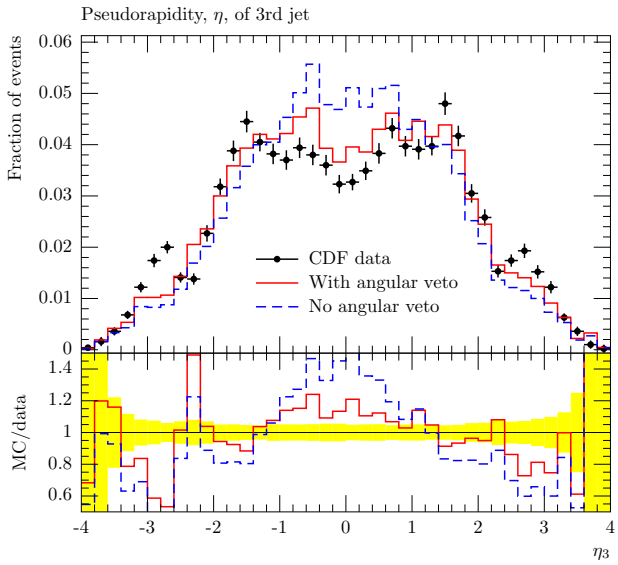

Figure 4: CDF's evidence for colour coherence in $p\bar{p}$ collisions at $\sqrt{s} = 1.8$ TeV. The pseudorapidity of the 3rd jet is plotted, uncorrected for detector effects, with the PYTHIA 6 Monte Carlo generator for comparison with angular vetoing turned on and off in the parton showers.

now preferentially uses a dipole shower ordered in transverse momentum and PYTHIA 8 only includes this version, see Section 14). Results are shown with angular ordering of the first initial-state emission switched off and on. We see that the dip in the data at central η_3 is not reproduced by the Monte Carlo simulation unless angular emission ordering is imposed to account for coherence effects. The comparison of these data with the latest versions of the main generators discussed in this review are shown in Section 18.

The general case of arbitrary $2 \to 2$ scattering is slightly more complicated, because a given hard process may have more than one colour flow. For example quark–gluon scattering $qg \to qg$, has three Feynman diagrams, with an s-channel or u-channel quark, or a t-channel gluon. One can show that there are two independent colour flows and, for example, the colour flow of the t-channel diagram can be written as the difference between the other two. The amplitude associated with each diagram is gauge-dependent, but the contribution of the sum of all diagrams to the amplitude for a given colour flow is gauge-invariant and is therefore physically meaningful. Finally, one finds that the interference between the amplitudes for different colour flows is

always suppressed by factors of the number of colours, N_c, and therefore that in the large-N_c limit (see Section 2.2), different colour flows can be considered as independent physical processes. One can therefore construct, for a given hard process configuration, probabilities for it to be in each of the colour flow states in the large-N_c limit. Having chosen a given colour flow, one can trace the colour lines through the hard process to find the colour partner of each parton. As shown in [47], this procedure results in an emission distribution that is correct up to terms that are suppressed not only by at least $1/N_c^2$, but are also dynamically suppressed, having no collinear enhancement.

In the large-N_c limit, a gluon has two colour connections and in the parton shower emits with colour factor C_A. In the dipole approach of Section 4.7, each line emits with a colour factor $C_A/2$, but typically in coherent parton showers a different approach has been used: One chooses one of the two colour partners with equal probabilities and generates a parton shower with colour factor C_A limited by the opening angle to the chosen partner. This procedure gives the correct inclusive distribution of emission, but as shown in [48] it produces too much event-to-event fluctuation, the wrong rate for any number of exclusive emissions and, in particular, a too high rate of non-emission. The correct procedure is the more dipole-like one in which each colour line emits with factor $C_A/2$ into a cone limited by its colour partner.

We make a final comment concerning the Lorentz invariance of the whole procedure. The coherence-improved parton shower described above was formulated in terms of an evolution in opening angle, which is manifestly not Lorentz invariant, but in practice it is usually implemented as an evolution in the energy of the emitter times the opening angle, $\tilde{q} \sim E\theta$. In the soft and collinear limits in which it is valid, this evolution *is* Lorentz invariant. However, its starting condition is not. In fact, one can show, [47], that the initial conditions of two colour-connected partons i and j are given by

$$\tilde{q}_{i,\max}\,\tilde{q}_{j,\max} = p_i \cdot p_j. \tag{19}$$

That is, depending on the choice of Lorentz frame in which the parton showering is performed, the maximum value of evolution variable for parton i, $\tilde{q}_{i,\max}$, and for parton j, $\tilde{q}_{j,\max}$, may take any values, but they must be related by Eq. (19). Although each shower is separately frame-dependent, provided colour-connected pairs of partons are developed in the same frame, the shower of the whole event is Lorentz-invariant. The same considerations apply also to the separation between initial- and final-state showers. One can think of

the corresponding boosts as being like a gauge transformation: changing the gauge moves radiation between different legs but the sum of emission from all legs is gauge invariant. This reflects the fact we have mentioned several times that we use the language of a classical branching process, because it is convenient, but it is derived from the underlying quantum structure of the gauge theory.

4.6. Quark mass effects

The parton showers we have described so far are for massless partons. In this section we shall consider how they are modified by parton mass effects. Although we discuss the explicit case of quarks, our comments are equally applicable to any massive coloured particle, for example squarks and gluinos in supersymmetry. We shall mainly consider the case of scattering or production processes with momentum transfers significantly larger than the quark mass since, as we shall see, radiation is suppressed in the threshold region, where the invariant mass of the coherent system of which the quark is a part is not much larger than its mass. We therefore work in a Lorentz frame in which the quark's energy is large relative to its mass, i.e. its velocity is close to c. We defer a more technical discussion of precisely how the quark mass is defined, which is ambiguous beyond the leading order of perturbation theory, until Appendix C.

In the soft limit, the universality of the amplitude to emit a gluon is unaffected by the parton mass. One can therefore derive a general formula for the angular distribution of soft gluons emitted by a dipole consisting of one or two massive (anti)quarks. It has the property that at large angles it is identical to the distribution produced by a massless quark of the same total momentum. This again accords with our picture of colour coherence – a soft wide angle gluon is not able to resolve the details of the colour line that emits it, all it sees is a colour charge moving in a given direction. The details of whether that colour charge is carried by one parton or a bundle of collinear partons and whether those partons are massless or massive do not affect it. On the other hand, the distribution is modified at small angles. Defining the ratio $m/E \equiv \theta_0$, which we assume to be small, we end up with a distribution that is identical to that from a massless quark, but with the replacement

$$\frac{\mathrm{d}\theta^2}{\theta^2} \to \frac{\theta^2\,\mathrm{d}\theta^2}{(\theta^2+\theta_0^2)^2}. \tag{20}$$

We see that emission at large angles, $\theta \gg \theta_0$ is indeed unaffected, but that it is suppressed at small angles, falling to zero in the exactly forward direction. In older parton shower algorithms, such as HERWIG [49], this was used as the basis for the 'dead cone approximation', in which the showering of massive partons was performed in an identical way to massless ones, but with a cutoff on opening angle at θ_0. With an appropriate choice of frame in which this evolution is performed, it can be shown to produce approximately the right amount of radiation, but it is clearly too brutal an approximation, producing too much radiation at angles a little above θ_0 and none at all below it.

While Eq. (20) is derived in the high energy limit, $\theta_0 \ll 1$, it shows that near threshold, where $\theta_0 \sim 1$, emission is suppressed at all angles. Indeed, the more general expression from which it is derived shows that at large angles, the emission probability is proportional to the velocity-squared of the emitting partons and hence that it goes to zero at threshold.

Ref. [50] considered the matrix elements for gluon emission in the decay of heavy objects to lighter partons with various colour, spin and parity quantum number assignments. It was found that the radiation pattern for finite gluon energy, while always suppressed in the forward direction, is significantly dependent on all of these parameters and in most cases not going exactly to zero even in the collinear limit. These are implemented in PYTHIA as process-dependent mass corrections.

The authors of Ref. [20] derived a generalization of the DGLAP splitting function to the massive case, which they called the quasi-collinear limit. This is defined as the limit of $p_t^2 \sim m^2 \ll Q^2$, where Q^2 is the hard scale. They found

$$P_{QQ}(z) \;=\; C_F \left[\tfrac{1+z^2}{1-z} - \tfrac{m^2}{p_Q \cdot p_g}\right], \qquad P_{gQ}(z) \;=\; T_R \left[z^2 + (1-z)^2 + \tfrac{2m^2}{(p_Q + p_{\bar{Q}})^2}\right]. \tag{21}$$

These are such that the subsequent limit $m \to 0$ at fixed $p_\perp$ smoothly recovers the massless behaviour. The limit $p_\perp \to 0$ at fixed m corresponds to the soft limit, if at fixed opening angle, and reproduces Eq. (20) or the collinear limit, if at fixed energy, and recovers the result of Ref. [50] for the generalization of the dead-cone suppression to finite energy. The quasi-collinear splitting functions are used in Herwig++ and SHERPA, while the matrix-element correction method of [50] is used in PYTHIA 8.

4.7. The dipole approach to parton showering

In discussing the parton shower approach to simulating radiation from the partons involved in a scattering process, we mentioned several times the alternative formulation in terms of emission from sets of colour dipoles. This approach was first used in the ARIADNE program [51], described in more detail in Section 12, and in fact is used by the majority of recent new implementations, including PYTHIA 8 [52], see Section 14, and SHERPA, with a choice of two different dipole shower implementations, [53, 54], see Section 15, as well as several standalone dipole cascade programs [55–57]. For most purposes it can be considered equivalent to the coherence-improved parton showers discussed already, but it does have some advantages, which we briefly describe in this section.

The basic observation is that, as discussed in Section 4.5 and in more detail in Section 8.3, in the large-N_c limit the colour structure of an arbitrarily-complicated system of partons can be decomposed as a colour flow, i.e. a set of colour lines each starting on an incoming quark, outgoing antiquark or gluon, connecting it with an outgoing quark, incoming antiquark or other gluon, and that in the soft-gluon and large-N_c limits, each of these lines emits independently. Whether the configuration was produced by a matrix-element calculation or by the parton shower itself, one can calculate, again in the large-N_c limit, the probabilities of different colour flows and hence choose in a given event a particular colour flow. One can quantify the validity of the dipole approximation as being the limit in which the transverse momentum of the emitted gluon, relative to the axes defined by the colour line from which it is emitted, is much smaller than any scales involved in the production of that colour line. It is therefore natural to use transverse momentum as the ordering variable for dipole showers.

The procedure is then to start from the hard process, decompose its colour structure as described in Section 4.5 and choose one colour flow. This gives a unique initial condition for the subsequent dipole evolution. Each colour line connecting a pair of partons effectively forms a colour–anticolour dipole and the emission from each dipole is generated independently. Although in the soft limit each dipole emits independently with a classical radiation pattern, emission with a finite transverse momentum results in a recoil. Since a gluon carries the colour lines of two dipoles, any recoil it experiences may affect the subsequent evolution of the neighbouring dipoles. Therefore the event is evolved globally, with the highest transverse momentum emission from any dipole being generated first, complete with its recoil, and its transverse mo-

mentum giving the upper limit for the subsequent evolution of the ensemble of dipoles. Although this shower is formulated in the soft limit, it was shown by [51] that collinear effects can be incorporated in the large-N_c limit by a simple modification to the rapidity distribution of the emitted gluon (which is flat in the soft limit). Recent implementations have gone further by using the dipole splitting functions and kinematics defined in the dipole subtraction method [19] to partition each dipole into 'monopole' pieces related to each of the two emitters of the dipole (with the other taking the role of spectator) each with its own colour factor, so that the collinear limit is exact in N_c and, like the coherence-improved parton shower, neglected terms are both N_c^2 and dynamically suppressed.

Some doubt was cast on the validity of the dipole shower method in Ref. [58], but it may be that the problem found there is an artefact of the toy model used [59, 60] and is not shared by full implementations. To our understanding, transverse-momentum-ordered dipole showers with collinear improvement are accurate to leading-collinear-logarithmic order and hence are formally as accurate as angular-ordered parton showers.

In fact, despite this formal equivalence, the dipole shower has some practical advantages. Firstly, the fact that it is transverse momentum ordered means that the hardest emission is generated first, making matrix element corrections significantly more straightforward to implement and obviating the need for truncated showers (see Section 5) from the internal lines. Secondly, the fact that emission is a $2 \to 3$ process, rather than $1 \to 2$, means that energy-momentum can be explicitly conserved, with all external partons on mass shell, at each step of the shower. In the parton shower approach, the initially on-shell parton develops some virtuality and momentum conservation must be violated at intermediate steps of generation. Only once all partons have developed their showers is a small amount of momentum shuffled between partons to restore its conservation. Finally, the problem mentioned in Section 4.5, of how to generate emission from the two colour lines of a gluon is obviated, since they simply radiate independently in the dipole approach. The kinematic variables used in dipole showers are Lorentz invariant and they naturally combine the radiation from colour-connected parton pairs, hence the issues discussed at the end of Section 4.5 are automatically satisfied by dipole showers.

We finally mention the extension of the dipole method to initial-state radiation. In the original implementation in ARIADNE [61], Section 12, there was no explicit initial-state radiation. The outgoing hadron remnant acted

as an emitter at one end of a dipole like any other parton except that, being an extended object, radiation in its collinear direction was suppressed. More recent dipole showers have formulated the evolution of dipoles containing an initial-state emitter in a more backward-evolution-like way, guided by the PDF set.

4.8. Summary

- Scattered, annihilated and created partons radiate gluons.
- Since gluons themselves are coloured, this radiation gives rise to further gluon radiation and parton multiplication.
- These showers can be simulated as an evolution in some appropriately chosen scale down from the scale of the hard process towards an infrared scale at which non-perturbative confinement effects set in.
- This evolution effectively sums to all orders terms enhanced by logarithms of the hard and soft scales, and can be formulated as coherence-improved parton showers or transverse-momentum-ordered dipole showers.
- Modern algorithms are extremely sophisticated implementations of all-order perturbative QCD. Although they use the probabilistic language of time-ordered sequential emission, they are derived from the full quantum structure of the underlying gauge theory, QCD.

Nevertheless, parton shower algorithms are certainly not the whole story in describing the exclusive structure of an event. Firstly, they are built on soft and collinear approximations to the full cross sections, while many of the observables we are interested in are explicitly sensitive to hard wide-angle emission and multi-jet final states, which can only be described accurately with the help of higher-order matrix elements, as discussed in Section 5. And secondly, they cannot be extended arbitrarily far into the infrared region where QCD becomes strongly-interacting and must be cut off at some scale beyond which non-perturbative models for hadronization and the distributions of partons in incoming hadrons (i.e. PDFs and primordial $k_\perp$) must be invoked, as described in Sections 7 and 8.

5. ME and NLO matching and merging

5.1. Introduction

In the previous sections we have described how to simulate partonic final states with matrix elements and with parton showers, and it should be clear to the reader that these approaches have different merits and shortcomings. While fixed-order matrix elements are excellent when simulating well separated, hard partons, they have problems when trying to describe collinear and soft partons, due to the occurrence of large logarithms. Also, obtaining the correct matrix element becomes very cumbersome when we have more than a handful of partons. With parton showers it is the other way around; hard, wide-angle emissions are poorly approximated, while soft and collinear parton emissions are well described even for very many partons. Clearly it would be desirable to combine the matrix element and parton shower approaches to get a good description of any partonic state. In particular, we note that a good description of soft and collinear multi-parton states is necessary for hadronization models such as string and cluster fragmentation (see Section 8) to work properly.

To combine fixed-order matrix elements with parton showers is, however, not a trivial task. The naïve procedure of simply adding a parton shower to an event generated with a matrix element generator does not work. One problem is related to the fact that tree-level matrix elements are *inclusive*, in that they give the probability of having *at least* n partons in a state calculated exactly to lowest order in α_{s}, while the corresponding state generated by a parton shower is *exclusive*, given by the probability that there are *exactly* n partons calculated approximately to all orders in α_{s}. Another problem is that care must be taken not to double count some regions of phase space or, conversely, to undercount other regions.

This problem can be understood on a more pictorial level in Fig. 5. There we have, for the process $e^+e^- \to$ jets, depicted the orders in the coupling constant α_{s} on the horizontal axis vs. the number of potentially occurring large logarithms of the type $L^m = \log(Q_{\mathrm{cm}}/Q_{\mathrm{jet}})^m$ on the vertical axis. Here, Q_{cm} is an energy scale of the order of the invariant mass of the produced system and Q_{jet} is related to the resolution scale of a given jet algorithm (see Section 2). The Born process is of order α_{s}^0 and typically associated with the production of two jets, the quark and antiquark in $e^+e^- \to q\bar{q}$. Clearly, for each additional emission, another factor of α_{s} is necessary, such that four jet production is of order α_{s}^2 and so on. Also, each emission can be related to at

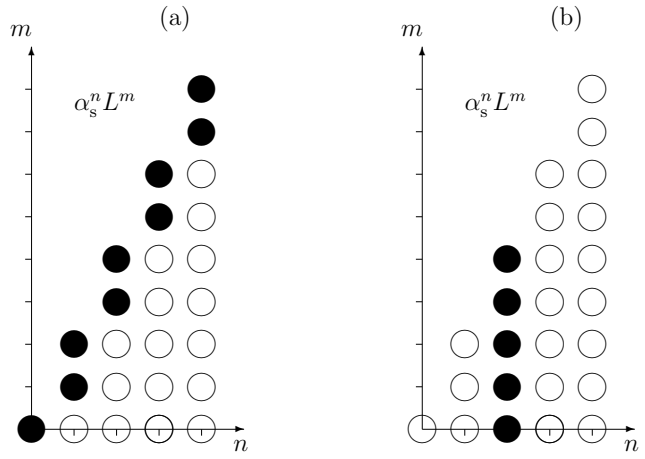

Figure 5: Pictorial view of the terms in the α_s-expansion that enter into a jet cross section in $e^+e^- \to$ jets. For each order in α_s, there are a number of large logarithms of the form $L^m = \log(Q_{\rm cm}/Q_{\rm jet})^m$ (vertical axis). For α_s^n the largest such logarithmic term is proportional to L^{2n}. For e.g. a 4-jet observable we want to correctly include all coefficients from α_s^2 and onwards. In (a) we see the terms that would be correctly included in a NLL parton shower (filled blobs), while in (b) we see the terms correctly included in a tree-level matrix element.

most two large logarithms, associated with the soft and collinear divergences, see the previous section on parton showers.

Now, the parton shower takes into account the exact leading and maybe even next-to-leading logarithms, i.e. it correctly takes into account all real emissions and virtual corrections at all orders of the type $\alpha_s^n L^{2n}$ and $\alpha_s^n L^{2n-1}$, while lower powers of L are treated approximately or completely omitted. The leading $\alpha_s^n L^{2n}$ term is easily obtained by an α_s-expansion of the Sudakov form factor in Eq. (15), while the next-to-leading term is obtained from the hard collinear emission and from coherent treatment of soft emissions in Section 4.3. The treatment of these logarithms will not impact on the total hadronic cross section, which is still given by the Born-level value, due to the probabilistic structure of the parton shower as discussed in Section 4.

On the other hand, differential distributions and observables sensitive to the pattern of additional QCD radiation will be defined by these logarithms. Stated in other words: the parton shower will not change the norm, but it will describe the shape of radiation-sensitive distributions.

Taken together, coherent parton showers will correctly include all filled blobs in Fig. 5a (equivalent to the terms $\alpha_s^n L^{2n}$ and $\alpha_s^n L^{2n-1}$). The natural

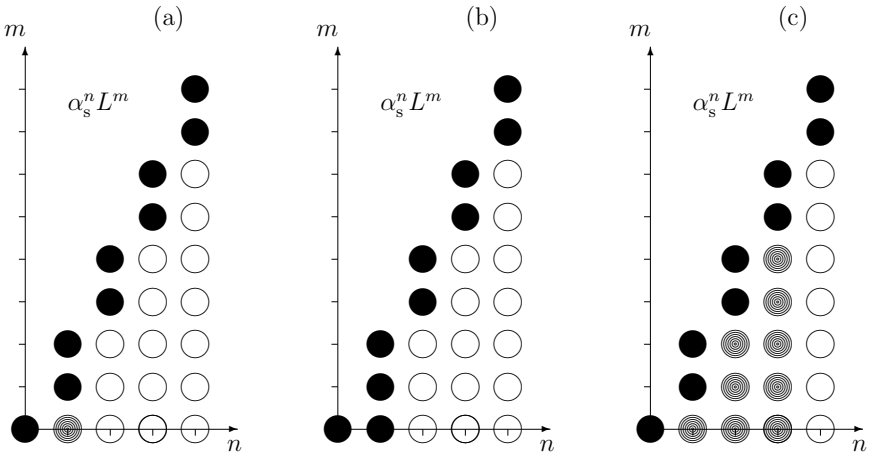

Figure 6: Pictorial view analogous to Fig. 5. (a) The terms included in tree-level matching of the first emission. Note that the $\alpha_s^1 L^0$ blob is only half filled, as it is correctly taken into account only in the real-emission contributions, not in the virtual ones, which means that the shapes of distributions will be correct but not their normalization. (b) The terms included in NLO matching of the first emission. (c) The terms included in tree-level CKKW-like merging up to 5-jet, where the half-filled blobs are only correctly taken into account for real-emission contributions above the merging scale.

question thus arises of how to include more terms into the picture in an exact way. To this end, a number of different procedures have been devised in the past two decades, and will be discussed is some detail in subsequent subsections:

- Tree-level matching:
  The first procedure for matching matrix elements with parton showers was invented decades ago by Bengtsson and Sjöstrand[62]. Similar techniques were later used also in [51, 63–66] and concentrated on correcting the first or hardest parton shower emission (Section 5.2.2). In our pictorial language, this amounts to including one extra blob as in Fig. 6a, of order $\alpha_s^1 L^0$, but *only on the shape*, while the norm for the inclusive process (its cross section) was still given at the LO Born-level.

- NLO matching:
  In order to include also the NLO correction to the total cross section of the inclusive sample, one could naively apply a constant K-factor, as discussed in Section 3.5. This, however, will not necessarily

be good enough for precision studies, since these higher-order corrections may also influence the kinematics of the Born-level configuration. Therefore, in the past decade much effort has been put into correcting parton showers also with exact next-to-leading-order (NLO) matrix elements, allowing to take into account the full effect of the $\alpha_s^1 L^0$-term (see Fig. 6b). Here the MC@NLO [67, 68] (Section 5.2.4) and POWHEG [69] (Section 5.2.3) procedures have been very successful for the correction of the first parton shower emission and for including the effect on the cross section. These ideas have been implemented in various programs, and we refer to the later parts of this section and to the descriptions of the individual event generators in Part II for the corresponding references.

- Multi-jet merging at LO:
  Another active area of developments in the last decade has been the treatment of multi-jet topologies, starting with the merging algorithm by Catani, Kuhn, Krauss and Webber (CKKW) [70] and a similar procedure developed in parallel by Lönnblad (later coined CKKW-L) [71]. In these procedures also the second and higher emissions in the parton shower were corrected to the corresponding tree-level matrix element, but at the price of introducing a technical merging scale above which the corrections are made (Section 5.3). So, the aim of these procedures is to simulate each jet multiplicity (with jets above the cut) with the corresponding tree-level matrix element, dressed with the parton shower. Pictorially it corresponds to taking into account all $\alpha_s^n L^{2n}$ and $\alpha_s^n L^{2n-1}$ blobs as in a normal PS, but also the impact *on the shape* of all the other blobs up to α_s^n for the n first real emissions above the cut, as indicated in Fig. 6c.

  The CKKW and CKKW-L approaches can be shown to maintain the logarithmic accuracy of the parton shower, at least in e^+e^- annihilations, without any double-counting of contributions. In addition, more pragmatic versions of the CKKW(-L) merging have been introduced, with less focus on the formal accuracy; the MLM approach by Mangano [72] (see also [73]) and the Pseudo-Shower algorithm by Mrenna and Richardson[74]. By now, the field has matured quite a lot, and in some recent publications the emphasis shifted to a more careful discussion of formal accuracy and its preservation, as in [75, 76].

- Multi-jet merging at NLO:
  For higher parton multiplicities, there have also been some suggestions for NLO corrections (Section 5.4). The MENLOPS procedure [77] simply combines POWHEG with CKKW so that the Born-level differential cross section becomes correct to NLO. The NL^3 procedure [78] and the procedure being implemented in the VINCIA program[55, 79] go further and try to also correct the higher jet cross sections to NLO, but so far no easily accessible implementation exists.

Clearly there are several different strategies for combining matrix elements and parton showers. As indicated above, it is useful to distinguish two groups of approaches. With *matching* we refer to those approaches in which high-order corrections to an inclusive process are integrated with the parton shower. The other strategy involves a *merging* scale, usually defined in terms of a jet resolution scale, where any parton produced above that scale is generated with a corresponding higher-order matrix element and, conversely, any parton produced below is generated by the shower.

5.2. Correcting the first emission

We start out by looking at the first emission in the parton shower. In a transverse-momentum-ordered parton shower, this is the hardest emission and will determine the main structure of the final state. Hence, it is important to get this right also far away from the soft and collinear regions where the parton shower is a good approximation.

5.2.1. The NLO cross section

To guide us we refer to the typical inclusive NLO cross section for a process with a given Born-level state, and we rewrite the schematic formula in Eq. (6) from Section 3.5 in a more explicit form,

$$\begin{aligned} \mathrm{d}\sigma^{\mathrm{NLO}} &= \mathrm{d}\Phi_0 \left[B(\Phi_0) + \alpha_\mathrm{s} V_1(\Phi_0) + \alpha_\mathrm{s} \int \mathrm{d}\Phi_{1|0} S_1(\Phi_1) \right] \\ &+ \mathrm{d}\Phi_1 \left[\alpha_\mathrm{s} R_1(\Phi_1) - \alpha_\mathrm{s} S_1(\Phi_1) \right] . \end{aligned} \tag{22}$$

Here we identify[9] the Born-level and the real-emission phase space Φ_0 and Φ_1, together with the corresponding tree-level matrix elements $B(\Phi_0)$ and $\alpha_s R_1(\Phi_1)$. We also have the virtual or loop contribution $\alpha_s V_1(\Phi_0)$ and the subtraction term $\alpha_s S_1(\Phi_1)$ which, when integrated over the one-particle phase-space element, $\Phi_{1|0}$, renders the first bracket finite, and also regularizes the real-emission term, making everything finite.

Typically, using the universality of soft and collinear divergencies, we can write the subtraction term in a factorized form as

$$S_1(\Phi_1) = B(\Phi_0) \otimes \tilde{S}(\Phi_{1|0}), \tag{23}$$

where $\tilde{S}(\Phi_{1|0})$ are the universal subtraction kernels with analytically known integrals. At this point it is useful to split the real-emission correction into one part containing all singularities, $R_1^{\rm s}$, and one non-singular part, $R_1^{\rm ns}$:

$$R_1(\Phi_1) = R_1^{\rm s}(\Phi_1) + R_1^{\rm ns}(\Phi_1)\,. \tag{24}$$

The splitting is quite arbitrary, as long as $R_1^{\rm s}$ contains all singularities, but will later be used for illustrating differences in some of the matching algorithms.

We can now write the inclusive NLO cross section

$$\begin{aligned} {\rm d}\sigma^{\rm NLO} &= {\rm d}\Phi_0 \left[B(\Phi_0) + \alpha_s V_1(\Phi_0) + \alpha_s \int {\rm d}\Phi_{1|0} S_1(\Phi_1) \right] \\ &+ {\rm d}\Phi_1 \alpha_s \left[R_1^{\rm s}(\Phi_1) - S_1(\Phi_1) \right] + {\rm d}\Phi_1 \alpha_s R_1^{\rm ns}(\Phi_1)\,, \end{aligned} \tag{25}$$

where, again, all individual terms in the sum are finite. We can now absorb the second bracket into the first and we can define the *NLO-weighted Born contribution*, $\bar{B}$, by integrating out the singular terms,

$$\begin{aligned} \bar{B}(\Phi_0) &= B(\Phi_0) + \alpha_s V_1(\Phi_0) + \alpha_s \int {\rm d}\Phi_{1|0} S_1(\Phi_1) \\ &+ \alpha_s \int {\rm d}\Phi_{1|0} \left[R_1^{\rm s}(\Phi_1) - S_1(\Phi_1) \right]. \end{aligned} \tag{26}$$

[9]Note that implicitly these terms also contain symmetry factors and parton luminosities.

Here we stress again that the S_1 can be written as a convolution of a Born term and a universal subtraction term, and in

$$\int \mathrm{d}\Phi_{1|0} S_1(\Phi_1) = B(\Phi_0) \otimes \int \mathrm{d}\Phi_{1|0} \tilde{S}(\Phi_{1|0}), \tag{27}$$

the integral over $\tilde{S}$ can be calculated analytically using dimensional regularization, allowing us to add it to the virtual part and thus explicitly cancel the divergences there. The integral over $R_1^{\mathrm{s}} - S_1$, in contrast, must typically be evaluated numerically through Monte Carlo integration.

We now arrive at a form of the inclusive NLO cross section,

$$\mathrm{d}\sigma^{\mathrm{NLO}} = \mathrm{d}\Phi_0 \bar{B}(\Phi_0) + \mathrm{d}\Phi_1 \alpha_{\mathrm{s}} R_1^{\mathrm{ns}}(\Phi_1), \tag{28}$$

which will serve as a starting point for our discussion about higher-order corrections to the parton shower approach.

5.2.2. The first emission in a parton shower

We now look at the inclusive cross section as given by the first emission in a parton shower:

$$\mathrm{d}\sigma^{\mathrm{PS}} = \mathrm{d}\Phi_0 B(\Phi_0) \left[\Delta(Q^2, Q_0^2) + \int_{Q_0^2} \frac{\mathrm{d}q_1^2}{q_1^2} \int \mathrm{d}z_1 \, \frac{\alpha_{\mathrm{s}}}{2\pi} P(z_1) \Delta(Q^2, q_1^2) \right], \tag{29}$$

where we have denoted the ordering variable q^2 (with Q^2 giving the starting scale, and Q_0^2 the cutoff scale for the shower). We note again that, performing the integral, the bracket is unity, reflecting the unitary nature of the parton shower.

In principle higher-order corrections will have two effects in a parton shower. They alter

1. the shape of distributions related to the first, hardest emission;
2. the norm — the total cross section — of the produced sample;

and there are methods that focus on one or the other, or both.

The first modification, which was also historically the first matching procedure [62], is simply to replace the splitting function above with the singular

part of the real emission matrix element,

$$\frac{\mathrm{d}q_1^2}{q_1^2}\mathrm{d}z_1\frac{\alpha_\mathrm{s}}{2\pi}P(z_1) \to \mathrm{d}\Phi_{1|0}\frac{R_1^\mathrm{s}(\Phi_1)}{B(\Phi_0)} \tag{30}$$

Two things are worth noting here:

- In the soft and collinear limits of the real-emission matrix elements, the effect of the extra emission factorizes into universal terms, which exhibit *exactly the same singularity structure as the splitting kernels employed in parton shower Monte Carlos*. These singularities, through the cut in the emission phase space, given by Q_0^2, lead to large logarithms, which in turn are resummed by the parton shower. The same large logarithms are, of course, then also encoded in R_1^s/B, and thus the logarithmic structure of the parton shower is preserved.

- In this transition, the one-particle phase space element of the parton shower is replaced by $\mathrm{d}\Phi_{1|0}$, the phase space element that, starting from a Born configuration, produces a real-emission phase space configuration. Clearly, if the one-particle emission phase space is not completely covered by the parton shower, the replacement above on its own will not be sufficient, since parts of the true available phase space will be left out. In this case, a hard matrix element correction, essentially through the non-singular term R_1^ns, is mandatory. This effect of not covering the full phase space may happen for two reasons:

  1. the parton shower does not completely cover the emission phase space. This is true, e.g. , for angular-ordered parton showers;
  2. the Born configuration exhibits zeros, due to polarization effects or similar, that are not present after the first emission. This happens, e.g. , for the zero in the lepton pseudo-rapidity distribution from hadronic W-boson production, as discussed in [80].

Note that the replacement above can fairly easily be carried over to the Sudakov form factor

$$\bar{\Delta}(Q^2, q^2) = \exp\left[-\int \mathrm{d}\Phi_{1|0(>q^2)}\alpha_\mathrm{s}\frac{R_1^\mathrm{s}(\Phi_1)}{B(\Phi_0)}\right], \tag{31}$$

using the so-called veto algorithm (see Appendix A.3).

We now get the inclusive cross section

$$\begin{aligned} \mathrm{d}\sigma^{\mathrm{PScorr}} &= \mathrm{d}\Phi_0 B(\Phi_0)\left[\bar{\Delta}(Q^2,Q_0^2)+\int \mathrm{d}\Phi_{1|0(>Q_0^2)}\alpha_{\mathrm{s}}\frac{R_1^{\mathrm{s}}(\Phi_1)}{B(\Phi_0)}\bar{\Delta}(Q^2,q_1^2)\right] \\ &+ \mathrm{d}\Phi_1\alpha_{\mathrm{s}}R_1^{\mathrm{ns}}(\Phi_1)\,, \end{aligned} \tag{32}$$

and by undoing the integral over the real emission we get the first emission of the parton cascade, properly weighted by the Sudakov form factor to give the higher-order $\alpha_{\mathrm{s}}^n L^{2n}$ and $\alpha_{\mathrm{s}}^n L^{2n-1}$ blobs in Fig. 5a, from which we can now continue with the subsequent emissions in the parton shower to get fully exclusive partonic final states.

The next logical step is to also achieve $\mathcal{O}(\alpha_{\mathrm{s}})$ accuracy at the cross section level. There are two ways to do this, which go under the names of POWHEG and MC@NLO, respectively.

5.2.3. POWHEG

The POWHEG approach, effectively, is an advanced matrix element reweighting procedure, where the Born-level term in front of the first square bracket in Eq. (32) is replaced by the NLO weighted Born-level term. Furthermore, the whole first-order real-emission term R_1 is used for R_1^{s}, so that $R_1^{\mathrm{ns}} = 0$. Thus

$$\mathrm{d}\sigma^{\mathrm{POWHEG}} = \mathrm{d}\Phi_0 \bar{B}(\Phi_0)\left[\bar{\Delta}(Q^2,Q_0^2)+\int \mathrm{d}\Phi_{1|0(>Q_0^2)}\alpha_{\mathrm{s}}\frac{R_1(\Phi_1)}{B(\Phi_0)}\bar{\Delta}(Q^2,q_1^2)\right], \tag{33}$$

and parton showering will give rise to similar emissions as the first term in Eq. (32) but with a global NLO-reweighting, $\bar{B}/B$, acting as a local K-factor.

Truncated and vetoed parton showers. Here we digress a bit to consider the problems arising if a parton shower is not ordered in hardness or $k_\perp$. In the POWHEG approach, the first emission is supposed to be the hardest one, and if the parton shower is not ordered in hardness one cannot simply add it to the states generated by POWHEG, as that would not ensure that the subsequent emissions would be less hard than the first one.

The simplest solution is to start the shower at its maximum possible ordering scale, but veto any emission that is harder than the first POWHEG one. However, as pointed out in [69], this means that the colour structure and kinematics of the parton shower would be altered, as the emission with

the highest ordering scale would be emitted from the +1-parton state rather than from the Born state, as it would have been in the normal shower.

The solution is to first reconstruct the parton shower variables (q_1^2, z_1) for the emission given by POWHEG. Then the shower is started from the corresponding Born-state with the maximum ordering variable Q^2 and is allowed to evolve down to q_1^2, vetoing any emission harder than the first emission. Then the (q_1^2, z_1) emission is inserted, and the shower can continue evolving, still vetoing any emission harder than the first emission. This procedure is called a truncated, vetoed shower[69].

5.2.4. MC@NLO

Having at hand the formula for the cross section in the POWHEG formalism allows us to discuss the alternative MC@NLO approach on the same footing. The main idea in MC@NLO is that the singular terms R_1^{s} are taken to be *identical* to the subtraction terms S_1. They in turn are given by the convolution $S_1 = B \otimes P$, i.e. by additionally identifying the universal subtraction terms with the parton shower splitting kernels. Therefore

$$\begin{aligned} \mathrm{d}\sigma^{\mathrm{MC@NLO}} &= \mathrm{d}\Phi_0 \left[B(\Phi_0) + \alpha_{\mathrm{s}} V_1(\Phi_0) + \alpha_{\mathrm{s}} B(\Phi_0) \otimes \int \mathrm{d}\Phi_{1|0} P(\Phi_{1|0}) \right] \\ &\quad \times \left[\Delta(Q^2, Q_0^2) + \int_{Q_0^2} \frac{\mathrm{d}q_1^2}{q_1^2} \int \mathrm{d}z_1 \, \frac{\alpha_{\mathrm{s}}}{2\pi} P(z_1) \Delta(Q^2, q_1^2) \right] \\ &+ \mathrm{d}\Phi_1 \alpha_{\mathrm{s}} \left[R_1(\Phi_1) - B(\Phi_0) \otimes P(\Phi_{1|0}) \right]. \end{aligned} \tag{34}$$

Again, undoing the integral in the second bracket, we obtain the first parton shower splitting, and we can continue the shower as before. In practice, two sets of events are given to the parton shower. The first set contain Born-level states given by the first bracket in Eq. (34), where the integral in the second bracket is simply undone by running the parton shower. The second set contains events with one extra parton, where the parton shower is added using suitable starting conditions. In this way the $\mathcal{O}(\alpha_{\mathrm{s}})$ contribution of the parton shower is removed and is instead replaced by the exact NLO result.

To $\mathcal{O}(\alpha_{\mathrm{s}})$, this is equivalent to POWHEG, however, we note that the real emission matrix element is not exponentiated in the Sudakov form factor (which is Δ rather than $\bar{\Delta}$). Also, contrary to POWHEG, it is not guaranteed that the weights of the generated states are positive definite, as one can easily

imagine having splitting functions that overestimate the real emission matrix element, rendering the last bracket negative.

5.3. Tree-level multi-jet merging and CKKW

An alternative way of choosing the R_1^{s} term is to introduce a cutoff, which we shall call the merging scale, Q^2_{MS} such that $R_1^{\mathrm{s}}(\Phi_1) = R_1(\Phi_1) \times \Theta(Q^2_{\mathrm{MS}} - q^2(\Phi_1))$. We then get a modified Born term compared to Eq. (26)

$$\tilde{B}(\Phi_0) = B(\Phi_0) + \alpha_{\mathrm{s}} V_1(\Phi_0) + \alpha_{\mathrm{s}} \int \mathrm{d}\Phi_{1|0(<Q^2_{\mathrm{MS}})} R_1(\Phi_1), \tag{35}$$

which we immediately identify as the NLO expression for the exclusive cross section with no partons above the scale Q^2_{MS}, in the full inclusive NLO cross section,

$$\mathrm{d}\sigma^{\mathrm{NLO}} = \mathrm{d}\Phi_0 \tilde{B}(\Phi_0) + \mathrm{d}\Phi_1 \alpha_{\mathrm{s}} R_1(\Phi_1) \Theta(q^2(\Phi_1) - Q^2_{\mathrm{MS}}). \tag{36}$$

We also see that the second term is exactly what we would get from a standard tree-level matrix element generator for the one-parton cross section with Q^2_{MS} as cutoff.

5.3.1. Merging for the first emission

Ignoring the NLO-reweighting of the Born term for the moment, we can now obtain a parton shower where the first emission is corrected to the tree-level matrix element if it is above Q^2_{MS}:

$$\begin{aligned} \mathrm{d}\sigma^{\mathrm{CKKW}} &= \mathrm{d}\Phi_0 B(\Phi_0) \left[\Delta(Q^2, Q_0^2) \right. \\ &\quad + \int_{Q_0^2} \frac{\mathrm{d}q_1^2}{q_1^2} \int \mathrm{d}z_1 \, \frac{\alpha_{\mathrm{s}}}{2\pi} P(z_1) \Theta(Q^2_{\mathrm{MS}} - q_1^2) \Delta(Q^2, q_1^2) \\ &\quad \left. + \int \mathrm{d}\Phi_{1|0} \alpha_{\mathrm{s}} \frac{R_1(\Phi_1)}{B(\Phi_0)} \Theta(q^2(\Phi_{1|0}) - Q^2_{\mathrm{MS}}) \Delta(Q^2, q_1^2) \right]. \end{aligned} \tag{37}$$

We see that the matrix element will fill the phase space above the merging scale (jet production) and the parton shower will fill the phase space below (jet evolution), effectively amounting to a phase space slicing into two disjoint regimes. This is the basis of the CKKW-based merging algorithms[70, 71].

A number of things are worth noting here:

1. The expression just exhibits the inclusive cross section for the first, hardest emission of a given Born configuration. The effect of the phase space slicing is made manifest, and leads to the two emission terms. The second of these emission terms, with $q^2 > Q^2_{\rm MS}$, is in fact generated differently from how the equation above suggests: In practice this term gives rise to a separate term contributing to the inclusive sample, but with a Born-level matrix element for a one-parton emission process as seed rather than the initial Born matrix element.
2. The equation above exhibits a new feature, namely a violation of unitarity, i.e. the square bracket does not integrate to one any more. As long as a reasonable range for the value of $Q^2_{\rm MS}$ is chosen, this does not have a big impact, though, and the total cross section of all contributions will be relatively stable with respect to changes in $Q^2_{\rm MS}$.
3. The equation above explicitly shows that the logarithmic accuracy of the parton shower is preserved in the merging.

5.3.2. Multi-jet merging

If we again undo the integrals in Eq. (37), we can as in Eq. (32) continue the cascade below q_1^2. However, as noted above, the second integral can then be thought of as an additional Born-level contribution for a one-parton emission process, for which we again can correct the first splitting. This would give us

$$\begin{aligned}
\mathrm{d}\sigma_1^{\rm CKKW} &= \mathrm{d}\Phi_1 \alpha_{\rm s} R_1(\Phi_1) \Theta(q^2(\Phi_{1|0}) - Q^2_{\rm MS}) \Delta(Q^2, q_1^2) \times \\
&\quad \Bigg[\Delta(q_1^2, Q_0^2) \\
&\quad + \int_{Q_0^2} \frac{\mathrm{d}q_2^2}{q_2^2} \int \mathrm{d}z_2 \, \frac{\alpha_{\rm s}}{2\pi} P(z_2) \Theta(Q^2_{\rm MS} - q_2^2) \Delta(q_1^2, q_2^2) \\
&\quad + \int \mathrm{d}\Phi_{2|1} \alpha_{\rm s} \frac{R_2(\Phi_2)}{R_1(\Phi_1)} \Theta(q^2(\Phi_{2|1}) - Q^2_{\rm MS}) \Delta(q_1^2, q_2^2) \Bigg] . \quad (38)
\end{aligned}$$

Clearly if we also have higher-order tree-level matrix elements, $R_3, R_4, \ldots$, available we can now continue to correct also higher parton multiplicities.

Further notes are in order.

- The Sudakov form factors can either be calculated analytically, as in the original CKKW scheme, or they can be generated by the shower

itself as in CKKW-L, where the form factor is interpreted strictly as a no-emission probability.

- If interpreted as no-emission probabilities, the Sudakov form factors are always below unity, and the reweighting can be implemented as a simple vetoing procedure (see Appendix A.3).

- In the MLM and Pseudo-Shower schemes, the Sudakov form factors are approximated by allowing the shower to radiate all the way down to its cutoff, Q_0^2, and this partonic state is then clustered with a jet algorithm with Q_{MS}^2 as resolution scale. The probability that these partonic jets are close to the original partons is then an approximation of the no-emission probability. The results are similar to those of CKKW(-L)[73], but it is not entirely clear how far the formal accuracy of the parton shower can be maintained.[10]

- Equating the Sudakov form factors in Eq. (15) with no-emission probabilities is only correct in final-state radiation. For initial-state emissions we must use the no-emission probability in Eq. (18), and it can be shown that this is related to the Sudakov form factor needed in the merging by a simple ratio of parton density function[82, 83] (see also [3]), such that

$$\Delta(q_i^2, q_{i+1}^2) = \frac{f(x, q_i^2)}{f(x, q_{i+1}^2)} \times \Delta(q_i^2, q_{i+1}^2; x). \tag{39}$$

  Hence, the procedure above needs to be amended with an extra reweighting with this PDF-ratio in the case of hadronic collisions.

- We have not considered the running of α_{s} in the parton shower. In practice, the matrix-element generators will use a fixed α_{s}, and in the CKKW-based algorithms, an additional weight, $\prod \alpha_{\mathrm{s}}^{\mathrm{PS}}(q_i^2)/\alpha_{\mathrm{s}}$, is introduced.

- If the parton shower is not ordered in hardness, or $k_\perp$, we cannot simply add a shower below the merging scale. Instead we must use the truncated, vetoed shower, described in Section 5.2.3, generalized to several hard emissions.

[10] See e.g. the discussion in [81].

5.4. Multi-jet NLO merging

If we look at Eq. (37), it is easy to see how we can reintroduce the NLO corrections from POWHEG in the CKKW-(L) matching schemes. What is needed is to replace the splitting function in the first integral with the same ratio R_1/B as in the second, and also reintroduce the corrected Sudakov form factors $\Delta \to \bar{\Delta}$. If we then also reweight all states with the dynamic K-factor $\bar{B}(\Phi_0)/B(\Phi_0)$, we arrive at the so-called MENLOPS procedure [77], where the inclusive cross section is correct to NLO, and the hardest emissions are corrected with tree-level matrix elements.

Lately, there has also been some progress in combining parton showers and matrix elements in such a way that also the cross sections for multi-jet final states becomes correct to next-to-leading order. The scheme called NL^3, suggested in [78], relies on being able to generate Born states with n extra partons above some merging scale exactly according to the exclusive NLO cross section, in the same way as in Eq. (35). From these states a shower is then allowed to evolve below the merging scale. To these event samples one can then add event samples generated according to the standard CKKW-L procedure, but these are reweighted such that the two first orders in α_s (corresponding to those in the NLO samples) are subtracted, by carefully expanding out the Sudakov form factors and the running of α_s.

The procedure is technically complicated and will not be described in detail here, and so far it has only been implemented for $e^+e^- \to$ jets. In the end (returning to the language of Figs. 5 and 6) the procedure corresponds to correctly taking into account the impact, both on shape *and* cross section, of all the blobs up to α_s^n together with all the $\alpha_s^k L^{2k}$ and $\alpha_s^k L^{2k-1}$ ones ($k > n$), for the n first real emissions above the cut, while all other emissions are only correct to $\alpha_s^n L^{2n}$ and $\alpha_s^n L^{2n-1}$ (corresponding to filling all the half-filled blobs in Fig. 6c).

5.5. Summary

- Fixed-order matrix elements and parton showers have different merits and shortcomings. They should be combined to get the best of both, for an optimal description of multi-parton states.

- Tree-level matrix elements cannot be blindly combined with a parton shower. The former are inclusive in nature, while the latter produces exclusive final states.

- Matrix elements must be supplemented with Sudakov form factors to give exclusive final states that can be combined with a parton shower.
- Special care must be taken if the parton shower is not ordered in hardness. When adding such a parton shower to a matrix-element-generated state it must therefore be properly truncated and vetoed.
- Combining next-to-leading-order matrix elements with parton showers for the first emission is now state of the art. For multi-leg matching and merging, the state of the art is still tree-level matrix elements.

Combining fixed-order matrix elements with parton showers is a very active research topic, and is important for giving reliable precision predictions for jet production from QCD. The last word is surely not said yet, and we are looking forward to many new ideas and improvements in the near future. In the long run it does not seem inconceivable that we will have generators producing results that are correct to next-to-next-to-leading order.

6. PDFs in event generators

Parton Distribution Functions play a central role in event generators, for the simulation of hard processes, parton showers and multiple parton interactions. The choice of PDF set therefore will influence both cross sections and event shapes.

To lowest order the function $f_i(x, \mu_F)$ describes the probability to find a parton of species i with a momentum fraction x when a proton is probed at a scale μ_F. This distribution cannot be predicted from first principles, since it depends on the non-perturbative physics of the proton wave function. With an ansatz for the initial distributions at some low scale μ_{F0}, the evolution towards larger scales is predicted by the DGLAP equations [35–37], however. Different tunes have been made, by comparing an evolved ansatz with relevant data, e.g. from Deeply Inelastic Scattering. Over the years many such tunes have been presented, with increasing accuracy as newer data have been added. Also the theoretical framework has seen some improvements. The CTEQ [84] and MRST/MSTW [85] collaborations have been especially diligent in regularly presenting updated tunes. These and others are available in the LHAPDF library [13].

Precision tests of QCD today normally involve comparisons with NLO matrix elements convoluted with NLO PDFs (Eq. (1)) both defined in the $\overline{\text{MS}}$

renormalization scheme. In general this allows a greatly improved description of data, relative to LO results. But NLO expressions are not guaranteed to be positive definite, and do not have a simple probabilistic interpretation. For PDFs, specifically, it is well known that the NLO gluon has a tendency to start out negative at small x for small scales, and only turn positive by the QCD evolution towards larger μ_F. In the MRST/MSTW sets the ansatz allows negative gluons, while the CTEQ ansatz is constructed to be positive definite. Either way, the NLO gluon PDF is very different from the LO one, also at larger scales. Specifically, it remains smaller in NLO than in LO at small x, which then typically is compensated by the NLO MEs being larger than the LO ones, by the presence of $\ln(1/x)$-enhanced terms.

In recent years the emphasis has been put on NLO PDFs, as offering the best description of hard-process data. The problem is that generators are largely of an LO character. That is, while several hard processes are implemented to NLO accuracy in some generators, notably in the MC@NLO and POWHEG frameworks, see Section 5, most are still only provided at LO, as are all the standard PS and MPI models, e.g. with LO splitting kernels in the showers. The latter two components additionally have most of their activity in the low-$p_\perp$ region, and the last one especially with low-x gluons. A usage of NLO PDFs with LO MEs here would be strongly questionable, since this combination typically undershoots the interaction rate obtained both in LO and NLO calculations.

Therefore the norm is for LO generators to use the few LO PDF fits that are still produced. In cases where the shape is more important than the absolute normalization — such as backwards evolution of ISR, where it is ratios of PDFs that sets the evolution rate — this may be perfectly adequate. But for absolute cross sections NLO calculations usually lie above LO ones, and this enhancement is needed to obtain a good description of data. This introduces a tension in LO PDF fits: a data set that is mainly sensitive to a particular x range prefers to have more of the total momentum of the proton located in that x range, at the expense of other x ranges. To address this issue, new Monte Carlo adapted PDFs have been presented, wherein the momentum sum rule $\sum_i \int_0^1 x f_i(x, \mu_F)\,\mathrm{d}x = 1$ is relaxed: MRST LO* and LO** [86], and CT09 MC1, MC2 and MCS [87]. By allowing the normalization to float, one typically finds a value 10 – 15% above unity, and the whole x range can be enhanced without tension. This should certainly not be viewed as a breaking of momentum conservation, but as a way to include an approximate K factor that can depend on the parton flavours and

momenta but not on the specific process.

Another trick introduced is to make use of pseudo-data, obtained by generating several different processes to NLO, but then fitting them to PDFs within an LO context [87]. That way it is possible to obtain a more uniform coverage over a large x range, and for different flavours. Additionally, of the above five sets, CT09 MCS does not relax the momentum sum rule, but instead optimizes renormalization and factorization scales process by process.

Note that much of the case for the modified LO sets is based on the LO PDF behaviour at small x and μ_F. In the opposite region, large x and μ_F, differences are not as clear-cut. Often the NLO corrections to the MEs there correspond to rescaling by an approximately constant factor. Then, if NLO PDFs provide a better shape than LO PDFs in that region, the combination of LO MEs and NLO PDFs makes sense. It is therefore possible to use one PDF set for the hard processes and another for the softer parton showers and multiple interactions.

To conclude, the new PDFs offer the hope of improved descriptions of data within generators, and have already started to be used, both by generator authors and by the experimental collaborations, as an alternative to normal LO ones. The outcome is still not clear; studies suggest that you can find distributions where the new sets do better than the traditional ones, and distributions where they do worse [88]. There can be no doubt, however, that these sets have put new tools in the hands of generator authors, and opened the way for further developments of PDFs especially well suited for generator applications.

- PDFs are used in generators for the description of hard processes, showers and MPIs.
- While NLO PDFs are appropriate for studies of hard processes, especially when combined with NLO MEs, they are not well suited for current LO shower and MPI models.
- New tricks have been introduced to improve the usefulness of LO PDFs in generators, and new sets have been presented, but currently there is no obvious winner.

7. Soft QCD and underlying event physics

Several distinct physics and modelling issues come under the heading of "soft QCD" and "underlying event". In Section 7.1 we discuss "primor-

dial $k_\perp$", a topic that lies on the intersection between parton showers and soft QCD. The rest of this section is devoted to a discussion of the different physics (sub-)processes that contribute to the total observed activity in hadron-hadron collisions. Thus, in Section 7.2, we give a brief introduction to — and dictionary of — the different QCD processes that form the dominant part of the total hadron-hadron cross section, and to the origin of the so-called "underlying event" and the associated "pedestal effect". In Section 7.3, we then take a closer look at models based on multiple parton interactions (MPI). Section 7.4 focuses on the particular issue of colour reconnections. Finally, Section 7.5 gives a very brief introduction to models of diffraction, in particular models based on pomerons.

For more specific details on the current implementations in each of the main generators, see the individual descriptions in Part II.

7.1. Primordial $k_\perp$

In Monte Carlo models, the term "primordial $k_\perp$" is used to refer collectively to any transverse momentum given to initial-state partons *beyond* that generated by the normal ISR shower evolution described in Section 4.4.

Physically, such additional momentum could come from several sources, as follows:

1. Fermi motion of confined partons inside their parent hadron, with a magnitude of order the inverse hadron radius $\sim \Lambda_{\rm QCD}$.
2. "Unresolved" ISR shower activity, coming from scales below the infrared cutoff.
3. Activity not accounted for, or incorrectly accounted for, by the particular shower model in question. In particular, this may be relevant for parton evolution involving low parton momentum fractions x, as was briefly discussed in Section 4.4.

Of these, only Fermi motion is relatively straightforward. It is also the only component that is genuinely "primordial", i.e. intrinsic to the incoming hadron. The others depend sensitively on issues that are inherently ambiguous in the shower description: whether the low-$p_\perp$ divergences in the parton shower are regulated by a sharp cutoff or by a smooth suppression (and in what variable), how $\alpha_{\rm s}$ is treated close to the cutoff, how the shower radiation functions and recoil effects behave, and whether any non-trivial low-x effects are included.

In the simplest possible treatment one lumps all these "unresolved" effects, regardless of origin, into a single number, called "primordial $k_\perp$". In each event, the beam-collinear partons extracted from each of the original hadrons can then be given a $p_\perp$ of this magnitude, typically distributed according to a Gaussian or similar distribution. (Since the beam remnant must necessarily take up the recoil from this kick, an upper cutoff is usually also enforced, limiting the amount by which the beam remnant is allowed to be kicked off axis by tails of this effect.)

However, even in this simplified case, the above discussion should serve to illustrate that the value of the "primordial $k_\perp$" should not really be perceived of as a universal constant. At the very least, the shower evolution equations imply that it must have some implicit dependence on the ISR cutoff — if we increase the shower cutoff, for instance, the primordial $k_\perp$ should increase slightly as well, to compensate for the now missing shower activity in the region that has been cut away. In current models, this scaling does not happen automatically, but must be taken care of by retuning the primordial $k_\perp$ if the ISR cutoff (or any other parameter affecting the infrared regularization of the initial-state shower) is changed. More troublingly, perhaps, since a lot of possible process-dependent physics effects have been "swept under the rug", there is also no strong reason why the same value of this primordial $k_\perp$ should work equally well for all processes or even in different phase space regions. Attempting to extract a value for it in several different, mutually complementary, processes and regions, could therefore be a valuable input to guide future modelling.

A next-to-simplest iteration can be obtained by letting the value of primordial $k_\perp$ scale with the Q^2 of the hard interaction [89]. This generates a minimum of process-dependence (e.g. partons entering a soft QCD scattering can now be given a smaller primordial $k_\perp$ than ones producing a Z boson), but still does not really address the underlying physics.

A first stab at a more physical model was made in [90], by including a non-perturbative function that depends explicitly on the phase space available for unresolved initial-state radiation, in addition to a smaller and more universal component to be modelled by a Gaussian. Although the data available at the time could not clearly differentiate this from the conventional models, the expectation is that this should generate a more realistic process- and collision-energy-dependence of the effective primordial $k_\perp$.

A secondary modelling issue, relevant to the MPI models discussed in the next subsection, is how much primordial $k_\perp$ is assigned to partons initiating

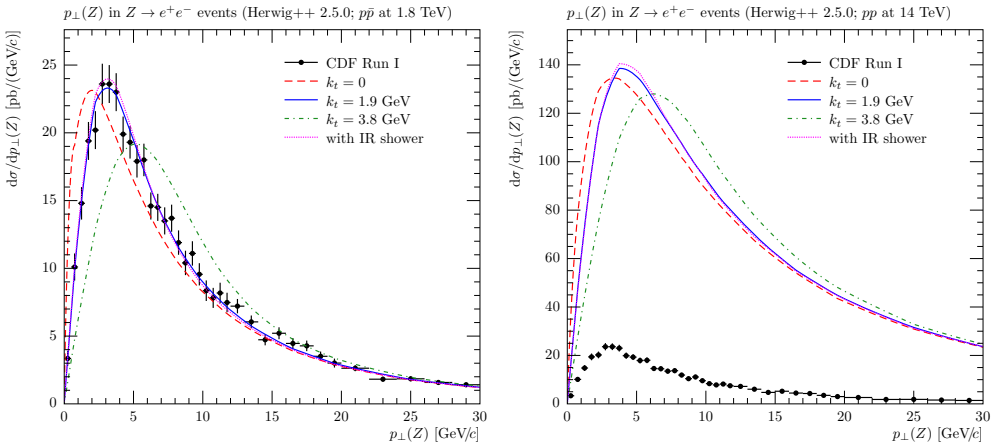

Figure 7: The low-$p_\perp$ peak of the $p_\perp$ distribution of lepton pairs in Drell-Yan events at the Tevatron, compared to CDF data [91]. A Monte Carlo model (Herwig++) is shown with four different choices for the "primordial $k_\perp$". a) $p\bar{p}$ at 1.8 TeV b) pp at 14 TeV.

multiple parton interactions, and how the associated recoil effects are distributed among those initiators and the remnant. Typically, MPI initiators are only assigned a primordial $k_\perp$ of the order of Fermi motion, although this is a model-dependent statement that may of course change, as models improve.

Empirically, the most important distribution for constraining the magnitude of this effect is the $p_\perp$ distribution of lepton pairs in Drell-Yan events. The peak of this distribution is extremely sensitive to infrared effects. In Fig. 7a, we compare the distribution measured by the CDF experiment [91] to a Monte Carlo model (Herwig++) with four different primordial-$k_\perp$ settings: 0 GeV (off), 1.9 GeV (the default in Herwig++), 3.8 GeV (twice the default), and the IR-augemented shower model [90]. To illustrate how these predictions scale with collider centre-of-mass energy, keeping the Q^2 of the hard interaction fixed, we also include a plot showing the $p_\perp$ of Drell-Yan pairs in pp collisions at 14 TeV in Fig. 7b; the distributions becomes broader, but the peak position stays relatively constant. A comparison of different generators on this distribution can be found in Fig. 18 in the comparisons section of the review (Section 18).

It is also worth noting that, depending on the model, details of how the transverse momenta generated by the initial-state parton shower and the primordial component are combined, the latter can also have a significant

effect well above the peak region. In the more primitive models, there is also the (probably artificial) possibility of a "double-peak" structure emerging at high energies, with a higher-$p_\perp$ peak generated by the perturbative shower and a low-$p_\perp$ one by primordial $k_\perp$.

As mentioned above, it is important to consider also complementary distributions, involving different scales or x values, to fully constrain this ambiguous component of Monte Carlo models. Good examples here would be the Drell-Yan process at different Q^2 values or at different rapidities. A systematic comparison to extractions in DIS could also be fruitful.

7.2. Soft QCD processes

Elastic and inelastic. Elastic scattering consists of all reactions of the type

$$A(p_A)B(p_B) \to A(p'_A)B(p'_B) \ , \tag{40}$$

where A and B are particles carrying momenta p_A and p_B, respectively. Specifically, the only exchanged quantity is momentum; all quantum numbers and masses remain unaltered, and no new particles are produced. Inelastic scattering covers everything else, i.e.

$$AB \to X \neq AB \ , \tag{41}$$

where $X \neq AB$ signifies that one or more quantum numbers are changed, or more particles are produced. The distinction between elastic and inelastic scattering is physically observable and is therefore quantum mechanically meaningful (see Section 16 for further discussion of this point). Thus, we divide the total hadron-hadron cross section into two physically distinguishable components,

$$\sigma_{\rm tot}(s) = \sigma_{\rm el}(s) + \sigma_{\rm inel}(s) \ , \tag{42}$$

where $s = (p_A + p_B)^2$ is the beam-beam centre-of-mass energy squared.

Diffractive and non-diffractive. If A or B are not elementary the inelastic final states may be further divided into "diffractive" and "non-diffractive" topologies. This is a qualitative classification, usually based on whether the final state looks like the decay of an excitation of the beam particles (diffractive), or not (non-diffractive), or upon the presence of a large rapidity gap somewhere in the final state which would separate such excitations. There are two schools of thought on how to specify this distinction more precisely:

1. Use a theoretical model, whose different physics subprocesses can each be uniquely assigned as diffractive or non-diffractive. However, different models produce different final-state spectra, and hence such a classification necessarily depends on the model used to make it. Furthermore, if the model allows for events of both diffractive and non-diffractive origin to populate the same phase space points, the interference terms between them have no unique assignments and hence the classification cannot be made quantum mechanically meaningful, see Section 16 for a more general discussion of this issue.
2. Use one or more physical observables, which guarantees that the definition will also be valid at the quantum level. In this case, the arbitrariness is instead reflected in the fact that one has to choose what one means by a "diffractive topology", at the level of a final-state observable, and this choice is without a unique "correct" answer. In general, one defines diffractive topologies as events that contain large rapidity gaps in the activity, consistent with (possibly multiple) decays of excited states, with "large" often taken to be somewhere in the range of 3–5 units of rapidity.

Types of diffraction. Given that an event has been labelled as diffractive either by a theoretical model or by a final-state observable, we may distinguish between three different classes of diffractive topologies, which it is possible to distinguish between physically, at least in principle. In double-diffractive dissociation (DD) events, both of the beam particles are diffractively excited and hence neither of them survive the collision intact. In single-diffractive dissociation (SD) events, only one of the beam particles gets excited and the other survives intact. The last diffractive topology is central diffraction (CD), in which both of the beam particles survive intact, leaving an excited system in the central region between them[11]. That is,

$$\sigma_{\rm inel}(s) = \sigma_{\rm SD}(s) + \sigma_{\rm DD}(s) + \sigma_{\rm CD}(s) + \sigma_{\rm ND}(s) \ , \tag{43}$$

where "ND" (non-diffractive, here understood not to include elastic scattering) contains no gaps in the event consistent with the chosen definition of diffraction. Further, each of the diffractively excited systems in the events labelled SD, DD, and CD, respectively, may in principle consist of several

[11]This latter topology also includes so-called "central exclusive production" [92].

subsystems with gaps between them. Eq. (43) may thus be defined to be exact, within a specific definition of diffraction, even in the presence of multi-gap events. Note, however, that different theoretical models almost always use different (model-dependent) definitions of diffraction, and therefore the individual components in one model are in general not directly comparable to those of another. It is therefore important that data be presented at the level of physical observables if unambiguous conclusions are to be drawn from them, see Section 16 for a more detailed discussion of this issue. Monte Carlo models of diffraction will be discussed briefly in Section 7.5 below.

Minimum bias and soft inclusive physics. The term "minimum bias" is an experimental term, used to define a certain class of events that are selected with the minimum possible selection bias, to ensure they are as inclusive as possible. This will be discussed in more detail in Section 16. In theoretical contexts the term "minimum bias" is often used with a slightly different meaning: to denote specific (classes of) inclusive soft QCD subprocesses in a given model. Since these two usages are not exactly identical, in this review we have chosen to reserve the term "minimum bias" to pertain strictly to definitions of experimental measurements, and instead use the term "soft inclusive physics" as a generic descriptor for the class of processes which generally dominate the various experimental minimum bias measurements in theoretical models.

Underlying event and jet pedestals. In events containing a hard parton-parton interaction, the underlying event represents the additional activity which is not directly associated with that interaction. There is some ambiguity in how one defines what is "associated" with the hard interaction, and what is not. Here, we shall define the underlying event to represent the additional activity *after* all bremsstrahlung off the hard interaction has already been taken into account. Specifically, initial-state radiation off the hard interaction is *not* included in our definition of the underlying event. Note also that the underlying event is usually much more active, with larger fluctuations, than soft-inclusive collisions at the same energy. This is called the "jet pedestal" effect (hard jets sit on top of a higher-than-average "pedestal" of underlying activity), and is interpreted as follows. When two hadrons collide at non-zero impact parameter, high-$p_\perp$ interactions can only take place inside the overlapping region. Imposing a hard selection cut therefore statistically biases the event sample toward more central collisions, which will also have

more underlying activity. The size of the pedestal, as a function of leading track $p_\perp$, is illustrated in Figs. 20–22 in the comparisons section of the review (Section 18).

Multiple interactions. In a hadron-hadron collision more than one pair of partons may interact, leading to the possibility of multiple interactions. In Monte Carlo modelling contexts, the most striking and easily identifiable consequence of multiple interactions is arguably the possibility of observing several hard parton-parton interactions in one and the same hadron-hadron event[12]. The main distinguishing feature of such jets is that they tend to form back-to-back pairs, with little total $p_\perp$. For comparison, jets from bremsstrahlung tend to be aligned with the direction of their "parent" partons. The fraction of multiple interactions that give rise to additional reconstructible jets is, however, quite small (how small depends on the exact jet definition used). Additional soft interactions, below the jet cutoff, are much more plentiful, and can give significant corrections to the colour flow and total scattered energy of the event. This affects the final-state activity in a more global way, increasing the multiplicity and summed transverse energy, and contributing to the break-up of the beam remnant in the forward direction.

To illustrate this we include in Fig. 8 a comparison between an ATLAS minimum bias measurement of the charged-track multiplicity at 7 TeV to a Monte Carlo model with and without MPI switched on (curves labelled as "default" and "no MPI", respectively). Clearly, the predicted multiplicity distribution without MPI is far too narrow, regardless of whether parton showers are included or not (curve labelled "no MPI, no shower"). This by itself is one of the strongest arguments that MPI must be included in realistic models of soft-inclusive physics.

The possibility of multiple interactions has also been implicit or explicit in many calculations of the total hadron-hadron cross section. Two recent and representative examples can be found in [94, 95]. The increase of the parton-parton cross section with CM energy is here directly driving an increase also of $\sigma_{\rm tot}(s)$.

The first detailed Monte Carlo model for perturbative MPI was proposed

[12] Additional jet pairs produced in this way are sometimes referred to as "minijets", and theoretically belong to a class of perturbative corrections called "higher twist", but in the interest of maintaining a compact terminology, we shall here just call them MPI jets.

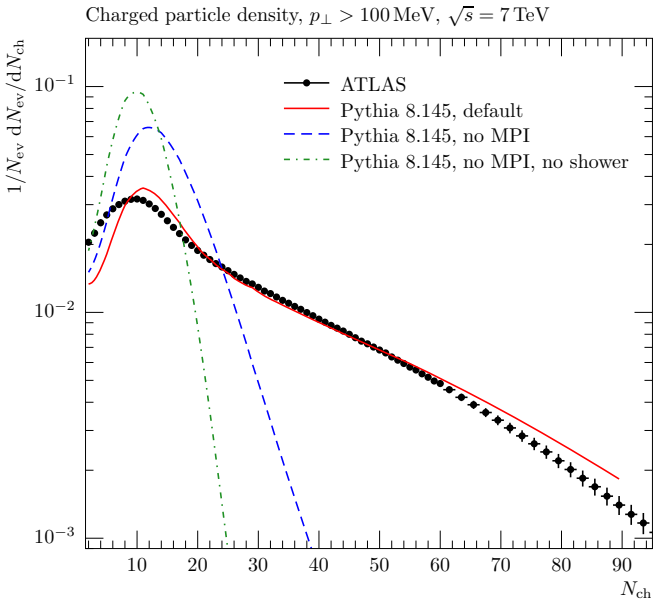

Figure 8: Models with and without MPI and parton showers, compared to the charged-particle multiplicity measured by the ATLAS experiment [93], for particles with $p_\perp > 100$ MeV, $|\eta| < 2.5$, and $c\tau > 10$ mm, in events that contain at least two such particles.

by Sjöstrand and van Zijl in [96], and most modern implementations employ a similar physical picture. Below, in section Section 7.3, we therefore first summarize the main points of this basic framework, pointing out the differences between the currently existing models as we go along. Some useful additional references to the history and development of the subject of multiple interactions also outside the Monte Carlo context can be found in the Perugia MPI workshop proceedings [97] and in the mini-reviews contained in [89, 98].

7.3. Models based on multiple parton interactions (MPI)

7.3.1. Basics of MPI

Consider first the cross section for a *single* parton-parton scattering, e.g. by t-channel gluon exchange (Rutherford scattering). This process, and simple variations of it, make up the vast majority of the total scattering processes occurring between coloured particles, and it is thus on this basic process that perturbative models of both soft inclusive and underlying event physics are currently built.

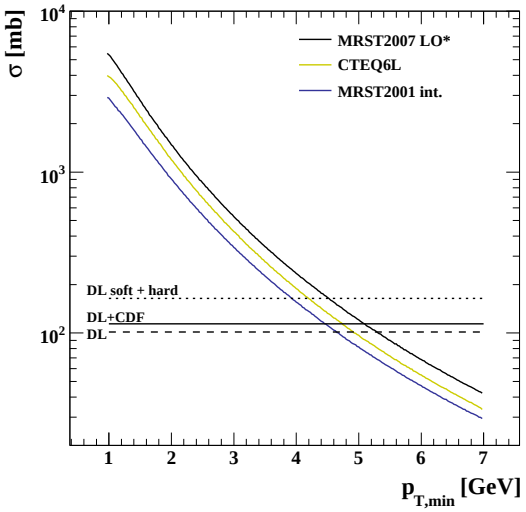

Figure 9: The inclusive jet cross section calculated at LO for three different proton PDFs, compared to various extrapolations of the non-perturbative fits to the total pp cross section at 14 TeV centre-of-mass energy. From [99].

An intuitive way of arriving at the idea of multiple interactions is to view hadrons simply as "bunches" of incoming partons. No physical law then prevents several distinct pairs of partons from undergoing scattering processes within one and the same hadron-hadron collision. The other key idea to bear in mind is that the exchanged QCD particles are coloured, and hence such multiple interactions, even when soft, can cause non-trivial changes to the colour topology of the colliding system as a whole, with potentially major consequences for the particle multiplicity in the final state.

In the soft QCD region, the t-channel gluon propagator almost goes on shell (reminiscent of the case of bremsstrahlung, described in detail in Section 4), causing the subprocess differential cross section to become very large, behaving roughly as:

$$\mathrm{d}\hat{\sigma}_{2j} \propto \frac{\mathrm{d}t}{t^2} \sim \frac{\mathrm{d}p_\perp^2}{p_\perp^4} , \tag{44}$$

An integration of this cross section from a lower cutoff $p_{\perp\mathrm{min}}$ to $\sqrt{s}$, using the full (leading-order) QCD $2 \to 2$ matrix elements folded with some recent parton-density sets, is shown in Fig. 9, for pp collisions at 14 TeV [99]. The solid curves, representing the calculated cross sections as functions of $p_{\perp\mathrm{min}}$,

are compared to a few of the Donnachie-Landshoff (DL) predictions [100, 101] for the total pp cross section $\sigma_{\rm tot}$, shown as horizontal lines with different dashing styles on the same plot. Physically, the jet cross section can of course not exceed the total pp one, yet this is what appears to be happening at scales of order 4–5 GeV in Fig. 9. How to interpret this behaviour?

Recall that the interaction cross section is an inclusive number. Thus, an event with two parton-parton interactions will count twice in σ_{2j} but only once in $\sigma_{\rm tot}$, and so on for higher multiplicities. In the limit that all the individual parton-parton interactions are independent and equivalent (to be improved on below), we have

$$\sigma_{2j}(p_{\perp\rm min}) = \langle n \rangle (p_{\perp\rm min})\ \sigma_{\rm tot}\ , \tag{45}$$

with $\langle n \rangle (p_{\perp\rm min})$ giving the average of the distribution in the number of parton-parton interactions above $p_{\perp\rm min}$ per hadron-hadron collision, and that number may well be above unity. This simple argument in fact expresses unitarity; instead of the total interaction cross section diverging as $p_{\perp\rm min} \to 0$ (which would violate unitarity), we have restated the problem so that it is now the *number of interactions per collision* that diverges.

Two important ingredients remain to be introduced in order to fully regulate the remaining divergence. The first is the correlation due to energy-momentum conservation — the interactions cannot use up more momentum than is available in the parent hadron — which will suppress the large-n tail of the naïve estimate above. This is handled slightly differently in the various models on the market. In the Pythia and Sherpa models, the multiple interactions are ordered in $p_\perp$, and the parton distributions for each successive interaction are explicitly constructed so that the sum of x fractions can never be greater than unity. In the Herwig++ model, instead the uncorrelated estimate of $\langle n \rangle$ above is used directly as an initial guess, but the actual generation of interactions stop once the energy-momentum conservation limit is exceeded (with the last "offending" interaction also removed from consideration).

Even with this suppression taken into account, however, the number of multiple interactions still grows uncomfortably fast as $p_{\perp\rm min} \to 0$. A second ingredient suppressing the number of interactions, at low-$p_\perp$ and x, is colour screening / saturation. Screening and saturation both roughly correspond to partons being unable to resolve each other as independent particles at low scales, but the underlying physics pictures are slightly different, as follows.

Screening is interpreted as an effect of the wavelength $\sim 1/p_\perp$ of the exchanged particle becoming larger than a typical colour-anticolour separation distance; it will then only couple to an average colour charge that vanishes in the limit $p_\perp \to 0$, hence leading to suppressed interactions. This screening effectively provides an infrared cutoff for MPI similar to that provided by the hadronization scale for parton showers. Saturation instead invokes explicit parton recombination effects to reduce the growth of the parton densities at low x. In either case, the product of cross section and parton densities is reduced. However, an important modelling distinction is therefore that the reduction takes place mainly as a function of $p_\perp$, for screening, whereas the x variable plays a central role in saturation arguments. As usual, the truth is likely to be a combination of both. Since most of the models considered in this review employ a screening-like cutoff, in $p_\perp$, we devote a bit more space to this possibility here.

A first estimate of an effective lower cutoff due to colour screening would be the proton size

$$p_{\perp\min} \simeq \frac{\hbar}{r_p} \approx \frac{0.2 \text{ GeV} \cdot \text{fm}}{0.7 \text{ fm}} \approx 0.3 \text{ GeV} \simeq \Lambda_{\text{QCD}} \,, \tag{46}$$

but empirically this appears to be too low. In current models, one replaces the proton radius r_p in the above formula by a "typical colour screening distance" d, i.e. an average size of a region within which the net compensation of a given colour charge occurs. This number is not known from first principles, so effectively this is simply a cutoff parameter, which can then just as well be put in transverse momentum space. The simplest choice is to introduce a step function $\Theta(p_\perp - p_{\perp\min})$, such that the perturbative cross section completely vanishes below the $p_{\perp\min}$ scale. This is the procedure followed in the original JIMMY model [102] (an add-on to the Fortran HERWIG generator), whose predictions therefore have a large dependence on the value of this parameter. The Herwig++ model [103] builds on this, and improves it by adding a set of "soft" scatterings below $p_{\perp\min}$, with a $p_{\perp\min}$-dependent cross section defined such that the two components add up to the total (inelastic non-diffractive) cross section [99], which should reduce the explicit dependence on $p_{\perp\min}$.

Alternatively, one may note that the jet cross section is divergent like

$\alpha_s^2(p_\perp^2)/p_\perp^4$, cf. Eq. (44), and that therefore a factor

$$\frac{\alpha_s^2(p_{\perp 0}^2 + p_\perp^2)}{\alpha_s^2(p_\perp^2)} \frac{p_\perp^4}{(p_{\perp 0}^2 + p_\perp^2)^2} \tag{47}$$

would smoothly regularize the divergences, now with $p_{\perp 0}$ as the free parameter to be tuned to data. This is the default in the current PYTHIA and SHERPA models. Note that, since this merely represents a "smoothed-out" variant of the Θ function cutoff above, there is still a strong dependence on the value of $p_{\perp 0}$. This is thus one of the main "tuning" parameters in such models.

The parameters do not have to be energy-independent, however. Higher energies imply that parton densities can be probed at smaller x values, where the number of partons rapidly increases. Partons then become closer packed and the colour screening distance d decreases. Just as the small-x rise varies like some power of x one could therefore expect the energy dependence of $p_{\perp\min}$ and $p_{\perp 0}$ to vary like some power of the centre-of-mass energy. Explicit toy simulations [104] lend some credence to such an ansatz, although with large uncertainties. One could also let the cutoff increase with decreasing x; this would lead to a similar phenomenology since larger energies probe smaller x values. Especially for models with strong dependence on this cutoff, the uncertainty on this energy and x scaling of the cutoff is a major concern when extrapolating between different collider energies.

As an alternative we therefore note that the introduction of so-called unintegrated parton densities, as used in the BFKL [41, 42], CCFM [43, 105], and LDC [106–108] approaches to initial-state radiation allows the possibility of replacing the $p_{\perp\min}$ or $p_{\perp 0}$ cutoff by parton densities that explicitly vanish in the $p_\perp \to 0$ limit [109]. This allows the possibility of an alternative implementation of multiple interactions [110] and may be a useful ingredient in future phenomenological models, possibly in combination with more explicit physical modelling of saturation effects.

7.3.2. Impact parameter dependence

As mentioned in Section 7.2, the so-called "pedestal effect" (see also Figs. 20–22) is partly driven by impact parameter dependence; in peripheral collisions, only a small fraction of events contain any high-$p_\perp$ activity, whereas central collisions are more likely to contain at least one hard scattering; a sample with a high-$p_\perp$ selection cut will therefore be biased towards

small impact parameters. The ability of a model to describe the shape of the pedestal (e.g. to describe both minimum bias data and underlying event distributions simultaneously) is therefore related to its modelling of the impact parameter dependence. A related effect is that, also for a fixed selected $p_\perp$, events at comparatively higher impact parameters should exhibit relatively less underlying event and vice versa.

All the models discussed here contain an explicit treatment of impact parameter, but we note that there are still substantial simplifications made. Most importantly, the impact parameter dependence is so far still assumed to be factorized from the x dependence, $f(x, b) = f(x)g(b)$, where b denotes impact parameter, a simplifying assumption that by no means should be treated as inviolate, see e.g. [111–113]. Also, the hadron-hadron impact parameter only enters in an averaged global sense, not as a vector, and the individual MPI are not assigned individual "locations" in transverse space.

In order to quantify the concept of hadronic matter overlap, one may assume a spherically symmetric distribution of matter inside a hadron at rest, $\rho(\mathbf{x})\,\mathrm{d}^3x = \rho(r)\,\mathrm{d}^3x$. The form of ρ is a matter of some uncertainty, with various more or less phenomenologically motivated choices available in models. The options range from simple parameteric forms in PYTHIA-based models, such as Gaussians, double Gaussians, exponentials [96], and forms interpolating between them [89], to a form based on the electromagnetic form factor in the HERWIG-based ones [114]. A possibility for future model refinements thus lies in the input of more detailed information on the flavour- or x-dependence of the transverse structure of the proton, e.g. obtained from sum rules, from analytic fits beyond the EM form factor, or from lattice studies.

For a collision with impact parameter b, the time-integrated overlap $\mathcal{O}(b)$ between the matter distributions of the colliding hadrons is given by

$$\mathcal{O}(b) \propto \int \mathrm{d}t \int \mathrm{d}^3x \;\rho(x, y, z)\,\rho(x + b, y, z + t)\;, \tag{48}$$

where the necessity to use boosted $\rho(\mathbf{x})$ distributions has been circumvented by a suitable scale transformation of the z and t coordinates, see [96]. The overlap function $\mathcal{O}(b)$ is identical to $A(b)$ in "JIMMY notation" [102, 103]. It is closely related to the $\Omega(b)$ of eikonal models (see, for example, [112, 115, 116]), but is somewhat simpler in spirit.

The larger the overlap $\mathcal{O}(b)$ is, the more likely it is to have interactions

between partons in the two colliding hadrons. In fact, to first approximation, there should be a linear relationship

$$\langle \tilde{n}(b) \rangle = k\mathcal{O}(b) \ , \tag{49}$$

where $\tilde{n} = 0, 1, 2, \ldots$ counts the number of interactions when two hadrons pass each other with an impact parameter b and k is an undefined constant of proportionality, to be specified below.

For each impact parameter, b, the number of interactions $\tilde{n}$ can be assumed to be distributed according to a Poissonian, modulo momentum conservation, with the mean value of the Poisson distribution depending on impact parameter, $\langle \tilde{n}(b) \rangle$. If the matter distribution has a tail to infinity (as, e.g., Gaussians do), one may nominally obtain events with arbitrarily large b values. In order to obtain finite total cross sections, it is therefore necessary to give a separate interpretation to the "zero bin" of the Poisson distribution, which corresponds to "no-interaction" events.

In the JIMMY [102] and Herwig++ [103] models the part of the pp cross section containing hard scatters is calculated from the area overlap function, the parton densities and the partonic cross section; the "no-interaction" possibility is then accounted for as a reduction of this cross section with respect to its value without allowing for MPI. The JIMMY model stops here, considering only hard events, and so it can only be applied to underlying event. As mentioned above, the Herwig++ model also permits the possibility of soft scatters (see also Section 13.6) and so can also be used to simulate soft-inclusive physics.

In the framework of [96], used by PYTHIA and SHERPA, the restriction to at least one perturbative scattering for soft inclusive scatters implies that the probability that two hadrons, passing each other with an impact parameter b, will produce a real event is given by

$$\mathcal{P}_{\rm int}(b) = \sum_{\tilde{n}=1}^{\infty} \mathcal{P}_{\tilde{n}}(b) = 1 - \mathcal{P}_0(b) = 1 - \exp(-\langle \tilde{n}(b) \rangle) = 1 - \exp(-k\mathcal{O}(b)) \ , \tag{50}$$

according to Poisson statistics. The average number of interactions per event at impact parameter b is now $\langle n(b) \rangle = \langle \tilde{n}(b) \rangle / \mathcal{P}_{\rm int}(b)$, where the denominator comes from the removal of hadron pairs that pass without interaction, i.e. which do not produce any events. While the removal of $\tilde{n} = 0$ from the potential event sample gives a narrower-than-Poisson interaction distri-

bution at each fixed b, the variation of $\langle n(b)\rangle$ with b gives a b-integrated broader-than-Poisson interaction multiplicity distribution.

Averaged over all b the relationship $\langle n\rangle = \sigma_{2j}/\sigma_{\rm nd}$ should still hold. Here, as before, σ_{2j} is the integrated interaction cross section for a given regularization prescription at small $p_\perp$, while the inelastic non-diffractive cross section $\sigma_{\rm nd}$ is taken from parameterization [100, 101, 117]. This relation can be used to solve for the proportionality factor k in Eq. (49). Note that, since now each event has to have at least one interaction, $\langle n\rangle > 1$, one must ensure that $\sigma_{2j} > \sigma_{\rm nd}$. The $p_{\perp 0}$ parameter has to be chosen accordingly small.

7.3.3. Perturbative corrections beyond MPI

There are essentially two perturbative modelling aspects which go beyond the introduction of MPI themselves. In particular, this concerns

1. Parton showers off the MPI.
2. Perturbative parton-rescattering effects.

Without showers, MPI models would generate very sharp peaks for back-to-back MPI jets, caused by unshowered partons passed directly to the hadronization model. However, with the exception of the oldest Pythia 6 model [96], all of the models discussed in this review do include such showers, and hence should exhibit more realistic (i.e. broader and more decorrelated) MPI jets — although not much can be said concerning their expected formal level of precision of course. A secondary effect is that a showered interaction also generates a larger hadronic multiplicity than an unshowered one. Therefore, a smaller total number of MPI is needed when tuning models incorporating such showers. More discussion of this tuning effect can be found in [118, 119]. On the initial state side of the MPI shower issue the main questions are whether and how correlated multi-parton densities are taken into account (for a recent treatment of this issue see e.g. [120] and references therein), and, as discussed previously, how the showers are regulated at low $p_\perp$ (or low x). Although none of the Monte Carlo models currently impose a rigorous correlated multi-parton evolution, all of them include some elementary aspects. The most significant for parton-level results is arguably momentum conservation, which is enforced explicitly in all the models, although in slightly different ways, as was discussed briefly above. The so-called "interleaved" models [52, 89] attempt to go a step further, generating an explicitly correlated multi-parton evolution in which flavour sum rules can be

imposed to conserve e.g. the total numbers of valence and sea quarks across interaction chains.

Perturbative rescattering in the final state can occur if partons are allowed to undergo several distinct interactions, with showering activity possibly taking place in between. This has so far not been studied extensively, but a first fairly complete model and exploratory study has been presented in the context of Pythia 8 [121]. The net effect there is a slight increase in the mean $p_\perp$ of the partonic final states, but more dramatic signatures have not yet been identified. In the initial state, parton rescattering effects may lead to saturation (discussed briefly in Section 7.3.1), or to the incoming partons carrying enhanced "primordial $k_\perp$" values (discussed in Section 7.1). It could also produce correlations between different MPI initiators, in particular in colour space. At the *parton level*, however, such colour correlations probably play a rather minor role. This is suggested both by an exploratory study of "intertwined" multiple interactions [52] (that is, letting several partons from the same shower chain undergo perturbative interactions, thus letting the perturbative shower evolution generate their colour correlations) which numerically found only very small effects, and by a more heuristic argument; that the multiple interactions are likely to be taking place slightly displaced from each other in space-time. Their "perturbative cross-talk" should therefore be suppressed by wave-function overlap factors, which mean they should only be able to emit coherently at rather small $p_\perp$ anyway. Compared to the usual perturbative subleading-colour ambiguities associated with parton shower Monte Carlos, this particular source of colour space ambiguity should therefore not represent any significant additional ambiguity *at the parton level*. The interleaved rescattering model of [121] is currently the only one to address emissions inside colour dipoles spanned *between* different MPI subsystems.

7.3.4. Non-perturbative aspects

Consider a hadron-hadron collision at a resolution scale of about 1 GeV. The system of coloured partons emerging from the short-distance phase (primary parton-parton interaction plus parton-level underlying event plus beam-remnant partons) must now undergo the transition to colourless hadrons.

In this context, it is useful to consider what happens to infrared safe, and infrared sensitive, observables separately. For infrared safe observables, such as energy flow and jet observables, the parton flow in phase space already gives quite a good approximation, and hadronization only gives small correc-

tions. (For precision studies, these must of course still be taken into account, see e.g. [122, 123].)

Infrared sensitive observables, on the other hand, such as individual hadron multiplicities and spectra are crucially dependent on the parton-parton correlations in colour space, and on the properties and parameters of the hadronization model used, pedagogical descriptions of which can be found in Section 8. Here, we concentrate on the specific issues connected with the structure of the underlying event in hadron collisions.

Keeping the short-distance parts unchanged, the colour structure *inside* each of the MPI systems is normally still described using just the ordinary leading-colour matrix-element and parton-shower machinery described in Sections 3 and 4. The crucial question, in the context of MPI, is then how colour is neutralized *between* different MPI systems, including also the remnants. Since these systems can lie at very different rapidities (the extreme case being the two opposite beam remnants), the strings or clusters spanned between them can have very large invariant masses (though normally low $p_\perp$), and give rise to large amounts of (soft) particle production. Indeed, in the context of soft-inclusive physics, it is precisely these "inter-system" clusters/strings which furnish the dominant particle production mechanism (cf. again Fig. 8), and hence their modelling is an essential part of the infrared physics description. For more on the physics of the string and cluster hadronization models, see Section 8.

On the left-hand side of Fig. 10 we give a simple sketch of what a $p\bar{p}$ collision containing two distinct parton-parton interactions might look like in (planar) colour space. The additional complications of parton showers and further MPI have been suppressed, so that we can focus entirely on the correlations *between* the two scatterings. Tracing the colour lines in this diagram and connecting each colour-connected parton pair in the final state by a dashed line results in the sketch shown to the right of the colour-flow diagram. In current hadronization models, each of these dashed lines would represent a string piece, or a cluster, as appropriate. The vertical axis roughly represents rapidity, with the beam-remnant partons at either extreme. The horizontal axis is intended to illustrate $p_\perp$. Thus, the $q'\bar{q}'$ pair from the primary parton-parton interaction (furthest to the left in the colour-flow diagram) are depicted at high $p_\perp$ and central rapidity, while the partons from the secondary interaction, $\bar{q}_{\mathrm{val}1}g$ are depicted at larger rapidities, with smaller transverse momenta.

The ambiguity in the colour correlations can be illustrated by comparing

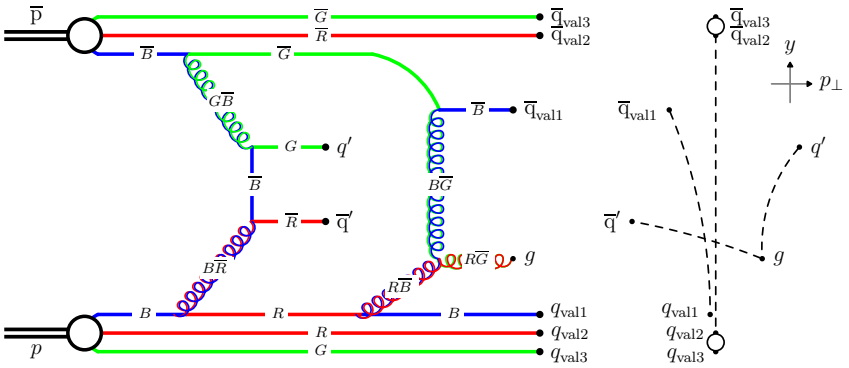

Figure 10: Left: example of colour assignments in a $p\bar{p}$ collision with two interactions. Explicit colour labels are shown on each propagator line. Right: The string/cluster topology resulting from the colour topology on the left, with horizontal and vertical axes illustrating transverse momentum and rapidity, respectively. On the right, the two undisturbed valence quarks in each of the beam remnant are represented as "diquarks" carrying the (anti-)baryon number of the original beam particles.

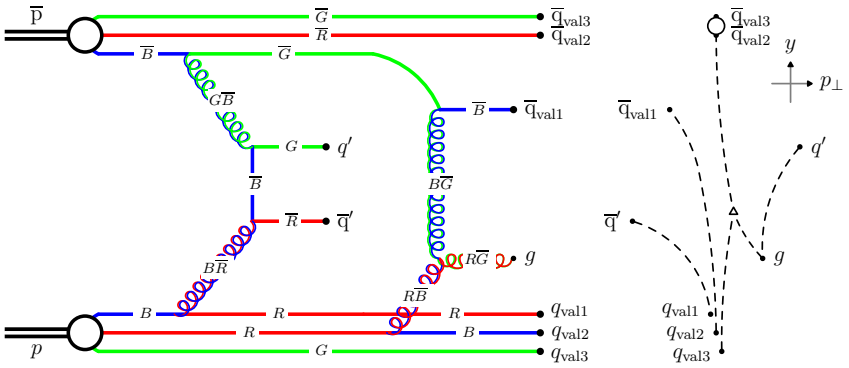

Figure 11: The same momentum and perturbative colour-flow configuration as in Fig. 10, but with the second gluon extracted from the proton now attached to a different quark line than that of the first gluon. The corresponding string topology reflects the change and now has become more complicated. The baryon number of the proton beam has been "liberated", as represented by the Δ symbol towards the middle of the diagram.

with Fig. 11 which shows exactly the same perturbative momentum and colour-space configuration, but now with the second gluon extracted from the proton attached to a different beam-remnant quark line than that of the first gluon. The corresponding string topology reflects the change and now has become more complicated. The baryon number of the proton beam has been "liberated", as represented by the Δ symbol towards the middle of the graph. As an aside, this also illustrates that the baryon number can migrate to the central region despite all the valence quarks remaining in the beam remnant; see [89] for an explicit Monte Carlo model of this effect. When adding more perturbative parton-parton interactions this ambiguity grows, and there appears to be very little one can say about it from perturbation theory.

In the HERWIG-based models the colour correlations are set up by first forcing the initiator of the primary parton-parton interaction to be a valence quark at low Q^2. The initiators of the subsequent MPI are then forced to be gluons, which are attached at random to the primary-interaction valence quark initiator. Since only one quark line is "disturbed" in this process, the beam baryon number remains in the remnant, with the two undisturbed valence quarks forming a "diquark" system (see Section 8).

In the old PYTHIA model the colour flow of the primary interaction is likewise taken as the basic skeleton onto which the underlying event interactions are added. In that model, the MPI final states can either be $q\bar{q}$ pairs, which form isolated single string pieces, or gg pairs, which either form a closed colour loop or are inserted to give kinks on the existing primary-interaction colour topology in a way that minimizes the total string length (equivalent to minimizing a measure of the classical potential energy). Again, since at most one quark in the beam remnant is directly "disturbed", the beam baryon number remains in the remnant. Empirically, the Tevatron data appear to prefer almost exclusively gg pairs that minimize the string length. This is indicative of very strong colour correlations between the MPI final states, although the model does not address the physical origin of them. (We return to this point below, under colour reconnections.)

In the new PYTHIA framework, described in [89], a more elaborate modelling of beam remnants was introduced, that allowed the tracing of colour flow in more detail and also allowed the beam baryon number to migrate away from the remnant. However, also in this modelling context, empirical comparisons to the Tevatron minimum bias data appear to require stronger colour correlations between the MPI final states than those naively generated

by the model.

This brings us from colour connections, to colour *reconnections*, which we shall discuss in the next section.

7.4. Colour reconnections

In a first study of colour rearrangements, Gustafson, Pettersson, and Zerwas (GPZ) [124] observed that, e.g. in hadronic WW events at LEP, colour interference effects and gluon exchanges may cause 'crosstalk' between the two W systems, leading e.g. to uncertainties in the W mass determination. In the GPZ picture, the corresponding changes occurred already at the perturbative QCD level, leading to predictions of quite large effects. Sjöstrand and Khoze (SK) [125, 126] subsequently argued against large perturbative effects and instead considered a non-perturbative scenario in which QCD strings can fuse or cut each other up (see e.g. [127]). These models resulted in effects much smaller than for GPZ, leading to a predicted total uncertainty on the W mass from this source of $\sigma_{M_W} < 40$ MeV.

Subsequently, several alternative models have been proposed, most notably by the Lund group, based on QCD dipoles [128–130], and by Webber based on clusters [131]. Apart from WW physics, colour reconnections have also been proposed to model rapidity gaps [132–135] and quarkonium production [136].

Experimental investigations of colour reconnections at LEP [137–140] were able to exclude at least the most dramatic scenarios, such as GPZ and extreme versions of SK with the recoupling strength parameter close to unity, but more moderate scenarios have not been excluded. Furthermore, in hadron collisions the initial state contains soft colour fields with wavelengths of order the confinement scale. The presence of such fields, unconstrained by LEP measurements, could impact in a non-trivial way the process of colour neutralization [132, 133]. And finally, the MPI produce an additional amount of displaced colour charges, translating to a larger density of hadronizing systems. It is not known to what extent the collective hadronization of such a system differs from a simple sum of independent systems, as will also be briefly mentioned in Section 8 on hadronization.

A new generation of colour-reconnection toy models have therefore been developed specifically with soft-inclusive and underlying event physics in mind [119, 141, 142], and also the cluster-based [131] and Generalized-Areal-Law [134] models have been revisited in that context. Although still quite crude, these models do appear to be able to describe significant features of

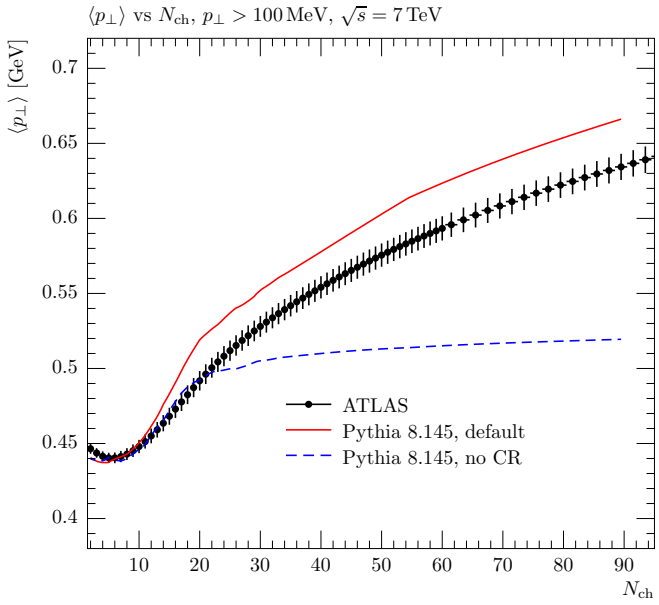

Figure 12: Models with and without colour reconnections compared to the $\langle p_\perp \rangle (N_{\rm ch})$ distribution measured by the ATLAS experiment [93], for particles with $p_\perp > 100$ MeV, $|\eta| < 2.5$, and $c\tau > 10$ mm, in events that contain at least two such particles.

the Tevatron and LHC data, such as the distribution of the mean $p_\perp$ of charged particles vs. the number of charged particles, $\langle p_\perp \rangle (N_{\rm ch})$. To illustrate this, we include in Fig. 12 a comparison between an ATLAS minimum bias measurement of the $\langle p_\perp \rangle (N_{\rm ch})$ distribution at 7 TeV and two Monte Carlo models, with and without colour reconnections switched on (curves labelled as "default" and "no CR", respectively). Without colour reconnections, the predicted $\langle p_\perp \rangle (N_{\rm ch})$ distributions appear to rise too slowly with $N_{\rm ch}$.

It is nonetheless clear that the details of the full fragmentation process in hadron-hadron collisions are still far from completely understood.

7.5. Diffraction and models based on pomerons

Essentially, the MPI-based models discussed above start from perturbatively calculable cross sections and attempt to extend these to low $p_\perp$ by a combination of resummations of soft perturbative effects and explicit modelling of non-perturbative effects.

It is also possible to start from a non-perturbative standpoint, using uni-

tarity to relate elastic and inelastic scattering processes through the optical theorem. In this language, the total cross section is driven by the exchange of "reggeons" and "pomerons" — colour-singlet fluctuations with leading $f\bar{f}$ and gg contents, respectively — with the latter dominating at high energies.

In this picture diffractive events originate from collisions between an effective flux of such (virtual) colour-singlet objects within the beam particles, leading to a characteristic spectrum that varies roughly like dM^2/M^2, with M the invariant mass of the diffractively excited system. (For multiple diffraction, the behaviour is a product of such factors.) An important modelling aspect is whether the pomerons are considered to have a substructure themselves. If so, partonic collisions between pomeron fluctuations can generate high-mass diffractive processes such as diffractive dijets and other hard central exclusive processes. If not, only the dM^2/M^2 spectrum is present.

Inelastic events are understood in terms of cut pomerons, which furnishes a relation between diffractive and non-diffractive scattering that is absent in the MPI-based models discussed above. The relation between MPI, diffraction, and pomerons is usefully discussed in [112].

Translated into the terminology used in this review, each cut pomeron corresponds to the exchange of a soft gluon, which results in two 'strings' being drawn between the two beam remnants. Uncut pomerons give virtual corrections that help preserve unitarity. A variable number of cut pomerons are allowed, which furnishes the equivalent of MPI in this language. However, note that cut pomerons were originally viewed as purely soft objects, and so generated only transverse momenta of order Λ_{QCD}, unlike the multiple interactions considered above. In DTUJET [143], PHOJET [144, 145] and DPMJET [146, 147], however, also hard interactions have been included, so that the picture now is one of both hard and soft pomerons, ideally with a smooth transition between the two. The three programs all make use of the Lund string hadronization description, however, and hence share the fundamental properties and ambiguities of this part of the modelling with the string-based MPI models discussed above.

7.6. Summary

- Several parton-parton interactions can occur within a single hadron-hadron collision. This is called multiple parton interactions (MPI).

- The hard perturbative tail of MPI is approximately proportional to $\mathrm{d}p_\perp^2/p_\perp^4$. This tail produces additional observable (pairs of) jets in the

underlying event. The oft repeated mantra that the underlying event is non-perturbative is thus a misconception.

- Most MPI *are* relatively soft, however, and do not lead to easily identifiable additional jets. Instead, they contribute to building up the total amount of scattered energy and cause colour exchanges between the remnants, thereby increasing the number of particles produced in the hadronization stage.

- Hadron-hadron collisions at small impact parameter have a higher number of MPI than peripheral ones. What the enhancement factor is depends on the shape of the hadron transverse mass distribution.

- A hadron-hadron collision with a large number of MPI has a higher probability of containing a hard jet than one with few MPI. This produces the "pedestal effect".

- The number of MPI is regulated by colour screening and saturation effects. The detailed behaviour of this regularization, including its dependence on collider centre-of-mass energy, is poorly known and represents one of the main uncertain / tunable aspects of the models.

- In addition to the MPI $2 \to 2$ scatterings, realistic models must also incorporate showers off the MPI, to describe the broadening and decorrelation of MPI jets.

- It is also possible to include perturbative rescattering effects, but this is so far not available in all models.

- At the non-perturbative level, the assumed structure of the beam remnant can be important, e.g. affecting the event structure at large rapidities and migration of the beam baryon number in rapidity.

- There are significant ambiguities concerning colour-space correlations, in particular *between* the various MPI systems. In current models some amount of *colour reconnections* appear to be necessary to properly describe minimum bias and underlying event data. This is probably the most poorly understood part of the modelling, however, and is associated with significant uncertainties.

- The distinction between the diffractive and non-diffractive components of the total inelastic hadron-hadron cross section is fundamentally ambiguous and must be interpreted with care, as discussed in Section 7.2. This issue is also discussed in Part III, there from the point of view of measurements.

- Diffractive processes are typically modelled as a separate class of processes driven by the exchange of so-called pomerons. These can be viewed either as purely soft objects or as having an internal partonic substructure. The latter provides a mechanism for generating high-mass diffractive processes such as diffractive dijets.

8. Hadronization

8.1. Definition and early developments

In the general context of QCD studies, the term "hadronization" has been used with somewhat different meanings. In the present context it refers to the specific model used in an event generator for the transition from the partonic "final" state to a complete representation of the actual hadronic final state. We should emphasize that this is a transition for which we still have only models, albeit inspired by QCD, because the only available rigorous approach to non-perturbative hadronic phenomena, lattice QCD, is formulated in Euclidean space-time and therefore cannot deal with inherently Minkowskian processes like the time-evolution of partons into hadrons.

Other "hadronization" meanings exist. When quantities that are calculable within perturbative QCD, for example hadronic event shapes in e^+e^- annihilation, are compared with experimental data, there are discrepancies that are commonly ascribed to "hadronization corrections". They are often estimated and corrected for by comparing the hadron-level prediction of an event generator with a parton-level result computed at the end of parton showering.[13] However, such a parton-level quantity is not really comparable to the result of a perturbative calculation, certainly not at fixed order, nor even when resummed to all orders, as the shower result depends on the scale and details of the cutoff that terminates it. The origin of the discrepancies is instead generic non-perturbative contributions that do not depend

[13]We strongly deprecate the correction of experimental data to "parton level" by this method. See Section 16 for discussion of this point.

on the detailed mechanism of hadron formation. They can be parameterized as power-suppressed terms related to the so-called infrared renormalon ambiguity of the perturbation series [148–151].

Another use of the term hadronization is to describe the parameterization of single-particle distributions from hard processes in terms of fragmentation functions – for recent reviews see [152, 153]. This is analogous to the parameterization of PDFs for incoming hadrons, and indeed similar factorization properties allow the scale dependence of the distributions to be predicted once they have been fitted at some scale, for example in e^+e^- annihilation. However once again such analyses do not illuminate the mechanism of hadron formation.

The earliest models for hadronic final states were based on isotropic or longitudinal phase space. On their own, these are mainly of interest at very low energies, and are not discussed further. The first model that points the way to current approaches is the Artru–Mennessier one [154], which manages to pioneer both string and cluster concepts. The code had a number of limitations, however, and never had a practical impact.

In contrast, the Field–Feynman model [155] a few years later kickstarted the whole field of hadronization studies by Monte Carlo simulation. It introduced an iterative recipe for the construction of realistic jets. By considering each outgoing parton separately, it became possible to write "independent fragmentation" generators for e^+e^- physics [156, 157].[14] These models soon became outdated since the independent fragmentation framework is not Lorentz invariant, is not safe under collinear emissions of partons, and also suffers from other deficiencies [158].

The two main hadronization classes in current use are the string and cluster ones. These are described in the following. The main difference is that the former transforms partonic systems directly into hadrons, while the latter employs an intermediate stage of cluster objects, with a typical mass scale of a few GeV.

[14] We note here that historically the terms "fragmentation" and "hadronization" have been used interchangeably, and we follow that usage in this Section, although in other contexts fragmentation can refer to the whole process of parton showering plus hadron formation.

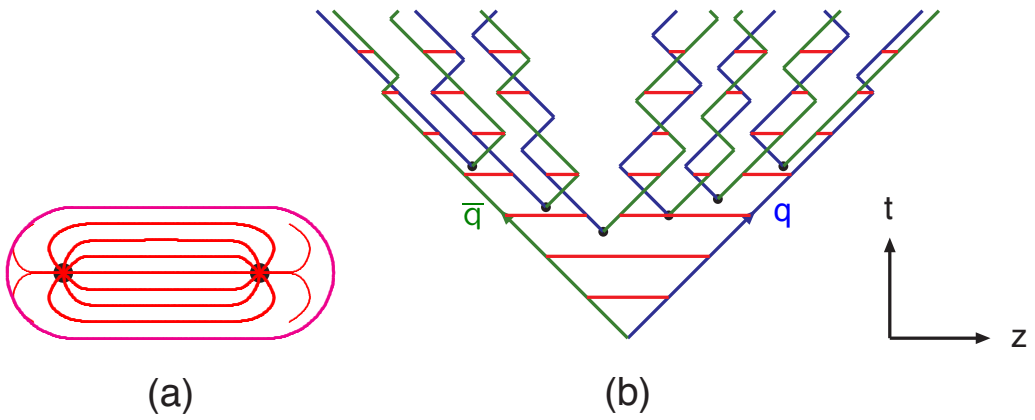

Figure 13: (a) A flux tube spanned between a quark and an antiquark. (b) The motion and breakup of a string system, with the two transverse degrees of freedom suppressed (diagonal lines are (anti)quarks, horizontal ones snapshots of the string field).

8.2. String model

An early string fragmentation model is that of Artru and Mennessier, introduced above. The most sophisticated and well-known string model is the Lund one, however. Its development began in 1977, followed by the first primitive Monte Carlo implementation in 1978. The core framework was complete by 1983 [159, 160]. Thereafter many different additions and alternatives have been studied, but only a few of them are available in the standard implementation in the PYTHIA event generator [161, 162]. It is this core Lund string framework that is presented here.

In QCD, a linear confinement is expected at large distances. This provides the starting point for the string model, most easily illustrated for the production of a back-to-back $q\overline{q}$ pair, e.g. in e^+e^- annihilation events. As the partons move apart, the physical picture is that of a colour flux tube being stretched between the q and the $\overline{q}$, Fig. 13a. The transverse dimensions of the tube are of typical hadronic sizes, roughly 1 fm. If the tube is assumed to be uniform along its length, this automatically leads to a confinement picture with a linearly rising potential, $V(r) = \kappa r$. From hadron mass spectroscopy the string constant κ, i.e. the amount of energy per unit length, is known to be $\kappa \approx 1$ GeV/fm ≈ 0.2 GeV^2.

This picture is also supported by lattice QCD calculations in the quenched approximation, i.e. with a gluonic field but no dynamical quarks. At small distances an additional Coulomb term is required, but the assumption of the

Lund model is that this term can be neglected in the overall production pattern of hadrons. Its influence would be felt in the properties of the individual hadrons, such as wave functions and masses, however.

In order to obtain a Lorentz covariant and causal description of the energy flow due to this linear confinement, the most straightforward approach is to use the dynamics of the massless relativistic string with no transverse degrees of freedom. The mathematical, one-dimensional string can be thought of as parameterizing the position of the axis of a cylindrically symmetric flux tube. The expression "massless" relativistic string is somewhat of a misnomer: κ effectively corresponds to a "mass density" along the string.

Now consider a simple $q\overline{q}$ two-parton event further. As the q and $\overline{q}$ move apart from the creation vertex, say along the $\pm z$ axis, the potential energy stored in the string increases, and the string may break by the production of a new $q'\overline{q}'$ pair, so that the system splits into two colour-singlet systems $q\overline{q}'$ and $q'\overline{q}$. These two systems move apart, and a widening no-field region opens up in between, Fig. 13b. For simplicity the quarks are shown as massless, so they move with the speed of light. If the invariant mass of either of these systems is large enough, further breaks may occur, and so on until only ordinary hadrons remain. Typically, a break occurs when the q and the $\overline{q}$ ends of a colour singlet system are 1–5 fm apart in the $q\overline{q}$ rest frame, but note that the higher-momentum particles at the outskirts of the system are appreciably Lorentz contracted.

At the end of the process, the string has broken by the creation of a set of new $q_i\overline{q}_i$ pairs, with i running from 1 to $n-1$ for a system that fragments into n primary hadrons (i.e. hadrons before secondary decays). Each hadron is formed by the quark from one break (or an endpoint) and the antiquark from an adjacent break: $q\overline{q}_1$, $q_1\overline{q}_2$, $q_2\overline{q}_3$, $\ldots$, $q_{n-1}\overline{q}$.

The space–time picture of string motion, e.g. in Fig. 13b, can be mapped onto a corresponding energy–momentum picture by noting that the constant string tension implies that the quarks obey

$$\left|\frac{\mathrm{d}E}{\mathrm{d}z}\right| = \left|\frac{\mathrm{d}p_z}{\mathrm{d}z}\right| = \left|\frac{\mathrm{d}E}{\mathrm{d}t}\right| = \left|\frac{\mathrm{d}p_z}{\mathrm{d}t}\right| = \kappa \ . \tag{51}$$

It follows that a hadron formed between vertices 1 and 2 has $E = \kappa\Delta z = \kappa(z_1 - z_2)$ and $p_z = \kappa\Delta t = \kappa(t_1 - t_2)$ [159]. The different breaks are spacelike separated, $(\Delta t)^2 - (\Delta z)^2 < 0$, i.e. they occur "independently" of each other in a causal sense. Nevertheless two adjacent breaks are constrained by the

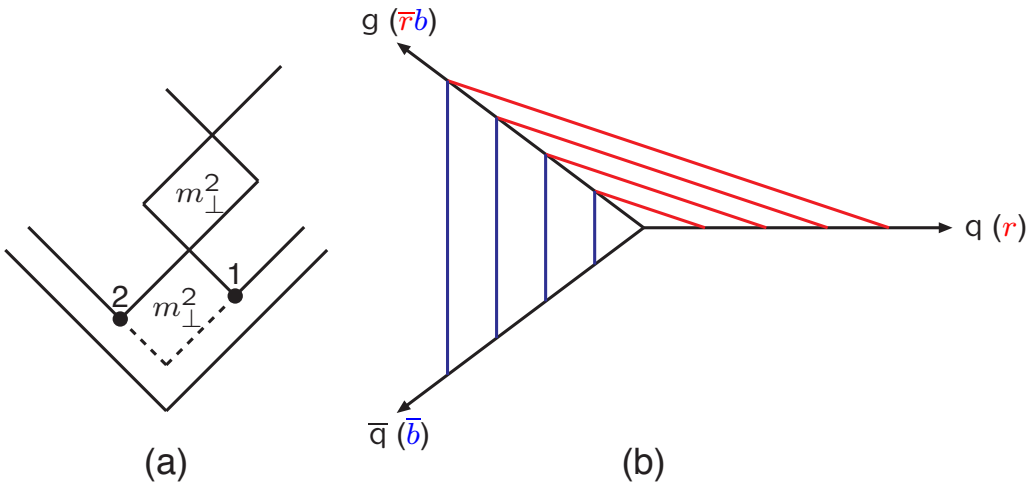

Figure 14: (a) conditions on nearby string breaks; (b) string motion in three-jet $q\overline{q}g$ events

fact that the string piece created by them has to be on the mass shell for the hadron being produced: $m_\perp^2 = m^2 + p_x^2 + p_y^2 = E^2 - p_z^2 = \kappa^2((\Delta z)^2 - (\Delta t)^2)$, Fig. 14a. Here transverse mass is introduced, since it is this quantity that becomes relevant for the (E, p_z) and (t, z) pictures, rather than normal mass, once transverse momentum fluctuations are introduced, see below. The total probability for an event to be formed can therefore be written as the product of $n-1$ breakup vertex probabilities times n delta functions for the (transverse) hadron masses.

Technically such an approach would be cumbersome. Fortunately an iterative procedure can be used to give the same result. Since there is no natural ordering, one is free to consider the breaks in any order. For instance, one can start at the q end of the system and iterate "left" towards the $\overline{q}$ end. Alternatively, one can start at the $\overline{q}$ end and iterate the other way, towards "right". Either approach should give the same overall answer, "left–right symmetry". Focusing on the production of a single hadron between vertices 1 and 2, Fig. 14a, the requirement reads $\mathcal{P}(1)\,\mathcal{P}(1 \to 2) = \mathcal{P}(2)\,\mathcal{P}(2 \to 1)$, where $\mathcal{P}(i)$ is the probability to reach vertex i by iteration from left/right and $\mathcal{P}(i \to j)$ the probability to take a step from vertex i to vertex j.

The solution to this equation can be written in terms of a fragmentation function $f(z)$, where z is the fraction of the remaining lightcone momentum

that the new hadron takes, with $E \pm p_z$ fraction for iteration to the left/right:

$$f(z) \propto \frac{1}{z}\,(1-z)^a\,\exp\left(-\frac{bm_\perp^2}{z}\right)\ , \tag{52}$$

where a and b are two free parameters (for the derivation see [163]).[15]

As a by-product, the derivation of $f(z)$ also gives the probability distribution in invariant time τ of $q'\overline{q}'$ breakup vertices. In terms of $\Gamma = (\kappa\tau)^2$, this distribution is $\mathrm{d}\mathcal{P}/\mathrm{d}\Gamma \propto \Gamma^a \exp(-b\Gamma)$, with the same a and b as above. In a given event, the connection between adjacent Γ values is given by the formula

$$\Gamma_2 = (1-z)\left(\Gamma_1 + \frac{m_\perp^2}{z}\right)\ , \tag{53}$$

where Γ_1 is the "old" and Γ_2 is the "new" value obtained after taking a step z for the production of a hadron with transverse mass $m_\perp$. The initial values at the q and $\overline{q}$ ends of the system are $\Gamma_0 = 0$. Note that $a = 0$ corresponds to a pure exponential decay as a function of the area swept out by the string, exactly as in the Artru–Mennessier model, but that correlations between adjacent Γ_i values is affected by the difference in mass spectra between the Lund and Artru–Mennessier models.

Heavy quarks, i.e. charm and bottom, are not produced at new string breaks (see below), but may be at the endpoints of a string. Unlike massless quarks, heavy quarks do not move along straight lines, which implies a changed area swept out by the string field. The argument of an exponential decay with area then leads to a modified shape [164]

$$f(z) \propto \frac{1}{z^{1+bm_Q^2}}\,(1-z)^a\,\exp\left(-\frac{bm_\perp^2}{z}\right)\ , \tag{54}$$

where m_Q is the heavy-quark mass.

The $f(z)$ formulae above, for the breakup of a system into a hadron and a remainder-system, strictly speaking only apply when the mass of the remainder-system is large. In a Monte Carlo program, it is therefore necessary to introduce a special procedure to cover the production of the last two particles. This contains no new physics, but has just to be constructed so

[15] A more complicated expression, with different a parameters for different flavours, is possible in principle, but only studied for baryon production.

that the place where one selects to "patch up" the fragmentation from the q end with that from the $\overline{q}$ one looks as closely like any other as is possible. In addition, steps are taken from the left and right ends of the system at random, so that the matching procedure is not applied at the same place in all events.

A related but different issue is what to do with a low-mass string, which occasionally may occur as part of an event with several separate strings. An attempt is then made to form an exclusive two-body state, with orientation preferentially along the string axis. If the string mass is too small for this to work, there is a possibility to let a small string collapse into one single hadron. To put this hadron on the mass shell, some shuffling of energy and momentum with other partons in the event is then necessary. This machinery thus has some similarities with the cluster fragmentation approach, but is in practice only used for a small fraction of the total particle production.

In a colour field a $q'\overline{q}'$ pair, where the q' and $\overline{q}'$ have no mass or transverse momentum, can classically be created in one point and then be pulled apart by the field. If the quarks have mass or transverse momentum, however, they must classically be produced at a certain distance so that the field energy between them can be transformed into the transverse mass $m_\perp$. Quantum mechanically, the quarks have to be created in one point and then must tunnel out to the classically allowed region. The production probability for this tunnelling process is proportional to

$$\exp(-\pi m_\perp^2/\kappa) = \exp(-\pi m^2/\kappa)\, \exp(-\pi p_\perp^2/\kappa)\ . \tag{55}$$

The factorization of the transverse-momentum and the mass terms leads to a flavour-independent Gaussian spectrum for the $q'\overline{q}'$ pairs. Since the string is assumed to have no transverse excitations, this $p_\perp$ is locally compensated between the quark and the antiquark of the pair, and $\langle p_{\perp q}^2 \rangle = \sigma^2 = \kappa/\pi \approx (250\ \mathrm{MeV})^2$. Experimentally a number closer to $\sigma^2 \approx (350\ \mathrm{MeV})^2$ is required, which could be explained as the additional effect of soft-gluon radiation below the shower cutoff scale. That radiation would have a non-Gaussian shape but, when combined with the ordinary fragmentation $p_\perp$, the overall shape is close to Gaussian, and is parameterized correspondingly in the program. Hadrons receive $p_\perp$ contributions from two $q'\overline{q}'$ pairs and have $\langle p_{\perp h}^2 \rangle = 2\sigma^2$.

The formula also implies a suppression of heavy quark production, $u : d : s : c \approx 1 : 1 : 0.3 : 10^{-11}$. Charm and heavier quarks hence are not expected

to be produced in the soft fragmentation. The suppression of $s\overline{s}$ production is left as a free parameter in the program, but the experimental value agrees qualitatively with theoretical prejudice.

A quark and an antiquark may combine to produce either a pseudoscalar or a vector meson. From counting the number of spin states one would expect the relative probability for pseudoscalar : vector to be 1 : 3. This should be modified by wave function effects, as manifested e.g. in the mass splitting between pseudoscalar and vector mesons, bringing the ratio closer to 1 : 1. The production of higher resonances is assumed to be low in a string framework. The four $L = 1$ multiplets are implemented, but are disabled by default, largely because several states are poorly known and thus may result in a worse overall description when included.

The simplest scheme for baryon production is that, in addition to quark–antiquark pairs, also antidiquark–diquark pairs are occasionally produced in the field, in a triplet–antitriplet representation. Such an assumption does not imply that a diquark should be considered as a single excitation of an elementary field, only that the soft chromoelectric field effectively acts on a diquark as if it were a single unit. Due to the large uncertainty in the definition of diquark masses, the tunnelling formula cannot be used directly to predict the expected rate of diquark production. Rather, from data a relative probability for diquark to quark production is determined to be $qq/q \approx 0.1$. Further parameters are needed to pin down the rates of individual diquarks, again for lack of well-defined diquark masses.

A more general framework for baryon production is the so-called popcorn model, in which diquarks as such are never produced, but rather baryons appear from the successive production of several $q'\overline{q}'$ pairs. Part of the time, the end result will be exactly the same $B\overline{B}$ situation as above, i.e. with an adjacent baryon B and antibaryon $\overline{B}$ sharing a diquark–antidiquark pair. However, further possibilities of the type $BM\overline{B}$, $BMM\overline{B}$, etc., can occur, where a varying number of mesons M are produced in between the baryon and antibaryon. The B and $\overline{B}$ then have just one $q'\overline{q}'$ pair in common, rather than two. In its present form, the program generates $B\overline{B}$ and $BM\overline{B}$ configurations with roughly equal probability, while $BMM\overline{B}$ and even longer meson chains are neglected.

A given quark–diquark pair may combine to produce either a spin 1/2 ("octet") or a spin 3/2 ("decuplet") baryon. Again higher resonances are neglected. A very important constraint is the fact that a baryon is a symmetric state of three quarks, neglecting the colour degree of freedom. When

a diquark and a quark are joined to form a baryon, it is therefore necessary to weight the different flavour and spin states by the probability that they form a symmetric three-quark system.

So far only the simplest possible system, $q\overline{q}$, has been considered. If several partons are moving apart from a common origin, the details of the string drawing become more complicated. For a $q\overline{q}g$ event, a string is stretched from the q end via the g to the $\overline{q}$ end, Fig. 14b, i.e. the gluon is an energy- and momentum-carrying kink on the string. It is assigned an incoherent sum of one colour charge and one anticolour one.

As a consequence of the gluon having two string pieces attached, the ratio of gluon/quark string forces becomes 2, a number that can be compared with the ratio of colour charge Casimir operators, $N_c/C_F = 2/(1 - 1/N_c^2) = 9/4$. In this, as in several other respects, the string model can therefore be viewed as a variant of QCD where the number of colours N_c is not 3 but infinite (cf. Section 2.2).

Note that the factor 2 above does not depend on the kinematical configuration: a smaller opening angle between two partons corresponds to a smaller string length drawn out per unit time, but also to an increased transverse velocity of the string piece, which gives an exactly compensating boost factor in the energy density per unit string length.

In an event with several gluons, these will still appear as kinks on the string between the q and $\overline{q}$ ends. It is also possible to have a closed gluon string, e.g. in $\Upsilon \to ggg$ decays.

One of the key predictions of the string model is that, in $q\overline{q}g$ events, the qg and $\overline{q}g$ angular regions should receive enhanced particle production, while the $q\overline{q}$ one should be depleted. This arises as a consequence of having fragmenting string pieces boosted into the former two regions, but not into the latter one. It was confirmed by JADE [165], which inspired the Leningrad study of perturbative coherence in such events [166]. It led to the picture of linked dipoles driving a perturbative evolution [51, 167], Section 4.7.

One of the key virtues of the string fragmentation approach is that it is collinear and infrared safe. That is, the emission of a collinear or soft gluon disturbs the overall string motion and fragmentation vanishingly little in the small-angle/energy limit [168]. Therefore the choice of lower cutoff scale for parton showers is not crucial: letting the shower evolve to smaller and smaller scales just adds smaller and smaller wrinkles on the string, which

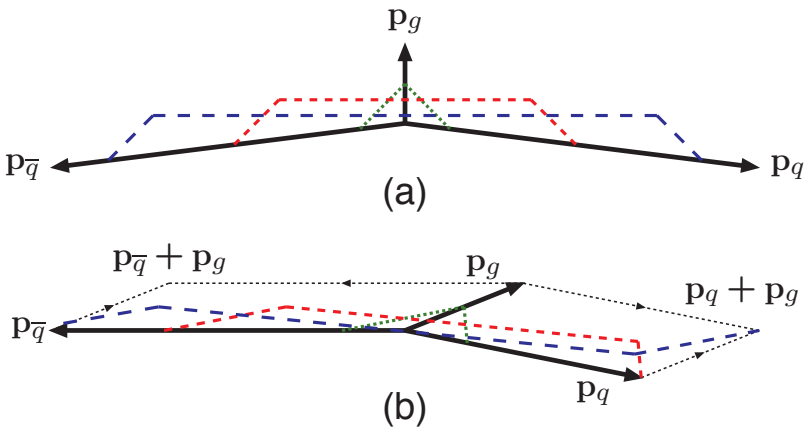

Figure 15: Snapshots in time of the string motion for (a) soft and (b) collinear gluon emission.

still maintains the same overall shape.[16]

To understand this point a bit better, consider the string motion without any fragmentation. A three-jet $q\overline{q}g$ event initially corresponds to having a string stretched from the q via the g to the $\overline{q}$, i.e. two string pieces, Fig. 14b. In the string piece between the g and the q ($\overline{q}$), g four-momentum is flowing towards the q ($\overline{q}$) end, and q ($\overline{q}$) four-momentum towards the g end. When the g has lost all its energy, the g four-momentum continues moving away from the middle, i.e. where the g used to be, and instead a third string region is formed there, consisting of inflowing q and $\overline{q}$ four-momentum.

For an energetic gluon it takes a long time for the gluon to lose its energy, and by then hadronization is already well under way. For a low-energy gluon, on the other hand, the third string region appears early, and the overall drawing of the string becomes fairly two-jetlike, Fig. 15a. In the limit of vanishing gluon energy, the two initial string regions disappear, and the ordinary two-jet event is recovered. Also for a collinear gluon, i.e. θ_{qg} (or $\theta_{\overline{q}g}$) small, the stretching becomes two-jetlike, Fig. 15b. In particular, the q string endpoint first moves out a distance $\mathbf{p}_q/\kappa$, and then a further distance $\mathbf{p}_g/\kappa$, a first half accreting gluon four-momentum and a second half re-emitting it. The end result is, approximately, that a string is drawn out as if there had

[16]In a generator implementation there are technical complications, however, and also an increasing time consumption, implying that it does not pay to take things to the extreme.

only been a single parton with energy $|\mathbf{p}_q + \mathbf{p}_g|$, such that the simple two-jet event again is recovered in the limit $\theta_{qg} \to 0$. These discussions for the three-jet case can be extended to the motion of a string with an arbitrary number of intermediate gluons.

The generalization of the left–right symmetry requirement to the fragmentation of multiparton configurations is not completely unique. A sensible physics ansatz is that the distribution in invariant time of breakup vertices should not depend on the exact shape of the string. The z variable no longer has any simple physical interpretation, but Eq. (52) and Eq. (53) taken together still provide a valid recipe for the relationship between adjacent Γ values. These Γ values themselves are always well defined and, if taken together with the constraint of hadrons being on mass shell, uniquely define the position of each breakup vertex.

Until now only the string model as such has been introduced. It is useful to briefly put it into the context of the generation of a complete event in hadronic collisions, a topic discussed in Section 7.3.4. String fragmentation is almost at the end of the generation chain, only followed by particle decays. It is applied when a number of partons have already been produced, by a combination of hard processes and parton showers, and with coloured left-over beam remnants. Since a remnant cannot be described by perturbative means, special rules are needed to assign colours to the individual partons in it, and to describe how the available remnant momentum is split between them. Some of these rules are based on common sense, such as that the average valence quark ought to carry more momentum than the sea one, but our ignorance also leads to some arbitrary decisions. With the remnant subdivided, and with colours traced in the large-N_c limit, the string topology can be constructed. The event that way can be split into a number of string systems. Mainly these will be open strings, with quarks or diquarks at the endpoints and with gluons in between, but closed gluon loops are also possible.

One special issue is that of baryon number flow if, say, (the colour of) two of the valence quarks of a proton are kicked out in different directions. For situations like these a three-quark system can be viewed as a Y-shaped topology: three strings, each with a quark at one endpoint, and at the other coming together in a junction. Each of the strings can break by the production of new $q'\overline{q}'$ pairs, but at the end of the process there will be one unmatched q' nearest to the junction in each string, and these three together give a baryon. Thus the baryon number is "carried" by the junction, and the

balance between the different string pieces pulling on the junction largely determines the net motion of this baryon [169]. Depending on the overall colour topology of an event it thereby becomes possible to transport the baryon number over large rapidity distances.

One potential weakness of the string model is that it is formulated in terms of the fragmentation of one single string in isolation, as you may expect it to be in e^+e^- annihilation events. If several strings are produced, they fragment independently of each other. For hadronic collisions the MPI framework is likely to lead to a picture where several strings overlap in space and time during the fragmentation process, however, especially at high collision energies. It is not unthinkable that this leads to collective phenomena bordering on those of the quark–gluon plasma expected in heavy-ion collisions, which then are not modelled by the standard string framework. For instance, a dense hadronic gas could lead to non-negligible rescattering corrections.

Finally, in addition to the basic ideas presented here, the string concept has been used as a starting point for various extensions, say for colour reconnections in W^+W^- events (see Section 7.3.4) or Bose–Einstein effects among identical mesons. Such effects are not included in simulations by default.

8.3. Cluster model

The cluster model of hadronization is based on the so-called preconfinement property of parton showers, discovered by Amati and Veneziano [170]. They showed that the colour structure of the shower at any evolution scale Q_0 is such that colour singlet combinations of partons (clusters) can be formed with an asymptotically universal invariant mass distribution. Here 'universal' means dependent only on Q_0 and the QCD scale Λ, and not on the scale Q or nature of the hard process initiating the shower, while 'asymptotically' means $Q \gg Q_0$. If in addition $Q_0 \gg \Lambda$, then the mass distribution of these colour singlet clusters, together with their (Q-dependent) momentum and multiplicity distributions, can be computed perturbatively [170, 171]. It turns out that the mass distribution is power-suppressed at large masses, the mean cluster multiplicity $\langle n \rangle$ rises faster than any positive power of $\ln Q$, and the asymptotic multiplicity distribution is a universal function of $n/\langle n \rangle$ (KNO scaling [172]).

The preconfinement mechanism can be seen most simply in the limit of a large number of colours N_c (cf. Section 2.2)[17]. To leading order in N_c,

[17]The proof of preconfinement is valid for any value of N_c. However, as in the string

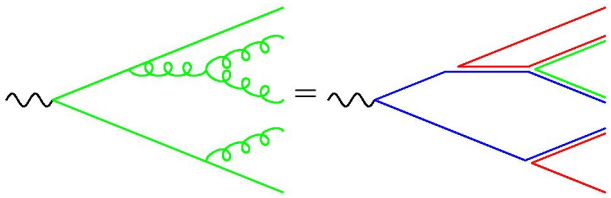

Figure 16: Colour structure of a parton shower to leading order in N_c.

the gluons in the shower can be represented by pairs of colour-anticolour lines that are connected at vertices (see Fig. 16). Then each colour line at the low-scale end of the shower is connected to an anticolour partner line at the same scale. In this limit the colour structure of the shower can be drawn on a plane, such that these colour-anticolour partners are adjacent. Adjacent partners can form colour singlets, whereas non-adjacent lines have a vanishing probability of doing so as $N_c \to \infty$. Furthermore, adjacency tends to imply closeness in phase space, leading to the suppression of large masses and an asymptotically universal mass distribution of adjacent objects.

A model of hadronization based on preconfinement was first proposed by Wolfram [173] and incorporated into an event generator for e^+e^- annihilation by Field, Fox and Wolfram [174, 175]. The key idea was to enforce non-perturbative splitting of gluons into quark-antiquark pairs at the shower cutoff scale Q_0. Then adjacent colour lines become quark-antiquark pairs that can form physical clusters with mesonic quantum numbers. For low values of the cutoff, the typical cluster invariant masses will be low and the hadrons from the decay of each cluster will be spread over a limited region of phase space. This leads naturally to a distribution of final-state hadrons closely connected to that of partons at the cutoff scale, i.e. to local parton-hadron duality [176, 177].

The enforced gluon splitting corresponds to an effective enhancement of the $g \to q\bar{q}$ vertex, which would be expected to reduce or even reverse the running of the QCD coupling at low scales. Thus this mechanism also agrees, at least qualitatively, with the notion of a finite effective low-scale value of α_S, which is suggested by studies of hadronization corrections to event shapes[150, 151, 178] and jet profiles [123].

model, subleading terms of order $1/N_c^2$ are neglected in the cluster hadronization model.

Another intriguing hint of enhanced gluon splitting is the high yield of soft photons in hadronic Z^0 decays [179, 180], which cannot be explained in terms of radiation from perturbatively produced quarks plus bremsstrahlung from initial-state leptons and final-state hadrons. This suggests a nonperturbative phase in which many charged particles are formed and propagate for significant times before hadronization, as might happen between gluon splitting and cluster formation.

Once the mechanism of gluon splitting has been adopted, a number of issues need to be addressed in building a quantitative model of hadronization. First of all, what should be the momentum distribution and flavours of the quarks produced in gluon splitting? The momentum distribution is not a major issue as long as the light flavours are treated as having constituent quark masses, $m_{u,d} \sim 300$ MeV, $m_s \sim 450$ MeV. Then the effective gluon mass at the end of showering, $m_g \sim Q_0 \sim 1$ GeV, is close to the threshold for splitting, and the kinematic range of quark momentum is too small for it to have much effect on the momenta and masses of the clusters.

On the other hand the flavour distribution in gluon splitting will clearly be important. At such low scales, kinematics will ensure that heavy flavours are forbidden and strangeness suppressed. However, these flavours can be pair-produced in cluster decays, as can baryon-antibaryon pairs. Baryons might also come from gluon splitting into light diquark-antidiquark pairs. Parameters can be introduced to tune the yields of different flavours, but generally the effects of kinematics work quite well as a first approximation.

The cluster mass distribution in e^+e^- annihilation into light-quark pairs, obtained from the HERWIG event generator, is shown in Fig. 17 for a wide range of centre-of-mass energies. One sees clearly the universality of the distribution and the typically low scale of cluster masses, determined by the shower cutoff, $Q_0 \sim 1$ GeV.

Once these clusters have been formed, how should they decay into the observed hadrons? The typical cluster masses are low enough for them to be treated as a smoothed-out spectrum of excited mesons, in which case quasi-two-body decay into less excited states seems to be preferred by Nature. Assuming that matrix element effects tend to average out, the simplest model is then to select at random among all two-body decay channels allowed by flavour and kinematics, with probabilities proportional to the available phase space for each, including spin degeneracy. The preference for decay directly to the lowest-mass states is somewhat offset by the larger number of spin states amongst excited hadrons. One must be careful to include full flavour

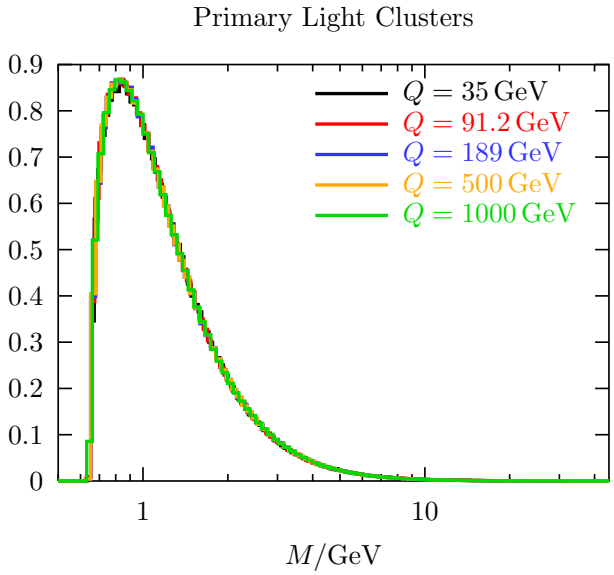

Figure 17: Invariant mass distribution of colour-singlet clusters in HERWIG.

multiplets of hadrons of each spin and parity, in order not to bias the flavour selection. This can entail some guesswork about the masses and decays of excited heavy-flavour hadrons that are not yet well established.

This basic model of cluster decay comes surprisingly close to fitting the hadron distributions observed in jet fragmentation, with virtually no free parameters other than the shower cutoff. The multiplicities of different flavours of mesons and baryons are determined by their masses and spins, and their transverse momenta relative to the jet axis are naturally limited by the phase space available in cluster decay. The characteristic differences between quark and gluon jets, with the latter having softer hadron spectra, higher multiplicities and wider profiles, all come from the higher rate of parton showering from gluons; apart from leading flavour effects, the relative proportions of different hadron species in all types of jets should be universal.

For a more refined description of hadronic final states, at the level demanded nowadays from event generators, the basic cluster model described above requires some adjustments. The sharp transition from perturbative to non-perturbative physics at the cutoff scale tends to over-suppress heavy states such as multiply-strange (e.g. Ω^-) and charmed baryons. A smoother transition over a range of scales would clearly be more physical. Light-

flavour baryon production comes mainly from the decay of mesonic clusters into baryon-antibaryon pairs. While this gives about the right multiplicities, it tends to produce pairs that are too closely correlated in rapidity. The requirement that each cluster should produce at least two hadrons leads to single-hadron distributions that are too low at high fractions of the jet momentum. This can be improved somewhat by allowing low-mass clusters to form a single hadron, transferring some four-momentum to a 'nearby' cluster. In reality the parton showering mechanism is not dominant at very high momentum fractions and more exclusive processes must take over.

A related problem is the treatment of high-mass clusters. Although the cluster mass distribution is mostly confined to low values, there is always a high-mass tail, as seen in Fig. 17, coming from events with very little parton showering. Again, exclusive hadron production would in fact predominate over these highly Sudakov-suppressed parton configurations. In the absence of such contributions, special treatment of high-mass clusters is required, as the model of isotropic phase-space decay is clearly unreasonable. The prescription commonly adopted is sequential binary fission, preserving the orientation along the axis defined by the constituent partons of the original cluster, until the sub-cluster masses fall below some value, typically $3-4$ GeV, after which the standard phase-space decay is resumed. The treatment of high-mass clusters thus becomes close to that of the string model, and indeed a smooth merging of the two models at intermediate cluster masses would seem well worth investigation.

The two cluster hadronization models in wide use [181, 182], incorporated in the Herwig and Sherpa generators respectively, differ in their detailed treatment of these issues but follow the basic approach outlined above. The reader is referred to the papers cited, the relevant sections below, and the generator manuals for further details.

An interesting recent development is the application of a statistical hadronization model to cluster decay [183]. In this way one may generate the spectra, multiplicities and flavour composition of the produced hadrons with few free parameters, while retaining the limited transverse momenta and jet structure which are difficult to explain if a statistical approach is applied directly to the whole final state.

As in the case of the string model, the basic cluster model does not include interaction between clusters, except for some momentum transfer to permit light ones to form single hadrons. There are optional schemes for colour reconnection between clusters, for example in W^+W^- hadronic decays, as

discussed in Section 7.3.4. There could be additional collective effects when the cluster density becomes high.

8.4. Summary

- Hadronization cannot be calculated from first principles, but has to be modelled. The two most commonly used model classes are the string and cluster ones.
- The string model is based on the assumption of linear confinement.
- A quark corresponds to an endpoint of a string, and a gluon to a kink on it, with partons ordered in colour along the string.
- The string offers a very predictive framework for how its space–time motion and breakup translates into an energy–momentum distribution of the primary hadrons. This framework also applies for complicated multiparton configurations, and has been successfully tested in e^+e^- collisions.
- The main (known) weakness of the string model is that there are many parameters related to flavour properties, which ultimately have to be pinned down from data itself.
- The cluster hadronization model is based on the preconfinement property of parton showers, which leads to colour-singlet parton clusters with a universal mass distribution at low scales.
- Cluster hadronization starts with non-perturbative splitting of gluons into quark-antiquark (and possibly diquark-antidiquark) pairs. Clusters are then formed from colour-connected pairs.
- Most clusters undergo quasi-two-body sequential phase-space decay. The limited cluster mass spectrum naturally leads to limited transverse momenta and suppression of heavy flavour, strangeness and baryon production.
- The decay of heavier clusters requires a more string-like initial stage of anisotropic decay into lighter clusters.

- When combined with angular-ordered parton showers, the cluster model gives a fairly good overall description of high-energy collider data, usually slightly less good than the string model but with fewer parameters.
- The busy environment of high-energy hadronic collisions could lead to nontrivial collective effects, currently not simulated either in string or in cluster models.

9. Hadron and tau decays

Following the hadronization phase of event generation a number of unstable hadrons are produced, which must be decayed into particles that are stable on collider timescales. This is an important part of the event simulation, because the observed final-state hadrons result from a convolution of hadronization and decay, so that a particular set of tuned hadronization parameters is applicable only in combination with a particular decay package.

Simulating hadron decays involves non-trivial modelling. At first glance it might seem that all the information needed to simulate these decays is readily available in the Particle Data Group (PDG)'s Review of Particle Physics [152], but the information on particle properties in the PDG is often insufficient and numerous choices have to be made. This is particularly true for members of excited meson multiplets, excited mesons containing heavy (bottom and charm) quarks, and baryons containing heavy quarks. The number of choices which have to be made increases as more excited meson and baryon multiplets are added to the simulation.

The first choice that must be made is which hadrons to include in the simulation. This choice is generator specific and is closely connected with the tuning of hadronization parameters. In the cluster model in particular it is important that all the light members[18] of a multiplet are included, as the absence of members can lead to isospin or $SU(3)$ flavour violation at an unphysical rate. All the general-purpose event generators include the lightest pseudoscalar, vector, scalar, even and odd charge conjugation pseudovector, and tensor multiplets of light mesons. In addition, some excited vector multiplets of light mesons are often included. Usually the mesons containing a single heavy quark, or heavy quarks with different flavours, from the same

[18]The hadrons containing only up, down and strange quarks.

multiplets are included, although particularly for bottom mesons the properties of the excited mesons are taken from theoretical models rather than the PDG. A large number of states containing $c\bar{c}$ or $b\bar{b}$ have been observed and usually most of these states are included in the simulation, with the exception of some recently discovered particles for which the quark model interpretation is unclear. While a large number of mesons are normally included, usually only the lightest octet, decuplet and singlet baryons are present, although both Herwig++ and Sherpa now include some heavier baryon multiplets. Although a number of baryons containing two heavy quarks have been observed these are not generally included in the standard generators as their production is rare.

Having selected the hadrons to use in the simulation, the choice of which decay modes to include and how to simulate them is closely related. Consider the example of the a_1 meson, which decays to three pions, $a_1 \to \pi\pi\pi$, where the dominant contribution takes place via an intermediate rho meson. If we choose to use a simple simulation without matrix element or off-shell effects, then this decay is best simulated as $a_1 \to \rho\pi$ followed by the decay of the rho meson to two pions. However, if a matrix element for the decay is included it is better to generate the three-body decay including the effect of the intermediate rho, and other suppressed contributions, in the matrix element for the decay.

Historically, the standard generators included few matrix elements for hadron decays and at best used a naïve Breit-Wigner smearing of the masses of the particles. More sophisticated simulation of hadronic decays was then performed using specialized external packages such as EvtGen [184] for hadron decays and TAUOLA [185–187] for tau decays. This still holds true for Pythia 8, while Herwig++ and Sherpa now include much better simulation of hadronic, and particularly tau lepton, decays. This was primarily motivated by the need to provide a better description of spin effects in tau decays. The perturbative production mechanism of the tau can have observable effects on its decay properties, which can be used to probe the properties of the Higgs boson and particles in BSM models. This is facilitated by using the same approach for both the perturbative and non-perturbative decays.

The decays of different types of hadron, and the tau lepton, are simulated in a variety of different ways. The light mesons and baryons which decay via the weak interaction typically have long lifetimes and therefore these decays do not need to be simulated in high energy collisions. The remaining strong and electromagnetic decays of the light mesons are normally simulated using

simple matrix elements based on parity and charge conjugation invariance. It is important that modes with relatively low branching ratios, for example pion Dalitz decay $\pi^0 \to e^+e^-\gamma$, are included as although they rarely occur for a single particle they can contribute significantly given the large rate for the production of light mesons.

The simulation of light baryon decays is often the most primitive part of the simulation, particularly in the external decay packages, as these were originally developed to simulate events at the B-factories, where baryons are rarely produced. The new hadron decay models have significant improvements for the simulation of baryon decays, typically using simple matrix elements based on the relevant conservation laws in the same way as for the light mesons.

While not a hadron, due to its mass the tau lepton primarily decays semi-leptonically to a tau neutrino and a small number of light mesons.[19] This can be simulated as the decay of the tau lepton to its associated neutrino and a virtual W boson. The matrix element can be written as

$$\mathcal{M} = \frac{G_F}{\sqrt{2}} L_\mu J^\mu, \qquad L_\mu = \bar{u}(p_{\nu_\tau})\,\gamma_\mu(1-\gamma_5)\,u(p_\tau), \tag{56}$$

where p_τ is the momentum of the τ and p_{ν_τ} is the momentum of the neutrino produced in the decay. The information on the decay products of the virtual W boson is contained in the hadronic current, J^μ. These currents are calculated either for low-energy effective theories or fits to experimental data. The currents for a large number of decays, from both modern theoretical models and experimental fits, are included in the most recent simulations of tau decay [185–189]. In some hadron decay models these currents are also used to simulate the weak decay of heavy mesons and baryons in the naïve factorization approximation [190, 191].

In recent years there has been a lot of interest in the decays of charm and, especially, bottom mesons motivated by the study of the CKM matrix and CP violation at the B-factories and the Tevatron. This has led to the development of detailed simulations, in particular the EvtGen package [184], for these decays. However, this package mainly concentrates on the simulation of B^0–$\overline{B}^0$ mixing and rare B-meson decays that are of interest for the

[19] The semi-leptonic branching ratio of the tau lepton is approximately 65% with the remaining 35% being fully leptonic decays.

study of CP violating phenomena.

While a large number of inclusive decay modes of the weakly decaying mesons containing a single charm or bottom quark have been observed, the branching ratios for these modes are insufficient to account for all the decays. The simulation of these decays therefore uses a combination of:

- a number of inclusive, generally low multiplicity, decays simulated using either a phase-space distribution, or matrix elements based on naïve factorization or experimental fits;
- partonic decays of the heavy quark, for example $b \to c\ell^-\bar{\nu}_\ell$, followed by the hadronization of the partonic final state including the spectator quark using the hadronization models described in Section 8 to simulate the remaining observed decay modes.

This approach for the simulation of heavy meson decays is sufficient in most collider physics applications. However, the simulation of the oscillations of B_d^0 and B_s^0 mesons and CP violation in B-meson mixing and decays are needed for both B-physics studies and some other applications that are sensitive to mixing phenomena.

Herwig++ and Pythia 8 include the oscillation of neutral B-mesons using the probability for the meson to oscillate into its antiparticle before it decays. Sherpa and EvtGen use a more sophisticated simulation including CP-violating effects and, for common decay modes of the neutral meson and its antiparticle, the interference between the direct decay and oscillation followed by decay.

While a number of decay modes of the weakly decaying charm baryons are known, very few weak decays of bottom baryons have been observed and, with the exception of the Λ_c^+, only ratios of the branching ratios are known. The simulation of the decays of the weakly decaying heavy baryons therefore uses a very small number of inclusive modes together with partonic decays for the majority of the decays.

A number of excited charm, and in the recent years, bottom mesons have been observed, although the properties of a number of the excited bottom mesons are uncertain. The strong and electromagnetic decays of excited bottom and charm mesons are normally treated in the same way as the decays of the light mesons, i.e. using simple matrix elements based on the relevant conservation laws.

While a number of charm baryons which decay via either electromagnetic or strong interactions have been observed, only the Σ_b and Σ_b^* bottom baryons, decaying via the electromagnetic and strong interactions respectively, have been observed. In general the baryons containing a single heavy quark required to complete the octet and decuplet baryon multiplets are included, although for many of the strongly decaying particles the masses and decay modes are based on theoretical models or the properties of the corresponding charmed baryons, rather than experimental results.

The decay rates of bottom- and charm-onium resonances to $\ell^+\ell^-$ and various partonic final states can be computed in terms of the quarkonium wavefunction, which is calculated in various models. As knowledge of the wavefunction is only needed to compute the width, which is taken from experimental results in event generators, the matrix elements can be used to simulate the decays of quarkonium states. In practice the simulation of the exclusive decays of these resonances is usually supplemented with the inclusion of a number of observed low multiplicity decay modes in a similar way as for weakly decaying charm and bottom hadrons.

EvtGen, Herwig++ and SHERPA include spin correlations between different decays in all hadron decays where matrix elements are used to calculate the distributions of the decay products, whereas PYTHIA 8 only includes correlations in certain decay chains. All the simulations include at least the generation of the masses of unstable particles according to the Breit-Wigner distribution, with improvements in some simulations for particles where new decay modes become kinematically accessible close to the particle's mass.

In summary:

- the simulation of hadron decays is based on a combination of experimental results and theoretically motivated assumptions which are required in order to generate exclusive events;
- the modern simulations of hadron decay are sophisticated, including matrix elements for many modes and spin correlations;
- given the close relationship between the hadron decay and hadronization models care should be taken when changing the hadron decay model, unless the hadronization parameters are retuned.

10. QED radiation

The simulation of electromagnetic radiation in general-purpose event generators uses one of two approaches. The most common is to use the same parton shower algorithm that was used for the simulation of QCD radiation. Indeed this is the preferred option for processes where the emission of both QCD and QED radiation is possible. The simulation of QED radiation proceeds in a similar way as for QCD radiation, with the evolution partner selected according to the charge, rather than the colour flow. This can cause problems in some processes where there are destructive contributions that would be suppressed by $1/N_c^2$ in QCD, but which are leading in QED. Despite these problems this is the most common approach in Monte Carlo simulations as both QED and QCD radiation can be generated at the same time. This interleaving of both types of radiation in one shower gives interesting phase space competition effects and could be used to shed light on the parton shower ordering variable[192].

An alternative to the parton shower is the Yennie-Frautschi-Suura (YFS) formalism [193] which proceeds by exponentiating the full eikonal distribution for soft photon emission, below a cut-off, together with the corresponding virtual corrections, given by the YFS form factor. In this approach, starting with the production of n particles, the cross section with the radiation of an additional n_γ photons can be written as

$$\begin{aligned}\sigma &= \frac{(2\pi)^4}{2\hat{s}}\prod_{i=1}^{n}\frac{\mathrm{d}^3 p_i}{(2\pi)^3 2p_i^0}|\overline{\mathcal{M}}|^2\delta^4\left(l_1+l_2-\sum_{i=1}^{n}p_i-\sum_{i=1}^{n_\gamma}k_i\right) \\ &\quad\times\sum_{n_\gamma=0}^{\infty}\frac{1}{n_\gamma!}\prod_{j=1}^{n_\gamma}\int\frac{\mathrm{d}^3 k_j}{k_j^0}\tilde{S}_{\mathrm{total}}(k_j)e^{Y_{\mathrm{total}}(\Omega)},\end{aligned} \tag{57}$$

where p_i are the momenta of the outgoing particles, k_i are those of the outgoing photons, l_i those of the incoming partons and $|\overline{\mathcal{M}}|^2$ is the spin summed/averaged matrix element for the leading-order process. The total dipole radiation function is

$$\tilde{S}_{\mathrm{total}}(k)=\sum_{i=0}^{n}\sum_{j=1,j>i}^{n}\frac{\alpha Z_i\theta_i Z_j\theta_j}{4\pi^2}\left(\frac{p_i}{p_i\cdot k}-\frac{p_j}{p_j\cdot k}\right)^2, \tag{58}$$

where $Z_{i,j}$ is the charge of the i,j^{th} particle in units of the positron charge

and $\theta_{i,j} = +1(-1)$ if the i, j^{th} particle is outgoing (incoming).

The total YFS form factor [193], $Y_{\text{total}}(\Omega)$, is a sum of contributions from pairs of charged particles:

$$Y_{\text{total}}(\Omega) = \sum_{i=0}^{n} \sum_{j>i}^{n} Y_{ij}(p_i, p_j, \Omega), \tag{59}$$

where Ω is used to symbolically indicate the dependence on the infrared cutoff on the photon energy. The YFS form factor for a pair of charged pairs is given by

$$Y_{ij}(p_i, p_j, \Omega) = 2\alpha \left(\mathcal{R}eB_{ij}(p_i, p_j) + \tilde{B}_{ij}(p_i, p_j, \Omega) \right). \tag{60}$$

The real emission piece, $\tilde{B}_{ij}$, is

$$\tilde{B}_{ij}(p_i, p_j, \Omega) = \frac{Z_i \theta_i Z_j \theta_j}{8\pi^2} \int_0^{|\mathbf{k}|<\omega} \frac{\mathrm{d}^3 k}{|\mathbf{k}|} \left(\frac{p_i}{k \cdot p_i} - \frac{p_j}{k \cdot p_j} \right)^2, \tag{61}$$

where ω is the upper limit on the photon energy. The virtual piece does not depend on the cutoff and is given by

$$B_{ij}(p_i, p_j) = -\frac{i Z_i \theta_i Z_j \theta_j}{8\pi^3} \int \mathrm{d}^4 k \frac{1}{k^2} \left(\frac{2p_i\theta_i - k}{k^2 - 2k \cdot p_i \theta_i} + \frac{2p_j\theta_j + k}{k^2 + 2k \cdot p_j \theta_j} \right)^2. \tag{62}$$

The standard technique to generating photons according to Eq. (57) works in two stages. First, the distribution is generated according to the leading-order result in which each photon is produced independently. A correction weight is then applied in order to give exactly the distribution in Eq. (57). The major advantage of this technique is that because the distribution used to generate the additional photons is known analytically, higher order corrections can be included exactly. It is this feature which allowed the construction of high precision Monte Carlo simulations for LEP physics [194–199] and is included in Sherpa for initial-state photon radiation in lepton collisions [200].

In the general-purpose event generators the parton shower approach is used in the majority of perturbative processes, where both QCD and QED radiation must be generated. However, both Herwig++ [201] and Sherpa [202] include the simulation of QED radiation using the YFS formalism in cases

where no QCD radiation is possible, i.e. for the leptonic decays of $W^{\pm}$ and Z^0 bosons, hadron and tau decays. In particular, the latter two applications simplify the decay tables considerably since many decay modes are produced by adding photons to simpler modes. In the previous generation of Monte Carlo simulations the production of QED radiation in particle decays was normally simulated using an interface to the PHOTOS program [203–205]. This program is based on the collinear approximation for the radiation of photons together with corrections to reproduce the correct result in the soft limit [203, 204]. Recently it has been improved to include the full next-to-leading order QED corrections for certain processes [205]. However, given the inherent problems with interfacing to external programs, the superior accuracy of the YFS formalism and the ability to systematically improve it, in Herwig++ and Sherpa the YFS approach is preferred.

In summary:

- QED radiation can be simulated using either a parton shower or YFS based approach;
- historically the parton shower approach has been more common in general-purpose event generators and is still used when both QED and QCD radiation is possible;
- both Herwig++ and Sherpa now use the YFS formalism for the simulation of QED radiation in particle decays.

11. BSM in general-purpose generators

We do not know what kind of physics beyond the Standard Model may be encountered at the LHC; if any is found, a variety of new physics models will need to be considered in order to determine its exact nature. Despite the large number of models, they can be split into two broad classes:[20]

1. models that contain either new effective operators which modify the cross sections and distributions for Standard Model processes, or only a few new particles which are generally produced as resonances, e.g. the ADD [208, 209] or Randall-Sundrum [210] extra-dimensional models;

[20] There are some scenarios such as Little Higgs [206, 207] and Leptoquark models which are intermediate between the two cases with only a small number of additional particles.

2. models that contain a large number of new particles, often new partners for each Standard Model particle, which can be produced in a variety of ways at the LHC and then decay, for example the Minimal Supersymmetric Standard Model (MSSM), Universal Extra Dimension models (UED) [211, 212] or Little Higgs models with T-parity [213, 214].

In general the first class of models are relatively simple to simulate with only minor changes to the Standard Model production processes that are present in all general purpose event generators. The simulation of the second class of models is more complicated. There are two approaches that have been adopted to simulate these models:

1. the production of the new heavy particles is simulated first, usually using a leading-order $2 \to 2$ scattering process, followed by the subsequent decay of the heavy particles, which often leads to long decay chains as the heavier BSM particles cascade decay into lighter ones;
2. a high multiplicity matrix element including all the final-state partons is used to simulate the process including the decays of any unstable heavy particles.

The first approach has the advantage of both computational simplicity and being able to easily simulate the fully inclusive BSM signal. However, while the second approach is more computationally expensive it has the advantage of correctly treating unstable intermediate particles and any correlation effects.

Methods have therefore been developed to allow all the correlation effects to be retained, in the approximation that only resonant diagrams are included and all interferences are neglected, while still simulating the production and decay of heavy particles separately [215–219]. Generally when using such methods the masses of the heavy particles are smeared using the Breit-Wigner distribution, although more sophisticated techniques have been developed [220]. Currently Herwig++ and Pythia 8 use the first of the above approaches, with Herwig++ using the methods of Refs. [219–221] to include spin correlations and off-shell effects. This also has the advantage that QCD radiation from new coloured particles can be simulated more easily. As Sherpa includes a sophisticated matrix element generator, it currently uses the second approach.

Historically models of new physics were implemented directly in the Monte Carlo event generators by hard coding the production and decay matrix elements. In recent years this has changed, with both Sherpa and Herwig++

using a method where the production processes and decays are automatically calculated from the Feynman rules, for arbitrary processes in SHERPA and for $2 \to 2$ scattering processes and $1 \to 2$ or 3 decays in Herwig++. It has also become increasingly common to use an external matrix element generator interfaced via the Les Houches Accord [222, 223] to simulate the hard scattering process. The most recent development is the FeynRules [224] package which can automatically calculate the Feynman rules in a given model from the Lagrangian in a form that can be used by a matrix element generator. SHERPA already uses this approach to allow a large range of models to be simulated and work is in progress to use it with Herwig++.

While in most cases models of new physics only require the simulation of the hard process, any subsequent decays, and the QCD radiation from the heavy particles, recently a number of more exotic models have been proposed where the nature of the new physics leads to changes in other parts of the Monte Carlo simulation. In general this occurs when the new model involves colour structures which do not occur in the Standard Model. Three situations have arisen.

Firstly, in R-parity violating SUSY models baryon number can be violated by a new operator which couples three particles in the fundamental, or anti-fundamental, representation of $SU(3)_C$ via the total antisymmetric tensor ϵ^{ijk}. This can be considered as a junction where three colour lines meet. This presents a problem both in the selection of the colour partners for the parton shower evolution and later in the hadronization stage. The simulation of these models, with the angular-ordered parton shower and cluster hadronization model [225, 226] and in the string model [169] (see Section 8.2), has been studied in detail with the selection of the colour partners for the perturbative radiation being done at random from among the potential partners, and after the shower a special treatment of three partons colour connected to the junction.

Secondly, in hidden valley models [227, 228] there are particles that are charged under a new strongly interacting gauge group. In these models, radiation of the gauge bosons of the new strong force by the new particle must be simulated both in the parton shower phase, as in [229], and in the subsequent hadronization.

Finally, some models have recently been proposed in which there are particles in representations of the $SU(3)_C$ group of the strong force other than those we know how to simulate (the fundamental and adjoint), for example particles in the sextet representation [230–232]. The simulation of

these particles is not currently possible in any of the general-purpose event generators.

In summary:

- most BSM models can be simulated either by incorporating changes to Standard Model production processes or by adding the production and decay of the new particles in the specific model;
- in general the production and decay of new particles are simulated separately in order to generate exclusive production processes;
- if new colour structures are present the parton shower and hadronization phases must also be modified.

Part II
Specific reviews of main generators

In this part we briefly review the MCnet event generators, referring back to Part I for the physics involved and the modelling options implemented in them. The first to be discussed, ARIADNE, has proved highly successful for e^+e^- and ep physics but is still under development for hadron-hadron collisions, as explained in Section 12. The next two, Herwig++ and PYTHIA 8, are new C++ generators based on earlier Fortran programs, while SHERPA is a wholly new C++ generator; all of these three are already extensively used for LHC physics, although still being actively improved as discussed in their respective Sections.

12. Ariadne

12.1. Introduction

The ARIADNE program [61] was the first parton shower generator to implement a dipole cascade. It uses the colour dipole model by Gustafson et al. [51, 167, 233], where gluon emissions are modelled as coherent radiation from two colour-connected partons.

For final-state radiation the ARIADNE cascade is rather similar to any other dipole-based cascade, such as the ones described in Sections 14 and 15. In e^+e^- annihilation into quarks, the first gluon emission is given by a dipole splitting function identical to the exact differential cross section for $e^+e^- \to q\bar{q}g$. Hence the matrix element matching described in Section 5.2.2 is automatically included. The next emission will then either come from the dipole between the quark and the gluon or from the dipole between the gluon and the antiquark, with a trivial generalization for subsequent emissions. The only difference in the subsequent emissions is the colour factors and the non-singular behaviour of the splitting functions, which in the soft and collinear limits coincide with the standard Altarelli–Parisi splitting functions in Eq. (12).

The recoils in the emissions are taken by both emitting partons in the radiating dipole. In this way all partons can be put on-shell in each step of the cascade. The way the recoils in the transverse direction are distributed between the radiating partons differs somewhat between different types of dipoles. For example in quark–gluon dipoles, the quark takes the full transverse recoil, so that the neighbouring dipole on the gluon side is minimally disturbed, while for a gluon–gluon dipole the transverse recoil is distributed so as to minimize the sum of the squared transverse momenta of the emitters. Apart from these recoils, all dipoles are treated independently.

The emissions are ordered (using appropriate Sudakov form factors) in a Lorentz-invariant transverse momentum defined as

$$p_\perp^2 = S_{\text{dip}}(1-x_1)(1-x_2), \tag{63}$$

where S_{dip} is the squared invariant mass of the dipole, and $x_i = 2E_i/\sqrt{S_{\text{dip}}}$ are the scaled energies of the partons after the emission in the dipole rest frame. The transverse momentum is also used as the scale in α_{s}. With an invariant definition of rapidity

$$y = \frac{1}{2}\ln\frac{1-x_1}{1-x_2} \tag{64}$$

it can easily be shown that the dipole splitting function is well approximated by $D(p_\perp, y) \propto dy\, d\ln p_\perp$, so apart from the running of α_{s}, the emission probability is essentially flat in the $(\ln p_\perp, y)$ plane, where the available phase space is given as an approximately triangular region, $\ln(p_{\perp\max}/p_\perp) \lesssim |y|$.

For final-state emissions, ARIADNE also includes the $g \to q\bar{q}$ splitting,

by simply dividing the normal Altarelli–Parisi splitting function between the two dipoles to which the gluon is connected [234].

12.2. Hadronic collisions

What makes ARIADNE truly unique is the handling of radiation in collisions where there are incoming hadrons. In a normal parton shower one would then apply a backwards evolution of initial-state splittings, and in more recent dipole shower implementations such as those in PYTHIA 8 and SHERPA (see Sections 14 and 15) dipoles are defined between e.g. incoming and outgoing partons in the hard interaction. The ARIADNE program, in contrast, uses the so-called Soft Radiation Model [233], where there are dipoles between the hadron remnants and the partons from the hard interactions.

Consider the process of deeply inelastic ep scattering. We can view it as a quark being kicked out of the proton by the virtual photon. The quark carries colour, while the corresponding anti-colour is continuing with the proton remnant down the beam pipe. From a semi-classical viewpoint we then would have a large dipole spanned between the struck quark and the proton remnant, and we could argue that this dipole would radiate gluons in the same way as a dipole between a q and $\bar{q}$ in an e^+e^--annihilation.

The difference between e^+e^- and ep is that in the former case the emitting $q\bar{q}$-pair is essentially point-like, while the proton remnant in the ep case is an extended object with about the same size as the proton itself. And, just as the emission of small-wavelength photons from an extended electric dipole antenna is suppressed, one can argue that high-$p_\perp$ emission of gluons in the proton direction should be suppressed [233]. In ARIADNE this is implemented by assuming that in any emission from a dipole connected to a hadron remnant, only a fraction

$$a = \left(\frac{\mu}{p_\perp}\right)^\alpha \tag{65}$$

of the remnant energy is available. Here μ is the inverse (transverse) size of the remnant (typically around 1 GeV), and α is a parameter related to the dimensionality of the remnant (1 would correspond to a string-like remnant, and 2 to a disc — the default value is 1). This gives a sharp cutoff in the phase space allowed for gluon radiation, but optionally also some emission outside this region is allowed with a power suppressed tail (in $p_\perp$).

One can relate this suppression to the ratios of parton densities which

enter the initial-state splittings in a conventional backward evolution shower (cf. Eq. (39)); however, especially in the remnant direction at small-x, the suppression in the ARIADNE case is much less severe. This shows up very distinctly in the case of forward jet rates at HERA (see e.g. [235]), where ARIADNE gives a much higher jet rate than conventional cascades, in better agreement with data. Comparing the Sudakov form factors one can see that the dipole shower in ARIADNE resums some large logarithms of $1/x$, similarly to what is done in BFKL evolution [236].

There is one additional peculiarity in ARIADNE related to the proton remnant. As only a part of the remnant takes part in the emission, only that part of it will receive a recoil. This means that there will be an extra gluon produced which is given some transverse momentum. This gluon will, however, also be suppressed by an additional Sudakov form factor corresponding to the probability that no standard emission would produce a higher $p_\perp$.

In e.g. W boson production in hadronic collisions, where there are no final-state coloured partons in the hard subprocess, the initial dipole will be spanned between the two remnants. In this case the recoil from emissions must also be shared with the W boson, which is done in a way described in [66].

As in the final-state cascade, the initial-state $g \to q\bar{q}$ splitting is not naturally described in terms of dipole radiation. Instead this is included as a standard backward-evolution step in a conventional initial-state shower. Also, the initial-state emission of a quark in a $q \to gq$ splitting may be included in the same way.

12.3. The ARIADNE *program and the LHC*

The ARIADNE program was initially written in Fortran, to be run together with the Fortran version of PYTHIA, simply replacing the PYTHIA parton shower with the dipole cascade. In principle it can be used to generate LHC events, but some care must be taken when generating processes with incoming gluons, such as Higgs production, since the initial-state emission of quarks in the $q \to gq$ splitting mentioned above was not implemented in the Fortran version.

The ARIADNE program is currently being rewritten in C++ using the THEPEG framework [237] (see section Section 13.2) and should soon be publicly available for generating dipole cascades for any Standard Model process. The aim is that it then will also be easily merged with matrix element generators using the CKKW-L algorithm (see Section 5.3). Possibly

it will also include NLO-merging (see Section 5.4), but this is conditional on whether the concept of recoil gluons, described briefly above, can be reformulated in a way that is compatible with a proper α_s expansion of the dipole emissions.

Finally it should be noted that the C++ version of ARIADNE is also used in conjunction with a new initial-state evolution model [238–240] based on Mueller's dipole evolution [241–243] formulated in impact-parameter space. The new program, called DIPSY [244] is mainly intended to generate soft QCD events, and can do so for both hadron collisions and heavy ion collisions.

13. Herwig++ and ThePEG

13.1. Introduction

Historically, Herwig++ is based on the event generator HERWIG (Hadron Emission Reactions With Interfering Gluons), which was first published in 1986 [39] and was developed throughout the era of LEP, with the latest major release version 6.5.10 [245, 246] in 2005[21]. From the beginning it has featured angular ordered parton showers to take colour coherence effects into account. The cluster hadronization model it uses (Section 8.3) was developed at the same time.

HERWIG was written in Fortran, but with the advent of the LHC it was decided to freeze its development and develop a new generator, with the same strengths as the old program, in C++. The idea was to not just rewrite the generator but to introduce physics improvements whenever they seemed necessary and feasible. The new generator, Herwig++, was first released only for e^+e^- annihilation in 2003 [247]. Since then it was further developed into a complete event generator for collider physics [248], with the current version 2.4.2 released in 2009. The code and its physics features are fully documented in the main reference [249], which will be updated as the code develops continually. Some distinctive physics features of Herwig++ are:

- Automatic generation of hard processes and decays with full spin correlations for many BSM models.
- Matching of many hard processes at NLO with the POWHEG method built in.

[21] Version 6.5.20, released in 2010, contains bug fixes.

- Angular ordered parton showers.
- Cluster hadronization.
- Sophisticated hadronic decay models, particularly for bottom hadrons and τ leptons.
- Hard and soft multiple partonic interactions to model the underlying event and soft inclusive interactions.

We will describe the most important details of the physics models in the remainder of this section.

13.2. ThePEG

Herwig++ is distributed as a comprehensive collection of plugin modules to ThePEG, the Toolkit for High Energy Physics Event Generation [237]. ThePEG provides all the infrastructure that is necessary to construct an event generator, handling e.g. random number generation, the event record, tuneable parameter settings, and most importantly, a mechanism to plug in physics implementations for all steps of event generation. Herwig++ provides such a set of plugins and comes with several complete generator setups for e^+e^-, ep and hadron-hadron collisions.

ThePEG's core component is the Repository, which holds the relations between all the different modules involved in a generator run and their tuneable parameter settings. It can be controlled through a simple command language in plain text, which is used to set up the modules involved in a generator run. Using such files at run time, the user can override any of the default parameters that Herwig++ comes with; no recompilations are necessary to change parameters, or to switch between physics models, different matrix elements or analyses.

ThePEG provides a reader for the Les Houches Accord event format [223] to read in parton-level events for further processing, an output module for HepMC events [250], as well as a native interface to Rivet [251], which avoids the overhead of having to pipe events through text files. Additionally, ThePEG can be linked to LHAPDF [13] to get direct access to any PDF sets that are available there.

The repository plugin structure allows for easy inclusion of user-defined modules. Any C++ object that inherits from the respective base classes in ThePEG can be used transparently in addition to, or instead of, one of

the default plugins. Any user code can be loaded at runtime as dynamically linked libraries. This allows modification of the program's behaviour without having to recompile the main program or needing to edit the core libraries. They can therefore always be installed centrally, possibly as part of a larger framework.

13.3. Hard processes

Three main mechanisms for simulating hard processes are available in Herwig++. First, there is a large set of hand-coded matrix elements for the most common subprocesses for hadron, lepton and DIS collisions. They are written using a reimplementation of the HELAS helicity amplitude formalism [252], which allows the spin correlations to be carried forward to the remaining event simulation consistently. Second, Herwig++ also contains a generic matrix element calculator for $2 \to 2$ processes, mainly used for BSM physics, which automatically determines the permitted diagrams for a set of given external legs from a list of active vertices. The third source of hard subprocesses is ThePEG's Les Houches reader, which allows parton-level events with any number of legs to be read from external sources.

For several processes, Herwig++ incorporates the full NLO corrections in the parton shower [253–255] using the POWHEG formalism (Section 5.2.3). An implementation of the CKKW merging scheme for tree-level multi-jet events (Section 5.3) will be included in an upcoming release [76].

13.4. BSM physics

The simulation of BSM physics in Herwig++ [220, 221] makes extensive use of ThePEG's plugin architecture. Each model is implemented in a model class, which holds the relevant new parameters, and a list of Feynman rules for its vertices. Based on this information, all possible production and decay matrix elements with up to four external legs are constructed and can be selected in the text-based input files. Herwig++ currently provides models to simulate processes in the MSSM [256, 257] and NMSSM [258] scenarios with an SLHA [259, 260] file reader to provide the relevant parameters, a model for universal extra dimensions [211, 261], an implementation of Randall-Sundrum [210] and ADD-type gravitons [208, 209], as well as a model of transplanckian scattering [262].

The production and decay matrix elements are all calculated using helicity amplitude techniques so that spin correlations between the production and decay of unstable particles can be generated using the approach of [219], as

described in Section 11. This ensures that Herwig++ can generate the spin correlations for individual decay chains in a computationally efficient way, while still allowing the simulation of inclusive BSM signals. The efficiency comes at the expense of neglecting interference effects with other decay chains leading to the same final state. Off-shell effects – including the suppression of decay modes close to threshold – are simulated using the approach of [220], which includes the running width of the unstable particle in the denominator of the Breit-Wigner propagator and in the calculation of the production matrix element for the particle.

13.5. Parton showering

The parton shower in Herwig++ is based on a new evolution variable $\tilde{q}$ [263], motivated from the branching of gluons off heavy quarks [20]. This is one of the possible choices in Eq. (10). As in HERWIG, the evolution in this variable ensures the angular ordering of parton shower emissions, to take colour coherence effects into account (see Section 4.5). In addition to the treatment of mass effects in the splitting functions and the showering of coloured particles in BSM models, the shower differs from HERWIG's implementation in the way it fills the available phase space for emissions. Considering only the first gluon emission from a $q\bar{q}$ pair, the new variable fills the soft gluon emission region of phase space without any overlap between the parton showers.

A so-called dead region is still present in the phase space, as in HERWIG, but is filled by either a hard matrix element correction or by higher order emissions. Potential discontinuities in the emission phase space at the transition from the parton shower to the hard emission region are avoided by applying a so-called soft matrix element correction: the emission rates in the parton shower overestimate the rates one would obtain from a full matrix element calculation. For each parton shower emission, the overestimated rate is then corrected down to the matrix element by a veto (see Appendix A.3) which reflects the relative emission probability between parton shower and matrix element, respectively. In Herwig++ there are matrix element corrections for $e^+e^- \to q\bar{q}$, Drell-Yan production of vector bosons in hadronic collisions, $gg \to h^0$ and for top decays. In order to fill the phase space smoothly, it should be noted that the starting scales of the parton shower are adjusted to the values that are given by the requirement of colour coherence, see Eq. (19). In Herwig++, these initial conditions cannot be altered,

e.g. by raising the initial evolution scale. Before the parton shower generates emissions, all heavy unstable particles in the partonic final state, which typically have a very narrow width, are decayed. All intermediate coloured lines are then also showered. These decays are done for the Higgs particle, electroweak gauge bosons, top quarks, and also e.g. supersymmetric particles (see Section 13.4).

13.6. Multiple parton interactions and beam remnants

The default model for the simulation of underlying event physics is a model for multiple partonic interactions [103]. Both hard and soft multiple partonic interactions are taken into account. The hard interactions are modelled as hard QCD $2 \to 2$ scatters with a transverse momentum above the cutoff value $p_\perp^{\min}$. The hard scattering centres are thought to be spatially distributed within the proton similarly to the charge, as measured in elastic electron–proton scattering, leading to the dipole form factor. However, a different width for the distribution of colour charges, quarks and gluons, parameterized by the inverse radius μ^2, is allowed. In the region $0 < p_\perp < p_\perp^{\min}$, soft scatters are generated with a transverse momentum distribution that has a Gaussian form, has an integral given by the soft parton-parton cross section, and is continuously matched with the perturbative distribution at $p_\perp = p_\perp^{\min}$ [116]. These constraints are sufficient to uniquely specify this distribution. The soft partons' longitudinal momentum distribution is taken to be like that of the low-energy sea, i.e. $xf(x) \approx$ flat. The spatial distribution of soft colour charges, given by a parameter μ^2_{soft}, is allowed to be different from the hard ones as otherwise it was not possible to obtain a model that is consistent with Tevatron data on multiple scattering [99]. The soft cross section and μ^2_{soft} are fixed from measurements of the total cross section and the elastic slope parameter, if available, or parameterizations of them otherwise.

After initial studies, good agreement with Tevatron underlying event measurements from Run I and II were found [103]. With the availability of first LHC data, e.g [93, 264] it became clear that the model suffered from the lack of a colour reconnection mechanism, which will be included in an upcoming release. It gives a very satisfactory description of these hard underlying event data.

13.7. Hadronization

Herwig++ uses the cluster hadronization model, described in Section 8.3. Its first step is a non-perturbative gluon splitting, where each gluon splits

isotropically in its rest frame into a $q\bar{q}$ pair of one of the three lightest flavours. We stress that at this stage all partons are treated as non-perturbative objects and acquire a constituent mass. The value of the gluon mass in particular is one of the important model parameters. After cluster formation we are left with a small number of heavier clusters of mass M, that will fission in binary sequential decays, whenever the condition

$$M^p \geq M_{\max}^p + (m_1 + m_2)^p \tag{66}$$

is fulfilled, where $m_{1,2}$ are the masses of the constituent partons of the cluster and $M_{\max}$ and p are the main parameters of the cluster hadronization model, chosen independently for light, charmed and bottom clusters. Once a cluster is split, a new particle-antiparticle pair of quarks or diquarks is taken out of the vacuum, chosen with adjustable weights. The kinematics of the new clusters preserve the original directions of the constituent particles and depend on whether they contain a perturbative parton or a beam remnant. Once clusters fall below the limit of Eq. (66), they decay isotropically in their rest frames into pairs of hadrons. The hadron species are determined according to available phase space and phenomenological weights for flavour multiplets. As heavier baryons tend to be suppressed in this approach [265], the choice between a baryonic or non-baryonic decay is made before the hadron species are selected. In some cases clusters will turn out to be too light to decay into a pair of hadrons; they will decay into a single light particle instead and share some momentum with a cluster close by in spacetime. For any cluster that contains a parton from the original hard process, e.g. a bottom quark, the resulting heavy meson retains the original parton direction in the cluster rest frame, up to some Gaussian smearing.

In addition to the hadronization of partonic final states, the implementation of the model in Herwig++ can also handle stable coloured particles or baryon number violating vertices, which both occur in BSM models.

As with all tuneable parameters, a detailed list and description can be found in the manual [249].

13.8. Hadron decays and QED radiation

The decays of both fundamental particles and unstable hadrons in Herwig++ are modelled in the same framework, using either a general matrix element based on the spin structure of the decay, or with a specific matrix element for important decay modes, with a particular emphasis on baryon decays.

This allows for a sophisticated treatment of off-shell effects, the treatment of excited baryonic multiplets, and for example the easy integration of the semileptonic τ lepton decays [188]. Spin correlation effects are included fully for the decays of all unstable particles [219] and are consistent with the preceding stages of event generation all the way back to the production matrix element. QED radiation in decays is simulated using the YFS formalism [201] (see Section 10). All the decay matrix elements have been extensively tested against external packages where available, and are in full agreement.

The particle properties such as masses, widths, lifetimes, decay modes and branching ratios that are used in Herwig++ can be found in the online interface to its database of particle properties at

`http://www.ippp.dur.ac.uk/~richardn/particles/`

13.9. Outlook

Herwig++ in its current version (2.4.2) is superior to its Fortran predecessor in almost all aspects of physics simulation and is the recommended version for new studies. Once this is true without any exceptions the version number will move to 3.0. The program package, together with ThePEG can be found at

`http://projects.hepforge.org/herwig/`

14. Pythia 8

14.1. Introduction

Pythia is a general-purpose event generator. It has been used extensively for e^+e^-, ep and $pp/p\overline{p}$ physics, e.g. at LEP, HERA and the Tevatron, and during the last 20 years has probably been the most used generator for LHC physics studies. As a building block it has also been used in heavy-ion physics and cosmic-ray physics.

The history of the Lund family of event generators began with Jetset [266–269] in 1978, which later was merged into Pythia [161, 270–274]. Over the years many new physics models, especially for perturbative and nonperturbative QCD, have been developed and tested in parallel with the respective code. Thus the Pythia 6 generator is the product of over thirty years of progress, but some of the code has not been touched in a very long time. New options have been added, but old ones seldom removed. The basic

structure has been expanded in different directions, well beyond what it was once intended for, making it rather cumbersome by now.

From the outset, all code was written in Fortran 77. For the LHC era, the experimental community made the decision to discontinue Fortran and move heavy computing to C++. Therefore it was logical also to migrate PYTHIA to C++, and in the process clean up and modernize various aspects. A first attempt in this direction was the PYTHIA 7 project [275, 276], however, early on this was redirected to become a generic administrative structure, and renamed THEPEG (see Section 13.2).

PYTHIA 8 is a clean new start, to provide a successor to PYTHIA 6. It is a completely standalone generator, but several optional hooks for links to other programs are provided. Work on it began in 2004, and the first fully operational version (8.100) was released in 2007 [162]. It is not yet as well tested and tuned as PYTHIA 6, and therefore not as much used, although a slow shift is underway. Since priority has been to be ready in time for LHC startup, some topics have not yet been addressed. Other parts of the PYTHIA 6 were deemed obsolete and are permanently dropped.

Here follows a very brief summary of the current PYTHIA 8.1 program. Much of the physics is the same as documented in the PYTHIA 6.4 manual [161] and the literature quoted there, with some relevant later updates [88, 121, 229, 277–279]. A complete manual also comes with the code distribution.

The physics summary below is split into core processes, the further perturbative evolution, and hadronization. An introduction to the code structure completes this outline.

14.2. Hard processes

Currently the program is only set up to handle collisions either between hadrons, such as p, $\overline{p}$, $\pi^{\pm}$ and π^0, or between same-generation leptons. That is, pp, $p\overline{p}$ and e^+e^- beam combinations can be used, but currently not ep, γp or $\gamma\gamma$.

PYTHIA contains an extensive list of hardcoded subprocesses, over 200, that can be switched on individually. These are mainly $2 \to 1$ and $2 \to 2$, some $2 \to 3$, but no multiplicities higher than that. Consecutive resonance decays may of course lead to more final-state particles, as will parton showers. A brief summary of the main sets of subprocesses is as follows:

- hard QCD processes, giving two high-$p_\perp$ partons;
- t-channel exchange of a γ^*/Z^0 or $W^{\pm}$, also giving two high-$p_\perp$ partons;

- prompt-photon production with one or two photons in the final state;
- a single γ^*/Z^0 or $W^\pm$ gauge boson, a pair of gauge bosons, or a gauge boson together with a parton;
- charmonium and bottomonium in the colour singlet and octet models;
- top and a hypothetical heavy fourth generation;
- Higgses within and beyond the Standard Model;
- Supersymmetry (in progress); and
- other exotic physics with new gauge bosons, left–right symmetry, leptoquarks, excited fermions, hidden valleys, or extra dimensions.

The subprocess cross sections have to be convoluted with PDFs to obtain the event rates. Several proton PDFs are hardcoded in Pythia for ease of use and speed. These include

- traditional LO sets such as GRV 94L, CTEQ 5L, 6L and 6L1, and MSTW 2008 LO;
- the newer-style Monte-Carlo-adapted modified LO sets MRST LO* and LO**, and CT09 MC1, MC2 and MCS; and
- two central members of NLO sets, namely MSTW 2008 NLO and CTEQ 66.00;

see Section 6. Further sets are available through an interface to the LHAPDF library. It is possible to use separate PDF sets for the hard interaction, on one hand, and for the subsequent showers and MPIs, on the other. Specifically, NLO sets are only intended to be used for hard subprocesses.

Obviously this list is far from complete, in terms of what will be required at the LHC. Furthermore Pythia does not have automatic code generation for new processes, unlike some other generators. The intention is that Pythia should be open to external input to the largest extent possible, however. That way specialists from many areas can contribute hard subprocesses, which thereafter are handled further by the normal Pythia machinery.

- If an external program can generate a Les Houches Event File [223], this can easily be read in by PYTHIA. A large number of programs can do just that. This includes general-purpose matrix-element programs, such as MadGraph or CompHep/CalcHep, and ready-made collections of processes, such as ALPGEN or AcerMC, see Section 3. It also includes several processes implemented in the POWHEG approach to NLO calculations, see Section 5.

- It is also possible to have a runtime link to C++ or Fortran programs, using the Les Houches Accord [222] structure to transfer information between the programs.

- You can implement your own hard process inside a class derived from a PYTHIA base class, send in a pointer to it, and then let PYTHIA handle the generation exactly as if it were an internal process. Notably MadGraph 5 will provide a facility whereby the complete code for such a class can be written automatically, ready to be linked.

PYTHIA is also open to input from other sources, such as the SUSY Les Houches Accord [259, 260].

14.3. Soft processes

The so-called soft processes are elastic, single and double diffractive, and nondiffractive, see Section 7.2. Together they are intended to offer an inclusive description of the total pp cross section, with the exception of some of the rare (and even hypothetical) processes that are better simulated separately. Thus the inelastic event sample includes high-$p_\perp$ physics as a tail of the low-$p_\perp$ one, in a consistent way, as provided by the MPI framework. To be precise, "soft" events contain an inclusive production of standard QCD $2 \to 2$ processes, prompt photons, charmonia and bottomonia, low-mass Drell-Yan pairs, and t-channel $\gamma^*/\mathrm{Z}^0/\mathrm{W}^\pm$ exchange, in their expected proportions, with the MPI approach ensuring that several of them can occur in the same event. One can alternatively use the same list as exclusive "hard" processes, if one is only interested in the high-$p_\perp$ tail, where a generation of the complete cross section would be inefficient.

Nondiffractive events provide the bulk of the inelastic cross section, i.e. what is observed in central detectors. Inside PYTHIA it is also referred to as the *minbias* component, but it does not have a one-to-one overlap with the experimental definition of minimum bias, see the warning in Section 7.2. The

nondiffractive component is expected to provide an even bigger fraction of the events that contain a hard process. Therefore, if the user requests an exclusive hard process, currently PYTHIA would always simulate the underlying event as being of the nondiffractive type.

Diffractive events are handled in the Ingelman–Schlein picture [280], wherein single diffraction is viewed as the emission of a pomeron pseudoparticle from one incoming proton, leaving that proton intact but with reduced momentum, followed by the subsequent collision between this pomeron and the other proton. The pomeron is, to first approximation, viewed as a glueball state with the quantum numbers of the vacuum, but by QCD interactions it will also have a quark content. The pomeron–proton collision can then be handled as a normal hadron–hadron nondiffractive event, displaying the same structure with MPI, ISR, FSR and the rest. Double diffractive events contain two pomeron–proton collisions.

Elastic scattering by default only includes strong interactions [117], but it is possible to switch on the QED Coulomb term and interference as well [281].

14.4. The perturbative evolution

The PYTHIA 8 showers are ordered in transverse momentum [52], both for ISR and for FSR. Also MPIs are ordered in $p_\perp$ [96]. This allows a picture where MPI, ISR and FSR are interleaved in one common sequence of decreasing $p_\perp$ values. This is most important for MPI and ISR, since they are in direct competition for momentum from the beams, while FSR mainly redistributes momenta between already kicked-out partons. The interleaving implies that there is one combined evolution equation

$$\begin{aligned} \frac{\mathrm{d}\mathcal{P}}{\mathrm{d}p_\perp} &= \left(\frac{\mathrm{d}\mathcal{P}_{\mathrm{MPI}}}{\mathrm{d}p_\perp} + \sum \frac{\mathrm{d}\mathcal{P}_{\mathrm{ISR}}}{\mathrm{d}p_\perp} + \sum \frac{\mathrm{d}\mathcal{P}_{\mathrm{FSR}}}{\mathrm{d}p_\perp} \right) \\ &\times \exp\left(- \int_{p_\perp}^{p_{\perp\mathrm{max}}} \left(\frac{\mathrm{d}\mathcal{P}_{\mathrm{MPI}}}{\mathrm{d}p'_\perp} + \sum \frac{\mathrm{d}\mathcal{P}_{\mathrm{ISR}}}{\mathrm{d}p'_\perp} + \sum \frac{\mathrm{d}\mathcal{P}_{\mathrm{FSR}}}{\mathrm{d}p'_\perp} \right) \mathrm{d}p'_\perp \right) \end{aligned} \quad (67)$$

that probabilistically determines what the next step will be. Here the ISR sum runs over all incoming partons, two per already produced MPI (including the hard process), the FSR sum runs over all outgoing partons, and $p_{\perp\mathrm{max}}$ is the $p_\perp$ of the previous step.

Starting from a large $p_\perp$ scale of the hard process, the decreasing $p_\perp$ of Eq. (67) can be viewed as an evolution towards increasing resolution; given

that the event has a particular structure when activity above some $p_\perp$ scale is resolved, how might that picture change when the resolution cutoff is reduced by some infinitesimal $\mathrm{d}p_\perp$? That is, let the "harder" features of the event set the pattern to which "softer" features have to adapt. It does not have a simple interpretation in absolute time; all the MPIs occur essentially simultaneously (in a simpleminded picture where the protons have been Lorentz contracted to pancakes), while ISR stretches backwards in time and FSR forwards in time.

14.5. Parton showering

The initial- and final-state algorithms are partly based on a dipole-type approach to recoils, see Section 4.7, but with some modifications.

In the simplest case, consider a colour dipole stretched between two final-state partons. The emission off such a dipole can be associated with either of the two ends, approximately in proportion to the respective $1/Q^2$ propagator, which gives a smooth transition across phase space for having it associated with either end, say $(1 \pm \cos\theta)/2$ in the soft-gluon limit. By this classification the radiator end is the one that branches into two, which implies changed kinematics, to be compensated by the recoiler end.

If the colour dipole is stretched between a final and an initial parton, radiation off the final end has to be compensated by a changed momentum for this incoming parton. The subdivision of radiation from the two dipole ends is also somewhat more delicate in this case, and necessitates the introduction of a special damping factor on emission from the final end.

ISR is described by backwards evolution [38], wherein branchings are constructed from the hard subprocess, back to the shower initiators. In each step the whole previously generated partonic system takes the recoil of the newly emitted parton. This applies whether the radiating initial dipole end has a colour partner in the initial or in the final state. In the latter case the pure dipole picture dictates that only this one partner should take the recoil, but such a picture would not give the correct resummation behaviour e.g. for Z^0 production, see Section 4.7, and is therefore rejected. Emissions are allowed partially to line up in azimuthal angle by colour flow, however, which retains some memory of the dipole structure.

The evolution variable is closely related to the transverse momemtum of a branching, but is not identical with it. Instead the lightcone-motivated relationships $p^2_{\perp\mathrm{evol}} = (1-z)Q^2$ for ISR and $p^2_{\perp\mathrm{evol}} = z(1-z)Q^2$ for FSR are

used to define the space- or time-like virtuality Q^2 of the off-shell intermediate parton, given the chosen $p_{\perp\text{evol}}$ and z. When kinematics are actually reconstructed, Lorentz invariant expressions for z are being used, based on ratios of invariant masses, which leads to a kinematical $p_{\perp\text{kin}} \leq p_{\perp\text{evol}}$. Specifically, as a function of emission angle, $p_{\perp\text{kin}}$ peaks at 90°, whereas Q^2 and hence $p_{\perp\text{evol}}$ keeps on rising with angle.

Both QCD and QED emissions are allowed, and fully interleaved. Currently allowed branchings in the shower are $q \to qg$, $g \to gg$, $g \to q\overline{q}$, $q \to q\gamma$, $\ell \to \ell\gamma$ and, for FSR only, $\gamma \to \ell^+\ell^-$ and $\gamma \to q\overline{q}$.

Many resonance decays involve full matching to NLO QCD matrix elements. For production, however, all internally implemented processes are LO only. Production of $\gamma^*/Z^0/W^\pm$ is matched to the real-emission corrections, so as to obtain the NLO $p_\perp$ spectrum, but without the NLO K-factor. Showers have been constructed so that they, by default, have a sensible behaviour over the full phase space, all the way up to the kinematical limit, for a wide range of processes, but they will not be perfect.

Final-state showers have a sharp lower cutoff, that should define the transition to hadronization. For ISR it is also possible to use a sharp cutoff, but a valid alternative is a smooth turn-off related to what is done for MPI below.

14.6. Multiple parton interactions and beam remnants

MPI modelling has traditionally been a hallmark of PYTHIA. The framework is extensively described in Section 7.3, and here only the basic principles are recapitulated, to put them in context.

The perturbative $2 \to 2$ QCD cross section, which is dominated by t-channel gluon exchange, diverges roughly like $\mathrm{d}p_\perp^2/p_\perp^4$. But this is based on the assumption of free incoming states, which is not the case when partons are confined in colour-singlet hadrons. Screening by nearby opposite colour charges will dampen the interaction of gluons with a large transverse wavelength. This is introduced by reweighting the interaction cross section by the factor in Eq. (47), where $p_{\perp 0}$ is a free parameter in the model. To be more precise, it is the physical cross section $\mathrm{d}\sigma/\mathrm{d}p_\perp^2$ that needs to be regularized, i.e. the convolution of $\mathrm{d}\hat{\sigma}/\mathrm{d}p_\perp^2$ with the two parton densities. One is thus at liberty to associate the screening factor with the incoming hadrons, half for each of them, instead of with the interaction. Such an association also gives a recipe to regularize the ISR divergence, as already noted.

The $p_{\perp 0}$ parameter can be energy-dependent, since higher energies probe partons at smaller x, where the parton density increases and thereby the

colour screening distance decreases. An ansatz $p_{\perp 0} \propto E_{\mathrm{CM}}^{\epsilon}$ is therefore assumed, with some small power ϵ.

The spatial shape of the proton determines the balance between peripheral and central collisions, as reflected for example in the width of the multiplicity distribution. Several different shapes are available, starting with a simple Gaussian ansatz.

Rescattering has been implemented, i.e. the possibility of one parton scattering several times. So far no good experimental signals have been found for it, and it is off by default.

For dedicated studies of two low-rate processes in coincidence, two hard interactions can be set in the same event, by a somewhat simplified duplication of the normal hard-process selection machinery. There are no Sudakov factors included for these two interactions, similarly to normal events with one hard interaction.

Rescaled parton densities are defined after each interaction, that take into account the nature of the previous partons extracted from the hadron. This guarantees energy–momentum–flavour conservation.

Currently there is only one scenario for colour reconnection in the final state, see Section 7.3.4, in which there is a certain probability for the partons of two subscatterings to have their colours interarranged in a way that reduces the total string length. (This is intermediate in character between the original strategy [96] and the more recent ones [119].)

At the end of the perturbative stage, a number of leftover partons are found in the proton beam remnants, with colour connections to the scattered partons, see Section 7.3.4. Primordial $k_{\perp}$'s are introduced both for the scattering subsystems and the remnants, colours are assigned to connect the subsystems and the remnants with each other, and leftover longitudinal momentum is split between the remnant partons. When necessary, the junction approach is used to keep track of the baryon number, see Section 8.2.

14.7. Hadronization

Hadronization is based solely on the Lund string fragmentation framework [159, 168], Section 8.2, which is at the origin of the JETSET program and thus of PYTHIA.

Particle data have been updated in agreement with the 2006 PDG tables [282]. Some updated charm and bottom decay tables have been obtained from the DELPHI and LHCb collaborations.

The BE_{32} model for Bose–Einstein effects [283] has been implemented, but is not on by default. It does a reasonable job with e^+e^- data but not so well for hadronic collisions.

14.8. Program structure and usage

The PYTHIA 8 homepage is at

`http://www.thep.lu.se/~torbjorn/Pythia.html`

and from there you can download the most recent version as a gzipped tar file, which also includes documentation as well as several example main programs illustrating different ways in which PYTHIA 8 can be used and linked. The documentation can also be accessed directly from the PYTHIA 8 homepage.

It is possible to perform analyses of the event record inside the main program. Alternatively events can be output to the HepMC format, from which they can be studied further, or sent on to detector simulation programs like Geant.

14.9. Summary

PYTHIA 8 by now offers a complete replacement of PYTHIA 6 for essentially all aspects related to LHC physics studies, and in many respects contains improved physics models and new features. While development of PYTHIA 6 has stopped, and new subversions will only be prompted by bug fixes, PYTHIA 8 is being further improved and extended in several directions. Experimental usage is still lagging behind, but interest is picking up, so one should expect a gradual phaseover during the next few years.

15. Sherpa

15.1. Introduction

SHERPA is a general-purpose event generator, capable of simulating the physics of lepton-lepton, lepton-hadron, and hadron-hadron collisions as well as photon induced processes. Unlike the programs ARIADNE, HERWIG and PYTHIA, it was constructed from the beginning in C++, and in contrast to the C++ versions of those programs some of the physics modules (such as the old parton shower, encoded in APACIC++, or the matrix element generator AMEGIC++) were established before the actual event generation framework. The construction paradigm of the SHERPA framework can be summarized as follows:

- *emphasis on strict modularity of physics modules*
  In fact the organization is such that physics modules are only connected through relatively unspecific event phase handlers, which in turn call interfaces to the underlying physics modules. These interfaces are constructed such that they can connect to various independent modules performing the same tasks. A prime example in SHERPA is the treatment of hard matrix elements, where various ME generators (see below) are available to SHERPA, but all of them accessible through one and the same `Matrix_Element_Handler`. This allows a comparably simple replacement of outdated modules, for instance the old APACIC++ parton shower.

- *bottom-up approach*
  The event organization within SHERPA is kept as simple as possible. In particular, there are no abstract overheads for possible event phases when there exists no corresponding physics module yet.

Traditionally SHERPA's main focus is on the perturbative event phase; SHERPA is a frontrunner in the automated generation of tree-level matrix elements and hosts two fully-fledged ME generators with highly advanced phase-space integration methods. In recent years, the scope there has widened to also include infrastructure to support the calculation of cross sections at NLO accuracy, by providing automated subtraction methods. In addition, the cornerstone of SHERPA's event simulation, from the beginning, was the multijet merging described in Section 5.3. Only quite recently the description of parton showering in SHERPA has been improved by the inclusion of a parton shower based on Catani-Seymour subtraction [54] and the development of a true dipole shower [53], the latter still awaiting full incorporation into the framework. Similarly, in the beginning hadronization in SHERPA was performed through an interface to the Fortran version of PYTHIA and only in recent years a new independent implementation of the cluster hadronization idea [182], see Section 8.3, has been added. Other additions include a complete model of hadron and τ decays and QED final-state radiation [202] and a simulation of the underlying event based on the multiple-parton scattering ideas of [96].

15.2. Hard processes

Tree-level matrix-element generators. Processes simulated by SHERPA are selected by defining initial and final states of the hard subprocess, generated

by the matrix element generator chosen, see below. These initial and final state also define the particles that will actually appear in the event record, following the philosophy outlined in Section 16.1.[22] To generate the cross sections for the hard subprocesses, SHERPA provides two built-in matrix-element generators, AMEGIC++ [5] and COMIX [6], as well as facilities for hard-coded matrix elements, see Appendix B.

AMEGIC++ is a Feynman diagram based generator that constructs tree-level amplitudes and suitable phase-space mappings from given sets of interaction vertices. The Feynman diagrams then get translated into helicity amplitudes using an algorithm similar to the one described in [284, 285] and extended to include also spin-two particles in [286]. The list of supported physics models covers:

- the complete Standard Model,
- extension of the SM by a general set of anomalous triple and quartic gauge couplings [287, 288],
- extension of the SM by a single complex scalar [289],
- extension of the SM by a fourth generation,
- extension of the SM by an axigluon [290–294],
- Two-Higgs-Doublet Model,
- Minimal Supersymmetric Standard Model [295],
- ADD model of large extra dimensions [208, 209].

Other new physics models can easily be invoked by providing model representations generated with the FeynRules program [224, 296]. Based on the information of all Feynman diagrams contributing to a given process, AMEGIC++ automatically constructs suitable phase-space mappings. For the actual integration all contributing channels are combined in a self-adaptive multi-channel integrator, see Appendix B.2, which automatically adjusts to

[22] It should be noted that in SHERPA projections on intermediate states in various schemes (narrow width or propagator, both with full spin correlations) are also available; these intermediate states, however, will typically *not* appear in the event record.

the relative importance of the single phase-space maps to minimize the variance. The efficiency of the integrator is further improved by applying the self-adaptive VEGAS [297] algorithm on single phase-space maps.

COMIX is especially suited for the simulation of highest-multiplicity processes. This generator is based on an extension of the colour-dressed Berends-Giele recursive relations to the full Standard Model, see Appendix B.1. Within COMIX any four-particle vertex of the Standard Model is decomposed into three-particle vertices. This leads to a significantly improved performance for large final-state multiplicities, compared to AMEGIC++. The summation (averaging) over colours in QCD and QCD-associated processes is performed in a Monte Carlo fashion and colour-ordered amplitudes can therefore be computed. Following the reasoning of [298], the colour-flow basis is employed throughout the code. As discussed in [299], this yields a certain correspondence between the large-N_c limit employed in parton-shower simulations and full QCD results, which is especially useful in the context of a merging with the parton shower, see Section 5.

Next-to-leading order event generation. The AMEGIC++ matrix-element generator has the further functionality to construct dipole-subtraction terms and their integrals over the one-parton emission phase space in the Catani–Seymour formalism [19] for arbitrary Standard Model processes [300]. When supplemented with corresponding one-loop amplitudes, using the Binoth-Les-Houches-Accord [27] interface structure, SHERPA is capable of generating parton-level events at next-to-leading order precision, see Section 3.5. This framework has for example been used to evaluate the QCD NLO corrections to $W/Z + 3$jets [301–303] and $W + 4$jets [304] production, with the loop amplitudes obtained from BLACKHAT [305]. In [306] the NLO corrections to ZZ+jet production have been calculated for the first time, relying on GOLEM [307] for the generation of the loop-amplitude expressions.

Besides the implementation of the Catani–Seymour dipole subtraction method, facilitating parton-level event generation at NLO, SHERPA also provides the possibility to generate hadron-level events at NLO accuracy using the POWHEG algorithm to combine NLO matrix elements with the SHERPA parton shower. This is achieved in a completely process-independent way, using a reformulation of the original POWHEG method, which was presented in [29]. The respective POWHEG generator is based on the same principles as the internal parton-shower module described in the following section.

15.3. Parton showering

SHERPA's default parton-shower algorithm, first presented in [54], is based on the Catani–Seymour dipole factorization formalism [19, 20]. The underlying key idea is to derive the corresponding shower splitting operators from the four-dimensional unintegrated dipole-subtraction terms by performing the large-N_c limit and summing and averaging over all spin degrees of freedom. Accordingly, one arrives at a completely factorized approximation for the real-emission process in terms of the underlying Born channel times a sum of suitable splitting operators that correctly account for (quasi-)collinear and soft emissions.

The emerging shower picture corresponds to sequential splittings of dipoles where, in the Catani–Seymour formulation, a dipole is made up of the actual parton that is supposed to split and a well-defined spectator parton that is colour-connected to the emitter. Four dipole configurations have to be considered, classified by the emitter/spectator being either in the final (F) or initial (I) state; FF, FI, IF and II. All dipole configuration are treated on an equal footing and as a consequence there is no formal distinction between initial- and final-state parton showers. Successive emissions are ordered in terms of the invariant transverse momentum between final-state splitting products or with respect to the emitting beam particle. At present the Catani–Seymour dipole shower in SHERPA implements all QCD splittings in the Standard Model and the MSSM as well as QED photon emissions [308].

In its original formulation presented in [54], the recoil strategy for the various types of dipole splittings closely followed the choice of the Catani–Seymour formalism [19, 20]. However, when considering initial-state splittings this can lead to the situation that only the first splitting of an initial–initial dipole transfers transverse momentum to the rest of the event. As an intuitive example, consider the shower evolution of a Drell-Yan event, which starts from just initial-initial dipoles. In the extreme case the gauge boson would get a finite recoil from the first splitting only, clearly at odds with the resummation of associated large logarithms. In [308, 309] alternative, crossing symmetric, recoil strategies were presented that avoid this peculiar feature. For the SHERPA implementation, [310] studied the impact of different recoil strategies in the context of deep-inelastic lepton scattering events.

The shower formulation based on Catani–Seymour dipole factorization offers two substantial advantages with respect to traditional parton showers,

which help to facilitate the merging with fixed-order matrix-element calculations:

- Due to the notion of specific spectator partons, four-momentum conservation is maintained locally, while only a single external particle, the spectator, takes the recoil when the splitting parton goes off-shell. This is important for the construction of a backward clustering algorithm based on the parton shower in the spirit of [75].

- The parton-shower model inherently respects QCD soft-colour coherence. By construction in Catani–Seymour factorization, the eikonal factor associated with soft gluon emission off a colour dipole, used to derive the angular ordering constrained in conventional parton showers, is exactly mapped onto two CS dipoles, which only differ by the role of emitter and spectator.

15.4. Matrix-element parton-shower merging

One of the key features of Sherpa is a generic implementation of the technique for combining tree-level matrix elements with parton showers that was presented in [75], see Section 5. The method was extensively tested and validated for multijet production in e^+e^- and hadron-hadron collisions, as well as deep-inelastic scattering processes, a scenario where event generators based on collinear factorization assumptions are unreliable due to a lack of matrix elements with sufficiently high final-state multiplicity [310]. An extension of the merging algorithm, which simulates hard QED radiation in a democratic approach, i.e. on the same footing as QCD radiation, was implemented in Sherpa and reported in [308]. It yields excellent agreement with existing experimental data on prompt photon production at both e^+e^- and hadron colliders. Although the novel merging technique implemented in recent versions of Sherpa has yielded significant improvements over the original CKKW algorithm, in the sense that results are more accurate and stable, the CKKW approach itself was already employed in former versions of Sherpa with great success [73, 311–313].

In order to realize the ME+PS merging, Sherpa makes use of its two internal tree-level matrix-element generators Amegic++ and Comix. Soft and collinear parton radiation is simulated by means of the internal parton shower. It should be noted that Sherpa implements its matrix-element parton-shower merging in a modular way, distributing only necessary tasks

to the matrix-element and parton-shower generators and handling all cross-module interaction in the overall framework. This means in particular that the matrix-element generator is only used to identify possible parton-shower histories in the matrix elements by testing for respective subamplitudes in the Feynman diagrams. The parton shower supplies information about the weight associated with a backward clustering that would reduce the actual partonic final state to the respective subamplitude. If external parton showers or matrix-element generators are provided by the user, they must be capable of performing these operations. If so, they can in turn be employed for automatic matrix-element parton-shower merging without any further adjustments of the SHERPA framework, see also Section 15.8.

The MENLOPS algorithm for merging lowest-multiplicity NLO matrix-elements with higher-order tree-level contributions as presented independently in [77] and [314] is fully implemented in the SHERPA generator [314]. It relies on the internal generic POWHEG generator described in Section 15.2, which drives the lowest-multiplicity simulation and interfaces to the Catani–Seymour dipole shower to generate additional parton radiation.

15.5. Multiple parton interactions and beam remnants

The multiple-interactions model used in SHERPA closely follows the original ideas of [96]. There are however important details where the approach deviates from the formalism in PYTHIA. Secondary interactions undergo parton-shower corrections in SHERPA, but the evolution does not interleave parton showers and additional hard scatterings. Care must then be taken when combining ME+PS merging with the modelling of multiple interactions. It is vital that the parton showers related to secondary collisions do not alter the initial jet spectra of the hard process. This can be achieved by a special jet veto procedure, which is described in some detail in [189].

The modelling of beam remnants in SHERPA is realized in such a way that only a minimal set of particles (quarks and diquarks, the latter as carriers of baryon number) is produced in order to reconstruct the constituent flavour configuration of an incoming hadron. The distribution of colour in the remnants is guided by the idea of minimizing the relative transverse momentum of colour dipoles spanning the outgoing partons. When including multiple parton interactions in the simulation, it is not always possible to accomplish free colour selection in the hard process and minimization of relative transverse momenta simultaneously. In such cases the colour configurations of

the matrix elements are kept but the configuration of the beam remnants is shuffled at random until a suitable solution is found.

In addition to the issues related to colour neutralization with the beam remnants, all shower initiators and beam partons obtain a primordial $k_\perp$, see Section 7.1. When tuning this distribution, for example by using the data shown in Fig. 18, the mean and width parameter values obtained are typically rather small (about $0.5 - 1.0$ GeV).

15.6. Hadronization

The idea underlying AHADIC++, SHERPA's module dealing with hadronization, is to take the interpretation of clusters as excited hadrons very literally, to compose clusters out of all possible flavours including diquarks and to have a flavour-dependent transition scale between clusters and hadrons. This results in converting only the very lightest clusters directly into hadrons, whereas slightly heavier clusters experience a competition between either being converted into heavy hadrons or decaying into lighter clusters. For all decays, QCD-inspired, dipole-like kinematics are chosen. In somewhat more detail, in AHADIC++, the hadronization of quarks and gluons proceeds as follows:

- Firstly, all gluons are forced to decay into quark or diquark-pairs, $q\bar{q}$ or $d\bar{d}$, and all remaining partons are brought on constituent mass shells. Recoils are compensated mainly through colour-connected particles.

- Subsequent decays of heavy clusters are modelled by first emitting a gluon from the $q\bar{q}$ pair and then splitting this gluon again.

- In all non-perturbative decays ($g \to q\bar{q}$ and cluster decays) the transverse momentum is limited to be smaller than a parameter $p_\perp^{\max}$, typically of the order of the parton-shower cutoff scale, and $p_\perp^2$ is chosen according to $\alpha_s(p_\perp^2 + p_0^2)/(p_\perp^2 + p_0^2)$, invoking a second parameter p_0 [23]. In this picture lighter-flavour pairs are preferentially produced due to available phase space; this is supplemented by weight parameters.

- The decays of clusters into hadrons are determined by various weights including flavour wave functions, phase-space factors, flavour and hadron-multiplet weights, and other dynamical measures.

[23] There is also the option to use a non-perturbative α_s coupling, agreeing with a measurement from the GDH sum rule [315].

15.7. Hadron decays and QED radiation

SHERPA's hadron decay module is quite exhaustive, with approximately 200 decay tables (one for each particle) consisting of more than 2500 decay channels. Each of them is modelled by isotropic decay and the branching ratio, but on top of that, spin-dependent matrix elements and even form factors can be included. This leaves SHERPA in a situation where for some decays various form factor models are available[24], while for others even the branching ratios are not well known and have to be estimated from symmetry principles and phase-space arguments.

In addition to the simulation of individual decays, non-trivial quantum effects are also modelled in SHERPA, including spin correlations in sequential decays and CP violation introduced by mixing phenomena or their interplay with direct CP violation in decays. For the latter, SHERPA allows the user to include separate decay tables for particles and antiparticles.

For QED FSR, the PHOTONS++ module [202] is invoked, which employs the YFS formalism (see Section 10) allowing for a systematic improvement of the eikonal approximation order-by-order in the QED coupling constant. $\mathcal{O}(\alpha)$ corrections are included for a number of processes, among them decays of vector particles into leptons, leptonic τ decays and some B decays. At present the module is only capable of handling single-particle initial states, i.e. particle decays possibly including QED FSR off the hard process. In contrast to some other implementations, however, it can deal with decays involving more than two charged particles.

15.8. Interfaces and extensions

Interfaces provided. SHERPA supports most of the commonly used standard interfaces for information input or output:

- parameters and interactions of new physics models can be incorporated through FeynRules generated input files [296],
- the spectra of supersymmetric models can be provided in the form of SLHA files [259, 260],

[24]There is a plethora of sources and models, for instance HQET [316–318], quark-model predictions [319–321] or QCD sum rules[322–325], all for heavy meson decays. In addition, form factor models for τ decays based on the Kuhn-Santamaria parameterization [326], or on Resonance Chiral Theory [327–330] have also been included.

- to link external parton densities the LHAPDF package is supported,
- hard-process configurations generated with either AMEGIC++ or COMIX can be output in the Les-Houches-Event-File format,
- one-loop amplitudes can be invoked using the Binoth-Les-Houches-Accord outlined in [27],
- fully showered and hadronized events can be output in the HepMC [250] or HepEvt format.

Extending SHERPA. Extensions of SHERPA can be provided in various ways. The easiest would certainly be to enhance the functionality of an existing module of the program, thus providing the code with the capability to, for example, simulate reactions in a new physics scenario. The most challenging, but nevertheless available option would be to supply a complete new module to the event-generation framework, encoding for example an alternative underlying event model. Considerable modifications of the core framework of SHERPA will only be necessary if an extension of the program requires cross-module interaction that has not been foreseen and therefore has not been implemented yet. In such cases, users are strongly encouraged to coordinate their efforts for implementing extensions with the authors of SHERPA. In most cases, however, existing structures will suffice to satisfy the needs for possible enhancements.

SHERPA provides the option of loading most possible extensions of the program package at runtime, using dynamically linked libraries. This mechanism is especially convenient to use in bigger software frameworks, where the SHERPA core library itself is just part of a larger event generation and analysis framework. It also allows the user to install SHERPA in a predefined location and to provide an extension of the program without altering its core modules.

For most of its extensions SHERPA employs a so-called "getter" mechanism to identify possibly available external sources. This means that an extension module is registered with the SHERPA instance at load time of its shared library, using a predefined protocol associated with the physics task of the extension module. An example would be an externally supplied parton shower, which registers using its name ("Apacic", for example) using the parton-shower identification protocol. At runtime, users can then specify

this name in the input card to enable the respective shower model in event generation.

The following extensions can currently be supplied to SHERPA using "getter" methods:

- *Analysis programs*
  Both the Rivet library and the HZTool library are interfaced using such extensions of SHERPA. These interfaces are distributed with the SHERPA package itself.

- *Parton distribution functions*
  Despite most PDFs being available nowadays within the LHAPDF library, it might, in some cases, become necessary to interface the code for a dedicated PDF. SHERPA provides this option and supplies, for example, in-house interfaces to photon PDFs.

- *Matrix elements*
  While there is little need to extend SHERPA with tree-level matrix elements, this option is nevertheless provided to allow implementation of special matrix elements, for example for upsilon production. Additionally, SHERPA provides the option of including external NLO virtual matrix elements, which can then be combined with automatically generated Born-level, real-emission and subtraction terms.

- *New physics models*
  Even though the usage of the FeynRules program package and its interface to SHERPA is strongly encouraged, SHERPA provides the option of implementing a new-physics scenario directly. The corresponding vertices will then be available for both internal matrix-element generators, AMEGIC++ and COMIX.

- *Helicity-amplitude building blocks*
  New helicity-amplitude building blocks might become necessary for exotic BSM scenarios. They can be provided for both internal matrix-element generators, AMEGIC++ and COMIX. Of course they will have a different underlying structure in each case.

- *Matrix-element generators*
  If necessary, a complete external matrix-element generator can be supplied. Note, however, that it must also satisfy the requirements imposed

by the possibility of merging matrix-element level events with parton showers. This means in particular that it must provide a clustering algorithm that identifies allowed parton-shower histories in tree-level matrix elements.

- *Parton-shower generators*
  If necessary, a complete external parton-shower model can be supplied. Such a parton shower must, however, comply with SHERPA's rules for matrix-element parton-shower merging, i.e. it must provide a related algorithm for computing the branching probability leading to tree-level matrix-element final states.

- *Hadron decayers*
  As already hinted at above, SHERPA already provides quite an extensive library for hadron decays. They can be further extended by providing form factors or "skeleton" matrix elements in the HADRONS++ package.

15.9. Summary

As with any other event generator, it is hard to conceive that SHERPA will ever reach a state of "perfection", where nothing is left to be done. However, for the near future, a number of enhancements are foreseen:

- Work on the automated implementation of the POWHEG algorithm, including non-trivial colour configurations and new-physics processes, will be finalized. Equipped with this tool, the path towards a multijet merging at NLO seems to be viable.

- A second, independent parton-shower formulation is ready to be fully included into the framework. This will allow systematic comparison of parton-shower effects with two independent modules in the same framework, a huge step forward.

- A new model for the simulation of soft inclusive physics and the underlying event, based on the multichannel eikonal approach of [331] is under way. It will supplement or replace the old model, based on MPI.

The current and future releases of the SHERPA package as well as the most recent documentation can be found at

http://projects.hepforge.org/sherpa/

Part III
The use of generators

16. Physics philosophy behind phenomenology and generator validation

As discussed in Section 1, Monte Carlo simulations are used in various ways when performing measurements in particle physics experiments that require the comparison of theoretical predictions with data. Similarly, measurements of SM processes in data provide important input to Monte Carlo tools. They provide validation of theoretical predictions and allow free parameters to be tuned.

There are some basic philosophies that experimentalists using Monte Carlo tools and making experimental measurements potentially useful for their validation should be aware of. These are discussed in this section.

16.1. Physical observables and Monte Carlo truth

When simulating a process with a Monte Carlo event generator it is important to make the distinction between "Monte Carlo truth" and "physical observables" (see also the discussion of Monte Carlo truth contained in the contribution by Buckley et al. in [332]).

It is often desired to specify a process in terms of intermediate objects as well as initial and final states, for example lepton pair hadroproduction via production and decay of a Z^0 boson. However, the intermediate objects are not physical observables, and in practice it is not always possible to classify the process in this way. In particular one must keep in mind that such a classification is only exact in the limit that all quantum interference effects can be neglected. Thus, although it may be convenient to model a double-slit experiment by shooting particles either through slit S (signal) or slit B (background), that distinction, as it stands, is not quantum mechanically meaningful when both slits are open.[25] Likewise, soft bremsstrahlung in

[25] "Background" here refers only to fundamentally *irreducible* background, which can produce the same final states as the signal.

particular depends strongly on interference effects (coherence, see Section 4 on parton showers), and hence the assignment of radiation as coming off this or that parton is inherently ambiguous. The one fail-safe way to make sure a distinction is quantum mechanically meaningful to all orders is well known: to classify an event according to the values of specific physical observables (such as where the photon struck the actual screen, in the case of the double-slit experiment).

The SHERPA event generator (see Section 15) goes so far as to insist that a process is defined in terms of initial and final states, such that it is not possible for a user to access any intermediate objects. All possible contributing subprocesses, as well as any interference terms between them, are then included in the calculation. While other event generators do allow the user to specify the process of interest in more detail, users should be aware of the possible limitations. In addition, when an experimental measurement is performed it should be presented in an unambiguous way, in terms of physical observables.

16.2. Making generator-friendly experimental measurements

For a measurement to be useful in the context of the development and improvement of Monte Carlo models, it must be well-defined in terms of the observed initial- and final-state particles, rather than in terms of intermediate unstable particles or a particular type of process. This is also a desirable attribute for any physical measurement to have meaning beyond a particular theoretical framework. Indeed, quantities not defined in terms of physical observables run the risk of not being quantum-mechanically meaningful.

The philosophy advocated here is that the data are "golden", and any dependence on current theoretical tools should be minimized to ensure the longevity and usefulness of the experimental result. Therefore corrections and extrapolations to different regions of phase-space using a Monte Carlo or other theoretical prediction should be minimized. This should not be confused with correcting for detector effects. In fact it is required that the effects of the detector (resolutions, efficiencies) are removed to within some stated systematic uncertainty, or at least quantified in terms of systematic uncertainties.

The initial state is generally the colliding beams, which are well known, although in some cases, for example almost-on-shell photons, they may be treated as a quasi-real initial state. The final state can be more problematic. In general the best approach is to define all particles with proper lifetimes

beyond some cut [118] (typically 30 ps) as being the "stable" final state of the event, and derive all event properties, cross section fiducial regions and so on from these. The result should be stated in terms of final-state particles within the acceptance of the detectors, without extrapolations into regions that are not measured. Statistics allowing, it is even better to split up the observed phase space into a few complementary regions, and quote the result for each separately, which can provide a non-trivial cross check on the ability of the models to interpolate among those regions.

If any theory-based corrections are applied (for example QED radiative corrections) they need to be clearly stated and quantified and the result without the correction should also be stated, since in principle these corrections would be included in the "ideal" Monte Carlo.

These guidelines are best illustrated with different examples of common measurements at collider experiments.

Measurements of charged-particle distributions ("minimum bias"). Typically distributions of charged particles, such as charged particle multiplicity, transverse momentum $p_\perp$ and pseudo-rapidity η distributions are made. These measurements are often referred to as "minimum bias", because the idea is usually to be as inclusive as possible and include the distributions of events in which it is known that an inelastic collision occurred. This is inferred from the detection of final-state particles (other than the incoming ones). Following the philosophy previously described, such a measurement should be made within a well-defined region of phase space. For example if a detector can reconstruct tracks from charged particles in the region $|\eta| < 2.5$ and $p_\perp > 100$ MeV, then the result should be expressed in terms of charged particles with the same (or tighter) kinematic cuts. Furthermore, if the distributions are normalized to the total number of events in the sample (as is often the case) it should be well defined what is meant by an event. For example an event could be defined as "any event with at least one charged particle with $|\eta| < 2.5$ and $p_\perp > 100$ MeV". This is a definition that can easily be reproduced at the generator level. Normalizing to all events from a pp collision is not well defined experimentally, as some minimal experimental criterion is required to detect a collision. The only way to correct distributions for events with no particles within the acceptance of the detector is to use a theoretical model or ad hoc extrapolation, which does not give any extra information from the data, and in fact contaminates the result with the model that is used to perform the correction.

Another important point for this type of analysis is the definition of the final state. As previously stressed, the result should be given in terms of final-state particles only. No claims should be made about the type of process that produced this final state, as it is not possible to state unambiguously what the process was. Historically many such measurements have been made for non-single-diffractive events. The reasoning is usually the use of a double-armed trigger, which selects events based on the presence of forward particles on both sides of the detector. These triggers are typically inefficient for single-diffractive events, where one of the colliding hadrons remains intact, resulting in a void of activity on one side of the detector. The distributions are often corrected for the remaining single-diffractive contribution, using a given Monte Carlo model. These models are very poorly constrained and unreliable, resulting in model dependent corrections with systematic uncertainties that are very difficult to quantify. A preferable approach is to leave the distributions uncorrected for a certain type of process.

To further suppress diffraction, one would instead add more requirements (more "bias") on the final state, such as the presence of more than one track in the fiducial region or the absence of large rapidity gaps in the event.

This particular example raises a more subtle issue, which is correcting for detector effects such as the trigger described previously. It is preferable to use a trigger that is as inclusive as possible, and highly efficient with respect to the event sample definition. It is also highly desirable to correct for the trigger efficiency using a data-driven approach. Relying on a model to correct for a trigger that does not overlap in phase-space with the particles being measured can also lead to unreliable results, as the prediction of the particle distributions in the region outside the measurement acceptance is model dependent. Again, the systematic uncertainties on these corrections can be large and very difficult to quantify. Alternatively the trigger signal should be corrected for detector effects and converted into a hadron-level definition to be included in the event definition discussed above (e.g. at least one charged particle in the region $3.0 < |\eta| < 5.0$ with $p_\perp > 50$ MeV).

Measurement of the $\ell^+\ell^-$ transverse momentum distribution in $Z^0/\gamma* \to \ell^+\ell^-$ events. An interesting measurement for constraining QCD initial-state radiation predictions is the $p_\perp$ of the Z^0 boson. There are features of such a measurement that illustrate many of the issues introduced above. The measurement that is actually made is of the di-lepton ($\ell^+\ell^-$) $p_\perp$, not the Z^0 $p_\perp$, as it is the final-state leptons that are detected. Correcting back to

the Z^0 $p_\perp$ traditionally involves two steps, both of which should be avoided. Firstly, QED radiation of photons from the final-state leptons would have to be corrected for, as the photons will carry off some fraction of the lepton and hence the Z^0 $p_\perp$. This involves using a model of QED radiation that is likely to have uncertainties and may neglect interference between photons emitted in the initial and final states. It may be argued that the experimental measurement should be comparable to a theoretical prediction that does not itself include the effects of QED radiation. Of course the ideal prediction should include all effects, but in reality this is not always practical. In this case the result should be given both with and without the QED corrections. Only presenting results corrected for QED effects implies that the best Monte Carlo generators must switch off part of the true process in order to compare to the data that has been corrected with another (potentially less accurate) model – which is an unnecessarily complicated procedure and in fact reduces the accuracy of the experimental result.

The correction of QED radiation is a subtle issue and should be treated with some caution. In the case of final-state electrons, the energy and hence $p_\perp$ measurement is typically made in a calorimeter. Any final-state photons that are emitted in a direction collinear to the electrons may, if they do not convert into e^+e^- pairs, end up in the same calorimeter cell(s) and hence can be indistinguishable from the electrons. Thus their energy will be automatically "clustered" back into the energy of the electron. Wide-angle radiation will of course not be included in the energy measurement. Depending upon the detector, it may therefore be preferable to define the electron in terms of a cone of electromagnetic particles, analogous to a hadronic jet. The size of this cone might be experiment specific, but it would be well defined and easily reproducible at the final-state particle level in a generator. See the contribution of Buckley et al. in [332] for a detailed discussion of this issue. Defining the final state in this way is also theoretically more reliable as the required corrections are smaller.

In the case of final-state muons the momentum is typically measured by a tracker that measures the curvature of charged particle tracks in a magnetic field. In this case the photons do not contribute to the particle momenta and only the di-muon momentum is measured. However, it should be noted that the effect of enhanced collinear radiation from muons is much less than that from electrons due to their larger mass.

The second correction required to "measure" the Z^0 $p_\perp$ is for the contribution from the virtual photon propagator and for Z^0/γ^* interference terms.

It is not possible to experimentally distinguish these contributions, although the Z^0 contribution can be greatly enhanced by making a cut on the invariant mass of the lepton pair in a window around the Z^0 boson mass, e.g. 66 $< M_{\ell\ell} <$ 116 GeV. Again, this definition is unambiguous and reproducible by any Monte Carlo generator and should therefore be preferred over claims of a process involving a particular propagator.

Another important issue that can be demonstrated in this example is the correction for the acceptance of the final-state leptons. The measurement can only be performed on leptons that fall within the acceptance; the result should therefore be presented in terms of leptons that pass certain kinematic cuts, e.g. $p_\perp > 25$ GeV and $|\eta| < 2.0$. An attempt to correct for the regions of phase space not measured can result in large extrapolations, using a certain prediction with its associated limitations and uncertainties. Again, this adds no information to the measurement and in fact reduces its accuracy, reliability and usefulness for validation and tuning.

Jet cross sections. Jets are designed to reflect and be sensitive to short-distance physics, but they are composed of hadrons. An example of poor practice which is fortunately by now almost extinct in current experimental measurements is the correction of jets to some "parton-level final state". While hadronization and other soft corrections do need to be evaluated in order to compare to perturbative QCD calculations, they are now typically applied to the theory rather than data, and in any case the data are almost invariably presented first in terms of final-state particles, even if later corrected in such comparisons. The soft QCD physics used in such corrections is typically the least theoretically constrained aspect of a given Monte Carlo program. Cases where, for example, the underlying event is corrected for at the same time as pile-up, or where even, bizarrely, the data are corrected directly from a detector level distribution to some "leading order" partonic state, are essentially useless for any theory comparison except possibly to the particular version of the particular Monte Carlo generator used to make the correction. Note that there are methods of correcting for, or reducing the effects of, underlying event which are well defined and model-independent, see for example [333].

16.3. Evaluation of MC-dependent systematic errors

Even if a measurement is defined in a model-independent way, as described above, there will still in general be model dependence in the correc-

tions applied to remove or quantify detector effects, since detector response is often evaluated using Monte Carlo tools. In addition it is often necessary to use Monte Carlo predictions of signal and background rates or kinematic distributions in order to extract the significance of a signal or place limits in the absence of a signal.

As a general rule, experimentalists should use all Monte Carlo generators that simulate the process of interest and potential backgrounds. While it is not always sufficient to take the difference between the result of two different generators or tunes as a systematic uncertainty, it is useful for getting an idea of the limitations of and differences between the predictions.

Often it is necessary to unfold a distribution, both for detector inefficiencies and resolutions. In some cases, such as a low detector efficiency that is localized in ϕ, the azimuthal angle around the beam-pipe, using a Monte Carlo to model the inefficiency will be very reliable. There is no physical significance to this region, so if the detector is well modelled and if the generator models the physics well in other ϕ regions, the modelling of the inefficiency will be robust. In other cases the underlying physics of the model used to do the unfolding can have a significant effect on the result. There are many different possible techniques for unfolding, which depend to varying degrees on the underlying model. The dependence on the model can be reduced by e.g. reweighting the Monte Carlo events to match the data for relevant kinematic distributions. Note that it is not necessarily only the distribution that is being unfolded that is relevant for the unfolding and sometimes unfolding in two dimensions, with a second distribution that is chosen because it is strongly correlated with the size of the correction, can be useful.

Residual uncertainties can be determined by comparing different Monte Carlo models or tunes, as long as the differences between the tunes are sufficiently large to cover the difference between Monte Carlo and data in relevant distributions.

A common Monte Carlo systematic is the modelling of a detector response to QCD jets. In general this depends upon the details of the detector and upon the fragmentation of the jets (charge-to-neutral ratio, energy partition, etc). The model dependence of a calibration may be tightly constrained by requiring that the simulation describes quantities such as the number of charged particles near jets, or the energy flow around jets, satisfactorily.

Finally, there are often MC-dependent systematic uncertainties associated with the modelling of the background and/or signal rates and kinematic distributions. Such uncertainties can be evaluated and minimized in the

manner described above, with the constraining requirements coming from comparisons between data and Monte Carlo in control regions. In addition, if any relevant measurements from the same or other experiments provide constraints on the Monte Carlo predictions used to extract the signal, these should be used in the assessment of the systematic uncertainties.

In general how to assess MC-dependent systematic uncertainties depends on the specific analysis. However, it is good practice to consider all possible constraints from data, whether it be control regions in the same measurement or different results. In addition the limitations of the Monte Carlo generator used should be understood, and different generators and tools should be considered.

17. Validation and tuning

Validation in the context of Monte Carlo generators means confronting a model with all relevant data that it claims to be able to describe. It is essential that the validation is global, because the model should describe the underlying physics and not just parameterize the data, otherwise it would not have any predictive power. In this sense validation is important for developing models as well as for debugging both code and physics models. Tuning means adjusting the free parameters of the model within their allowed ranges to improve the description of the relevant data.

17.1. Generator validation and tuning strategies

As mentioned, generator validation must simultaneously consider a range of observables to be meaningful and predictive beyond the observables considered. The choice of observables must also be limited according to the model being considered: poor description of an observable whose responsible process is not modelled conveys little information.

For tuning, similarly, a range of observables is required for predictivity and to obtain a generally usable single set of parameters. Again, depending on the suitability of observables to the model being tuned, it may or may not be *possible* to describe all data simultaneously: this in itself may be a useful result for model development. The optimization of MC parameters to the chosen observables may be performed manually – guided by the expected physical behaviour of the models – or by a more automated method driven by the quality of the fit to data. In both approaches, some sampling of the parameter space is typical to ascertain the generator behaviour in response to

parameter changes. The allowed ranges of parameter values in this sampling typically span all values for which the underlying physical picture is valid, although scans of more restricted ranges are usually necessary to produce a final tune.

The choice of reference data is important since all simulations lack some known physics effects. Generator tuning should primarily optimize phenomenological simulation aspects, and not make up for shortcomings in modelling of event aspects that should be robustly described by calculable QCD. For example, tuning a Monte Carlo generator that contains only a $2 \to 2$ scattering matrix element to high jet-multiplicity data will tend to distort the parton shower and underlying event in an attempt to make up for the lack of higher multiplicity matrix elements. However, there are modelling aspects that do not fall neatly into either a perturbative or non-perturbative definition, e.g. the primordial $k_\perp$ as discussed in Section 7.1. The parameters of these models are perfectly valid for use in tuning – with appropriate care. For example, while a primordial $k_\perp$ width may have no numerical upper limit in the generator implementation, a tuned value located far into the perturbative regime would be an abuse of the model and suggest deficiencies elsewhere.

As general-purpose event generators contain models for many processes, most have of order 15 or more tuning parameters. This defines a parameter space whose dimensionality is far too high for comprehensive exploration, even with an automated sampling method. The practical consequence is that factorization of the parameters into minimal sets suitable for each group of observables has been found to be important. Hence, tuning of generators usually occurs in several distinct stages, in the following order:

- *Hadronization and final-state fragmentation:* The flavour and kinematic structure of the final-state shower and hadronization mechanisms are assumed to be universal between e^+e^- and hadron colliders. As e^+e^- observables (e.g. event shapes and identified particle rates and $p_\perp$ spectra) may be described by a generator without first requiring a reasonable tune of initial-state hadron collider effects, these are typically used to tune final-state shower and hadronization parameters. Flavour structure and kinematics may themselves be factorized to some extent, perhaps with iteration.

  Some typical parameters for tuning of fragmentation kinematics are the α_s/Λ_{QCD} values and IR-cutoff for the final-state shower, the string

tension and fragmentation function parameters for string hadronization models, and the gluon constituent mass and cluster momentum smearing in cluster hadronization models. Light and heavy quark fragmentation kinematics are often treated separately, which permits further factorization to charm- and bottom-specific observables without compromising the statistically dominant light fragmentation. Tuning of flavour parameters in hadronization – for string hadronization in particular – introduces an extra collection of parameters for, e.g. , enhancement and suppression of strangeness/charm/beauty, η/η' and baryon fractions. A final semi-distinct group of parameters may be available for adjusting the admixtures of different orbitally excited hadron states: whether these are considered in tuning depends on the purpose at which the tuning is aimed.

The recent availability of identified particle data from hadron colliders such as RHIC and the LHC is of interest from the point of view of hadronization tuning, but violates the desirable feature of not requiring a viable initial-state effect tune before beginning. At present, such data have not been included in tunings: they are, however, of great interest for validating the assumption that hadronization parameters tuned to e^+e^- observables will remain valid in a hadron collider environment.

- *Initial-state parton shower:* Once a reasonable tune of final-state parameters has been obtained, the typical next step is to tune the initial-state (space-like) parton shower parameters. The reason for tuning this before the soft QCD effects is that we desire the shower to be tuned to observables with little MPI/beam-remnant contamination, and then use the full flexibility of the heavily-parameterized MPI machinery to make the final best fit to data. This way, we avoid the danger of absorbing effects which should be perturbatively describable into the relatively unconstrained MPI modelling.

  Some typical observables for initial-state shower tuning are dijet azimuthal decorrelations (from the Tevatron and the LHC, with concern that $2 \to 2$ matrix elements are not abused to include third hard jet contributions) and hadron collider jet shapes. Typical parameters are the shower IR-cutoff, the shower $\alpha_{\mathrm{s}}/\Lambda_{\mathrm{QCD}}$, and perhaps a scaling factor for the α_{s} evaluation scale and the starting scale for the parton cascade. The philosophy of what shower parameters are available for

tuning varies according to generator: some permit use of multiple α_s definitions, while others insist that the same values be used throughout the generator, perhaps based on the value specified in the PDF.

- *MPI and beam remnant effects:* As discussed above, since MPI modelling is the element of Monte Carlo modelling least constrained by *ab initio* QCD calculation, it is left untuned until the final stage. There may be many parameters in MPI models – essentially all modelling aspects described in Section 7.3 can introduce one or more parameters. The key parameters common to most eikonal MPI models are the $p_{\perp\min}$ cutoff/regulator for perturbative $2 \to 2$ scattering, the parameterization of the scaling of this cutoff with collision energy, the hadronic matter distribution/overlap, and any parameters relating to colour-reconnection of either strings or clusters. The primordial $k_\perp$ width is often considered as part of this tuning step, as it may affect soft QCD observables as well as the peak region of the Z^0 $p_\perp$ spectrum. As MPI models generate multiple scattering from low-x gluons extracted from the beam-remnants, they are profoundly affected by the choice of PDF. Hence, distinct MPI tunings are required for each PDF. The most obvious parameter affected by a change of PDF is $p_{\perp\min}$: when using a PDF with a large low-x gluon fraction, the MPI model will require more screening of the divergent partonic cross section than for a PDF with a smaller amount of soft gluon. Accordingly, tunes with PDFs such as LO* [86] which have a lot of low-x gluon tend to have higher $p_{\perp\min}$ values than tunes of the same generator using e.g. the CTEQ6L1 [334] PDF.

  The observables for MPI tuning are minimum bias and underlying event data from as many hadron colliders as possible. As a key feature of soft QCD modelling is the scaling of MPI activity with the collider center-of-mass energy, a wide range of collision energies is desirable. Experimental tunings may place emphasis on the collider of most interest – currently the LHC – for the purpose of best describing the soft QCD backgrounds to hard-process simulations at that collider. To date the most comprehensive MPI tunes have included data from the CERN S$p\bar{p}$S, RHIC, the Tevatron, and the LHC. HERA data have not yet been included in hadron collider MPI tuning, but whether a single tune can describe both $e^{\pm}p$ and $pp/p\bar{p}$ data is a strong check on the domain of validity of the generator's MPI model [335]. LHC results on

identified particle distributions in minimum bias and underlying event data will provide another test of currently unprobed model details.

The Rivet [251] package for MC generator validation and the Professor [336] system for generator tuning have become established tools in both the collider theory and experiment communities. Their strength is in systematically verifying event simulations and optimizing their parameters, where required and physically sensible. Both tools are described in the following sections.

17.2. Rivet

Rivet is a Monte Carlo *validation* tool: it encodes MC equivalents of an ever more comprehensive set of high-energy collider analyses which are particularly useful for testing the physics of MC generators. Rivet does not itself produce generator tunings, but provides a standard set of analyses by which to verify the accuracy of a given generator with a given tuning. These analyses are based upon a set of calculational tools that make writing of new analyses by either phenomenologists or experimentalists relatively straightforward.

Several fundamental design principles have been derived from the experience on Rivet's predecessor system, HZTool [337, 338], and from iteration of the Rivet design:

- No generator steering: Rivet relies entirely on being provided, by unspecified means, with events represented by the HepMC [250] event record.

- No generator-specific analyses: official Rivet analyses are specifically not allowed to use the generator-specific portions of the supplied event records. Apart from a few very limited exceptions, all analyses are based solely on physical observables, i.e. those constructed from stable particles (those with HepMC status 1) and physical decayed particles (those with status 2). This approach is fully compatible with the approach to robust generator phenomenology discussed in Section 16.2.

- Rivet can be used as a C++ library to be interfaced with generator author or experiment analysis frameworks, as a Python module for construction of higher-level tools (for example, much of the Rivet documentation is generated this way), or as a command line tool (which

itself makes use of the Python interface). This exemplifies a general philosophy to keep the tools simple and flexible, rather than constrain Rivet's applicability to a pre-defined collection of specific tasks.

Internally, Rivet analyses are based on a comprehensive set of calculational tools called *projections*, which perform standard computations such as jet algorithms (using FastJet [339]), event shape observables, and a variety of other common tasks. Use of projections allows, e.g.

- simplification of analysis code;
- encapsulation of complexities arising from the ban on use of event record internal entities (the summation of photon momenta around charged leptons during vector boson reconstruction is a good example);
- and efficiency gains over pure library functions, via a complex (but hidden) system of automatic projection result caching.

Users can write their own analyses using the Rivet components and use them via the Rivet programming interface (API) or command-line tool without re-compiling Rivet, due to use of an analysis "plugin" system. Separation between generator and Rivet on the command-line is most simply achieved by using the HepMC plain text `IO_GenEvent` format via a UNIX pipe (a.k.a. FIFO): this avoids disk access and writing of large files, and the CPU penalty in converting event objects to and from a text stream is in many cases outweighed by the general-purpose convenience. For generator-specific use of Rivet, the programmatic interface allows HepMC objects to be passed directly in code, without this computational detour. While this method requires some up-front integration into generator frameworks, eliminating the temporary conversions to and from a plain text format provides a significant performance gain, and the API control gives more flexibility, e.g. in use of resulting histograms, than is possible with the command-line tool. A sister tool, AGILe [340], is provided for convenient control of several legacy Fortran-based generators, while the MCnet generators either feed a HepMC text stream into Rivet, or in several cases use the direct programmatic interface.

Reference data for the standard analyses are included in the Rivet package as a set of XML files in the AIDA [341] format. After several years of re-development as part of the CEDAR [340] project, the HepData [342]

database of HEP experimental results is used to directly export data files usable by Rivet from its Web interface at `http://hepdata.cedar.ac.uk/`: this can be used by anyone developing new analyses based on papers in HepData. Analysis histograms are directly booked using the reference data as a binning template, ensuring that data and MC histograms are always maximally consistent.

The most recent version of Rivet at the time of writing is 1.4.0. This release focuses on quality control of official analyses, and was largely driven by requirements of LHC experiment MC tuning studies, by validation requirements of MCnet ME/PS merging algorithm developments, and by increasingly wide use of weighted events to cover disparate phase space regions in single MC runs. Development of Rivet has also driven much of the feature development and bug-fixing in HepMC in recent years, in particular improving the treatment of physical units, propagation of cross section information in the event record (supported by all MCnet generators), and a more complete event weighting system.

With the increasing user demand for Rivet functionality, major effort has been devoted to making the command-line tools and post-processing scripts intuitive, comprehensive and bug-free. The emphasis on usability also led to making Rivet analyses "self-documenting": each analysis has a structured set of metadata specifying name, authors, run conditions, a description, etc., which is used (via the Python interface) to provide interactive help, HTML documentation, and a reference section in the Rivet manual.

The next major stage of development is the upgrade of Rivet's histogramming and data analysis code, which is currently rather basic. The developing data analysis library will be of general-purpose usefulness, but will provide some features particularly useful for MC validation and tuning analyses, such as parallel handling of event weight vectors for integrated event re-weighting, and non-contiguous histogram binning as required by several experimental analyses. The upgrade will also enable statistically accurate combination of runs, allowing for greater parallelization of Rivet analyses that require large event statistics: this major development will mark Rivet version 2.0.0.

17.3. Professor

The Professor system builds on the output of MC validation analyses such as those in Rivet, by optimizing generator parameters to achieve the best possible fit to reference data. The main description of Professor's details

is found in reference [336], so we will only summarize it here. The most recent version of Professor at the time of writing is 1.1.0.

Fundamentally, generator tuning is an example of the more general problem of optimizing a very expensive function with many parameters: the volume of the space grows exponentially with the number of parameters and the CPU requirements of even a single evaluation of the function mean that any attempt to scan the parameter space will fail for more than a few parameters. Here, the expensive function is running a generator with a particular parameter set to recreate a wide range of analysis observables, using a package such as Rivet. The approach adopted by Professor is to parameterize the expensive function based on a non-exhaustive scan of the space: it is therefore an approximate method, but its accuracy is systematically verifiable and it is currently the best approach available.

The MC parameterization is generated by independently fitting a function to each of the observable bin values, approximating how they vary in response to changes in the parameter vector. One approach to fitting the functions would be to make each function a linear combination of algebraic terms with n coefficients α_i, then to sample n points in the parameter space. A matrix inversion would then fix the values of α_i. However, use of a pseudoinverse for rectangular matrices allows a more robust coefficient definition with many more samples than are required, with an automatic least-squares fit to each of the sampled "anchor points": this is the method used by Professor. By aggregating the parameterizations of all the observable bins under a weighted goodness of fit (GoF) measure a numerical optimization can be used to create an "optimal" tune. The GoF currently used in Professor is a heuristic function based on a χ^2, but augmented with inclusion of all available errors – as opposed to the traditional Pearson definition which uses the number of MC events in each bin as the sole uncertainty measure in the denominator. In practice, many different semi-independent (sampled with replacement) combinations of MC runs are used to provide a systematic handle on the degree of variation expected in tunes as a result of the inputs, to avoid the problem that a single "maximum-information" tune may not be typical of the parameter space.

The Professor tools have been used in tuning of several generators, including the MCnet ones already featured, particularly for the hadronization and soft QCD multiple-scattering aspects of event generation, where theory is least predictive and generators have most free parameters. Initial studies focused on the Pythia 6 MC generator [161], as this had already been the

focus of a CDF tuning campaign and was well understood. It was found that the parameterization method worked well in all cases, and a range of systematic methods and tools were developed to check the accuracy of the approximations, such as line-scans through the parameter space. Parameter spaces and observables with discontinuous behaviours – e.g. some aspects of cluster hadronization – remain problematic for any method that assumes smooth parameterizations. Several approaches exist to handle this, including parameter transformation, use of separate parameterizations in distinct regions, and manually avoiding tuning across such discontinuities. As discussed in Section 17.1, factorization of the total parameter space into block diagonal tuning stages is required: with Professor, $\mathcal{O}(10)$ parameters at a time has been found to be a practical maximum.

Much of the effort in constructing a generator tune is now focused on the development of a set of fit weights for the observables in a tune: different applications may wish to place different emphases on different observables, e.g. LHC vs. Tevatron data, or underlying event vs. minimum bias data. Once a set of weights has been chosen, it is a matter of logistics to create equivalent tunes for different PDFs: this permits a more accurate measure of the systematic effect of PDF choice than was previously possible. In the particular case of MPI model tuning to soft QCD observables, this approach has shown that much of the effect of PDF changes can be absorbed into typical MPI model parameter choices.

The intermediate parameterizations have proven useful in their own right: the `prof-I` GUI tool provides interactive visualization of observable responses to parameter changes and is useful for MC developers as a model-exploration and debugging tool. The usefulness of fast parameterization is not limited to MC generators, and Professor has been used for other studies from extra-solar planets to exploration of supersymmetric model phenomenology. As the LHC era matures, the demand for "new" tunes will naturally reduce – to be replaced with a need for more accurate assessments of systematic uncertainty. Professor will remain a useful tool for this purpose, as the MC parameterizations can be used for construction of tune-error estimates. In one approach, parameter points sampled from the multi-dimensional Gaussian distribution defined by the numerical minimizer covariance matrix are mapped into observables using the parameterizations, defining error bands for given statistical confidences. Alternatively, the same covariance matrix can be used slightly differently to construct Hessian "error tunes", or "eigentunes". The latter approach is already in use by LHC ex-

perimental collaborations to improve the accuracy of MC-derived modelling systematics for detailed LHC physics studies.

18. Illustrative results

In this section we show results from the Herwig++, Pythia 8 and Sherpa MC generators described in Part II, compared to data from a variety of collider experiments from LEP to the LHC. In all these plots, the versions and tunes shown are: for Herwig++, a pre-release copy of version 2.5.0 with the default tune to the MRST LO** PDF; for Pythia 8, version 8.145 with tune 4C and the CTEQ6L1 PDF; and for Sherpa, version 1.2.3 with the default tune and the CTEQ6L1 PDF. All the analyses shown are in Rivet.

It should be emphasised here that the generators have not yet been optimally tuned to LHC data overall, or indeed to any of the particular plots shown. The intention here is rather to give an "existence proof" of output from the programs. Therefore the success or otherwise of a generator in fitting the data should not at this stage be taken as a true measure of its performance. As stated in the figure captions, as tuning progresses the plots will be updated and archived at `http://mcplots.cern.ch/`.

Fig. 18 shows the Z^0 transverse momentum distribution in $p\bar{p}$ collisions at $\sqrt{s} = 1.8$ TeV, compared with CDF data [91]. As discussed in Section 7.1, the position and shape of the peak in this distribution is sensitive to the modelling of non-perturbative effects generically termed "primordial $k_\perp$".

In Fig. 19 we show results on soft QCD processes compared with ATLAS minimum bias data [93].

Figs. 20–22 show observables relevant to the underlying event, discussed in Section 7, compared to ATLAS data at 900 GeV and 7 TeV [343]. Various indicators of event activity are measured in the transverse region, i.e. at $60^\circ - 120^\circ$ in azimuth, relative to the leading-$p_\perp$ charged particle. Fig. 23 shows similar results for the Tevatron, in the transverse region relative to the leading jet, and in the towards region, i.e. closer than 60° in azimuth, relative to the Z^0 direction in Drell-Yan events, compared to CDF data [344].

Some results on final states in e^+e^- annihilation at the Z^0 peak are shown in Figs. 24–25, together with ALEPH data [345, 346]. Other plots relevant to jet fragmentation are shown in Figs. 26–28.

Finally Fig. 29 shows results from the MCnet generators on the colour-coherence test discussed in Section 4.5 (already displayed in Fig. 4 for the earlier generator Pythia 6), again compared with CDF data [46].

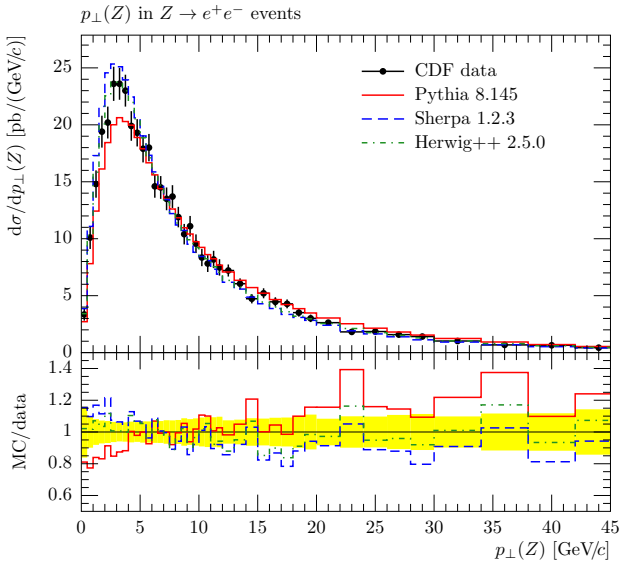

Figure 18: CDF 2000 Z^0 $p_\perp$ peak [91]. The location of the peak is very sensitive to the degree of "primordial $k_\perp$" smearing in the generator, and the higher-$p_\perp$ region is affected by the parton shower. In all cases, the generators have been run with LO matrix elements, and the MC normalization is fixed to that of the data, to alleviate the requirement for an NLO cross-section. An up-to-date version of this plot can be found at `http://mcplots.cern.ch/`.

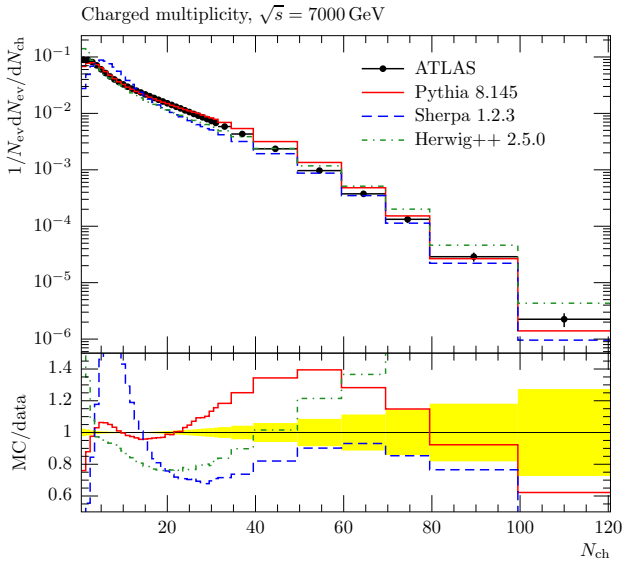

(a) Charged multiplicity

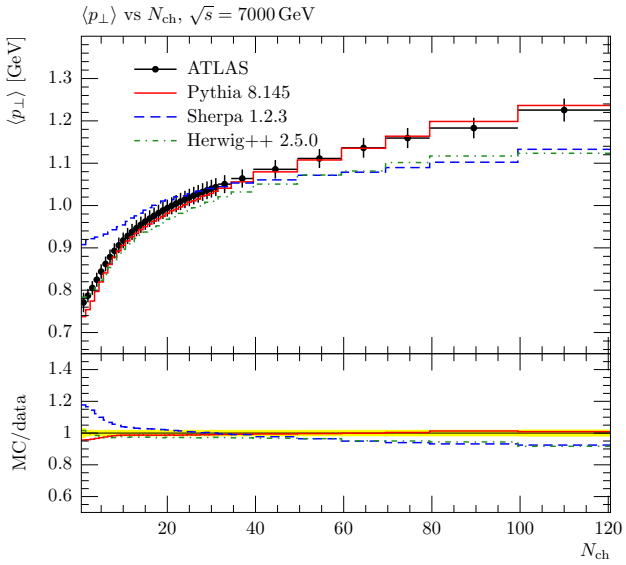

(b) $\langle p_\perp \rangle$ vs. N_{ch}

Figure 19: ATLAS minimum bias charged particle distributions at 7 TeV, with a charged particle $p_\perp$ cut of $p_\perp > 500$ MeV, $|\eta| < 2.5$, $c\tau > 10\,\text{mm}$ [93]. The MC description of these observables is dominated by the tuning of the MPI models: the inclusive charged multiplicity is dependent on the level of MPI activity, and the correlation between $\langle p_\perp \rangle$ and N_{ch} is affected by colour reconnection, as described in Section 7. Up-to-date versions of these plots can be found at `http://mcplots.cern.ch/`.

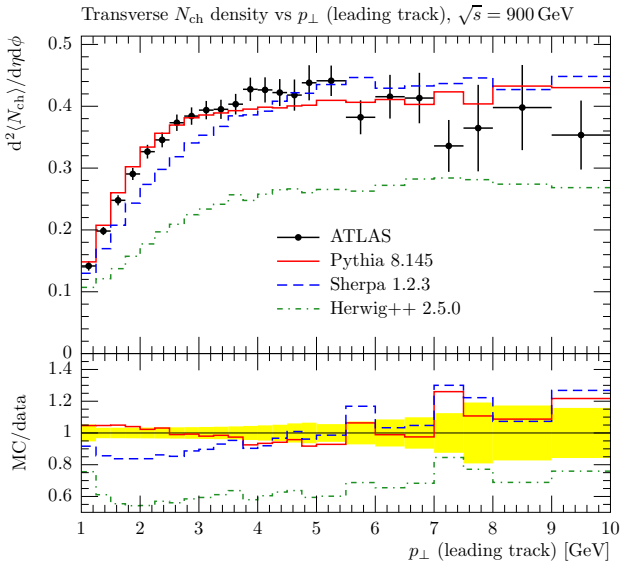

(a) Transverse N_{ch} at 900 GeV

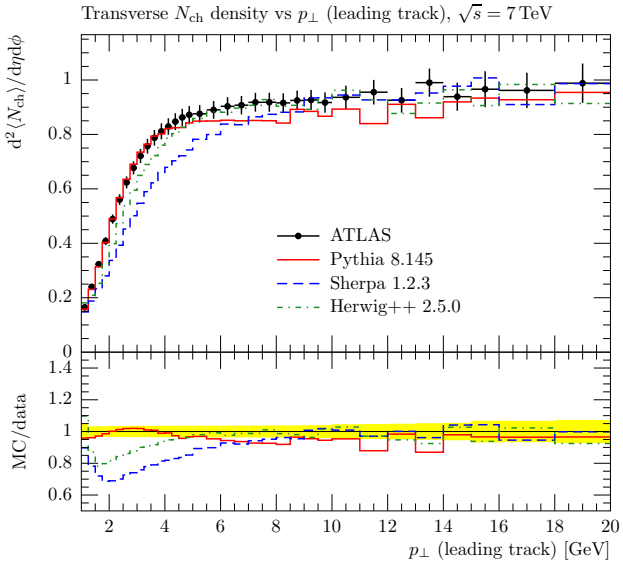

(b) Transverse N_{ch} at 7 TeV

Figure 20: ATLAS 900 GeV and 7 TeV underlying event observables, showing the dependence of MPI activity on the $p_\perp$ of the leading charged particle in the event, with a charged particle $p_\perp$ cut of $p_\perp > 500$ MeV, $|\eta| < 2.5$, $c\tau > 10\,\mathrm{mm}$ [343]. The MC description of these observables is dominated by the tuning of the MPI models, as described in Section 7. Up-to-date versions of these plots can be found at `http://mcplots.cern.ch/`.

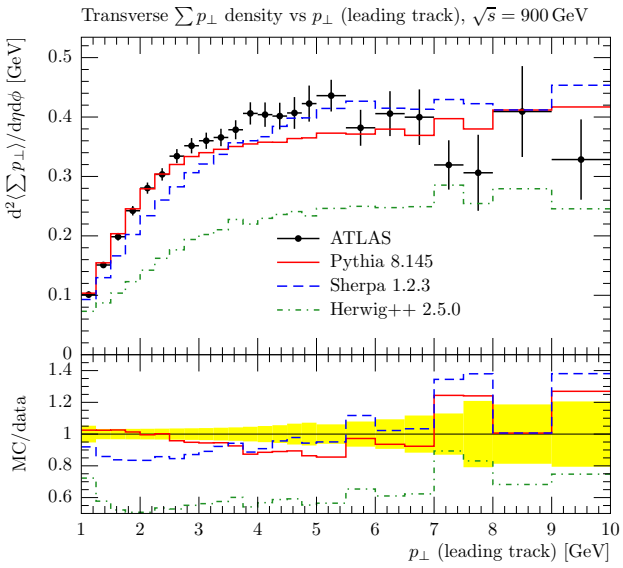

(a) Transverse $p_\perp^{\text{sum}}$ at 900 GeV

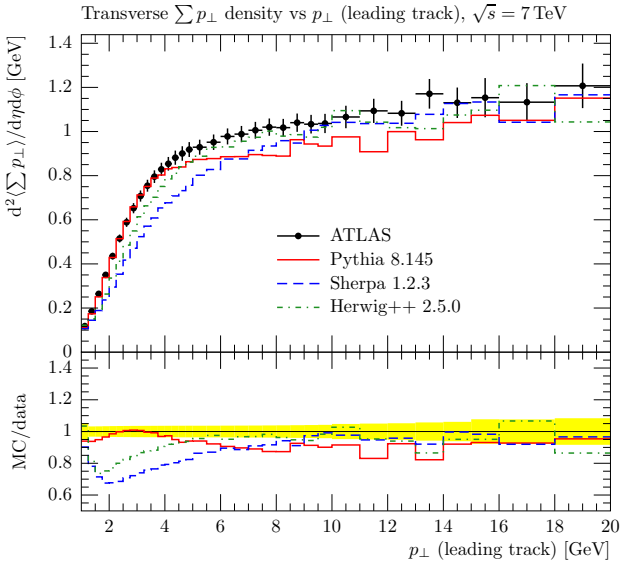

(b) Transverse $p_\perp^{\text{sum}}$ at 7 TeV

Figure 21: ATLAS 900 GeV and 7 TeV underlying event observables, showing the dependence of MPI activity on the $p_\perp$ of the leading charged particle in the event, with a charged particle $p_\perp$ cut of $p_\perp > 500$ MeV, $|\eta| < 2.5$, $c\tau > 10\,\text{mm}$ [343]. The MC description of these observables is dominated by the tuning of the MPI models, as described in Section 7. Up-to-date versions of these plots can be found at `http://mcplots.cern.ch/`.

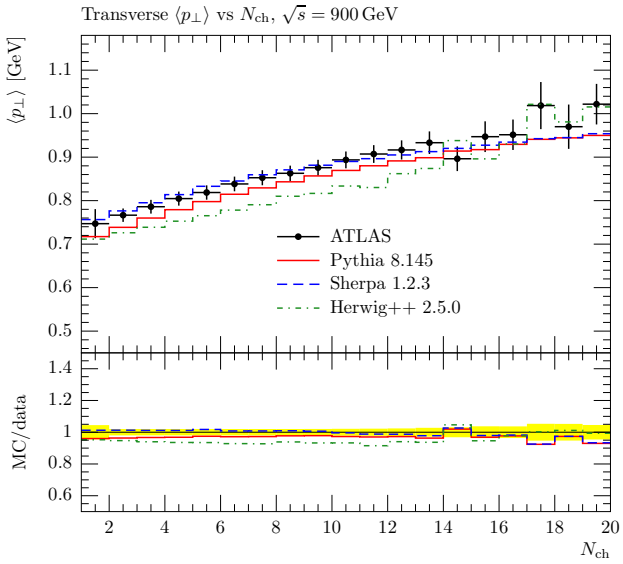

(a) Transverse $\langle p_\perp \rangle$ vs. $N_{\rm ch}$ at 900 GeV

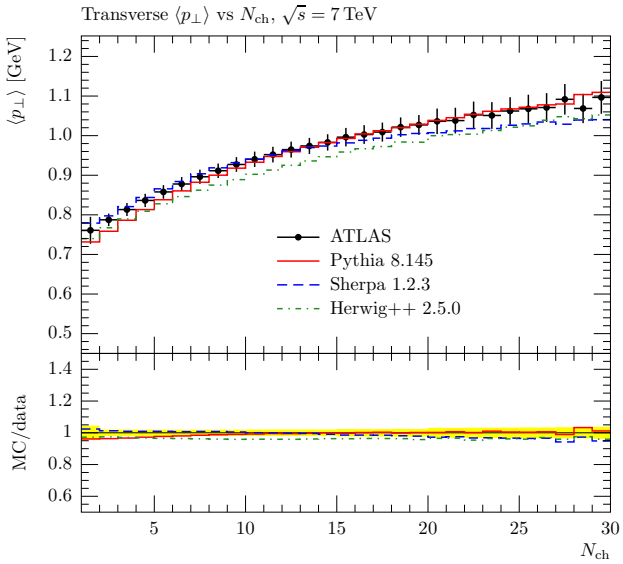

(b) Transverse $\langle p_\perp \rangle$ vs. $N_{\rm ch}$ at 7 TeV

Figure 22: ATLAS 900 GeV and 7 TeV underlying event $\langle p_\perp \rangle$ vs. $N_{\rm ch}$ correlation in the region transverse to the leading charged particle, with a charged particle $p_\perp$ cut of $p_\perp > 500$ MeV, $|\eta| < 2.5$, $c\tau > 10\,\text{mm}$ [343]. The MC description of these observables is dominated by the tuning of the MPI models, as described in Section 7. Up-to-date versions of these plots can be found at `http://mcplots.cern.ch/`.

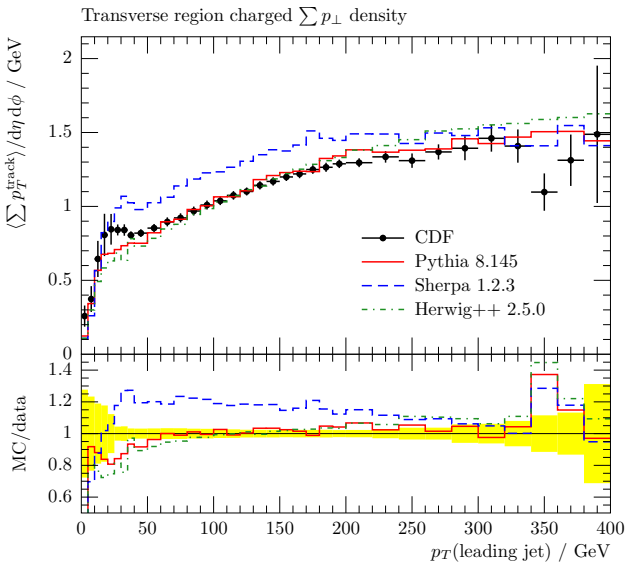

(a) CDF Run 2 transverse $p_\perp^{\text{sum}}$ in leading jet events at 1960 GeV

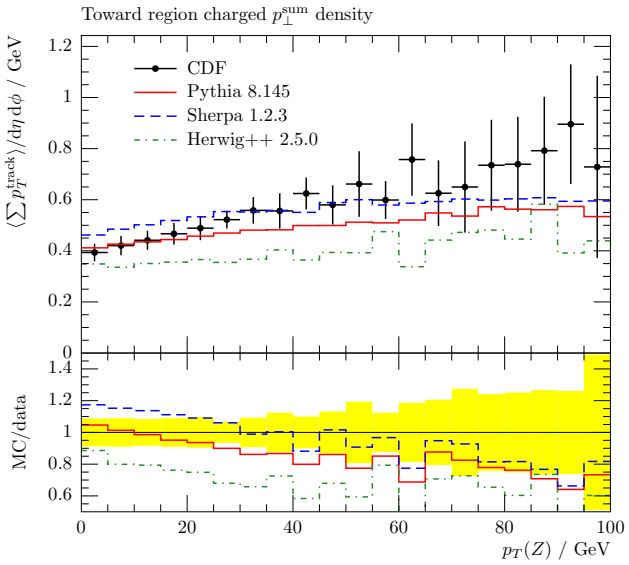

(b) CDF Run 2 towards $p_\perp^{\text{sum}}$ in Drell-Yan events at 1960 GeV

Figure 23: CDF Run 2 underlying event profile observables: the $p_\perp^{\text{sum}}$ is shown in the transverse region for leading jet events, and the towards region in Drell-Yan events [344]. Up-to-date versions of these plots can be found at `http://mcplots.cern.ch/`.

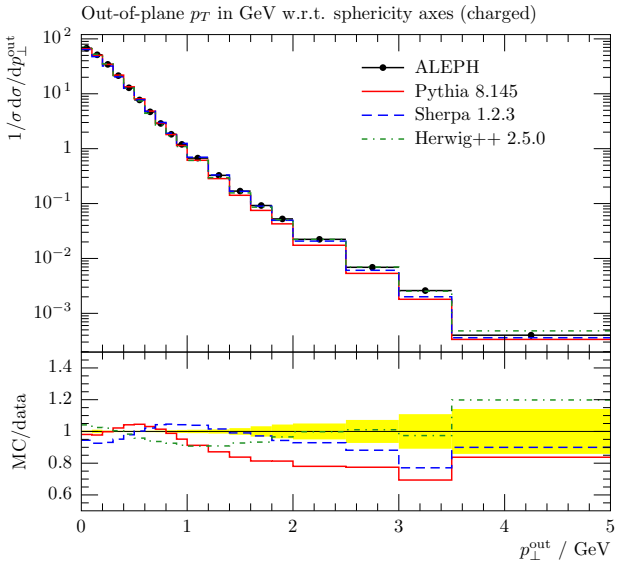

(a) Summed out-of-event-plane $p_\perp$ [345]

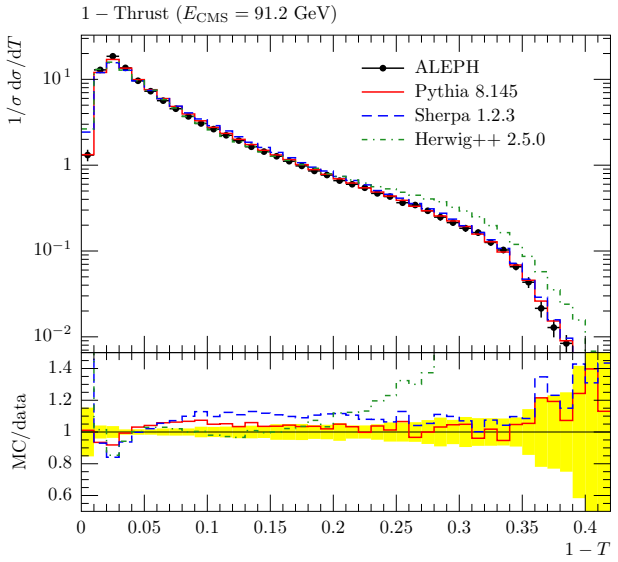

(b) $1 - \mathrm{Thrust}$ [346]

Figure 24: e^+e^- event shapes measured by ALEPH at 91 GeV [345, 346]. Up-to-date versions of these plots can be found at `http://mcplots.cern.ch/`.

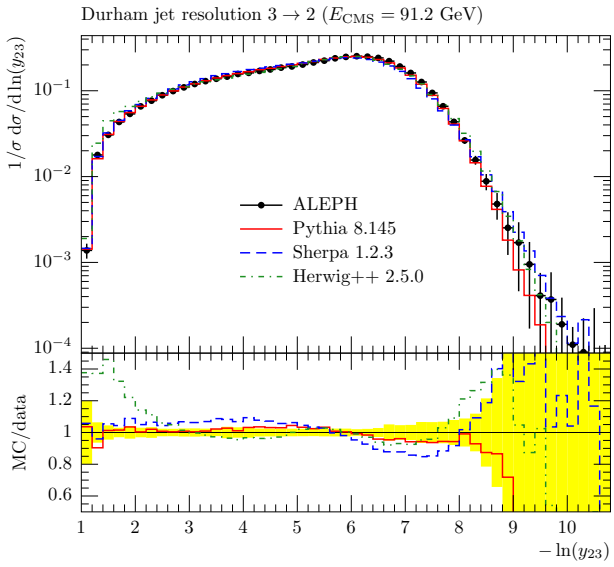

(a) Differential 3-jet rate

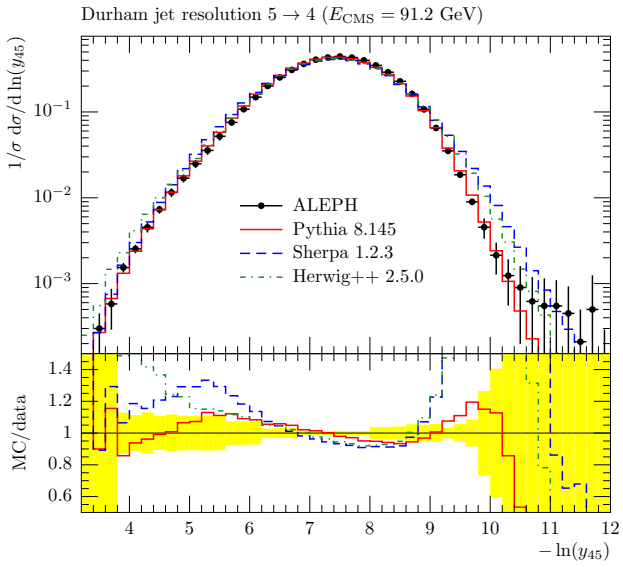

(b) Differential 5-jet rate

Figure 25: e^+e^- differential jet rates measured by ALEPH at 91 GeV [346]. The quantity $y_{n-1,n}$ is the value of the $k_\perp$-jet resolution at which n jets are just resolved. Up-to-date versions of these plots can be found at `http://mcplots.cern.ch/`.

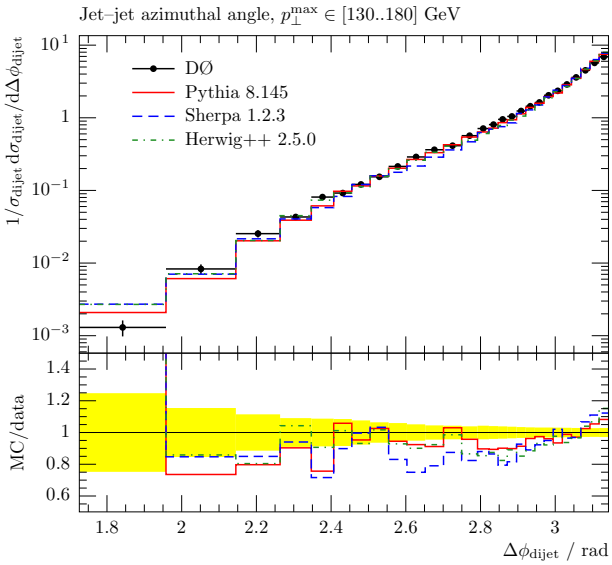

(a) DØ dijet azimuthal decorrelation [347]

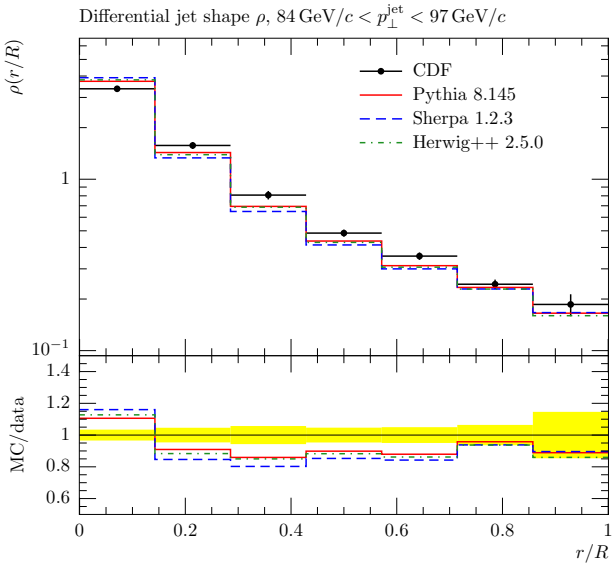

(b) Hadron collider jet shapes: CDF [348]

Figure 26: Hadron collider shower-sensitive observables: dijet azimuthal decorrelation and jet shapes measured by DØ and CDF in Run 2 [347, 348]. The azimuthal decorrelation is a measure of the influence of three-jet configurations and shower emissions in disrupting a purely back-to-back two-parton configuration. Jet shapes measure the distribution of (transverse) momentum as a function of radius within jets. Up-to-date versions of these plots can be found at `http://mcplots.cern.ch/`.

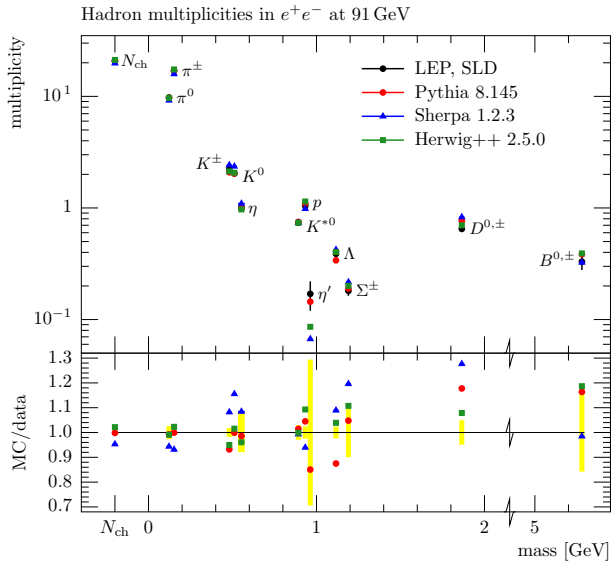

(a) LEP/SLD identified particle multiplicities [152]

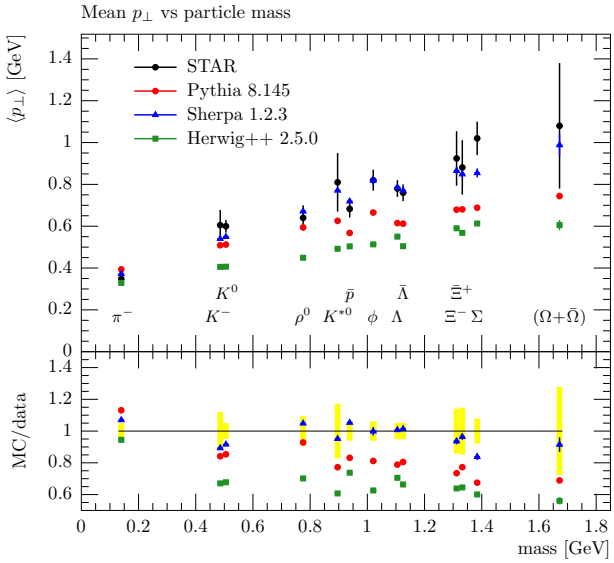

(b) STAR identified particle mean $p_\perp$ [349]

Figure 27: Identified hadron multiplicities in e^+e^- collisions at the Z peak and $\langle p_\perp \rangle$ vs. particle mass in pp collisions at 200 GeV. These observables are determined primarily by the tuning of the hadronization models, both the flavour and kinematic aspects, but the overall multiplicities are also strongly dependent on the tuning of the parton showers (and MPI models, for the hadron collider observables). Up-to-date versions of these plots can be found at `http://mcplots.cern.ch/`.

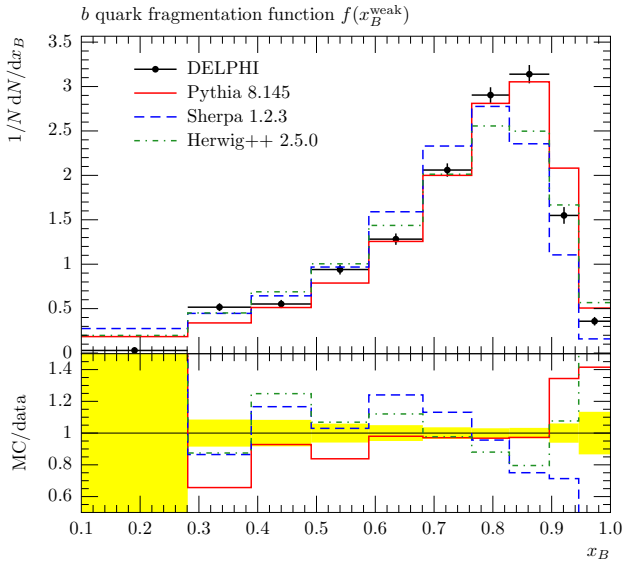

Figure 28: DELPHI B fragmentation function $x_B = 2E_B/\sqrt{s}$ for weakly decaying b hadrons [350]. Most Monte Carlo models apply a special fragmentation function treatment to heavy quarks, but this observable is not entirely decoupled from light quark fragmentation parameters. An up-to-date version of this plot can be found at `http://mcplots.cern.ch/`.

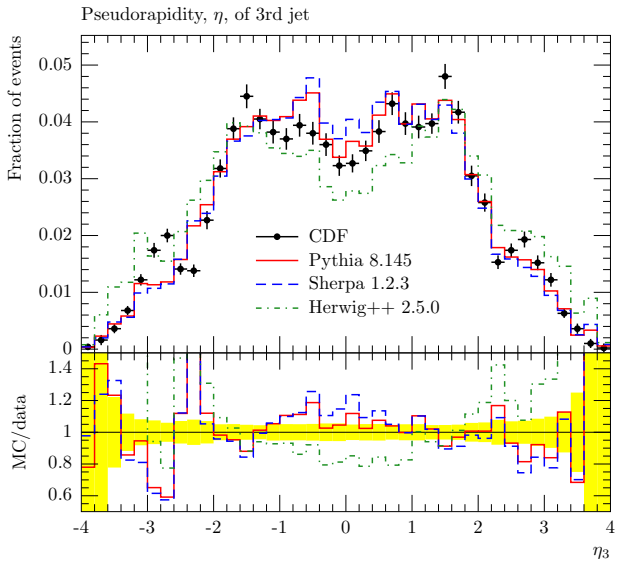

Figure 29: CDF's evidence for colour coherence in $p\bar{p}$ collisions at $\sqrt{s} = 1.8$ TeV [46]. The pseudorapidity of the third jet is plotted, uncorrected for detector effects, with the Herwig++, Pythia 8 and Sherpa Monte Carlo generators. All these generators include colour coherence effects via either angular-ordered parton showers (Herwig++) or transverse-momentum-ordered dipole showers (Pythia 8, Sherpa), and hence correctly exhibit a dip at central rapidity. The correlated fluctuations between MC samples are due to statistical errors on the detector-smearing correction factors taken from the CDF paper. An up-to-date version of this plot can be found at `http://mcplots.cern.ch/`.

Acknowledgements

This work was supported by the European Union as part of the EU Marie Curie Research Training Network MCnet (MRTN-CT-2006-035606). We are most grateful to the members of the MCnet network for their dedication and hard work, which underlie many of the new developments reviewed here.

We thank André Hoang for permission to use his lectures at the 2009 MCnet summer school as the basis for Appendix C and for his and Iain Stewart's comments on the manuscript.

JMB's work is supported in part by a Royal Society Wolfson Research Merit Award. SG acknowledges support from the Helmholtz Alliance "Physics at the Terascale". SH's work was supported by the US Department of Energy under contract DE–AC02–76SF00515. LL and TS acknowledge support from the Swedish Research Council (contract numbers 621-2007-4157, 621-2008-4252 and 621-2009-4076). ELN's work is supported in part by a Royal Society University Research Fellowship. MHS's work is supported in part by an IPPP Associateship and in part by a Royal Society Wolfson Research Merit Award. SS acknowledges support by the German Federal Ministry of Education and Research (BMBF). BW acknowledges the support of a Leverhulme Trust Emeritus Fellowship.

Part IV
Appendices

Appendix A. Monte Carlo methods

Appendix A.1. Generating distributions

We give here a very brief review of the numerical methods used in Monte Carlo event generators. The basic requirement of such a generator is to produce a set of representative points in the phase space of the process under study, in such a way that the density of points follows the probability distribution predicted for that process. The simplest case is that of a single variable x to be distributed in the region $[x_{\min}, x_{\max}]$ with probability distribution proportional to $f(x) \geq 0$. Then if $R \in [0, 1]$ is a uniform pseudo-random

number, we want to generate x such that

$$\int_{x_{\min}}^{x} f(x')\,\mathrm{d}x' = R\int_{x_{\min}}^{x_{\max}} f(x')\,\mathrm{d}x' \ . \tag{A.1}$$

If the indefinite integral of $f(x)$ is a known function $F(x)$ then this is equivalent to solving

$$F(x) = R\,F(x_{\max}) + (1-R)\,F(x_{\min}) \ . \tag{A.2}$$

If the inverse function F^{-1} is known, the problem is solved. Otherwise, the solution can often be obtained quite fast numerically, because the positivity of $f(x)$ ensures that $F(x)$ is monotonic.

If the indefinite integral of $f(x)$ is not known, or if the method of numerical solution is too slow, then the *hit-or-miss* method can be used. Here we suppose that a function $g(x) \geq f(x)$ on the interval $[x_{\min}, x_{\max}]$ has a known indefinite integral $G(x)$ that can be inverted or solved for x. Then we generate the distribution according to $g(x)$ and accept the resulting point with probability $f(x)/g(x)$, i.e. if $f(x) > R'g(x)$ where $R' \in [0,1]$ is another uniform pseudo-random number. In particular we can choose a constant $g(x) = g_u \geq \max\{f(x), x \in [x_{\min}, x_{\max}]\}$, generate points uniformly as

$$x = R\,x_{\max} + (1-R)\,x_{\min} \ , \tag{A.3}$$

and accept those points that satisfy $f(x) > R'g_u$. However this may be very inefficient (many points may be rejected) if $f(x)$ is very non-uniform or if g_u is chosen too large.

Appendix A.2. Monte Carlo integration and variance reduction

In reality the phase space is multi-dimensional. Then it is important to appreciate that the Monte Carlo method is based on the concept of an integral as an average. Suppose we have a matrix element-squared $f(\mathbf{x})$ which is a function of the n-component vector $\mathbf{x}$, and we want to integrate it over a region V of $\mathbf{x}$-space, for example to compute a cross section:

$$I[f] = \int_V \mathrm{d}^n x\, f(\mathbf{x}) \ . \tag{A.4}$$

Standard methods of integration (Simpson's, Gaussian, ...) are too laborious and/or inaccurate for n large (say $n > 3$). However, if N points $\{\mathbf{x}_i, i =$

$1, \ldots, N\}$ are distributed (pseudo-)randomly in V, then the central limit theorem of statistics tells us that the *mean value* of f on those points is an unbiased estimator of the integral,

$$I[f] \simeq \langle f \rangle = \frac{1}{N} \sum_{i=1}^{N} f(\mathbf{x}_i) \; , \tag{A.5}$$

and that the estimated error $E[f]$ on this evaluation is given by the *variance* of f,

$$\mathrm{Var}(f) = \langle (f - \langle f \rangle)^2 \rangle = \langle f^2 \rangle - \langle f \rangle^2 \; , \tag{A.6}$$

as

$$E[f] = \sqrt{\frac{\mathrm{Var}(f)}{N-1}} \; . \tag{A.7}$$

Thus the error decreases as the inverse square root of the number of points, independent of the dimensionality of the integral. Furthermore, for a given number of points, the error will be less if the variance of the integrand is small.

The variance can be reduced by a change of variables that "flattens" the integrand. Consider the mapping $\mathbf{x} \to \mathbf{y}(\mathbf{x})$ with Jacobian

$$\left| \frac{\partial(\mathbf{y})}{\partial(\mathbf{x})} \right| = g(\mathbf{x}) \; . \tag{A.8}$$

Then

$$I[f] = \int_{V'} \mathrm{d}^n y \, \frac{f(\mathbf{x})}{g(\mathbf{x})} \; , \tag{A.9}$$

where V' is the region in $\mathbf{y}$-space corresponding to V in $\mathbf{x}$-space. If $h = f/g$ is a function with less variance than f itself then the error will be reduced by distributing points uniformly in $\mathbf{y}$-space. This is known as *importance sampling*. To obtain a set of points distributed according to $f(\mathbf{x})$, as desired for an event generator, we can now apply the hit-or-miss method, accepting points with probability h/h_{lim}, where h_{lim} is an upper bound on the value of h in V'. The Monte Carlo efficiency, as measured by the fraction of points accepted, $\langle h \rangle / h_{\mathrm{lim}}$, will usually also be increased as a result of the variance reduction.

In some applications, for example NLO cross section calculations, the integrand $f(\mathbf{x})$ can contain integrable singularities. Although these would give

a finite result if they were calculated analytically, their variance is divergent and hit-or-miss Monte Carlo will fail to converge. Variance reduction, with a carefully chosen generated distribution $g(\mathbf{x})$, becomes mandatory in such cases.

More sophisticated methods for variance reduction, such as *stratified* or *multichannel sampling*, are also applied in Monte Carlo generators, particularly when dealing with matrix elements that have sharp peaks due to resonance production or matrix element singularities close to the physical region, as discussed in Appendix B.

If it is difficult to arrive at an acceptable efficiency by reducing the variance of the integrand and/or finding a good upper bound on it, one may wish to resort to generating *weighted events*. In that case the phase-space points $\{\mathbf{x}_i\}$ (or $\{\mathbf{y}_i\}$ if some variance reduction has been achieved) are used to represent events, but each event has a different weight f_i (or h_i) when contributions to observables are computed. In that case one has to take account of the variance of the weights when computing error on observables. That means, for example, that one must keep track of the sum of the squared weights as well as the weights contributing to each bin of a histogram. In contrast the error for the *unweighted events* obtained from hit-or-miss is just given by the square root of the number of events in the bin.

An example of a situation in which weighted events can be useful is in the study of jet hadroproduction, where the distribution of jet transverse energy E_T falls very rapidly, roughly as E_T^{-5}. If events are generated according to the relevant hard subprocess matrix elements multiplied by $p_\perp^5$, where $p_\perp$ is the transverse momentum of the hardest final-state parton in the subprocess, and then weighted by $p_\perp^{-5}$, event properties can be explored over the full range of jet E_T without generating huge event samples.

For further details of general Monte Carlo methods see, for example, [351] and the relevant section of the Review of Particle Physics [352].

Appendix A.3. Veto method

It often happens in event generators that one wishes to generate an ordered sequence of values $\{q_i\}$ of some variable q, for example the evolution variable of a parton shower, according to a distribution function with a rather complicated form, in this case the relevant Sudakov form factor. The *veto method*, a variant of hit-or-miss, is a useful way of achieving this.

Suppose that, given Q, we wish to generate $0 < q_1 < Q$ such that the probability that $q_1 < q$ is $F(q)/F(Q)$, where $F(q)$ is a monotonically in-

creasing function with $F(0) = 0$, e.g. the Sudakov form factor $\Delta(Q^2, q^2)$ in Eq. (15)[26] In simple cases we can do this as in Eq. (A.2), by solving the equation $F(q_1) = RF(Q)$ where $R \in [0, 1]$ is a uniform pseudo-random number. However, if $F(q)$ is too complicated for this, but its derivative $f(q) = \mathrm{d}F/\mathrm{d}q$ is known, and we can find a simpler monotonic function $G(q) \geq 0$ with derivative $g(q)$ such that $f(q)/F(q) < g(q)/G(q)$ for $q < Q$, we can proceed as follows:

1. Solve $G(q') = R\,G(Q)$ for q', where R is a random number as above.
2. If $f(q')/F(q') > R'\,g(q')/G(q')$, where R' is another random number, set $q_1 = q'$.
3. Otherwise *veto* this choice of q_1, i.e. set $Q = q'$ and go back to step 1 to find $q'' < q'$.

To see that this generates the correct probability $P(q_1 < q) = F(q)/F(Q)$, we note first that the probability distribution of q' from step 1 is $dP/dq' = g(q')/G(Q)$, and the probability of vetoing q' is

$$P_{\mathrm{veto}}(q') = 1 - \frac{f(q')G(q')}{F(q')g(q')} \; . \tag{A.10}$$

Now the probability of finding $q_1 < q$ with no veto is

$$P(q_1 < q)_{0-\mathrm{veto}} = \frac{G(q)}{G(Q)} \; , \tag{A.11}$$

while the probability of finding $q_1 < q$ after one veto is

$$\begin{aligned} P(q_1 < q)_{1-\mathrm{veto}} &= \int_q^Q \mathrm{d}q' \frac{g(q')}{G(Q)} P_{\mathrm{veto}}(q') \frac{G(q)}{G(q')} \\ &= \frac{G(q)}{G(Q)} \int_q^Q \mathrm{d}q' \left[\frac{g(q')}{G(q')} - \frac{f(q')}{F(q')} \right] \\ &= \frac{G(q)}{G(Q)} \left[\ln \frac{G(Q)}{G(q)} - \ln \frac{F(Q)}{F(q)} \right] \; . \end{aligned} \tag{A.12}$$

[26]Strictly speaking, Eq. (15) requires $q^2 > 2Q_0^2$ where $Q_0 > 0$ and $\Delta(Q^2, 2Q_0^2) > 0$. We consider here the case that $Q_0 \to 0$, and discuss below the effect of $Q_0 > 0$.

Similarly the probability of finding $q_1 < q$ after two vetoes is

$$P(q_1 < q)_{2-\text{veto}} = \frac{1}{2!}\frac{G(q)}{G(Q)}\left[\ln\frac{G(Q)}{G(q)} - \ln\frac{F(Q)}{F(q)}\right]^2 , \qquad \text{(A.13)}$$

where the $1/2!$ comes from the fact that the vetoes are ordered, $q'' < q' < Q$. Summing over all numbers of vetoes gives an exponential series,

$$\begin{aligned} P(q_1 < q) &= \sum_{n=0}^{\infty}\frac{1}{n!}\frac{G(q)}{G(Q)}\left[\ln\frac{G(Q)}{G(q)} - \ln\frac{F(Q)}{F(q)}\right]^n \\ &= \frac{G(q)}{G(Q)}\exp\left[\ln\frac{G(Q)}{G(q)} - \ln\frac{F(Q)}{F(q)}\right] = \frac{F(q)}{F(Q)} , \qquad \text{(A.14)} \end{aligned}$$

as required.

As a simple example, suppose we have an upper bound $a > f(q)/F(q)$ for all $q < Q$. Then we can take $G(q) = \exp(aq)$, so that step 1 gives $q' = Q + (\ln R_1)/a$, and veto q' if $f(q')/F(q') < aR_2$. As in simple hit-or-miss, the method remains valid but becomes less efficient (more vetoes) if a is larger than necessary.

Once a value of q_1 has been accepted, q_2 can be generated by repeating steps 1–3 with Q replaced by q_1, and so on to create a decreasing ordered sequence $\{q_i\}$. In the case of a parton shower, the sequence terminates at q_n when the step 1 with $Q = q_n$ produces a value of q' less than the shower cutoff Q_0.

Appendix B. Evaluation of matrix elements

In this section we review in more detail the generation and evaluation of hard subprocess matrix elements and the related methods to integrate over the phase space of outgoing particles.

Appendix B.1. Matrix element calculation

Summation versus sampling. When calculating the cross section for a given process, an integral over the relevant phase space has to be performed, typically through Monte Carlo methods. Then, for each phase-space point (i.e. for each set of incoming and outgoing momenta) the matrix element squared has to be evaluated. This involves a summation and averaging over the unobserved quantum numbers of the outgoing and incoming particles,

respectively. On the level of squared amplitudes the summation can be performed analytically, involving algebraic relations such as completeness relations or the Dirac trace algebra, which yields an analytical result for the squared matrix elements, that can in turn be expressed by Lorentz-invariant combinations of the four-momenta of the involved particles. This method is typically applied for matrix elements of low final-state multiplicity, which are pre-computed and implemented explicitly in the event generators. On the level of numerically evaluated amplitudes, on the other hand, one may choose between a summation over all quantum states such as helicities and colours for a given phase-space configuration and a Monte Carlo sampling over these states, together with the phase-space integration. The computational complexities for summation and sampling for matrix elements with n external lines naively differ by the n^{th} power of the number of possible states, i.e. usually $\mathcal{O}(2^n)$ for the possible helicity assignments and $\mathcal{O}(3^{n_3}8^{n_8})$ for the possible colour assignments of n_3 external quarks and n_8 external gluons. By suitably eliminating common subexpressions of the matrix elements, one can, however, often reduce these naive factors quite considerably. The decision whether to sum or to sample over helicity and colour degrees of freedom is therefore strongly dependent on the process and the particle multiplicity. Corresponding comparisons have been presented, e.g. in [6]. This issue will not be discussed further here. We will, however, discuss different techniques to efficiently deal with coloured states, as the sum over colours usually poses the most severe restriction on the ability to evaluate high-multiplicity matrix elements.

Pre-computed matrix elements. Traditionally, the matrix elements acting as seeds for event generation have been related to processes with low multiplicity of two or maximally three particles in the final state. For such processes, analytical results are usually available, and consequently they are used in all event generators. With the advent of multijet merging methods and agreements for interface structures, the importance of incorporating such matrix elements directly into MC programs has diminished, such that in the new generation of event generators only a few pre-computed analytic matrix elements are available. On the other hand, due to the incorporation of matching methods for NLO matrix elements, some explicit next-to-leading order results are now direct inputs for event generation, just as leading-order results were previously. This situation is likely to change, as with the advent of general methods to automate the computation of NLO virtual corrections

the need for explicit calculations may slowly disappear.

The helicity method. Textbook methods of squaring full matrix elements and summing over helicity and colour through the application of completeness relations yields a rather large number of terms: for N Feynman diagrams in this method $N(N-1)/2$ contributions must be evaluated. An obvious way of reducing this number is to directly evaluate the amplitudes, yielding complex numbers, before summing and squaring them and before sampling over the phase space. In order to compute the individual numerical values of the amplitudes, an efficient representation in terms of external momenta and helicities is mandatory. A first solution to this problem was achieved in [284]. The basic idea is to replace all momentum-dependent terms appearing in an amplitude through suitably chosen spinor products. This substitution can always be achieved, since spinors are the simplest representations of the Lorentz group and their products correspondingly yield the minimal representation of a Lorentz-invariant complex number. One can, for example, identify the numerator of a fermion propagator as

$$\not{p} + \mu \;= \frac{1}{2} \sum_{\lambda} \left[u(\lambda,p)\bar{u}(\lambda,p) \;\left(1 + \frac{\mu}{\sqrt{p^2}}\right) + v(\lambda,p)\bar{v}(\lambda,p) \;\left(1 - \frac{\mu}{\sqrt{p^2}}\right)\right] , \tag{B.1}$$

and the polarization vector of a spin-1 boson with momentum $p+q$ can be written as

$$\epsilon_\mu(p+q) \;= \frac{1}{\sqrt{4p\cdot q}} \bar{u}(\lambda,q)\gamma_\mu u(\lambda,p)\,. \tag{B.2}$$

In such a way, and employing a Chisholm identity for terms of the form $\bar{u}\gamma^\mu u \times \bar{u}\gamma_\mu u$, every amplitude containing fermion interactions can be decomposed into spinor products of the form $\bar{u}u$ and $\bar{v}v$, see [284, 285, 353, 354]. In the context of tree-level matrix-element generators, the corresponding elementary building blocks are usually referred to as Lorentz functions. They are implemented in a similar form in any of the automated matrix-element generators listed above.

Feynman-diagram based methods. Having at hand the basic Lorentz functions to decompose amplitudes into terms that can be evaluated numerically in a straightforward manner, the remaining problem is the generation of

these amplitudes. Traditionally this is achieved through the construction of Feynman diagrams – an algorithm with improved efficiency using recursive relations will be discussed later. The diagrammatic approach has been followed for instance in MadGraph [9] and AMEGIC++ [5]. In both programs, Feynman-diagram-like topologies, i.e trees with binary or tertiary vertices, are generated and then filled with the actual interactions given by the physics model in question. The resulting objects are translated into so-called helicity amplitudes, i.e. into products of the Lorentz functions discussed in the previous paragraph. In so doing, some manipulations may be performed, trying to identify common subexpressions and either factoring them out or storing them such that identical pieces need to be calculated only once. In both cases, the programs write out the helicity amplitudes in a high-level programming language to be compiled and linked to the original program. The resulting libraries are then employed to calculate cross sections, to generate parton-level events and to pass these events on to a parton-shower simulation, for instance, using Les Houches Event Files, see Appendix B.3.

Skeletons. In Herwig++ only a few pre-computed squared matrix elements are available. The authors of this code have, however, compensated for this by a low-level matrix-element generator, which is capable of constructing helicity amplitudes for processes with up to four external particles (i.e. $2 \to 2$ scattering and $1 \to 3$ decay processes). Depending on the spin of those particles, the algorithm identifies all possible topologies (s, t, and u-channel as well as four-point interactions) for the process in question, with the corresponding propagators being specified by the Feynman rules given in an internal format. These topologies are then directly mapped onto the respective prefabricated helicity amplitudes. This algorithm greatly alleviates the task of integrating the cross sections efficiently: the knowledge of topologies and propagators allows for a direct translation into prefabricated integration channels, forming a multi-channel integrator, see Appendix B.2. For further details of the implementation of this algorithm we refer to [221].

Recursive techniques. There are several techniques for computing tree-level matrix elements that employ different versions of recursive relations. With increasing number of particles involved in the scattering they are superior to diagram-based methods, as they naturally implement an optimal common subexpression elimination. One such method, which we shall consider as an example of a recursive technique in this context, is the Berends-Giele

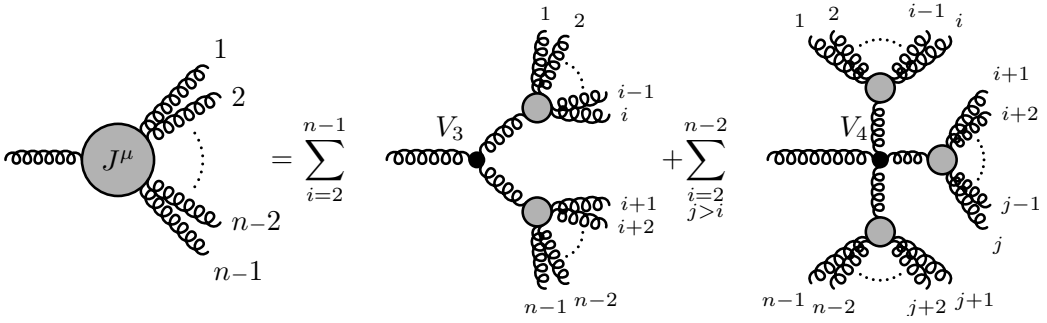

Figure B.30: Pictorial representation of the Berends-Giele recursive relations.

algorithm [355–359]. It has recently been improved to incorporate an efficient way to deal with colour [298], rendering it essentially equivalent to the Dyson-Schwinger methods employed for instance in HELAC [360], and comparable in efficiency with the ALPHA algorithm of [361], implemented in AlpGen [4] and O'Mega [11].

The basic idea of the Berends-Giele recursion algorithm can be summarized as follows. At first, an $n-1$-point gluon off-shell current, J^μ, is defined, which represents the sum of all colour-ordered Feynman diagrams with $n-1$ external on-shell legs and a single off-shell leg with polarization μ. This off-shell current can then be decomposed into lower-point off-shell currents, which are joined by the elementary gluon interaction vertices, thus forming a bigger part of the full scattering amplitude. This algorithm is schematically depicted in Fig. B.30. A full n-gluon amplitude is finally obtained by amputating the off-shell propagator and contracting the remaining quantity with the external polarization of gluon n.

Similar recursions exist for the off-shell quark currents [355] and for the full Standard Model [6]. They can, in fact, be defined for any theory allowing the construction of Feynman diagrams. A further improvement of this method was recently obtained through a decomposition of all four-particle vertices into three-particle ones. Such a decomposition reduces the computational complexity for many-particle final states, as the numerical effort grows approximately like N^n, with N the average number of legs in elementary vertices of the theory.

Treatment of colour. Several methods have been suggested over the past decades to optimize the computation of amplitudes including QCD particles

with respect to the colour degrees of freedom. There are two essentially different approaches: the textbook method would be to compute colour-ordered quantities, i.e. sets of Feynman diagrams or off-shell currents with all colour information combined into kinematics-independent prefactors. When assembling the full matrix element, colour-factors and kinematics-dependent functions are then treated separately. An alternative approach is to directly include colour in the diagrams or off-shell currents and to devise, for example, recursive relations which depend on the colour quantum numbers.

The latter approach has been very successful in the past, leading to the construction of advanced tree-level matrix-element generators, capable of dealing with very large final-state multiplicities [4, 6, 7, 360]. The textbook approach, on the other hand, is often much more convenient to use, especially when insight into the analytical structure of the computation is necessary. It also usually leads to a significant acceleration of matrix-element computations for low-multiplicity final states.

Although a number of possible colour bases exist [362–364], which have been used for several numerical comparisons in the past [298], the one that is widely adopted today is the colour-flow basis [7, 299]. The reason for its superior speed in the computation of large-multiplicity QCD amplitudes lies not only in the milder growth in the number of possible colour-ordered amplitudes, but also in the fact that every colour coefficient multiplying the kinematics-dependent functions in squared matrix elements consists only of delta functions, which are trivial to evaluate in a Monte Carlo program.

Appendix B.2. Phase-space integration

MC integration and sampling methods. Once the matrix element for a given process has been constructed, one is left with the task of performing the related integral over the phase space of the initial- and final-state particles. Taking account of the unknown momentum fractions of the initial-state partons, the dimension of this phase space is $(3n-4)+2$ at hadron colliders, with the integrand (the matrix element squared) typically exhibiting a challenging structure with pronounced peaks. While the large dimensionality renders traditional quadrature methods useless and enforces the usage of MC techniques, the difficult structures pose a serious threat to the convergence of the integration. This means that highly advanced sampling algorithms need to be introduced, which are dubbed phase-space integrators or "integration channels". From the formal point of view, all integration channels dealing with the same final state are equal, as they must finally yield exactly the

same value of the MC integral. However, they usually differ greatly in the rate of convergence and in practice one would obviously prefer to use the channel leading to the smallest error in the shortest time.

Multi-channel integration. To generate an adequate phase-space integrator for realistic $2 \to n$-particle processes, several existing channels can be combined using the multi-channel method [365]. Symbolically one can write a single channel as a map X from uniformly distributed random numbers $\vec{x} \in [0,1]^{3n-4}$ to the four-momenta $\vec{p} = (p_1, \ldots, p_n)$ of final-state particles, The corresponding MC weight g is then given by

$$\frac{1}{g} = \frac{\mathrm{d}\Phi_n(X(\vec{x}))}{\mathrm{d}\vec{x}} \tag{B.3}$$

where Φ_n represents the n-particle phase space. The multi-channel method now combines several maps X_i into a new map X as follows:

$$\mathrm{X}(\vec{x}, \tilde{\alpha}) = X_k(\vec{x}) \;, \quad \text{for} \quad \sum_{l=1}^{k-1} \alpha_l < \tilde{\alpha} < \sum_{l=1}^{k} \alpha_l \;, \tag{B.4}$$

requiring an additional random number $\tilde{\alpha}$ and arbitrary coefficients α_k with $\alpha_k > 0$ and $\sum_k \alpha_k = 1$. The corresponding MC weight is given by

$$G = \sum_k \alpha_k \; g_k \;. \tag{B.5}$$

The coefficients α_k can be adapted to minimize the variance of the phase-space integral.

Brief review of phase-space factorization. Consider the $2 \to n$ scattering process in Eq. (1), where we label incoming particles by a and b and outgoing particles by $1 \ldots n$. The corresponding partonic n-particle differential phase space element reads

$$\begin{aligned} \mathrm{d}\Phi_n(a,b;1,\ldots,n) = &\left[\prod_{i=1}^{n} \frac{\mathrm{d}^4 p_i}{(2\pi)^3}\, \delta(p_i^2 - m_i^2)\Theta(p_{i0})\right] \\ &\times (2\pi)^4 \delta^{(4)}\left(p_a + p_b - \sum_{i=1}^{n} p_i\right) \;, \end{aligned} \tag{B.6}$$

where m_i are the on-shell masses of the outgoing particles. Following Ref. [366], the n-particle phase space can be factorized as

$$\begin{aligned} \mathrm{d}\Phi_n(a,b;1,\ldots,n) = \mathrm{d}\Phi_{n-m+1}(a,b;\pi,m+1,\ldots,n) \\ \times \frac{\mathrm{d}s_\pi}{2\pi}\,\mathrm{d}\Phi_m(\pi;1,\ldots,m)\;, \end{aligned} \tag{B.7}$$

where $\pi = \{1\ldots m\}$ indicates an s-channel virtual particle. Eq. (B.7) allows one to decompose the complete phase space into building blocks corresponding to s- and t-channel two-body decay processes of the form $\mathrm{d}\Phi_2(\{12\};1,2)$ and $\mathrm{d}\Phi_2(a,b;1,2)$. We refer to these objects as phase-space vertices, while the integral $\mathrm{d}s_\pi/2\pi$, introduced in Eq. (B.7), is called a phase-space propagator. There is a close correspondence between matrix element computation and phase-space generation, justifying this notation. Even though s- and t-channel decay seem identical, since both represent a solid angle integration, in practice one would use different sampling strategies [367].

Sequential algorithm for phase-space integration. One of the most efficient general approaches to sampling the phase space of multi-particle processes is to employ a sequential algorithm, constructing the full phase space based on the pole structure of one of the Feynman diagrams that contribute to the matrix element. This technique was suggested very early on in the history of MC programs [367]. It is then also possible to construct a separate integrator for each possible graph and employ multi-channel methods to optimize the integration [365]. The method provides a general way to adapt to the assumed pole structure of arbitrarily complicated matrix elements. It is nowadays widely used by the most advanced general-purpose phase-space generators [5–8, 10, 368, 369]. The core algorithm can be formulated as recursive relations in terms of the phase-space propagators and vertices.

The difference between the various phase-space generators available today is usually only *how* these recursive equations are employed. If the basic building blocks are used to build "phase-space diagrams", we obtain an integrator which is suitable for combination with a diagram-based matrix-element generator. If the recursion is implemented as is, the resulting phase-space generator is best combined with a recursive method to compute the matrix elements.

Other algorithms. Other algorithms for phase-space integration exist, which are often less general, but potentially more efficient for their purpose. One

of them is the HAAG method [370], which is designed to produce momenta distributed approximately according to a QCD antenna function for an n-particle process, which reads

$$A_n(p_0, p_1, ..., p_{n-1}) = \frac{1}{(p_0 p_1)(p_1 p_2)...(p_{n-2} p_{n-1})(p_{n-1} p_0)}. \tag{B.8}$$

Different antennae can be obtained from permutations of the momenta $\{p_i\}$. Generally, like the sequential phase-space integrator described above, HAAG relies on phase-space factorization over time-like intermediate momenta. The main difference lies in the sequence of factorization and in the sampling technique for the basic vertices, which resembles the phase-space sampling in a dipole shower.

An important, simple but universally applicable phase-space integrator is Rambo [371]. It is widely used because the underlying algorithm requires no information about the integrand. This makes Rambo the preferred default choice if no time is to be spent on the construction of a dedicated integration channel for the process in question. Rambo assumes an unconstrained phase space, i.e. a phase space where four-momentum conservation does not hold, to generate initial particle momenta. These momenta are in turn boosted and rescaled to arrive at a physically meaningful phase-space point. The conformal transformation thus applied is associated with an additional weight. Rambo can be used for massless and massive particles alike, where massive particles simply require an additional step in the algorithm.

Appendix B.3. Interface structures

Les Houches Event Files. The Les Houches Event File (LHEF) format offers a simple structure for transferring parton-level events to general purpose event generators that subsequently accomplish parton showering and hadronization. While the original version proposed in [222] was based on exchanging two Fortran common blocks, in the recent version the information is embedded in a minimal XML-style file structure [223].

All information specifying the actual run that produced the events, e.g. the incoming beams, their energies and the PDF set used, is collected in a header structure. This is supplemented by information on the cross sections and the event weighting strategy.

For each parton-level event all necessary information is stored in a separate structure, listing, amongst other things, the incoming and outgoing

particle momenta, their flavour and potential mother–daughter relations as well as the event's weight. Most importantly for subsequent showering, each event carries a definite colour flow, determined according to some algorithm by the matrix-element generator code.

The LHEF format to output parton-level events is supported by all the major matrix-element generator programs and has proved to be a robust tool for interfacing them with general-purpose event generators, greatly boosting the set of available processes for the latter.

Binoth Les Houches Accord. It is apparent from Eq. (6) that calculating a cross section at NLO is a very modular task. This is exploited by the Binoth Les Houches Accord, see Ref. [27]. It defines a standard for passing the virtual times Born contribution of an one-loop calculation to a tree-level MC program that deals with the generation of the corresponding Born and real-emission processes, as well as the differential and integrated subtraction terms.

In an initialization stage the one-loop provider (OLP) and the MC program exchange information on the calculational scheme. Then, for a given set of Born level momenta, the OLP returns the coefficients of the $1/\epsilon^2$ and $1/\epsilon$ poles and the finite term. This is sufficient to compose the full cross section calculation within a tree-level generator that implements the necessary subtraction terms [300, 372–374]. This interface structure was used recently to calculate the NLO corrections to $W + 3$ jets [302] and $t\bar{t} + 2$ jets [375].

Implementing your own ME into MCs. Of course, the various event generators also support, to varying degrees, implementations of matrix elements by their users. This option is particularly interesting for models with unorthodox particle content or to study small fragments of larger models.

Appendix C. Top quark mass definitions

One of the important applications of Monte Carlo event generators is in the experimental measurement of Standard Model parameters. An example where they are particularly heavily used is the top quark mass determination. As we will discuss in this Appendix, this application warrants a deeper investigation of precisely how the top quark mass is defined. Our aim is not to review this entire field, but rather to give just enough background information to set the scene for a discussion of the mass definition used in

event generators. For more technical details we refer to the literature and in particular [376–379], whose approach we largely follow.

Most of our discussion applies equally well to any coloured massive object (i.e. with mass in the perturbative regime, $m \gg \Lambda_{QCD}$): the bottom quark and more marginally the charm quark, but also any new coloured particles that are discovered at the LHC, such as squarks, excited quarks or other quark partners. However, we will see that the width of the particle plays an important role in our discussion and it seems likely that the top quark is unique in this regard: its decay width (1.5 GeV) is above the typical scale of confinement so the top decays before it can hadronize and its production and decay should, in principle, be fully calculable in perturbation theory. At the same time, its width is not so far above the confinement scale and is certainly a lot smaller than its mass, so events containing top quarks are able to evolve significantly between its production and decay and parton showers and high-order perturbative effects are very important. The bottom quark's lifetime is much longer and in many, but not all, BSM scenarios those of new coloured particles are much shorter.

We begin our discussion by recalling that in renormalized quantum field theory, parameters that appear in the Lagrangian do not have a unique physical interpretation, but rather are theoretical constructs that serve as stepping stones to making physical predictions. In particular, for each parameter that we renormalize, we have to choose what quantity to keep fixed, corresponding to the choice of renormalization scheme. In the case of particle masses, at one loop order, we have to consider self-energy corrections that are divergent in the ultraviolet,

$$m_0 \to m_0 + \Sigma(m_0), \tag{C.1}$$

where

$$\Sigma(m) = \frac{3}{4} C_F \frac{\alpha_\mathrm{s}}{\pi} m \left(\frac{1}{\epsilon} + \text{finite} \right) + \mathcal{O}(\alpha_\mathrm{s}^2) \tag{C.2}$$

is the on-shell quark self-energy in $d = 4 - 2\epsilon$ dimensions. The choice of scheme corresponds to a choice of mass parameter m^{scheme},

$$m^{\text{scheme}} = m_0 + \delta m \tag{C.3}$$

and a reexpression of Σ as a function of m^{scheme}, such that in

$$m_0 \to m^{\text{scheme}} + \Sigma'(m^{\text{scheme}}), \qquad \Sigma'(m) = \Sigma(m) - \delta m, \tag{C.4}$$

Σ' is finite. The text-book wisdom is that the choice of scheme is a purely technical issue, because at a given order of perturbative theory the corresponding ambiguity is one order higher and therefore, if calculated to sufficiently high order, the scheme-dependence becomes irrelevant. However, this means firstly that it remains a very important practical issue, because one scheme may result in a perturbative expansion that converges much more rapidly than another. If we use the systematic rate of convergence as a criterion for our preferred choice of scheme, and find that this rate is different for different physical observables, we will conclude that the 'best' choice of scheme is an observable-dependent statement. And secondly, the fact that QCD perturbation theory is at best an asymptotic series means that one is not able to calculate to infinite orders of perturbation theory and one must seek a scheme that is well-defined also at the non-perturbative level.

Before proceeding to discuss specific schemes that are in use, we briefly mention that if one includes electroweak corrections in the self-energy, then one obtains an imaginary part from the fact that the top quark can decay to a quasi-on-shell W boson. Including this in the all-orders quark propagator, one obtains the imaginary part that gives rise to the width term in the Breit-Wigner distribution. Thus, from a technical point of view, one can view the renormalized top quark mass as a complex parameter whose imaginary part gives the top width.

Of the several top quark mass definitions on the market, we can divide them into two categories: long-distance, which practically means the pole mass scheme, and short-distance, for example the $\overline{\text{MS}}$ mass or jet mass schemes, which we define briefly below.

The pole mass is defined by analogy with the mass definition used in most QED calculations. Conceptually, one imagines taking the particle to infinity and measuring its classical mass in isolation. Even though this cannot be physically done for a quark in QCD, one can make it an operational definition at any finite order of perturbation theory, with the mass parameter defined to be the real part of the position of the pole in the complex momentum space. At the one-loop level, this amounts to defining $\delta m = \Sigma(m)$ in Eq. (C.3).

The archetypal short-distance scheme is the $\overline{\rm MS}$ one[27]. There, one defines

$$\delta m(\mu) = \frac{3}{4} C_F \, \frac{\alpha_{\rm s}}{\pi} \, m \, \frac{(4\pi)^\epsilon}{\Gamma(1-\epsilon)} \, \frac{1}{\epsilon} \, . \tag{C.5}$$

That is, one subtracts only the divergent term itself and associated universal ϵ-dependent constants.

The difference between the masses in any two schemes can be calculated as a perturbative series in $\alpha_{\rm s}$. In particular, the difference between the pole and $\overline{\rm MS}$ masses is simply the ultraviolet-regular part of the self-energy. Crucial information about the mass schemes can be obtained by examining the infrared behaviour of this difference. At one-loop level, it contains the integral over gluon loop momenta, weighted by the running coupling evaluated at the scale of the loop momentum,

$$m^{\rm pole} - m^{\overline{\rm MS}} \stackrel{q \ll m}{\sim} C_F \int \frac{{\rm d}^3 q}{2(2\pi)^3} \, \frac{\alpha_{\rm s}(q)}{q^2} \; \sim \; C_F \int {\rm d}q \, \alpha_{\rm s}(q). \tag{C.6}$$

This integral is ill-defined in all-order perturbation theory, since it involves an integral over the region where $\alpha_{\rm s}$ becomes large. In a perturbative expansion in powers of $\alpha_{\rm s}(\mu)$, this shows up as a set of factorially-growing terms, such that perturbation theory does not converge. Technically, this gives rise to an ambiguity in the all-order result, known as the renormalon ambiguity, of order Λ_{QCD}: the bottom line is that one cannot, perturbatively, relate $m^{\rm pole}$ and $m^{\overline{\rm MS}}$ to each other with an accuracy of better than Λ_{QCD}. This indicates that one (or possibly both) of these definitions is unsuitable for making perturbative calculations with an accuracy better than this.

Further insight can be gained by calculating simple physical quantities in the two schemes. For example, one can calculate the static interquark potential and show that it has exactly the same renormalon ambiguity as the self-energy correction. Therefore a prediction of the total energy of a static quark-antiquark system in the pole mass scheme, which absorbs all of the self-energy into the mass definition, leaves a renormalon ambiguity in the

[27]Note that the choice of renormalization scheme used for particle masses is totally independent of the choice of renormalization scheme used for coupling constants. In particular, using $\overline{\rm MS}$ for $\alpha_{\rm s}$ does not require us to use the $\overline{\rm MS}$ scheme also for the top mass. In fact, the two schemes are unrelated to each other, except operationally: in both one subtracts only the epsilon pole and associated universal constants.

prediction of this physical quantity. On the other hand, short-distance mass schemes do not subtract it, allowing it to cancel between the self-energy and the potential, leaving a perturbatively-calculable physical prediction. This argument shows that, for this observable, a short-distance mass is preferable. In fact, for every observable that has been analysed in sufficient detail to make this comparison, the same conclusion has been reached. The practical results also bear it out: the perturbative series for total top production cross sections, the top quark decay width and electroweak corrections such as the ρ parameter, all converge significantly faster if expressed in terms of the $\overline{\rm MS}$ mass rather than the pole mass. But is this what is measured experimentally?

It is possible to extract a value of the top mass from a measurement of the $t\bar{t}$ cross section [380, 381], which is unambiguously the $\overline{\rm MS}$ mass, but this is considerably less precise than direct measurements from the final-state properties. These direct measurements are highly non-trivial conceptually, precisely because the top quark is not isolated, but rather is produced as part of a system, evolves by the emission of gluons, decays to a b quark, which evolves further and then hadronizes to form a jet. While there are many refinements in the experimental techniques, they are all based in one way or another on the measurement of this jet momentum, and of the decay products of the W that accompanies it (either a lepton and neutrino or two jets). Our goal is therefore to understand the connection between the properties of this jet and the mass of the top quark that contributed to it. However, it also contains hadrons produced by radiation from other partons in the event, including the initial-state partons, and by the underlying event. In the absence of a first-principles understanding of these effects, the experiments model them with event generators, so that the experimental measurement can effectively be thought of as a measurement of the top mass parameter of the particular event generator used. We assume that this measurement itself is well understood, and concentrate on the final step of the analysis: the relation of this parameter to some quantity that can be defined perturbatively and related to other mass schemes, for example the $\overline{\rm MS}$ one.

As a point of principle, it is not possible to make this connection. Parton shower algorithms are based on leading logarithmic perturbation theory and as such are not accurate enough to fix the scheme – different schemes will only differ by next-to-leading logarithmic corrections. Nevertheless, by speculating about how an ideal all-order algorithm would work, we can obtain an order-of-magnitude result for the mass parameter that appears in parton shower algorithms.

This argument is facilitated by the approach developed in [376]. This showed that all short-distance mass schemes in use can be defined perturbatively with reference to the pole mass, an auxiliary mass scale, R, and the scale used to renormalize $\alpha_{\rm s}$, μ,

$$m^{\rm pole} = m(R,\mu) + R\left[\sum_{n=1}^{\infty} \alpha_{\rm s}^n(\mu)\, C_n\Big(\frac{\mu}{R}\Big)\right], \tag{C.7}$$

where the series in square brackets does not depend explicitly on m, only implicitly through R. Renormalization group arguments can then be used to derive the joint dependence of m on R and μ, which has a leading logarithm at the $n^{\rm th}$ order $\ln^n R/\mu$. Moreover, since the perturbation theory in which m is used must also be μ dependent, large logarithms may arise at all orders of the perturbative expansion of the observable being calculated, or the expression for m, or both, unless μ and R are chosen to be of order the physical scale for the observable being calculated. One also observes in calculating the terms in Eq. (C.7) that the renormalon ambiguity arising from the square brackets is equal to that in $m^{\rm pole}$, showing that the short-distance mass m does not contain a renormalon ambiguity.

Different schemes fall into different classes, with the $\overline{\rm MS}$ scheme having $R \sim m$, threshold mass schemes such as the 1S, PS and kinetic mass schemes typically used in B physics having $R \sim \alpha_{\rm s} m$ and the jet mass scheme discussed below having $R \sim \Gamma_t$, the top quark decay width. Using the insight from this renormalization group approach, one can view R as a new factorization scale above which physics is integrated out into the mass definition. Since the infrared contribution to the self-energy (the right-hand side of Eq. (C.6)) is positive definite, one expects in this picture that the series in brackets will be positive in general, which it is for all of the mass definitions in practical use.

With this physical picture in mind, we can describe the action of an idealized parton shower event generator. It would describe the production and evolution of the system containing a top quark using a properly-matched combination of fixed-order matrix elements and parton showers to sufficient accuracy (at least next-to-leading order and next-to-leading logarithmic respectively). This evolution would describe the state of the system down to scales of order the top decay width, whereupon the top quark would decay. It would also describe the evolution of the partons involved in the decay from

the scale of the energy release ($\sim m$) down to the top width. Finally, for the evolution of the system at scales from Γ_t down to the parton shower's infrared cutoff, the system of partons produced by the previous steps should be considered the external partons that emit, including the b quark but not the t quark. Consideration of this evolution shows that the jet distributions are affected by physics at all scales, but that only the physics at scales above Γ_t is sensitive to the value of the top quark mass. Therefore the mass that is reconstructed from such a measurement has, in principle, all logarithmic physics at scales above Γ_t integrated into it. We can conclude that perturbation theory will converge quickest with a mass definition defined at a reference scale $R \sim \Gamma_t$. This was illustrated in [378, 379] for the simpler case of $e^+e^- \to t\bar{t}$, where it was explicitly shown that a suitably-defined jet mass scheme indeed gave quicker convergence, with much smaller order-to-order changes in the shape of the top hemisphere mass distribution than in the $\overline{\rm MS}$ scheme, for example. The final step of the argument is to state that, if the idealized all-orders calculation converges quickest with such a scheme, then the scheme-independent leading-order leading-log results will be most similar to them if their mass parameter is chosen to be of order the jet mass.

In practice, current parton shower algorithms do not interrupt the evolution at scale $\Gamma_t \sim 1.5$ GeV, although an implementation was attempted in Pythia 6 and some effects of it studied for $e^+e^- \to t\bar{t}$ [382]. They rather continue it down to their infrared cutoffs $Q_0 \sim 1$ GeV. That is, they shower the events as if $\Gamma_t < Q_0$. Despite the small difference between these two scales, it means that in principle one can repeat the argument above and state that the parton shower results are most similar to an all-orders calculation in a scheme in which $R \sim Q_0$. That is, we can state as the final result for the likely relation between the top quark mass measured using a given Monte Carlo event generator ("MC") and the pole mass as [383]

$$m^{\rm pole} = m^{\rm MC} + Q_0 \Big[\alpha_{\rm s}(Q_0)\, c_1 + \ldots \Big], \tag{C.8}$$

where $Q_0 \sim 1$ GeV and c_1 is unknown, but presumed to be of order 1 and, according to the argument above, presumed to be positive. Given that $\alpha_{\rm s}(1\ {\rm GeV})$ is also of order 1, this states that $m^{\rm pole}$ could be of order 1 GeV higher than the value measured by the Tevatron experiments (and hence that $m^{\overline{\rm MS}}$ could be of order 1 GeV higher than the value obtained by assuming that the measured value is actually $m^{\rm pole}$). Since the current experimental

uncertainty is ± 1.1 GeV [384], clarifying this relation clearly demands more attention.

References

[1] B. R. Webber, Monte Carlo Simulation of Hard Hadronic Processes, Ann. Rev. Nucl. Part. Sci. 36 (1986) 253–286.

[2] G. P. Salam, Towards Jetography, Eur. Phys. J. C67 (2010) 637–686. arXiv:0906.1833, doi:10.1140/epjc/s10052-010-1314-6.

[3] R. K. Ellis, W. J. Stirling, B. R. Webber, QCD and collider physics, Camb. Monogr. Part. Phys. Nucl. Phys. Cosmol. 8 (1996) 1–435.

[4] M. L. Mangano, M. Moretti, F. Piccinini, R. Pittau, A. D. Polosa, ALPGEN, a generator for hard multiparton processes in hadronic collisions, JHEP 07 (2003) 001. arXiv:hep-ph/0206293.

[5] F. Krauss, R. Kuhn, G. Soff, AMEGIC++ 1.0: A Matrix Element Generator In C++, JHEP 02 (2002) 044. arXiv:hep-ph/0109036.

[6] T. Gleisberg, S. Höche, Comix, a new matrix element generator, JHEP 12 (2008) 039. arXiv:0808.3674, doi:10.1088/1126-6708/2008/12/039.

[7] A. Kanaki, C. G. Papadopoulos, HELAC: A package to compute electroweak helicity amplitudes, Comput. Phys. Commun. 132 (2000) 306–315. arXiv:hep-ph/0002082.

[8] C. G. Papadopoulos, PHEGAS: A phase-space generator for automatic cross-section computation, Comput. Phys. Commun. 137 (2001) 247–254. arXiv:hep-ph/0007335.

[9] T. Stelzer, W. F. Long, Automatic generation of tree level helicity amplitudes, Comput. Phys. Commun. 81 (1994) 357–371. arXiv:hep-ph/9401258.

[10] F. Maltoni, T. Stelzer, MadEvent: automatic event generation with MadGraph, JHEP 02 (2003) 027. arXiv:hep-ph/0208156.

[11] M. Moretti, T. Ohl, J. Reuter, O'Mega: An optimizing matrix element generator, arXiv:hep-ph/0102195.

[12] W. Kilian, T. Ohl, J. Reuter, WHIZARD: Simulating Multi-Particle Processes at LHC and ILC, arXiv:0708.4233.

[13] M. R. Whalley, D. Bourilkov, R. C. Group, The Les Houches Accord PDFs (LHAPDF) and LHAGLUE, arXiv:hep-ph/0508110.

[14] F. Bloch, A. Nordsieck, Note on the Radiation Field of the electron, Phys. Rev. 52 (1937) 54–59. doi:10.1103/PhysRev.52.54.

[15] T. Kinoshita, Mass singularities of Feynman amplitudes, J. Math. Phys. 3 (1962) 650–677.

[16] T. D. Lee, M. Nauenberg, Degenerate Systems and Mass Singularities, Phys. Rev. 133 (1964) B1549–B1562. doi:10.1103/PhysRev.133.B1549.

[17] W. T. Giele, E. W. N. Glover, Higher-order corrections to jet cross sections in e^+e^- annihilation, Phys. Rev. D46 (1992) 1980–2010. doi:10.1103/PhysRevD.46.1980.

[18] W. T. Giele, E. W. N. Glover, D. A. Kosower, Higher order corrections to jet cross-sections in hadron colliders, Nucl. Phys. B403 (1993) 633–670. arXiv:hep-ph/9302225, doi:10.1016/0550-3213(93)90365-V.

[19] S. Catani, M. H. Seymour, A general algorithm for calculating jet cross sections in NLO QCD, Nucl. Phys. B485 (1997) 291–419. arXiv:hep-ph/9605323.

[20] S. Catani, S. Dittmaier, M. H. Seymour, Z. Trocsanyi, The dipole formalism for next-to-leading order QCD calculations with massive partons, Nucl. Phys. B627 (2002) 189–265. arXiv:hep-ph/0201036.

[21] D. A. Kosower, Antenna factorization of gauge-theory amplitudes, Phys. Rev. D57 (1998) 5410–5416. arXiv:hep-ph/9710213.

[22] D. A. Kosower, Antenna factorization in strongly-ordered limits, Phys. Rev. D71 (2005) 045016. arXiv:hep-ph/0311272, doi:10.1103/PhysRevD.71.045016.

[23] A. Gehrmann-De Ridder, T. Gehrmann, E. W. N. Glover, Antenna subtraction at NNLO, JHEP 09 (2005) 056. arXiv:hep-ph/0505111.

[24] A. Daleo, T. Gehrmann, D. Maître, Antenna subtraction with hadronic initial states, JHEP 04 (2007) 016. arXiv:hep-ph/0612257.

[25] S. Frixione, Z. Kunszt, A. Signer, Three-jet cross-sections to next-to-leading order, Nucl. Phys. B467 (1996) 399–442. arXiv:hep-ph/9512328, doi:10.1016/0550-3213(96)00110-1.

[26] S. Frixione, A general approach to jet cross sections in QCD, Nucl. Phys. B507 (1997) 295–314. arXiv:hep-ph/9706545, doi:10.1016/S0550-3213(97)00574-9.

[27] T. Binoth, et al., A proposal for a standard interface between Monte Carlo tools and one-loop programs, Comput. Phys. Commun. 181 (2010) 1612–1622. arXiv:1001.1307, doi:10.1016/j.cpc.2010.05.016.

[28] S. Alioli, P. Nason, C. Oleari, E. Re, A general framework for implementing NLO calculations in shower Monte Carlo programs: the POWHEG BOX, JHEP 06 (2010) 043. arXiv:1002.2581, doi:10.1007/JHEP06(2010)043.

[29] S. Höche, F. Krauss, M. Schönherr, F. Siegert, Automating the Powheg method in Sherpa, arXiv:1008.5399.

[30] J. D. Jackson, Classical Electrodynamics, Wiley, New York, 1999.

[31] F. E. Low, Bremsstrahlung of very low-energy quanta in elementary particle collisions, Phys. Rev. 110 (1958) 974–977. doi:10.1103/PhysRev.110.974.

[32] V. V. Sudakov, Vertex parts at very high-energies in quantum electrodynamics, Sov. Phys. JETP 3 (1956) 65–71.

[33] A. E. Chudakov, Ser. Fiz., Izv. Akad. Nauk SSSR 19 (1955) 650.

[34] D. Amati, A. Bassetto, M. Ciafaloni, G. Marchesini, G. Veneziano, A Treatment of Hard Processes Sensitive to the Infrared Structure of QCD, Nucl. Phys. B173 (1980) 429. doi:10.1016/0550-3213(80)90012-7.

[35] V. N. Gribov, L. N. Lipatov, Deep inelastic *e-p* scattering in perturbation theory, Sov. J. Nucl. Phys. 15 (1972) 438–450.

[36] Y. L. Dokshitzer, Calculation of the structure functions for deep inelastic scattering and e^+e^- annihilation by perturbation theory in quantum chromodynamics, Sov. Phys. JETP 46 (1977) 641–653.

[37] G. Altarelli, G. Parisi, Asymptotic freedom in parton language, Nucl. Phys. B126 (1977) 298–318.

[38] T. Sjöstrand, A model for initial state parton showers, Phys. Lett. B157 (1985) 321.

[39] G. Marchesini, B. R. Webber, Monte Carlo Simulation of General Hard Processes with Coherent QCD Radiation, Nucl. Phys. B310 (1988) 461. doi:10.1016/0550-3213(88)90089-2.

[40] S. Catani, B. R. Webber, G. Marchesini, QCD coherent branching and semiinclusive processes at large x, Nucl. Phys. B349 (1991) 635–654. doi:10.1016/0550-3213(91)90390-J.

[41] I. I. Balitsky, L. N. Lipatov, The Pomeranchuk Singularity in Quantum Chromodynamics, Sov. J. Nucl. Phys. 28 (1978) 822–829.

[42] E. A. Kuraev, L. N. Lipatov, V. S. Fadin, The Pomeranchuk Singularity in Nonabelian Gauge Theories, Sov. Phys. JETP 45 (1977) 199–204.

[43] S. Catani, F. Fiorani, G. Marchesini, Small-x behavior of initial state radiation in perturbative QCD, Nucl. Phys. B336 (1990) 18–85.

[44] G. Marchesini, B. R. Webber, Final states in heavy quark leptoproduction at small x, Nucl. Phys. B386 (1992) 215–235. doi:10.1016/0550-3213(92)90181-A.

[45] H. Jung, G. P. Salam, Hadronic final state predictions from CCFM: the hadron-level Monte Carlo generator CASCADE, Eur. Phys. J. C19 (2001) 351–360. arXiv:hep-ph/0012143.

[46] F. Abe, et al., Evidence for color coherence in $p\bar{p}$ collisions at $\sqrt{s} = 1.8$ TeV, Phys. Rev. D50 (1994) 5562–5579. doi:10.1103/PhysRevD.50.5562.

[47] R. K. Ellis, G. Marchesini, B. R. Webber, Soft Radiation in Parton Parton Scattering, Nucl. Phys. B286 (1987) 643. doi:10.1016/0550-3213(87)90456-1.

[48] A. Schofield, M. H. Seymour, Gaps Between Jets in Parton Showers (in preparation).

[49] G. Marchesini, B. R. Webber, Simulation of QCD coherence in heavy quark production and decay, Nucl. Phys. B330 (1990) 261. doi:10.1016/0550-3213(90)90310-A.

[50] E. Norrbin, T. Sjöstrand, QCD radiation off heavy particles, Nucl. Phys. B603 (2001) 297–342. arXiv:hep-ph/0010012.

[51] G. Gustafson, U. Pettersson, Dipole formulation of QCD cascades, Nucl. Phys. B306 (1988) 746.

[52] T. Sjöstrand, P. Z. Skands, Transverse-momentum-ordered showers and interleaved multiple interactions, Eur. Phys. J. C39 (2005) 129–154. arXiv:hep-ph/0408302.

[53] J.-C. Winter, F. Krauss, Initial-state showering based on colour dipoles connected to incoming parton lines, JHEP 07 (2008) 040. arXiv:0712.3913.

[54] S. Schumann, F. Krauss, A parton shower algorithm based on Catani-Seymour dipole factorisation, JHEP 03 (2008) 038. arXiv:0709.1027.

[55] W. T. Giele, D. A. Kosower, P. Z. Skands, A Simple shower and matching algorithm, Phys. Rev. D78 (2008) 014026. arXiv:0707.3652, doi:10.1103/PhysRevD.78.014026.

[56] Z. Nagy, D. E. Soper, Parton showers with quantum interference, JHEP 09 (2007) 114. arXiv:0706.0017, doi:10.1088/1126-6708/2007/09/114.

[57] M. Dinsdale, M. Ternick, S. Weinzierl, Parton showers from the dipole formalism, Phys. Rev. D76 (2007) 094003. arXiv:0709.1026.

[58] Y. L. Dokshitzer, G. Marchesini, Monte Carlo and large angle gluon radiation, JHEP 03 (2009) 117. arXiv:0809.1749.

[59] Z. Nagy, D. E. Soper, Final state dipole showers and the DGLAP equation, JHEP 05 (2009) 088. arXiv:0901.3587, doi:10.1088/1126-6708/2009/05/088.

[60] P. Skands, S. Weinzierl, Some remarks on dipole showers and the DGLAP equation, Phys. Rev. D79 (2009) 074021. arXiv:0903.2150, doi:10.1103/PhysRevD.79.074021.

[61] L. Lönnblad, Ariadne version 4: A program for simulation of QCD cascades implementing the colour dipole model, Comput. Phys. Commun. 71 (1992) 15–31.

[62] M. Bengtsson, T. Sjöstrand, Coherent Parton Showers Versus Matrix Elements: Implications of PETRA - PEP Data, Phys. Lett. B185 (1987) 435. doi:10.1016/0370-2693(87)91031-8.

[63] M. H. Seymour, A simple prescription for first-order corrections to quark scattering and annihilation processes, Nucl. Phys. B436 (1995) 443–460. arXiv:hep-ph/9410244, doi:10.1016/0550-3213(94)00554-R.

[64] M. H. Seymour, Matrix-element corrections to parton shower algorithms, Comp. Phys. Commun. 90 (1995) 95–101. arXiv:hep-ph/9410414.

[65] G. Miu, T. Sjöstrand, W production in an improved parton-shower approach, Phys. Lett. B449 (1999) 313–320. arXiv:hep-ph/9812455, doi:10.1016/S0370-2693(99)00068-4.

[66] L. Lönnblad, Small x effects in W + jets production at the Tevatron, Nucl. Phys. B458 (1996) 215–230. arXiv:hep-ph/9508261.

[67] S. Frixione, B. R. Webber, Matching NLO QCD computations and parton shower simulations, JHEP 06 (2002) 029. arXiv:hep-ph/0204244.

[68] S. Frixione, B. R. Webber, The MC@NLO 3.3 Event Generator, arXiv:hep-ph/0612272.

[69] P. Nason, A new method for combining NLO QCD with shower Monte Carlo algorithms, JHEP 11 (2004) 040. arXiv:hep-ph/0409146, doi:10.1088/1126-6708/2004/11/040.

[70] S. Catani, F. Krauss, R. Kuhn, B. R. Webber, QCD matrix elements + parton showers, JHEP 11 (2001) 063. arXiv:hep-ph/0109231.

[71] L. Lönnblad, Correcting the colour-dipole cascade model with fixed order matrix elements, JHEP 05 (2002) 046. arXiv:hep-ph/0112284.

[72] M. Mangano, The MLM Matching procedure(in preparation).

[73] J. Alwall, et al., Comparative study of various algorithms for the merging of parton showers and matrix elements in hadronic collisions, Eur. Phys. J. C53 (2008) 473–500. arXiv:0706.2569.

[74] S. Mrenna, P. Richardson, Matching matrix elements and parton showers with Herwig and Pythia, JHEP 05 (2004) 040. arXiv:hep-ph/0312274.

[75] S. Höche, F. Krauss, S. Schumann, F. Siegert, QCD matrix elements and truncated showers, JHEP 05 (2009) 053. arXiv:0903.1219.

[76] K. Hamilton, P. Richardson, J. Tully, A modified CKKW matrix element merging approach to angular-ordered parton showers, JHEP 11 (2009) 038. arXiv:0905.3072, doi:10.1088/1126-6708/2009/11/038.

[77] K. Hamilton, P. Nason, Improving NLO-parton shower matched simulations with higher order matrix elements, JHEP 06 (2010) 039. arXiv:1004.1764, doi:10.1007/JHEP06(2010)039.

[78] N. Lavesson, L. Lönnblad, Extending CKKW-merging to one-loop matrix elements, JHEP 12 (2008) 070. arXiv:0811.2912, doi:10.1088/1126-6708/2008/12/070.

[79] P. Skands, The Vincia Monte Carlo (in preparation).

[80] S. Alioli, P. Nason, C. Oleari, E. Re, NLO vector-boson production matched with shower in POWHEG, JHEP 07 (2008) 060. arXiv:0805.4802, doi:10.1088/1126-6708/2008/07/060.

[81] N. Lavesson, L. Lönnblad, Merging parton showers and matrix elements – back to basics, JHEP 04 (2008) 085. arXiv:0712.2966, doi:10.1088/1126-6708/2008/04/085.

[82] F. Krauss, Matrix elements and parton showers in hadronic interactions, JHEP 0208 (2002) 015. arXiv:hep-ph/0205283.

[83] N. Lavesson, L. Lönnblad, W+jets matrix elements and the dipole cascade, JHEP 07 (2005) 054. arXiv:hep-ph/0503293.

[84] H.-L. Lai, et al., New parton distributions for collider physics, arXiv:1007.2241.

[85] A. D. Martin, W. J. Stirling, R. S. Thorne, G. Watt, Parton distributions for the LHC, Eur. Phys. J. C63 (2009) 189–295. arXiv:0901.0002, doi:10.1140/epjc/s10052-009-1072-5.

[86] A. Sherstnev, R. S. Thorne, Parton Distributions for LO Generators, Eur. Phys. J. C55 (2008) 553–575. arXiv:0711.2473, doi:10.1140/epjc/s10052-008-0610-x.

[87] H.-L. Lai, et al., Parton Distributions for Event Generators, JHEP 04 (2010) 035. arXiv:0910.4183, doi:10.1007/JHEP04(2010)035.

[88] T. Kasemets, T. Sjöstrand, A Comparison of new MC-adapted Parton Densities, arXiv:1007.0897.

[89] T. Sjöstrand, P. Z. Skands, Multiple interactions and the structure of beam remnants, JHEP 03 (2004) 053. arXiv:hep-ph/0402078.

[90] S. Gieseke, M. H. Seymour, A. Siodmok, A Model of non-perturbative gluon emission in an initial state parton shower, JHEP 06 (2008) 001. arXiv:0712.1199, doi:10.1088/1126-6708/2008/06/001.

[91] A. A. Affolder, et al., The transverse momentum and total cross section of e^+e^- pairs in the Z boson region from $p\bar{p}$ collisions at $\sqrt{s} = 1.8$ TeV, Phys. Rev. Lett. 84 (2000) 845–850. arXiv:hep-ex/0001021, doi:10.1103/PhysRevLett.84.845.

[92] V. A. Khoze, A. D. Martin, M. G. Ryskin, Prospects for new physics observations in diffractive processes at the LHC and Tevatron, Eur. Phys. J. C23 (2002) 311–327. arXiv:hep-ph/0111078.

[93] The ATLAS collaboration, Charged-particle multiplicities in pp interactions measured with the ATLAS detector at the LHC, arXiv:1012.5104.

[94] E. Avsar, On the High Energy Behaviour of The Total Cross Section in the QCD Dipole Model, JHEP 0804 (2008) 033. arXiv:0803.0446, doi:10.1088/1126-6708/2008/04/033.

[95] A. Grau, R. M. Godbole, G. Pancheri, Y. N. Srivastava, Soft Gluon k(t)-Resummation and the Froissart bound, Phys.Lett. B682 (2009) 55–60. arXiv:arXiv:0908.1426, doi:10.1016/j.physletb.2009.10.080.

[96] T. Sjöstrand, M. van Zijl, A multiple-interaction model for the event structure in hadron collisions, Phys. Rev. D36 (1987) 2019.

[97] P. Bartalini, R. Field, R. Chierici, M. Cacciari, A. Moraes, et al., Multiple partonic interactions at the LHC. Proceedings, 1st International Workshop, MPI'08, Perugia, Italy, October 27-31, 2008arXiv:1003.4220.

[98] G. Gustafson, Multiple scattering, underlying event, and minimum biasarXiv:0712.1941.

[99] M. Bähr, J. M. Butterworth, M. H. Seymour, The Underlying Event and the Total Cross Section from Tevatron to the LHC, JHEP 01 (2009) 065. arXiv:0806.2949, doi:10.1088/1126-6708/2009/01/065.

[100] A. Donnachie, P. V. Landshoff, Total cross sections, Phys. Lett. B296 (1992) 227–232. arXiv:hep-ph/9209205.

[101] A. Donnachie, P. V. Landshoff, Does the hard pomeron obey Regge factorization?, Phys. Lett. B595 (2004) 393–399. arXiv:hep-ph/0402081, doi:10.1016/j.physletb.2004.05.068.

[102] J. M. Butterworth, J. R. Forshaw, M. H. Seymour, Multiparton Interactions in Photoproduction at HERA, Z. Phys. C72 (1996) 637–646. arXiv:hep-ph/9601371.

[103] M. Bähr, S. Gieseke, M. H. Seymour, Simulation of multiple partonic interactions in Herwig++, JHEP 07 (2008) 076. arXiv:0803.3633.

[104] J. Dischler, T. Sjöstrand, A Toy model of color screening in the proton, Eur.Phys.J. C3 (2001) 2. arXiv:hep-ph/0011282.

[105] M. Ciafaloni, Coherence effects in initial jets at small Q^2/s, Nucl. Phys. B296 (1988) 49–74.

[106] B. Andersson, G. Gustafson, J. Samuelsson, The linked dipole chain model for DIS, Nucl. Phys. B467 (1996) 443–478.

[107] B. Andersson, G. Gustafson, H. Kharraziha, Investigations into the BFKL mechanism with a running QCD coupling, Phys.Rev. D57 (1998) 5543–5554. arXiv:hep-ph/9711403, doi:10.1103/PhysRevD.57.5543.

[108] H. Kharraziha, L. Lönnblad, The linked dipole chain Monte Carlo, JHEP 03 (1998) 006. arXiv:hep-ph/9709424.

[109] G. Gustafson, L. Lönnblad, G. Miu, Gluon distribution functions in the k(T) factorization approach, JHEP 0209 (2002) 005. arXiv:hep-ph/0206195.

[110] G. Gustafson, L. Lönnblad, G. Miu, Hadronic collisions in the linked dipole chain model, Phys.Rev. D67 (2003) 034020. arXiv:hep-ph/0209186, doi:10.1103/PhysRevD.67.034020.

[111] P. Hagler, et al., Nucleon Generalized Parton Distributions from Full Lattice QCD, Phys.Rev. D77 (2008) 094502. arXiv:arXiv:0705.4295, doi:10.1103/PhysRevD.77.094502.

[112] D. Treleani, Double parton scattering, diffraction and effective cross section, Phys.Rev. D76 (2007) 076006. arXiv:arXiv:0708.2603, doi:10.1103/PhysRevD.76.076006.

[113] B. Blok, Y. Dokshitzer, L. Frankfurt, M. Strikman, The four jet production at LHC and Tevatron in QCDarXiv:1009.2714.

[114] J. R. Forshaw, J. Storrow, Mini - jets and the total inelastic photoproduction cross-section, Phys.Lett. B268 (1991) 116–121. doi:10.1016/0370-2693(91)90933-H,10.1016/0370-2693(91)90933-H.

[115] C. Bourrely, J. Soffer, T. T. Wu, Impact picture phenomenology for $\pi^{\pm}p$, $K^{\pm}p$ and pp, $\bar{p}p$ elastic scattering at high-energies, Eur.Phys.J. C28 (2003) 97–105. arXiv:hep-ph/0210264, doi:10.1140/epjc/s2003-01159-7.

[116] I. Borozan, M. H. Seymour, An eikonal model for multiparticle production in hadron-hadron interactions, JHEP 09 (2002) 015. arXiv:hep-ph/0207283.

[117] G. A. Schuler, T. Sjöstrand, Hadronic diffractive cross-sections and the rise of the total cross-section, Phys.Rev. D49 (1994) 2257–2267. doi:10.1103/PhysRevD.49.2257.

[118] C. Buttar, et al., Standard Model Handles and Candles Working Group: Tools and Jets Summary Report, arXiv:0803.0678.

[119] P. Z. Skands, Tuning Monte Carlo Generators: The Perugia Tunes, arXiv:1005.3457.

[120] J. R. Gaunt, W. Stirling, Double Parton Distributions Incorporating Perturbative QCD Evolution and Momentum and Quark Number Sum Rules, JHEP 1003 (2010) 005. arXiv:0910.4347, doi:10.1007/JHEP03(2010)005.

[121] R. Corke, T. Sjöstrand, Multiparton interactions and rescattering, JHEP 01 (2009) 035. arXiv:0911.1909, doi:10.1007/JHEP01(2010)035.

[122] A. Bhatti, et al., Determination of the jet energy scale at the Collider Detector at Fermilab, Nucl. Instrum. Meth. A566 (2006) 375–412. arXiv:hep-ex/0510047, doi:10.1016/j.nima.2006.05.269.

[123] M. Dasgupta, L. Magnea, G. P. Salam, Non-perturbative QCD effects in jets at hadron colliders, JHEP 02 (2008) 055. arXiv:0712.3014, doi:10.1088/1126-6708/2008/02/055.

[124] G. Gustafson, U. Pettersson, P. M. Zerwas, Jet Final States in W W Pair Production and Color Screening in the QCD Vacuum, Phys. Lett. B209 (1988) 90. doi:10.1016/0370-2693(88)91836-9.

[125] T. Sjöstrand, V. A. Khoze, Does the W mass reconstruction survive QCD effects?, Phys. Rev. Lett. 72 (1994) 28–31. arXiv:hep-ph/9310276, doi:10.1103/PhysRevLett.72.28.

[126] T. Sjöstrand, V. A. Khoze, On Color rearrangement in hadronic W^+W^- events, Z. Phys. C62 (1994) 281–310. arXiv:hep-ph/9310242, doi:10.1007/BF01560244.

[127] X. Artru, Classical String Phenomenology. 1. How Strings Work, Phys. Rept. 97 (1983) 147. doi:10.1016/0370-1573(83)90081-9.

[128] G. Gustafson, J. Häkkinen, Color interference and confinement effects in W pair production, Z. Phys. C64 (1994) 659–664. doi:10.1007/BF01957774.

[129] L. Lönnblad, Reconnecting colored dipoles, Z. Phys. C70 (1996) 107–114. doi:10.1007/s002880050087.

[130] C. Friberg, G. Gustafson, J. Häkkinen, Colour connections in e^+e^- -annihilation, Nucl. Phys. B490 (1997) 289–305. arXiv:hep-ph/9604347, doi:10.1016/S0550-3213(97)00064-3.

[131] B. R. Webber, Colour reconnection and Bose-Einstein effects, J. Phys. G24 (1998) 287–296. arXiv:hep-ph/9708463, doi:10.1088/0954-3899/24/2/003.

[132] W. Buchmuller, A. Hebecker, A Parton model for diffractive processes in deep inelastic scattering, Phys. Lett. B355 (1995) 573–578. arXiv:hep-ph/9504374, doi:10.1016/0370-2693(95)00721-V.

[133] A. Edin, G. Ingelman, J. Rathsman, Soft colour interactions as the origin of rapidity gaps in DIS, Phys. Lett. B366 (1996) 371–378. arXiv:hep-ph/9508386, doi:10.1016/0370-2693(95)01391-1.

[134] J. Rathsman, A generalised area law for hadronic string reinteractions, Phys. Lett. B452 (1999) 364–371. arXiv:hep-ph/9812423, doi:10.1016/S0370-2693(99)00291-9.

[135] R. Enberg, G. Ingelman, N. Timneanu, Soft color interactions and diffractive hard scattering at the Tevatron, Phys.Rev. D64 (2001) 114015. arXiv:hep-ph/0106246, doi:10.1103/PhysRevD.64.114015.

[136] A. Edin, G. Ingelman, J. Rathsman, Quarkonium production at the Tevatron through soft color interactions, Phys. Rev. D56 (1997) 7317–7320. arXiv:hep-ph/9705311, doi:10.1103/PhysRevD.56.7317.

[137] G. Abbiendi, et al., Color reconnection studies in $e^+e^- \to W^+W^-$ at $\sqrt{s} = 183$ GeV, Phys. Lett. B453 (1999) 153–168. arXiv:hep-ex/9901019, doi:10.1016/S0370-2693(99)00309-3.

[138] G. Abbiendi, et al., Colour reconnection in $e^+e^- \to W^+W^-$ at $\sqrt{s} =$ 189 GeV – 209 GeV, Eur. Phys. J. C45 (2006) 291–305. arXiv:hep-ex/0508062, doi:10.1140/epjc/s2005-02439-x.

[139] S. Schael, et al., Test of colour reconnection models using three-jet events in hadronic Z decays, Eur. Phys. J. C48 (2006) 685–698. arXiv:hep-ex/0604042, doi:10.1140/epjc/s10052-006-0017-5.

[140] J. Abdallah, et al., Study of leading hadrons in gluon and quark fragmentation, Phys. Lett. B643 (2006) 147–157. arXiv:hep-ex/0610031, doi:10.1016/j.physletb.2006.10.040.

[141] M. Sandhoff, P. Z. Skands, Colour annealing - a toy model of colour reconnectionsPresented at Les Houches Workshop on Physics at TeV Colliders, Les Houches, France, 2-20 May 2005.

[142] P. Z. Skands, D. Wicke, Non-perturbative QCD effects and the top mass at the Tevatron, Eur.Phys.J. C52 (2007) 133–140. arXiv:hep-ph/0703081, doi:10.1140/epjc/s10052-007-0352-1.

[143] P. Aurenche, F. W. Bopp, R. Engel, D. Pertermann, J. Ranft, et al., DTUJET-93: Sampling inelastic proton proton and anti-proton - proton collisions according to the two component dual parton model, Comput.Phys.Commun. 83 (1994) 107–123. arXiv:hep-ph/9402351, doi:10.1016/0010-4655(94)90037-X.

[144] R. Engel, Photoproduction within the two component dual parton model. 1. Amplitudes and cross-sections, Z.Phys. C66 (1995) 203–214. doi:10.1007/BF01496594.

[145] R. Engel, J. Ranft, Hadronic photon-photon interactions at high-energies, Phys.Rev. D54 (1996) 4244–4262. arXiv:hep-ph/9509373, doi:10.1103/PhysRevD.54.4244.

[146] J. Ranft, The Dual parton model at cosmic ray energies, Phys.Rev. D51 (1995) 64–84. doi:10.1103/PhysRevD.51.64.

[147] S. Roesler, R. Engel, J. Ranft, The Monte Carlo event generator DPMJET-III, arXiv:hep-ph/0012252.

[148] B. R. Webber, Estimation of power corrections to hadronic event shapes, Phys. Lett. B339 (1994) 148–150. arXiv:hep-ph/9408222, doi:10.1016/0370-2693(94)91147-9.

[149] G. P. Korchemsky, G. F. Sterman, Nonperturbative corrections in resummed cross-sections, Nucl. Phys. B437 (1995) 415–432. arXiv:hep-ph/9411211, doi:10.1016/0550-3213(94)00006-Z.

[150] Y. L. Dokshitzer, B. R. Webber, Calculation of power corrections to hadronic event shapes, Phys. Lett. B352 (1995) 451–455. arXiv:hep-ph/9504219, doi:10.1016/0370-2693(95)00548-Y.

[151] Y. L. Dokshitzer, G. Marchesini, B. R. Webber, Dispersive Approach to Power-Behaved Contributions in QCD Hard Processes, Nucl. Phys. B469 (1996) 93–142. arXiv:hep-ph/9512336, doi:10.1016/0550-3213(96)00155-1.

[152] C. Amsler, et al., Review of particle physics, Phys. Lett. B667 (2008) 1. doi:10.1016/j.physletb.2008.07.018.

[153] S. Albino, The hadronization of partons, Rev. Mod. Phys. 82 (2010) 2489–2556. arXiv:0810.4255.

[154] X. Artru, G. Mennessier, String model and multiproduction, Nucl. Phys. B70 (1974) 93–115.

[155] R. D. Field, R. P. Feynman, A parametrization of the properties of quark jets, Nucl. Phys. B136 (1978) 1. doi:10.1016/0550-3213(78)90015-9.

[156] P. Hoyer, P. Osland, H. G. Sander, T. F. Walsh, P. M. Zerwas, Quantum Chromodynamics and Jets in e^+e^-, Nucl. Phys. B161 (1979) 349. doi:10.1016/0550-3213(79)90217-7.

[157] A. Ali, E. Pietarinen, G. Kramer, J. Willrodt, A QCD Analysis of the High-Energy e^+e^- Data from PETRA, Phys. Lett. B93 (1980) 155. doi:10.1016/0370-2693(80)90116-1.

[158] T. Sjöstrand, Some comments on jet fragmentation models and α_s determinations, Z. Phys. C26 (1984) 93. doi:10.1007/BF01572546.

[159] B. Andersson, G. Gustafson, G. Ingelman, T. Sjöstrand, Parton Fragmentation and String Dynamics, Phys. Rept. 97 (1983) 31–145. doi:10.1016/0370-1573(83)90080-7.

[160] B. Andersson, The Lund model, Vol. 7, Camb. Monogr. Part. Phys. Nucl. Phys. Cosmol., 1997.

[161] T. Sjöstrand, S. Mrenna, P. Skands, PYTHIA 6.4 physics and manual, JHEP 05 (2006) 026. arXiv:hep-ph/0603175.

[162] T. Sjöstrand, S. Mrenna, P. Skands, A brief introduction to PYTHIA 8.1, Comput. Phys. Commun. 178 (2008) 852–867. arXiv:0710.3820.

[163] B. Andersson, G. Gustafson, B. Söderberg, A General Model for Jet Fragmentation, Z. Phys. C20 (1983) 317. doi:10.1007/BF01407824.

[164] M. G. Bowler, e^+e^- production of heavy quarks in the string model, Z. Phys. C11 (1981) 169.

[165] W. Bartel, et al., Particle Distribution in Three Jet Events Produced by e^+e^- Annihilation, Z. Phys. C21 (1983) 37. doi:10.1007/BF01648774.

[166] Y. I. Azimov, Y. L. Dokshitzer, V. A. Khoze, S. I. Troian, The String Effect and QCD Coherence, Phys. Lett. B165 (1985) 147–150. doi:10.1016/0370-2693(85)90709-9.

[167] G. Gustafson, Dual description of a confined colour field, Phys. Lett. B175 (1986) 453.

[168] T. Sjöstrand, Jet fragmentation of nearby partons, Nucl. Phys. B248 (1984) 469. doi:10.1016/0550-3213(84)90607-2.

[169] T. Sjöstrand, P. Z. Skands, Baryon number violation and string topologies, Nucl. Phys. B659 (2003) 243. arXiv:hep-ph/0212264, doi:10.1016/S0550-3213(03)00193-7.

[170] D. Amati, G. Veneziano, Preconfinement as a Property of Perturbative QCD, Phys. Lett. B83 (1979) 87. doi:10.1016/0370-2693(79)90896-7.

[171] A. Bassetto, M. Ciafaloni, G. Marchesini, Color Singlet Distributions and Mass Damping in Perturbative QCD, Phys. Lett. B83 (1979) 207. doi:10.1016/0370-2693(79)90687-7.

[172] Z. Koba, H. B. Nielsen, P. Olesen, Scaling of multiplicity distributions in high-energy hadron collisions, Nucl. Phys. B40 (1972) 317–334. doi:10.1016/0550-3213(72)90551-2.

[173] S. Wolfram, Parton and hadron production in e^+e^- annihilation. Largely based on a talk given at 15th Rencontre de Moriond, Les Arcs, France, Mar 9-21, 1980.

[174] G. C. Fox, S. Wolfram, A Model for Parton Showers in QCD, Nucl. Phys. B168 (1980) 285. doi:10.1016/0550-3213(80)90111-X.

[175] R. D. Field, S. Wolfram, A QCD Model for e^+e^- Annihilation, Nucl. Phys. B213 (1983) 65. doi:10.1016/0550-3213(83)90175-X.

[176] Y. I. Azimov, Y. L. Dokshitzer, V. A. Khoze, S. I. Troyan, Similarity of Parton and Hadron Spectra in QCD Jets, Z. Phys. C27 (1985) 65–72. doi:10.1007/BF01642482.

[177] Y. I. Azimov, Y. L. Dokshitzer, V. A. Khoze, S. I. Troyan, Humpbacked QCD Plateau in Hadron Spectra, Zeit. Phys. C31 (1986) 213. doi:10.1007/BF01479529.

[178] M. Dasgupta, G. P. Salam, Event shapes in e^+e^- annihilation and deep inelastic scattering, J. Phys. G30 (2004) R143. arXiv:hep-ph/0312283, doi:10.1088/0954-3899/30/5/R01.

[179] J. Abdallah, et al., Evidence for an excess of soft photons in hadronic decays of Z^0, Eur. Phys. J. C47 (2006) 273–294. arXiv:hep-ex/0604038, doi:10.1140/epjc/s2006-02568-8.

[180] J. Abdallah, et al., Study of the Dependence of Direct Soft Photon Production on the Jet Characteristics in Hadronic Z^0 Decays, Eur. Phys. J. C67 (2010) 343–366. arXiv:1004.1587, doi:10.1140/epjc/s10052-010-1315-5.

[181] B. R. Webber, A QCD Model for Jet Fragmentation Including Soft Gluon Interference, Nucl. Phys. B238 (1984) 492. doi:10.1016/0550-3213(84)90333-X.

[182] J.-C. Winter, F. Krauss, G. Soff, A modified cluster-hadronization model, Eur. Phys. J. C36 (2004) 381–395. arXiv:hep-ph/0311085, doi:10.1140/epjc/s2004-01960-8.

[183] C. Bignamini, F. Becattini, F. Piccinini, MCSTHAR++, a Monte Carlo code for the microcanonical hadronization, arXiv:1006.2722.

[184] D. J. Lange, The EvtGen particle decay simulation package, Nucl. Instrum. Meth. A462 (2001) 152–155. doi:10.1016/S0168-9002(01)00089-4.

[185] P. Golonka, et al., The tauola-photos-F environment for the TAUOLA and PHOTOS packages, release II, Comput. Phys. Commun. 174 (2006) 818–835. arXiv:hep-ph/0312240, doi:10.1016/j.cpc.2005.12.018.

[186] S. Jadach, Z. Was, R. Decker, J. H. Kuhn, The tau decay library TAUOLA: Version 2.4, Comput. Phys. Commun. 76 (1993) 361–380. doi:10.1016/0010-4655(93)90061-G.

[187] S. Jadach, J. H. Kuhn, Z. Was, TAUOLA: A Library of Monte Carlo programs to simulate decays of polarized tau leptons, Comput. Phys. Commun. 64 (1990) 275–299. doi:10.1016/0010-4655(91)90038-M.

[188] D. Grellscheid, P. Richardson, Simulation of Tau Decays in the Herwig++ Event Generator, arXiv:0710.1951.

[189] T. Gleisberg, S. Höche, F. Krauss, M. Schönherr, S. Schumann, F. Siegert, J. Winter, Event generation with Sherpa 1.1, JHEP 02 (2009) 007. arXiv:0811.4622, doi:10.1088/1126-6708/2009/02/007.

[190] M. Wirbel, B. Stech, M. Bauer, Exclusive Semileptonic Decays of Heavy Mesons, Z. Phys. C29 (1985) 637.

[191] M. Bauer, B. Stech, M. Wirbel, Exclusive Nonleptonic Decays of D, D_s, and B Mesons, Z. Phys. C34 (1987) 103.

[192] M. H. Seymour, Soft isolated photon production as a probe of the parton shower mechanism, Z. Phys. C64 (1994) 445–452. doi:10.1007/BF01560106.

[193] D. R. Yennie, S. C. Frautschi, H. Suura, The Infrared Divergence Phenomena and High-energy Processes, Ann. Phys. 13 (1961) 379–452.

[194] S. Jadach, B. F. L. Ward, YFS2: The Second Order Monte Carlo for Fermion pair Production at LEP/SLC with the initial-state radiation of two hard and multiple soft photons, Comput. Phys. Commun. 56 (1990) 351–384. doi:10.1016/0010-4655(90)90020-2.

[195] S. Jadach, B. F. L. Ward, Z. Was, Coherent exclusive exponentiation for precision Monte Carlo calculations, Phys. Rev. D63 (2001) 113009. arXiv:hep-ph/0006359, doi:10.1103/PhysRevD.63.113009.

[196] S. Jadach, B. F. L. Ward, Z. Was, The precision Monte Carlo event generator KK for two- fermion final states in e^+e^- collisions, Comput. Phys. Commun. 130 (2000) 260–325. arXiv:hep-ph/9912214, doi:10.1016/S0010-4655(00)00048-5.

[197] W. Placzek, S. Jadach, Multiphoton radiation in leptonic W-boson decays, Eur. Phys. J. C29 (2003) 325–339. arXiv:hep-ph/0302065, doi:10.1140/epjc/s2003-01223-4.

[198] S. Jadach, W. Placzek, M. Skrzypek, B. F. L. Ward, Z. Was, The Monte Carlo program KoralW version 1.51 and the concurrent Monte Carlo KoralW&YFSWW3 with all background graphs and first order corrections to W pair production, Comput. Phys. Commun. 140 (2001) 475–512. arXiv:hep-ph/0104049, doi:10.1016/S0010-4655(01)00296-X.

[199] S. Jadach, W. Placzek, M. Skrzypek, B. F. L. Ward, Z. Was, The Monte Carlo event generator YFSWW3 version 1.16 for W pair production and decay at LEP2/LC energies, Comput. Phys. Commun. 140 (2001) 432–474. arXiv:hep-ph/0103163, doi:10.1016/S0010-4655(01)00288-0.

[200] A. Schälicke, F. Krauss, R. Kuhn, G. Soff, Implementing initial state radiation for lepton induced processes in AMEGIC++, JHEP 12 (2002) 013. arXiv:hep-ph/0203259.

[201] K. Hamilton, P. Richardson, Simulation of QED radiation in particle decays using the YFS formalism, JHEP 07 (2006) 010. arXiv:hep-ph/0603034.

[202] M. Schönherr, F. Krauss, Soft photon radiation in particle decays in SHERPA, JHEP 12 (2008) 018. arXiv:0810.5071, doi:10.1088/1126-6708/2008/12/018.

[203] E. Barberio, Z. Was, PHOTOS: A Universal Monte Carlo for QED Radiative Corrections. Version 2.0, Comput. Phys. Commun. 79 (1994) 291–308.

[204] E. Barberio, B. van Eijk, Z. Was, PHOTOS: A Universal Monte Carlo for QED Radiative Corrections in Decays, Comput. Phys. Commun. 66 (1991) 115–128.

[205] P. Golonka, Z. Was, PHOTOS Monte Carlo: a precision tool for QED corrections in Z and W decays, arXiv:hep-ph/0506026.

[206] N. Arkani-Hamed, et al., The Minimal Moose for a Little Higgs, JHEP 08 (2002) 021. arXiv:hep-ph/0206020.

[207] N. Arkani-Hamed, A. G. Cohen, E. Katz, A. E. Nelson, The littlest Higgs, JHEP 07 (2002) 034. arXiv:hep-ph/0206021.

[208] N. Arkani-Hamed, S. Dimopoulos, G. R. Dvali, The hierarchy problem and new dimensions at a millimeter, Phys. Lett. B429 (1998) 263–272. arXiv:hep-ph/9803315, doi:10.1016/S0370-2693(98)00466-3.

[209] I. Antoniadis, N. Arkani-Hamed, S. Dimopoulos, G. R. Dvali, New dimensions at a millimeter to a Fermi and superstrings at a TeV, Phys. Lett. B436 (1998) 257–263. arXiv:hep-ph/9804398, doi:10.1016/S0370-2693(98)00860-0.

[210] L. Randall, R. Sundrum, A large mass hierarchy from a small extra dimension, Phys. Rev. Lett. 83 (1999) 3370–3373. arXiv:hep-ph/9905221, doi:10.1103/PhysRevLett.83.3370.

[211] T. Appelquist, H.-C. Cheng, B. A. Dobrescu, Bounds on universal extra dimensions, Phys. Rev. D64 (2001) 035002. arXiv:hep-ph/0012100, doi:10.1103/PhysRevD.64.035002.

[212] H.-C. Cheng, K. T. Matchev, M. Schmaltz, Bosonic supersymmetry? Getting fooled at the CERN LHC, Phys. Rev. D66 (2002) 056006. arXiv:hep-ph/0205314, doi:10.1103/PhysRevD.66.056006.

[213] I. Low, T parity and the littlest Higgs, JHEP 10 (2004) 067. arXiv:hep-ph/0409025, doi:10.1088/1126-6708/2004/10/067.

[214] J. Hubisz, P. Meade, Phenomenology of the littlest Higgs with T-parity, Phys. Rev. D71 (2005) 035016. arXiv:hep-ph/0411264, doi:10.1103/PhysRevD.71.035016.

[215] J. C. Collins, Spin correlations in Monte Carlo event generators, Nucl. Phys. B304 (1988) 794. doi:10.1016/0550-3213(88)90654-2.

[216] I. G. Knowles, Angular correlations in QCD, Nucl. Phys. B304 (1988) 767. doi:10.1016/0550-3213(88)90653-0.

[217] I. G. Knowles, A linear algorithm for calculating spin correlations in hadronic collisions, Comput. Phys. Commun. 58 (1990) 271–284. doi:10.1016/0010-4655(90)90063-7.

[218] I. G. Knowles, Spin Correlations in Parton - Parton Scattering, Nucl. Phys. B310 (1988) 571. doi:10.1016/0550-3213(88)90092-2.

[219] P. Richardson, Spin correlations in Monte Carlo simulations, JHEP 11 (2001) 029. arXiv:hep-ph/0110108.

[220] M. A. Gigg, P. Richardson, Simulation of Finite Width Effects in Physics Beyond the Standard Model, arXiv:0805.3037.

[221] M. Gigg, P. Richardson, Simulation of beyond standard model physics in Herwig++, Eur. Phys. J. C51 (2007) 989–1008. arXiv:hep-ph/0703199, doi:10.1140/epjc/s10052-007-0364-x.

[222] E. Boos, et al., Generic user process interface for event generators, arXiv:hep-ph/0109068.

[223] J. Alwall, et al., A standard format for Les Houches Event Files, Comput. Phys. Commun. 176 (2007) 300–304. arXiv:hep-ph/0609017.

[224] N. D. Christensen, C. Duhr, FeynRules - Feynman rules made easy, Comput. Phys. Commun. 180 (2009) 1614–1641. arXiv:0806.4194, doi:10.1016/j.cpc.2009.02.018.

[225] M. J. Gibbs, A. Ringwald, B. R. Webber, J. T. Zadrozny, Monte Carlo simulation of baryon and lepton number violating processes at high-energies, Z. Phys. C66 (1995) 285–302. arXiv:hep-ph/9406266, doi:10.1007/BF01496603.

[226] H. K. Dreiner, P. Richardson, M. H. Seymour, Parton shower simulations of R-parity violating supersymmetric models, JHEP 04 (2000) 008. arXiv:hep-ph/9912407.

[227] M. J. Strassler, K. M. Zurek, Echoes of a hidden valley at hadron colliders, Phys. Lett. B651 (2007) 374–379. arXiv:hep-ph/0604261, doi:10.1016/j.physletb.2007.06.055.

[228] M. J. Strassler, Possible effects of a hidden valley on supersymmetric phenomenology, arXiv:hep-ph/0607160.

[229] L. Carloni, T. Sjöstrand, Visible Effects of Invisible Hidden Valley Radiation, arXiv:1006.2911.

[230] C.-R. Chen, W. Klemm, V. Rentala, K. Wang, Color Sextet Scalars at the CERN Large Hadron Collider, Phys. Rev. D79 (2009) 054002. arXiv:0811.2105, doi:10.1103/PhysRevD.79.054002.

[231] T. Han, I. Lewis, T. McElmurry, QCD Corrections to Scalar Diquark Production at Hadron Colliders, JHEP 01 (2010) 123. arXiv:0909.2666, doi:10.1007/JHEP01(2010)123.

[232] E. L. Berger, Q.-H. Cao, C.-R. Chen, G. Shaughnessy, H. Zhang, Search for Color Sextet Scalars in Early LHC Experiments, arXiv:1005.2622.

[233] B. Andersson, G. Gustafson, L. Lönnblad, U. Pettersson, Coherence effects in deep inelastic scattering, Z. Phys. C43 (1989) 625.

[234] B. Andersson, G. Gustafson, L. Lönnblad, Gluon splitting in the color dipole cascades, Nucl. Phys. B339 (1990) 393–406.

[235] A. Aktas, et al., Forward jet production in deep inelastic scattering at HERA, Eur. Phys. J. C46 (2006) 27–42. arXiv:hep-ex/0508055.

[236] J. Rathsman, Differences between Monte Carlo models for DIS at small-x and the relation to BFKL dynamics, Phys. Lett. B393 (1997)

181–187. arXiv:hep-ph/9610535, doi:10.1016/S0370-2693(96)01637-1.

[237] L. Lönnblad, ThePEG, Pythia7, Herwig++ and Ariadne, Nucl. Instrum. Meth. A559 (2006) 246–248. doi:10.1016/j.nima.2005.11.143.

[238] E. Avsar, G. Gustafson, L. Lönnblad, Energy conservation and saturation in small-x evolution, JHEP 07 (2005) 062. arXiv:hep-ph/0503181.

[239] E. Avsar, G. Gustafson, L. Lönnblad, Small-x dipole evolution beyond the large-N(c) limit, JHEP 01 (2007) 012. arXiv:hep-ph/0610157.

[240] E. Avsar, G. Gustafson, L. Lönnblad, Difractive Excitation in DIS and pp Collisions, JHEP 12 (2007) 012. arXiv:arXiv:0709.1368[hep-ph].

[241] A. H. Mueller, Soft gluons in the infinite momentum wave function and the BFKL pomeron, Nucl. Phys. B415 (1994) 373–385.

[242] A. H. Mueller, B. Patel, Single and double BFKL pomeron exchange and a dipole picture of high-energy hard processes, Nucl. Phys. B425 (1994) 471–488. arXiv:hep-ph/9403256.

[243] A. H. Mueller, Unitarity and the BFKL pomeron, Nucl. Phys. B437 (1995) 107–126. arXiv:hep-ph/9408245.

[244] C. Flensburg, G. Gustafson, L. Lönnblad, The DIPSY Monte Carlo (in preparation).

[245] G. Corcella, et al., HERWIG 6: an event generator for hadron emission reactions with interfering gluons (including supersymmetric processes), JHEP 01 (2001) 010. arXiv:hep-ph/0011363.

[246] G. Corcella, et al., HERWIG 6.5 release note, arXiv:hep-ph/0210213.

[247] S. Gieseke, A. Ribon, M. H. Seymour, P. Stephens, B. Webber, Herwig++ 1.0: An event generator for e^+e^- annihilation, JHEP 02 (2004) 005. arXiv:hep-ph/0311208.

[248] M. Bahr, et al., Herwig++ 2.3 release note, arXiv:0812.0529.

[249] M. Bähr, et al., Herwig++ Physics and Manual, Eur. Phys. J. C58 (2008) 639–707. arXiv:0803.0883, doi:10.1140/epjc/s10052-008-0798-9.

[250] M. Dobbs and J. B. Hansen, The HepMC C++ Monte Carlo event record for High Energy Physics, Comput. Phys. Commun. 134 (2001) 41–46. doi:10.1016/S0010-4655(00)00189-2.

[251] A. Buckley, et al., Rivet user manual, arXiv:1003.0694.

[252] H. Murayama, I. Watanabe, K. Hagiwara, HELAS: HELicity amplitude subroutines for Feynman diagram evaluations, KEK-91-11.

[253] K. Hamilton, P. Richardson, J. Tully, A positive-weight next-to-leading order Monte Carlo simulation of Drell-Yan vector boson production, JHEP 10 (2008) 015. arXiv:0806.0290, doi:10.1088/1126-6708/2008/10/015.

[254] K. Hamilton, P. Richardson, J. Tully, A positive-weight Next-to-Leading Order Monte Carlo Simulation for Higgs boson production, JHEP 04 (2009) 116. arXiv:0903.4345, doi:10.1088/1126-6708/2009/04/116.

[255] K. Hamilton, A positive-weight next-to-leading order simulation of weak boson pair production, arXiv:1009.5391.

[256] H. E. Haber, G. L. Kane, The Search for Supersymmetry: Probing Physics Beyond the Standard Model, Phys. Rept. 117 (1985) 75–263. doi:10.1016/0370-1573(85)90051-1.

[257] J. F. Gunion, H. E. Haber, Higgs Bosons in Supersymmetric Models. 1, Nucl. Phys. B272 (1986) 1. doi:10.1016/0550-3213(86)90340-8.

[258] U. Ellwanger, C. Hugonie, A. M. Teixeira, The Next-to-Minimal Supersymmetric Standard Model, Phys. Rept. 496 (2010) 1–77. arXiv:0910.1785, doi:10.1016/j.physrep.2010.07.001.

[259] P. Skands, et al., SUSY Les Houches accord: interfacing SUSY spectrum calculators, decay packages, and event generators, JHEP 07 (2004) 036. arXiv:hep-ph/0311123.

[260] B. Allanach, et al., SUSY Les Houches Accord 2, Comp. Phys. Commun. 180 (2009) 8–25. arXiv:0801.0045, doi:10.1016/j.cpc.2008.08.004.

[261] H.-C. Cheng, K. T. Matchev, M. Schmaltz, Radiative corrections to Kaluza-Klein masses, Phys. Rev. D66 (2002) 036005. arXiv:hep-ph/0204342, doi:10.1103/PhysRevD.66.036005.

[262] G. F. Giudice, R. Rattazzi, J. D. Wells, Transplanckian collisions at the LHC and beyond, Nucl. Phys. B630 (2002) 293–325. arXiv:hep-ph/0112161, doi:10.1016/S0550-3213(02)00142-6.

[263] S. Gieseke, P. Stephens, B. Webber, New formalism for QCD parton showers, JHEP 12 (2003) 045. arXiv:hep-ph/0310083.

[264] G. Aad, et al., Charged-particle multiplicities in pp interactions at $\sqrt{s} = 900$ GeV measured with the ATLAS detector at the LHC, Phys. Lett. B688 (2010) 21–42. arXiv:1003.3124, doi:10.1016/j.physletb.2010.03.064.

[265] A. Kupco, Cluster hadronization in HERWIG 5.9, arXiv:hep-ph/9906412.

[266] T. Sjöstrand, The Lund Monte Carlo for Jet Fragmentation, Comput. Phys. Commun. 27 (1982) 243.

[267] T. Sjöstrand, The Lund Monte Carlo for e^+e^- Jet Physics, Comput. Phys. Commun. 28 (1983) 229. doi:10.1016/0010-4655(83)90041-3.

[268] T. Sjöstrand, The Lund Monte Carlo for Jet Fragmentation and e^+e^- Physics: Jetset Version 6.2, Comput. Phys. Commun. 39 (1986) 347–407. doi:10.1016/0010-4655(86)90096-2.

[269] T. Sjöstrand, M. Bengtsson, The Lund Monte Carlo for Jet Fragmentation and e^+e^- Physics. Jetset Version 6.3: An Update, Comput. Phys. Commun. 43 (1987) 367. doi:10.1016/0010-4655(87)90054-3.

[270] H. U. Bengtsson, The Lund Monte Carlo for high p_t physics, Comput. Phys. Commun. 31 (1984) 323. doi:10.1016/0010-4655(84)90018-3.

[271] H. U. Bengtsson, G. Ingelman, The Lund Monte Carlo for high p_t physics, Comput. Phys. Commun. 34 (1985) 251. doi:10.1016/0010-4655(85)90003-7.

[272] H.-U. Bengtsson, T. Sjöstrand, The Lund Monte Carlo for Hadronic Processes: Pythia Version 4.8, Comput. Phys. Commun. 46 (1987) 43. doi:10.1016/0010-4655(87)90036-1.

[273] T. Sjöstrand, High-energy physics event generation with PYTHIA 5.7 and JETSET 7.4, Comput. Phys. Commun. 82 (1994) 74–90. doi:10.1016/0010-4655(94)90132-5.

[274] T. Sjöstrand, et al., High-energy physics event generation with PYTHIA 6.1, Comput. Phys. Commun. 135 (2001) 238–259. arXiv:hep-ph/0010017, doi:10.1016/S0010-4655(00)00236-8.

[275] L. Lönnblad, Development strategies for PYTHIA version 7, Comput. Phys. Commun. 118 (1999) 213–228. arXiv:hep-ph/9810208, doi:10.1016/S0010-4655(98)00200-8.

[276] M. Bertini, L. Lönnblad, T. Sjöstrand, Pythia version 7-0.0: A proof-of-concept version, Comput. Phys. Commun. 134 (2001) 365–391. arXiv:hep-ph/0006152, doi:10.1016/S0010-4655(00)00206-X.

[277] R. Corke, T. Sjöstrand, Improved Parton Showers at Large Transverse Momenta, arXiv:1003.2384.

[278] S. Navin, Diffraction in Pythia, arXiv:1005.3894.

[279] R. Corke, T. Sjöstrand, Interleaved Parton Showers and Tuning Prospects, arXiv:1011.1759.

[280] G. Ingelman, P. E. Schlein, Jet Structure in High Mass Diffractive Scattering, Phys. Lett. B152 (1985) 256. doi:10.1016/0370-2693(85)91181-5.

[281] D. Bernard, 1, et al., The Real Part of the Proton - anti-Proton Elastic Scattering Amplitude at the Center-Of-Mass Energy of 546 GeV, Phys. Lett. B198 (1987) 583. doi:10.1016/0370-2693(87)90922-1.

[282] W. M. Yao, et al., Review of particle physics, J. Phys. G33 (2006) 1–1232. doi:10.1088/0954-3899/33/1/001.

[283] L. Lönnblad, T. Sjöstrand, Modelling Bose-Einstein correlations at LEP 2, Eur. Phys. J. C2 (1998) 165–180. arXiv:hep-ph/9711460, doi:10.1007/s100520050131.

[284] R. Kleiss, W. J. Stirling, Spinor techniques for calculating $p\bar{p} \to W^{\pm}/Z^0$+jets, Nucl. Phys. B262 (1985) 235–262.

[285] A. Ballestrero, E. Maina, S. Moretti, Heavy quarks and leptons at e^+e^- colliders, Nucl. Phys. B415 (1994) 265–292. arXiv:hep-ph/9212246, doi:10.1016/0550-3213(94)90112-0.

[286] T. Gleisberg, F. Krauss, K. T. Matchev, A. Schälicke, S. Schumann, G. Soff, Helicity formalism for spin-2 particles, JHEP 09 (2003) 001. arXiv:hep-ph/0306182.

[287] T. Appelquist, C. W. Bernard, Strongly interacting Higgs bosons, Phys. Rev. D22 (1980) 200. doi:10.1103/PhysRevD.22.200.

[288] T. Appelquist, G.-H. Wu, Electroweak chiral Lagrangian and new precision measurements, Phys. Rev. D48 (1993) 3235–3241. arXiv:hep-ph/9304240, doi:10.1103/PhysRevD.48.3235.

[289] A. Dedes, T. Figy, S. Höche, F. Krauss, T. E. J. Underwood, Searching for Nambu-Goldstone Bosons at the LHC, JHEP 11 (2008) 036. arXiv:0807.4666.

[290] J. C. Pati, A. Salam, Mirror Fermions, J/psi Particles, Kolar Mine Events and Neutrino Anomaly, Phys. Lett. B58 (1975) 333–337. doi:10.1016/0370-2693(75)90667-X.

[291] L. J. Hall, A. E. Nelson, Heavy Gluons and Monojets, Phys. Lett. B153 (1985) 430. doi:10.1016/0370-2693(85)90487-3.

[292] P. H. Frampton, S. L. Glashow, Chiral Color: An Alternative to the Standard Model, Phys. Lett. B190 (1987) 157. doi:10.1016/0370-2693(87)90859-8.

[293] P. H. Frampton, S. L. Glashow, Unifiable Chiral Color With Natural GIM Mechanism, Phys. Rev. Lett. 58 (1987) 2168. doi:10.1103/PhysRevLett.58.2168.

[294] J. Bagger, C. Schmidt, S. King, Axigluon Production in Hadronic Collisions, Phys. Rev. D37 (1988) 1188. doi:10.1103/PhysRevD.37.1188.

[295] K. Hagiwara, et al., Supersymmetry simulations with off-shell effects for the CERN LHC and an ILC, Phys. Rev. D73 (2006) 055005. arXiv:hep-ph/0512260.

[296] N. D. Christensen, et al., A comprehensive approach to new physics simulations, arXiv:0906.2474.

[297] G. P. Lepage, VEGAS - An Adaptive Multi-dimensional Integration Program, CLNS-80/447.

[298] C. Duhr, S. Höche, F. Maltoni, Color-dressed recursive relations for multi-parton amplitudes, JHEP 08 (2006) 062. arXiv:hep-ph/0607057.

[299] F. Maltoni, K. Paul, T. Stelzer, S. Willenbrock, Color-flow decomposition of QCD amplitudes, Phys. Rev. D67 (2003) 014026. arXiv:hep-ph/0209271.

[300] T. Gleisberg, F. Krauss, Automating dipole subtraction for QCD NLO calculations, Eur. Phys. J. C53 (2008) 501–523. arXiv:0709.2881.

[301] C. F. Berger, et al., Precise Predictions for W + 3 Jet Production at Hadron Colliders, Phys. Rev. Lett. 102 (2009) 222001. arXiv:0902.2760, doi:10.1103/PhysRevLett.102.222001.

[302] C. F. Berger, et al., Next-to-Leading Order QCD Predictions for W+3-Jet Distributions at Hadron Colliders, Phys. Rev. D80 (2009) 074036. arXiv:0907.1984, doi:10.1103/PhysRevD.80.074036.

[303] C. F. Berger, et al., Next-to-Leading Order QCD Predictions for Z, γ^*+3-Jet Distributions at the Tevatron, Phys. Rev. D82 (2010) 074002. arXiv:1004.1659, doi:10.1103/PhysRevD.82.074002.

[304] C. F. Berger, et al., Precise Predictions for W + 4 Jet Production at the Large Hadron Collider, arXiv:1009.2338.

[305] C. F. Berger, et al., An Automated Implementation of On-Shell Methods for One- Loop Amplitudes, Phys. Rev. D78 (2008) 036003. arXiv:0803.4180, doi:10.1103/PhysRevD.78.036003.

[306] T. Binoth, T. Gleisberg, S. Karg, N. Kauer, G. Sanguinetti, NLO QCD corrections to ZZ+jet production at hadron colliders, Phys. Lett. B683 (2010) 154–159. arXiv:0911.3181, doi:10.1016/j.physletb.2009.12.013.

[307] T. Binoth, J. P. Guillet, G. Heinrich, E. Pilon, C. Schubert, An algebraic / numerical formalism for one-loop multi-leg amplitudes, JHEP 10 (2005) 015. arXiv:hep-ph/0504267.

[308] S. Höche, S. Schumann, F. Siegert, Hard photon production and matrix-element parton-shower merging, Phys. Rev. D81 (2010) 034026. arXiv:0912.3501, doi:10.1103/PhysRevD.81.034026.

[309] S. Plätzer, S. Gieseke, Coherent Parton Showers with Local Recoils, arXiv:0909.5593.

[310] T. Carli, T. Gehrmann, S. Höche, Hadronic final states in deep-inelastic scattering with Sherpa, Eur. Phys. J. C67 (2010) 73. arXiv:0912.3715, doi:10.1140/epjc/s10052-010-1261-2.

[311] F. Krauss, A. Schälicke, S. Schumann, G. Soff, Simulating W/Z + jets production at the Tevatron, Phys. Rev. D70 (2004) 114009. arXiv:hep-ph/0409106, doi:10.1103/PhysRevD.70.114009.

[312] F. Krauss, A. Schälicke, S. Schumann, G. Soff, Simulating W/Z + jets production at the CERN LHC, Phys. Rev. D72 (2005) 054017. arXiv:hep-ph/0503280.

[313] T. Gleisberg, F. Krauss, A. Schälicke, S. Schumann, J.-C. Winter, Studying W^+W^- production at the Fermilab Tevatron with Sherpa, Phys. Rev. D72 (2005) 034028. arXiv:hep-ph/0504032.

[314] S. Höche, F. Krauss, M. Schönherr, F. Siegert, NLO matrix elements and truncated showers, arXiv:1009.1127.

[315] A. Deur, V. Burkert, J. P. Chen, W. Korsch, Determination of the effective strong coupling constant $\alpha_{s,g_1}(Q^2)$ from CLAS spin structure function data, Phys. Lett. B665 (2008) 349–351. arXiv:0803.4119, doi:10.1016/j.physletb.2008.06.049.

[316] M. Neubert, Heavy-quark symmetry, Phys. Rept. 245 (1994) 259–396. arXiv:hep-ph/9306320.

[317] I. Caprini, L. Lellouch, M. Neubert, Dispersive bounds on the shape of $\bar{B} \to D^{(*)} l\bar{\nu}$ form factors, Nucl. Phys. B530 (1998) 153–181. arXiv:hep-ph/9712417, doi:10.1016/S0550-3213(98)00350-2.

[318] J. D. Richman, P. R. Burchat, Leptonic and semileptonic decays of charm and bottom hadrons, Rev. Mod. Phys. 67 (1995) 893–976. arXiv:hep-ph/9508250.

[319] N. Isgur, D. Scora, B. Grinstein, M. B. Wise, Semileptonic B and D decays in the quark model, Phys. Rev. D39 (1989) 799. doi:10.1103/PhysRevD.39.799.

[320] D. Scora, N. Isgur, Semileptonic meson decays in the quark model: An update, Phys. Rev. D52 (1995) 2783–2812. arXiv:hep-ph/9503486, doi:10.1103/PhysRevD.52.2783.

[321] J. L. Goity, W. Roberts, Soft pion emission in semileptonic B-meson decays, Phys. Rev. D51 (1995) 3459–3477. arXiv:hep-ph/9406236, doi:10.1103/PhysRevD.51.3459.

[322] P. Ball, R. Zwicky, New results on $B \to \pi, K, \eta$ decay form factors from light-cone sum rules, Phys. Rev. D71 (2005) 014015. arXiv:hep-ph/0406232, doi:10.1103/PhysRevD.71.014015.

[323] P. Ball, R. Zwicky, $B_{d,s} \to \rho, \omega, K^*, \Phi$ decay form factors from light-cone sum rules reexamined, Phys. Rev. D71 (2005) 014029. arXiv:hep-ph/0412079, doi:10.1103/PhysRevD.71.014029.

[324] P. Ball, G. W. Jones, $B \to \eta^{(\prime)}$ form factors in QCD, JHEP 08 (2007) 025. arXiv:0706.3628.

[325] T. M. Aliev, M. Savci, Semileptonic decays of pseudoscalar mesons to scalar f_0 meson, arXiv:hep-ph/0701108.

[326] Kühn, Johann H. and Santamaría, A., τ Decays to pions, Z. Phys. C48 (1990) 445–452. doi:10.1007/BF01572024.

[327] S. Weinberg, Phenomenological Lagrangians, Physica A96 (1979) 327.

[328] J. Gasser, H. Leutwyler, Chiral Perturbation Theory to One Loop, Ann. Phys. 158 (1984) 142. doi:10.1016/0003-4916(84)90242-2.

[329] J. Gasser, H. Leutwyler, Chiral perturbation theory: Expansions in the mass of the strange quark, Nucl. Phys. B250 (1985) 465. doi:10.1016/0550-3213(85)90492-4.

[330] G. Ecker, J. Gasser, A. Pich, E. de Rafael, The role of resonances in chiral perturbation theory, Nucl. Phys. B321 (1989) 311. doi:10.1016/0550-3213(89)90346-5.

[331] M. G. Ryskin, A. D. Martin, V. A. Khoze, Soft processes at the LHC, I: Multi-component model, Eur. Phys. J. C60 (2009) 249–264. arXiv:0812.2407, doi:10.1140/epjc/s10052-009-0889-2.

[332] J. Butterworth, F. Maltoni, F. Moortgat, P. Richardson, S. Schumann, et al., The Tools and Monte Carlo working group Summary Report, arXiv:1003.1643.

[333] M. Cacciari, G. P. Salam, S. Sapeta, On the characterisation of the underlying event, JHEP 04 (2010) 065. arXiv:0912.4926, doi:10.1007/JHEP04(2010)065.

[334] J. Pumplin, D. R. Stump, J. Huston, H. L. Lai, P. Nadolsky, W. K. Tung, New generation of parton distributions with uncertainties from global QCD analysis, JHEP 0207 (2002) 012. arXiv:hep-ph/0201195.

[335] T. Carli, T. Gehrmann, S. Hoeche, Hadronic final states in DIS with Sherpa, arXiv:1006.5696.

[336] A. Buckley, H. Hoeth, H. Lacker, H. Schulz, J. E. von Seggern, Systematic event generator tuning for the LHC, Eur. Phys. J. C65 (2010) 331–357. arXiv:0907.2973, doi:10.1140/epjc/s10052-009-1196-7.

[337] J. Bromley, et al., HZTOOL: A package for Monte Carlo-data comparison at HERA (version 1.0)Prepared for Workshop on Future Physics at HERA (Preceded by meetings 25-26 Sep 1995 and 7-9 Feb 1996 at DESY), Hamburg, Germany, 30-31 May 1996.

[338] B. M. Waugh, et al., HZTool and Rivet: Toolkit and framework for the comparison of simulated final states and data at colliders, arXiv:hep-ph/0605034.

[339] M. Cacciari, FastJet: A code for fast k_t clustering, and more, arXiv:hep-ph/0607071.

[340] A. Buckley, CEDAR: tools for event generator tuning, PoS ACAT2007 (2007) 050. arXiv:0708.2655.

[341] Aida – Abstract Interfaces for Data Analysis, http://aida.freehep.org/.

[342] A. Buckley, M. Whalley, HepData reloaded: reinventing the HEP data archive, arXiv:1006.0517.

[343] G. Aad, et al., Measurement of underlying event characteristics using charged particles in pp collisions at $\sqrt{s} = 900$ GeV and 7 TeV with the ATLAS detector, arXiv:1012.0791.

[344] T. Aaltonen, et al., Studying the Underlying Event in Drell-Yan and High Transverse Momentum Jet Production at the Tevatron, Phys. Rev. D82 (2010) 034001. arXiv:1003.3146, doi:10.1103/PhysRevD.82.034001.

[345] R. Barate, et al., Studies of quantum chromodynamics with the ALEPH detector, Phys. Rept. 294 (1998) 1–165. doi:10.1016/S0370-1573(97)00045-8.

[346] A. Heister, et al., Studies of QCD at e^+e^- centre-of-mass energies between 91 and 209 GeV, Eur. Phys. J. C35 (2004) 457–486. doi:10.1140/epjc/s2004-01891-4.

[347] V. M. Abazov, et al., Measurement of Dijet Azimuthal Decorrelations at Central Rapidities in $p\bar{p}$ Collisions at $\sqrt{s} = 1.96$ TeV, Phys. Rev. Lett. 94 (2005) 221801. arXiv:hep-ex/0409040, doi:10.1103/PhysRevLett.94.221801.

[348] D. E. Acosta, et al., Study of jet shapes in inclusive jet production in $p\bar{p}$ collisions at $\sqrt{s} = 1.96$ TeV, Phys. Rev. D71 (2005) 112002. arXiv:hep-ex/0505013, doi:10.1103/PhysRevD.71.112002.

[349] B. I. Abelev, et al., Strange particle production in $p + p$ collisions at $\sqrt{s} = 200$ GeV, Phys. Rev. C75 (2007) 064901. arXiv:nucl-ex/0607033, doi:10.1103/PhysRevC.75.064901.

[350] G. Barker, et al., A Study of the b-Quark Fragmentation Function with the DELPHI Detector at LEP IPresented at ICHEP 2002. arXiv:DELPHI2002-069CONF603.

[351] F. James, Monte Carlo theory and practice, Rept. Prog. Phys. 43 (1980) 1145.

[352] K. Nakamura, Review of particle physics, J. Phys. G37 (2010) 075021. doi:10.1088/0954-3899/37/7A/075021.

[353] A. Ballestrero, E. Maina, S. Moretti, Heavy quark production at e^+e^- colliders in three and four jet events, Phys. Lett. B294 (1992) 425–430. doi:10.1016/0370-2693(92)91544-J.

[354] A. Ballestrero, E. Maina, S. Moretti, Heavy quark production at e^+e^- colliders in multi-jet events and a new method of computing helicity amplitudes, arXiv:hep-ph/9405384.

[355] F. A. Berends, W. T. Giele, Recursive calculations for processes with n gluons, Nucl. Phys. B306 (1988) 759.

[356] F. A. Berends, W. Giele, The six-gluon process as an example of Weyl-van der Waerden spinor calculus, Nucl. Phys. B294 (1987) 700.

[357] R. Kleiss, H. Kuijf, Multi-gluon cross-sections and five jet production at hadron colliders, Nucl. Phys. B312 (1989) 616.

[358] F. A. Berends, W. T. Giele, H. Kuijf, Exact expressions for processes involving a vector boson and up to five partons, Nucl. Phys. B321 (1989) 39.

[359] F. A. Berends, W. T. Giele, H. Kuijf, On six-jet production at hadron colliders, Phys. Lett. B232 (1989) 266.

[360] P. D. Draggiotis, R. H. P. Kleiss, C. G. Papadopoulos, Multi-jet production in hadron collisions, Eur. Phys. J. C24 (2002) 447–458. arXiv:hep-ph/0202201.

[361] F. Caravaglios, M. Moretti, An algorithm to compute Born scattering amplitudes without Feynman graphs, Phys. Lett. B358 (1995) 332–338. arXiv:hep-ph/9507237, doi:10.1016/0370-2693(95)00971-M.

[362] M. L. Mangano, S. J. Parke, Z. Xu, Duality and multi-gluon scattering, Nucl. Phys. B298 (1988) 653.

[363] V. del Duca, A. Frizzo, F. Maltoni, Factorization of tree QCD amplitudes in the high-energy limit and in the collinear limit, Nucl. Phys. B568 (2000) 211–262. arXiv:hep-ph/9909464.

[364] V. Del Duca, L. J. Dixon, F. Maltoni, New color decompositions for gauge amplitudes at tree and loop level, Nucl. Phys. B571 (2000) 51–70. arXiv:hep-ph/9910563.

[365] R. Kleiss, R. Pittau, Weight optimization in multichannel Monte Carlo, Comput. Phys. Commun. 83 (1994) 141–146. arXiv:hep-ph/9405257, doi:10.1016/0010-4655(94)90043-4.

[366] F. James, Monte-Carlo phase space, CERN-68-15.

[367] E. Byckling, K. Kajantie, N-particle phase space in terms of invariant momentum transfers, Nucl. Phys. B9 (1969) 568–576.

[368] A. Cafarella, C. G. Papadopoulos, M. Worek, HELAC-PHEGAS: A generator for all parton level processes, Comput. Phys. Commun. 180 (2009) 1941–1955. arXiv:0710.2427, doi:10.1016/j.cpc.2009.04.023.

[369] J. Alwall, et al., MadGraph/MadEvent v4: The new web generation, JHEP 09 (2007) 028. arXiv:0706.2334.

[370] A. van Hameren, C. G. Papadopoulos, A hierarchical phase space generator for QCD antenna structures, Eur. Phys. J. C25 (2002) 563–574. arXiv:hep-ph/0204055.

[371] R. Kleiss, W. J. Stirling, S. D. Ellis, A new Monte Carlo treatment of multiparticle phase space at high energies, Comput. Phys. Commun. 40 (1986) 359.

[372] R. Frederix, T. Gehrmann, N. Greiner, Automation of the Dipole Subtraction Method in MadGraph/MadEvent, JHEP 09 (2008) 122. arXiv:0808.2128, doi:10.1088/1126-6708/2008/09/122.

[373] R. Frederix, S. Frixione, F. Maltoni, T. Stelzer, Automation of next-to-leading order computations in QCD: the FKS subtraction, JHEP 10 (2009) 003. arXiv:0908.4272, doi:10.1088/1126-6708/2009/10/003.

[374] M. Czakon, C. G. Papadopoulos, M. Worek, Polarizing the Dipoles, JHEP 08 (2009) 085. arXiv:0905.0883, doi:10.1088/1126-6708/2009/08/085.

[375] G. Bevilacqua, M. Czakon, C. G. Papadopoulos, M. Worek, Dominant QCD Backgrounds in Higgs Boson Analyses at the LHC: A Study of $pp \to t\bar{t}+2$ jets at Next-To-Leading Order, Phys. Rev. Lett. 104 (2010) 162002. arXiv:1002.4009, doi:10.1103/PhysRevLett.104.162002.

[376] A. H. Hoang, A. Jain, I. Scimemi, I. W. Stewart, Infrared Renormalization Group Flow for Heavy Quark Masses, Phys. Rev. Lett. 101 (2008) 151602. arXiv:0803.4214, doi:10.1103/PhysRevLett.101.151602.

[377] S. Fleming, A. H. Hoang, S. Mantry, I. W. Stewart, Jets from massive unstable particles: Top-mass determination, Phys. Rev. D77 (2008) 074010. arXiv:hep-ph/0703207, doi:10.1103/PhysRevD.77.074010.

[378] S. Fleming, A. H. Hoang, S. Mantry, I. W. Stewart, Top Jets in the Peak Region: Factorization Analysis with NLL Resummation, Phys. Rev. D77 (2008) 114003. arXiv:0711.2079, doi:10.1103/PhysRevD.77.114003.

[379] A. Jain, I. Scimemi, I. W. Stewart, Two-loop Jet-Function and Jet-Mass for Top Quarks, Phys. Rev. D77 (2008) 094008. arXiv:0801.0743, doi:10.1103/PhysRevD.77.094008.

[380] V. M. Abazov, et al., Combination of $t\bar{t}$ cross section measurements and constraints on the mass of the top quark and its decays into charged Higgs bosons, Phys. Rev. D80 (2009) 071102. arXiv:0903.5525, doi:10.1103/PhysRevD.80.071102.

[381] U. Langenfeld, S. Moch, P. Uwer, Measuring the running top-quark mass, Phys. Rev. D80 (2009) 054009. arXiv:0906.5273, doi:10.1103/PhysRevD.80.054009.

[382] V. A. Khoze, T. Sjöstrand, Color correlations and multiplicities in top events, Phys. Lett. B328 (1994) 466–476. arXiv:hep-ph/9403394, doi:10.1016/0370-2693(94)91506-7.

[383] A. H. Hoang, I. W. Stewart, Top Mass Measurements from Jets and the Tevatron Top-Quark Mass, Nucl. Phys. Proc. Suppl. 185 (2008) 220–226. arXiv:0808.0222, doi:10.1016/j.nuclphysbps.2008.10.028.

[384] The Tevatron Electroweak Working Group, Combination of CDF and D0 Results on the Mass of the Top Quark, arXiv:1007.3178.